Joining of Advanced Ceramics to Metals

Karim Khene

BEng

A thesis submitted in partial fulfilment of the requirements of the Nottingham Trent University for the degree of Doctor of Philosophy

January 2003

The Nottingham Trent University

Abstract

A novel method for ceramic-to-metal joining, applicable for a wide range of emerging ceramic matrix composites (CMC) and cermets was developed. It combined singularity removal from the free surface and the introduction of a functional gradient zone, achieved by introducing a 'dome-flat' concept. This shaping was done by CNC electrical discharge machining (EDM) of the CMC by the preshaped metal part. These novel interfaces were modelled and the differential thermal expansion-induced stresses generated during brazing were predicted for 10mm, 20mm and 30mm diameter joints using finite element analysis (FEA). An experimental programme was conducted to validate the finite element analysis results as indicated by samples' residual strengths using tensile testing. It proved that removal of the excessive stress concentration associated with the peripheral region of simple flat interfaced joints, allowed useful joints to be manufactured with dome or dome-flat interface geometries in diameters up to 30mm in the Syalon 501/AISI 321 system despite its high coefficient of thermal expansion (CTE) ratio approaching 3.5:1. Thus, for lower CTE mismatch systems, diameters in excess of 30mm can be joined. For large joints, the strength limiting factor was shown to be more likely due to the decreasing strength attributable to increased ceramic cross section, than to the effects of induced differential thermal strains from joining. Active metal brazing was selected to manufacture the ceramic-to-metal joints and guidelines were presented for the production of strong joints. EDM machining proved invaluable for manufacturing the dome-flat geometry interfaces required with a good degree of accuracy and with near perfect interfacial conformity. For generating even more complex interfaces, non-contact EDM becomes the only viable machining method for generating ceramic surfaces of high complexity. Copper interlayers generally raised joints' strengths and resulted in more consistency in tensile tests. Techniques were developed for the accurate machining of complex interlayers and a tool design was proposed for producing precision cast or sintered metal interlayers on an industrial scale. Microhardness testing was used to monitor the differential thermal stress-induced strains at joints interfaces and, although braze-contamination hardening within the stainless steel and any copper interlayers accompanied the differential strain-induced hardening, the results provided evidence to support the predicted size effect on residual stress and strain in metal/ceramic joints. The strongest joints produced in this investigation had tensile strengths up to 52MPa and were found in 20mm diameter Syalon 501/AISI 321 stainless steel joints containing copper interlayers. The importance of balancing cooling rate across each interface of a joint was noted. For the soft copper interlayer used, the opportunity for recrystallisation to persist to as low a temperature as possible during cooling from brazing was an advantage. In addition it was beneficial to allow the full potential of the thermal stress-relaxing design features comprising the stainless steel featheredges and the copper interlayers to be realised to the limits of their strain absorbing capacity. Further work was proposed which would further increase the level of complexity of the interface by replacing the flat interface across the central region of the joint by a region of repeated interpenetration such as a 3-D sine wave, capitalizing on the ease of complex interface profile machining demonstrated through non-contact electrical discharge machining of ceramics.

Acknowledgements

I should like to express my thanks and appreciation to all the staff of the Nottingham Trent University who helped me throughout this project.

In particular my director of studies Dr. John Huddleston and my second supervisor Dr Martyn Lacey for their tireless supervision and continuous support and help to overcome the challenging nature of this project.

I should also like to thank all the technicians who assisted me during my research, Dr Chris Trueman for his help with the EDM, Judith Kipling for her valuable assistance in the lab, Alan Tye and Ralph James for machining graphite and test samples and all the others who I have not mentioned here.

Thanks are also due to Mark Deven of Buehler for helping me to establish satisfactory metallographic procedures.

Finally I should like to thank my family for their support over the years and my friends and colleagues from the Faculty Research Institute for their ongoing friendship and encouragement.

Thank you all.

Joining of Advanced Ceramics to Metals

Table of Contents

Chapter 1

Background to Research

1.1 Aims of the investigation

Much research has been conducted since the late 1980's in the area of joining ceramics to metals. This has resulted in a body of knowledge exemplified by the popular texts by Nicholas[1], Schwartz[2] and Morrell[3]. This has been accompanied by conferences[4, 5] and published works on the fundamental nature of ceramic to metal interfaces typically by Rűhle and Mader[6].

The process and materials-related work has highlighted the development of special brazes and adhesives (still both on-going) and thermodynamic factors including interfacial chemical reactions. Practical investigations have been accompanied by finite element modelling, particularly with regard to the magnitude of residual stresses generated within such joints caused by any mismatch between the thermal expansion coefficients of the joint members as well as by differences in their physical properties.

The amount of research conducted into methods of reducing these levels of residual stress has been relatively modest. Tinsley[7] and Tinsley et al[8] showed the residual stress reduction that could be gained by generating curved mating interfaces, though few others workers have considered non -planar interfaces.

By the same token, there has been little investigation into joining large areas or of the effect upon residual stress magnitude and joint integrity of increasing interfacial area. Most investigators have limited their practical and modelling studies to small metal to ceramic interface areas, typically between 5-10mm diameter and of simple cross section shape.

Concurrently, significant advances have been taken place in the development of advanced technical structural ceramics.

Running alongside these investigations into metal-ceramic joining, invariably using the simple monolithic ceramic materials silicon nitride, silicon carbide, alumina and zirconia, there have been profound developments in ceramics themselves with, for example the introduction of fibre-reinforced ceramics (like SiC fibre- reinforced SiC) and of ceramics containing particulate dispersoids. Where these particulates are electrically conductive (eg. the nitrides carbides, borides, and carbonitrides of titanium, zirconium and hafnium) and of sufficient concentration to facilitate the formation of electrically conductive pathways through the ceramic's microstructure, the composite material becomes amenable to shaping by electrical discharge machining (EDM). This non-contact machining process imposes no mechanical forces on the ceramic being machined. Furthermore, over half a centry this process has become an established and sophisticated toolroom process for shaping metals, especially moulds and dies, capable through its CNC control and closely controlled and infinitely variable power supply, to be able to generate with great accuracy, if necessary, the most complex of surface profiles.

It is the aim, therefore of this present investigation to exploit the novel ceramic shaping approach of using EDM in conjunction with one of these electrically conductive ceramic composites to generate a range of interface profiles in order to investigate the effects of increasing joint interfacial area (up to 10 times larger than studied by most researchers) on joint integrity and residual stress level. The study will utilise finite element analysis modelling in conjunction with an extensive practical programme of joints manufacture and evaluation. Joints with and without a soft metal interlayer will be investigated.

Whilst metal-to-ceramic joint specimens with large interfacial area might be expected to exhibit wide statistical variation in strength, and be associated with considerable cost implications, it is nevertheless anticipated that, whilst formal joint strength-to-interfacial area size relationships may not be obtainable from the proposed study, strong trends will be identified and some clarity emerge on the limiting size of interfacial area that can be joined.

Finally, and most importantly, it is hoped that a method can be demonstrated for effective joining of ceramics to metals using existing tool room techniques, which will be applicable to larger and less conventional cross sectional shapes.

To extend the work carried out by Tinsley [7] in his investigation to reduce residual stresses at the interface between metal-ceramic joints using 10mm diameter samples, two lines of investigation will be investigated during this project. The first will study the effect on the principal tensile stresses, which are potentially harmful to the ceramic, when using a 2mm thick-curved copper interlayer in a ceramic-metal system i.e. Syalon 501/ AISI 321. The second is to study the effects of changing the size and interface type of the test samples from 10mm dome, to 20mm dome-flat to 30mm dome-flat on the thermally induced residual stresses from joining. Both lines of investigation will be conducted using finite element analysis supported by experimental methods involving the production, mechanical testing and microscopical evaluation of joints.

The ideal outcome from the present study would be the development of a ceramic-to-metal joining approach which would be easy to apply, appropriate for a wide range of ceramics and metals and most importantly be able to accommodate parts of any size, small or large.

1.2 Introduction

Advanced ceramics have been identified as potential candidates for high-temperature structural applications because of their high-temperature resistance, low density, and excellent corrosion and wear resistance. In order to expand the application of these materials, joining them to metals has become a necessity.

In recent years interest has risen in ceramics as high performance materials. The two main reasons for this interest are:

(a) The necessity for high strength materials which can be used at high temperatures.
(b) The potential that ceramics possess for further development and improvement.

Ceramics enjoy several major advantages over metals and other materials. They have heat resistance, wear and abrasion resistance, hardness (at least three times those of engineering alloys), lightness and resistance to erosion and corrosion. It is true that ceramics in general are inferior in terms of brittleness, in particular their low impact and thermal shock resistances create major restrictions on their applications. The ionic and covalent bonds in ceramics give them a structure in which atoms and ions cannot move easily, thus relaxation of stress is less likely to occur. That characteristic has the disadvantage that breakage will result from comparatively small faults. It is not unusual for ceramic objects to shatter suddenly without warning. This is particularly likely to occur in a ceramic-metal joint owing to differential contraction/expansion-induced interfacial stresses, the crack running along the ceramic side of the interface.

The problems with poor thermal shock resistance have been overcome to some extent with the development of silicon nitride and silicon carbides, as well as sialons, all of which have excellent strength, relatively low thermal expansion coefficient and, for silicon carbide high thermal conductivity.

Most of the work carried out, in the field of ceramic joining in the past looked principally into ways of joining ceramics to metals, typically as presented by Schwartz[2]. Techniques were investigated to overcome problems encountered from material incompatibilities such as mismatch of coefficients of expansion, surface reaction and the residual stresses formed from metal-ceramic joining following a change in the temperature during processing or in subsequent service.

The need for reliable joining between ceramics and metals has long been recognised. This started centuries ago with the practice of mechanical attachment of gemstones in jewellery. Recent industrial applications in many sectors have led to the development of various manufacturing processes for joining ceramics to metals, including the familiar moly-manganese process.

The role of ceramics in engineering is changing rapidly with critical new application areas, as new structural and electrical materials are developed. Even though ceramics enjoy many physical property advantages over metals, the use of ceramics still depends on their incorporation into metallic structures.

The development of novel materials for the sectors of transport, medicine, energy, and information technology has been gaining crucial importance. Products of today and tomorrow are required to be more efficient, long-lived, environment-friendly and less expensive. In order to achieve this many constraints have to be addressed when joining ceramics to metals. Good examples are those of problems met during fabrication of assemblies in the electronic sector, or in the aerospace industry where components are exposed to very high temperature for long periods of time in highly corrosive environment.

1.3 Importance of joining ceramics to metals

Joining facilitates the use of structural ceramics in cases where structures cannot be made in one piece or in cases where joining is the only feasible and economical way. Joined ceramics can be made stronger than other materials, either by combining stronger components or by introducing compressive stresses into the system from either strong fibres as in composites, or from the mating metal parts as in some automotive applications. Joined parts can be made with shapes and tolerances not readily achievable otherwise. A good example of the potential of joining can be seen in the manufacture of the complex internal passages for cooling flows in heat exchangers.

Tinsley's work on joining Syalon 101 and 501 to stainless steel AISI 321 will be further examined and extended in the present investigation. The ceramic-to-metal joining concept is not new. During recent years, techniques described by Nicholas[1] and Schwartz[2] have been developed, and most of them have proved reliable and effective up to a limited degree. This current work is not concerned with developing completely new techniques for joining ceramics to metals, rather to investigate the effects and implications of interface geometry and size of components on the generation of residual stresses at the interfaces, and looking into novel ways to reduce or eliminate them and so allow the production of larger and more reliably jointed parts. Many papers highlight the importance of joining[9-11]

Application	Technique	Ceramic	Metal
Dental implants	Diffusion bonding	Al_2O_3	Nb, Ti
Lenses	Adhesives	Glass	Steel, Polymers
Housing for semiconductors	Metallising & hard brazing	Al_2O_3	FeNi, Cu
Turbo charger	Active brazing	Si_3N_4	Ni-alloys
Feedthroughs	Active brazing	Al_2O_3	FeNi, Cu
Turbines blades	Form fitting	Si_3N_4	Stainless Steel
Lamps	Glass filler material brazing	Glass	W, Mo
Solid oxide fuel cells	Glass filler material brazing	ZrO_2	Cr-alloys
Hip implants	Form fitting	Al_2O_3	Stainless Steel

Table1.1: Examples of ceramic - metal joint application[2]

The range of applications as presented by Schwartz[2], Unal et al[12] and Peteves et al[13] for ceramics is considerable. Ceramics are used in the aerospace, automotive, and electronics industries. Although many applications rely on the high temperature capabilities, the majority depend on the corrosion and wear resistance of advanced ceramics. Good examples are found in cutting tools, die parts, nozzles and ceramic armour. Advanced ceramics are also used in molten metal handling where inertness and thermal shock resistance are important. Table 1.1 shows examples of current applications for ceramic-to-metal joining.

1.4 Existing joining techniques

1.4.1 Mechanical Fastening

There are different ways to join together mechanically two dissimilar materials [14-16]. These are often simple in design and usually involve bolts or screw threads. The problem with the latter is that a ceramic screw thread requires expensive machining and can result in cracking of the ceramic. Mechanical fastening[2] is a cheap technique usually used for [9-10] locating parts rather then joining them. Using this method, damaged parts can be replaced easily. Bolting, threading and clamping are the most used methods[17, 18], however it is best to avoid them when working with ceramics as cracks can be easily initiated. It is the practice to use washers or gaskets of soft metal typically aluminium, copper and lead to relax potentially dangerously high contact stresses, which could fracture ceramic parts.

The use of threads in ceramics introduces non-uniform loads, which may cause the ceramic to fracture. For ground surfaces of ceramics parts with accurate dimensions, shrink fitting can be used. Under careful control of temperature to accommodate the difference in CTE between ceramics and metals, highly accurate fitting can be achieved after cooling, in tightly connected parts. During processing one should take care to avoid thermal shock damage to the ceramic

1.4.2.Friction Welding

This method described by Weiss[19], Suthoff[20] and Greitman and Weiss al[21] consists of using friction to induce heat to generate solid phase joints between ceramic and metal. While the ceramic component is kept stationary, the metal part is spun at high speed. This generates a lot of heat, and metal is stressed above its yield stress creating a liquid at the metal/ceramic interface. The two parts are than brought to rest under axial load, the molten metal created by friction solidifying to form the joint.

1.4.3 Adhesives

Schwartz[2] and Broring Vegla et al[22] state that using adhesives is a simple and cheap method of joining ceramics to metals. Adhesives provide a good load distribution over the contact area and generate strong joints at low temperature. Some organic adhesives form strong joints up to 170°C or higher. In practice adhesives are not used for high temperature application.

1.4.4 Diffusion bonding

Diffusion bonding was described by various authors[23--32] as a solid-state joining process by which two nominally flat surfaces are joined at high temperature under mechanical pressure in an inert atmosphere. This process is used to join similar or dissimilar materials. For diffusion bonding to be successful the two candidate surfaces are carefully prepared, ensuring a good surface finish free of irregularities or cavities which may be detrimental to the joint integrity (a ratio of 1:50 is typical for roughness asperity height to roughness wavelength). The temperature required for diffusion bonding usually ranges between 0.5 and 0.8 of the absolute melting temperature of the metal. To avoid macroscopic deformation the pressure used in the process is typically a small fraction of the yield stress of the metal at room temperature. Depending on the joint system used, time can vary from a few minutes to several hours. The precise value for each of the variables for a bond in a particular material is chosen such that, ideally, parent metal microstructures and properties are attained after bonding and there is no gross macroscopic deformation, although in practice this may occur up to a few percent locally.

Various authors[33-37] describe diffusion bonding and highlight its difference from brazing. In diffusion bonding the bond strength matches that of the base metal typically up to 200MPa. During joining minimal distortion take place resulting in well-defined interfacial geometries. Unlike brazed joints, those made by diffusion bonding can be used safely at high temperatures.

The disadvantage of diffusing bonding is the high cost involved when using high temperatures and pressure and, often-sophisticated equipment.

Diffusion bonding occurs in five stages:

- Point contact between the two surfaces
- Plastic deformation of the metal reducing the asperities and increasing the contact areas until the local stress decreases below the yield stress.
- Removal of voids at the interface as well as a simultaneous migration of the interface out of a planar orientation and away from the voids.

- Removal of the remaining voids by diffusion.
- Grain boundary rearrangement and volume diffusion.

1.4.5 Active metal brazing

Active metal brazing has been described in many sources[34, 38-44]. It is commonly used in joining ceramics and metals for structural applications. The active metal, which is ordinarily alloyed in low concentration with other metals, has a strong affinity for the ceramic substrate anion. When the braze is melted at the interface between a metal and a ceramic, the active metal will migrate to the ceramic surface where oxidation/reduction reactions take place to promote adhesion through the formation of an intermediate compound. Active metal brazing will be outlined in fuller detail in Chapter 2.

1.4.6 Microwave joining

This method of joining utilises microwaves to heat ceramic materials to temperatures high enough to accomplish the joining of parts. Papers presented by Klein[45] Palaith and Silberglitt[46] and Binner et al[47] describe this technique.

The process is both rapid and efficient making this technique well suited to various aspects of processing ceramics including joining. Although interest in microwave processing has increased noticeably in the last decade, this technology is still largely in a developmental stage.

In microwave heating, heat is generated within materials unlike other techniques which require external heating sources. A consequence of this is that microwave-heated materials become hotter inside than outside, rather than the reverse as is common in conventionally heated materials. Advantages of this internal volumetric heating are that both small and large parts can be heated rapidly and uniformly, a characteristic, which is especially attractive for ceramic materials. For ceramic-to-ceramic joining applications microwave processing offers the possibilities of:

(1) rapid heating with modest power levels compared to conventional techniques,

(2) localised heating of joint regions through sample configuration and joint design,

(3) Selective heating of materials,

(4) On-line process control.

While still in a developmental stage, the application of microwave processing techniques to joining appears to be a viable and versatile approach. This method is suitable for ceramic joining but not for metal.

1.5 Evaluation and inspection techniques for metal-ceramic joints

When testing ceramic - metal joints it is required to know about the integrity and the quality of the components as well as to investigate the reliability of joints. Different types of testing exist which will be described below.

1.5.1 Destructive testing methods

1.5.1.1 Shear tests

The shear strength is calculated from the fracture load divided by the area of the joined surface. This method discussed by Unal et al[48] generates two problems:

1 The shear stress applied is not a simple shear at the joint region, there is always a tensile stress present due to a bending moment.

2 Once the test sample is held in position between the test tools, a compressive force is induced. This creates an additional unknown, making the evaluation for the shear stress inaccurate.

Neither of the problems mentioned in 1 and 2 can be ignored, therefore shear tests cannot be used as exact evaluations.

1.5.1.2 Tensile tests

Advanced ceramic materials need adequate methods to test their tensile properties. Conventional equipment will not grip ceramics adequately due to the material's extreme hardness. With tension testing, a larger material volume can be loaded; however, conventional tension testing requires precision-machined test specimens to minimize stress concentrations at the attachment. Precision machining also minimizes uncontrollable bending when force is applied to the specimen. Easy self-alignment of the specimen into the tensile axis of the machine is a vital requirement to prevent unacceptable bend stresses becoming imposed on the ceramic specimen.

1.5.1.3 Bend tests

Bend tests techniques were described by Schwartz[2] and Üstündag, et al[49]. The most common bend tests for ceramics are the three- point and four-point bend tests. The main problem with other types of tests is that with ceramic samples it is difficult to grip them in the machine. In bend tests, however there are no gripping stresses. The simply supported test piece simply experiences compressive stresses on one face and tensile stresses on the opposite face. Because the tensile strength is smaller than the compressive strength in ceramic materials the fracture is likely to start on the tensile surface, which explained the relation between the compressive and the tensile strength in the material. The value of tensile strength is approximately half of the modulus of rupture.

1.5.2 Non destructive testing

In this section various non-destructive evaluation techniques for ceramics are presented. These techniques for ceramics and ceramic-metal systems include ultrasonic, radiography, x-ray computed tomography, and acoustic emission.

Advanced ceramics have been identified as potential candidates for high-temperature structural applications because of their high-temperature resistance, lightweight, and excellent corrosion and wear resistance as described by Lehman et al[50]. In order to expand the application of these materials, the use of appropriate non-destructive evaluation (NDE) approaches is critical to effective process control and reliable performance in service. NDE techniques have been addressed by many authors [51-55].

Usually non-destructive testing is performed so it does not affect future usefulness and serviceability in order to detect, locate, measure, and evaluate flaws, to assess integrity, properties, and composition, and to measure geometrical characteristics. The defect information obtained from these techniques is then evaluated to determine if the component meets specified acceptance criteria.

1.5.2.1 Ultrasonic testing

Ultrasonic testing was described by Netzelmann et al[56] as one of the most widely used NDE techniques for quality control and service-integrity evaluation because of its relatively inexpensive cost and the convenience of data acquisition. Generally, ultrasonic testing can be used to detect flaws, determine the size, shape, and location of defects, and identify discontinuities in materials. Also, the determination of ultrasonic velocities can be used to measure the modulus of elasticity or Young's modulus of materials. The ultrasonic testing technique has been reviewed by many authors [51-55].

In ultrasonic testing, beams of high-frequency sound waves are introduced into materials so as to detect both surface and internal flaws as described in the ASM Handbook[57]. The sound waves travel through the material (with some attendant loss of energy) and are deflected at interfaces and/or defects. The deflected beam can be displayed and analysed to assess the presence of flaws or discontinuities. Most ultrasonic inspections are performed at frequencies between 0.1 MHz and 25 MHz.

1.5.2.2 Radiography

There are two primary applications of radiography: determining inherent material properties and evaluating manufacturing features. In radiography, radiation is passed through the subject part or material and a detector senses variations in the intensity of the radiation exiting the sample, thereby enabling a profile of the internal defect distribution to be seen as explained in the ASNT Handbook[58]. The resulting two-dimensional radiation pattern can be visualized using photographic films or fluorescent screens. Using this technique, a wide range of material thickness levels can be assessed, as can complex shapes that would be difficult to scan using an ultrasonic technique.

In general, radiographic NDE can be classified according to the type of radiation employed: x-ray, gamma, or neutron.

NDE using x-ray or gamma rays includes capturing and processing a shadow photograph. Specifically, the varying amounts of transmitted radiation cause ionization in the emulsion surface of the film, forming a latent image. The radiographic sensitivity of the resulting photograph is limited by the quality of the shadow image, by the scatter of radiation in the test object, by the test environment, and by the nature of the film emulsion.

In neutron radiography, the image is essentially a two-dimensional shadow display representing the intensity distribution of thermal neutrons passing through an object. As compared to x-ray or gamma-ray radiography, the attenuation characteristics of neutron energy are different. Here, the total neutron cross section is the criterion for utilizing neutron radiography, whereas density and atomic number (linear absorption coefficient) are the main parameters in x-ray and gamma-ray radiography. Generally, neutron radiography complements conventional x-ray and gamma-ray radiography as it can detect flaws and material conditions that other methods cannot effectively assess.

Although radiography has numerous advantages, it is not without certain drawbacks. For example, access to opposite sides of the test object is required, and some structures are not amenable to study (e.g., components in radioactive or high-temperature environments). To maximize the likelihood of detection, cracks must be oriented nearly parallel to the beam. Delaminations are almost always undetectable. Finally, the use of radiography is a health risk, and the technique is expensive.

In their review, Kim and Liaw[59], quoted the neutron radiography work conducted by Nir-El et al to detect various types of discontinuities (e.g., voids and bulk-density reduction) and to determine the structure and composition of lithium-based ceramics and glasses.

Kim and Liaw[59] also cited Lewis et al who conducted extensive work with Si_3N_4 composites and $Al/Si/Al_2O_3$ composites to contrast the capabilities of neutron and x-ray radiography. They found that neutron radiography was capable of producing good-quality images on a wider range of ceramic composites than x-ray radiography and that it was better suited for examining thicker sections in these materials.

Highly sensitive microfocus x-ray radiography was used to detect and measure micrometer-sized defects in ZrO_2 pellets introduced by Ekinci et al[60]. Artificial flat-bottom holes and saw cuts of different depths were made to the pellets to use as calibration standards.

1.5.2.3 X- ray computed tomography

X- ray computed tomography (CT) was also reviewed by Kim and Liaw[59]. X-ray computed tomography provides a cross-sectional view of an object's interior and is well suited to characterizing a material's integrity. In essence, CT is an advanced form of x-ray radiography. Conventional radiography provides a two-dimensional presentation of a three-dimensional object as the image plane is approximately normal to the X-ray beam. CT creates a digital representation of a thin slice parallel to the X-ray beam. Typical slice thickness ranges from 0.025 mm to 3 mm, with pixel sizes (picture elements) ranging from 0.025 mm to 1 mm.

Recently, CT has been extensively used to characterize ceramic components, including ceramic failure analysis, composite-structure developments, and microstructural characterization in ceramic composites.

1.5.2.4 Acoustic emission

Acoustic emission can be a very powerful NDE technique for the in-situ monitoring of damage evolution during mechanical testing. When a material is subjected to stress, it may experience micro-damage before fracture; these conditions produce small stresses or ultrasonic waves in the material and acoustic emissions are generated. For ceramic materials, an increase in acoustic emissions occurs before fracture, providing a potential means of either detecting crack initiation or predicting when failure is imminent. Acoustic emissions can be detected by AE piezoelectric sensors (transducers), which convert wave pulses into electrical impulses that can be amplified and displayed. More on acoustic emission is presented in papers[53-55].

Generally, AE equipment includes piezoelectric transducers, amplifiers, single- and multi-channel signal processing systems, acoustic-event counters, and coordinate plotters.

In terms of ceramic-based materials, the rate and intensity of acoustic emissions may be used to detect the initiation and propagation of cracks and delaminations, and acoustic emission NDE can be used to predict static and fatigue failure.

Pollinger[61] et al showed the importance of non-destructive evaluation (NDE) to improve the quality of inspection in aircraft auxiliary power unit and propulsion engine turbine hot sections, industrial power generation turbines and automotive hybrid vehicle turbo generators. They also showed the future needs for NDE techniques as structural engineering ceramics components are increasingly used in industry.

1.6 Difficulties when joining ceramics to metals

Most of the disadvantages in ceramic-metal systems arise from differences in coefficient of thermal expansion (C.T.E) [62-64]. Metals generally expand and contract more than ceramics, inducing stress in the joint, leading to poor joint strength and frequent cracking in the ceramic member.

Ceramic	C.T.E./K^{-1} X10^{-6}	Metal	C.T.E./K^{-1} X10^{-6}	Compound	C.T.E./K^{-1} X10^{-6}
Si_3N_4	4.6	Ni	16.3	Ti_3SiC_2	9.2
SiC	3.2	Al	26.5	Ti_5Si_3	9.5
Al_2O_3	8.0	Ti	8.5		
ZrO_2 (cubic)	11.8	W	6.6		
Syalon*101	3.04	Mo	5.8		
Syalon*201	3.4	Incusil[I]	19.7		
Syalon*501	5.6	Nimonic75	17.1		
AlN	5.3	Stainless Steel(410)	14.0		
		Kovar [L]<550°C	5.3		

Table 1.2-Comparison of CTE for different materials.

[L]kovar is trade name of Westinghouse Electric Company.

*Syalon101, 201 and 501 are registered products of International Syalons Ltd.

[I]Incusil ABA is a commercial braze alloy (WESCO, Belmont, CA)

1.6.1 Residual stresses

The mismatch of C.T.E between the two materials often leads to failure in ceramic-metal systems during cooling following joining where differential thermal strain induces residual internal stresses. Repeated thermal cycling in service further compounds the problem. In most cases these residual stresses are sufficient to initiate cracks in the ceramics at the interface (Gao et al [65]) between the ceramic and the metal, causing the ceramic to break. In a few commercial cases ceramics and metals are satisfactorily joined. A good example of this can be found in a nickel-based alloy, which has been successfully joined to an alumina substrate in the electronic components of a commercial satellite[66].

Highly demanding service conditions, for ceramic-metal joints to operate in extreme environments involve rapid heating to elevated temperature followed by fast cooling rate [62] putting the systems into a dynamic thermal mismatch situation where the metal gains or loses temperature faster than the ceramic. Designing such joint systems requires much care in selecting suitable materials with appropriate properties to meet the needs of advanced applications in respect to efficiency, reliability and safety.

1.6.2 Reaction layer formation

The strength and integrity of a joint in a ceramic-metal system is not only affected by the amount of residual stresses induced after cooling, as mentioned earlier, but also by the formation of a reaction layer [64, 67, 68], between the two materials.

In the case of diffusion bonding, the metal under elevated temperature and pressure deforms to make intimate contact with the ceramic. Two situations may arise, either the metal recrystallizes to form a uniform interface or reacts with the ceramic in which case atoms from both ceramic and metal move from the parent material to diffuse into the other material (host). There are also cases where chemical reaction takes place creating a laminated structure and thus new interfaces. The diffusion process usually removes voids at the interface and simultaneously existing voids in the inner region of the metal; this phenomenon is known as the Kirkendall effect. In some situations, gases created during the process cause pores and voids to remain at the interface affecting joint integrity. In the case of active metal brazing of ceramic-metal systems, the braze melts to react chemically with both materials. It is common for metals, which wet ceramics to react with them, making the brazing process successful.

The ceramic-metal interface's structure can take one of the following types:

- **Non-reactive:** These interfaces are microscopically planar and coherent (epitaxial) or incoherent.
- **Penetrative:** These are created by penetration of the melted metal into the ceramic lattice during joining at elevated temperatures and pressures, and more often when mixtures of metal and ceramic powders are used as the interlayer.
- **Reactive:** This is the most common interface observed between metal/ceramic systems.
- **Diffusive:** Interfacial reaction layers are usually of brittle nature, which in the majority of cases develop obeying parabolic laws. Strength usually increases up to a certain thickness of the reaction layer, and decreases noticeably beyond that optimum thickness.

The width of the reaction zone (x) obtained in diffusion bonding[23-25] can be estimated from the following expression.

$$X = K_o t^n \exp(-Q / RT) \qquad \textbf{Equation 1.1}$$

Where

K_o = constant for diffusion

n = Time exponent(~ 0.5)

Q = Activation energy

R = Gas constant

t = Time

T = Absolute temperature

The activation energy (Q) is directly dependent on the diffusion parameters, namely grain boundary and surface diffusion. The rate of diffusion follows normally an increase from lattice to boundary to surface. According to equation 1.1 the reaction layer width increases with temperature. The thickness of the reaction layer can be roughly estimated from the following equation.

$$X = k\,(Dt)^{1/2} \qquad \textbf{Equation1.2}$$

Where

k = Constant reaction layer

X = The thickness of the reaction layer

D = Diffusion coefficient in the interlayer

t = Time

In order to produce sound ceramic-metal joints acceptable for commercial use, the formation of reaction products and the evaluation of optimum thickness need to be fully understood[26, 69].

The problem of excessive stress build up in metal ceramic joints resulting from differential thermal strain can be significantly reduced by the use of simple or complex metallic interlayers and controlled cooling rate. These methods of reducing induced stresses will be presented in section 3.3.

1.7 Theoretical study of ceramic to metal systems

1.7.1 Finite element analysis

Following changes in temperatures during manufacture or service, ceramic-metal systems are subjected to internal thermal stresses known as residual stresses[70, 71] Although these thermally induced stresses can be calculated analytically, the use of a more recent technique based on finite element analysis (FEA)[72] gives more flexibility in terms of speed, accuracy and freedom in design.

Finite Element Analysis (FEA)[73] software has improved noticeably since the early days, owing to new powerful features, such as fast processors and more memory RAM and ROM becoming available, allowing more sophisticated tasks to be carried out accurately. With the emergence of windows-based applications, producing complicated designs and exporting them between different softwares is now possible, giving designers more flexibility and a wider freedom of choice in their modelling tasks, reducing considerably the amount of experimentation needed. Computer simulation is a valuable tool to simulate experiments and predict results before conducting experimental work, hence reducing experimental expenses and giving a better judgement on the expected output of an experiment.

1.7.2 Elastic versus Plastic Finite Element Modelling

Most of the work published on finite element analysis[74-76] in the area of ceramic-metal joining has been carried out using linear elastic calculation, although non-linear analysis was used in the analysis of a joint in a high vacuum device. The disadvantage of purely elastic analysis is that it often tends to predict unrealistically high residual stress in joints, far greater than the level of stress needed either to break the ceramic or yield the metal. In reality, plastic deformation in the metal part can play a role in reducing the thermally induced stresses.

1.7.3 Two-D versus Three-D finite element modelling

The axisymmetry of cylindrical joints, similar to specimen used in the authors' experiments (dome and Dome-flat samples) can be an advantage to simplify analytical problems thereby allowing a 2-D model to be used to represent a 3-D sample.

The 2-D modeling in FEA is more convenient then a 3-D application which is more time consuming and costly.

The 2-D modelling of our joints was undertaken using eight noded quadratic elements. This analysis was somewhat simplified by its symmetry, so that only half of the sample needed to be modelled. Following analysis, stress contour plots can be obtained for the plane considered, which is parallel to the sides of the sample. Graphs of stress variations along selected node paths are also available.

1.8 Conclusions

Ceramic-metal joined structures are being developed for use in a variety of applications to obtain properties not available in monolithic materials, but joints operating over a wide temperature range may experience large destructive interfacial stresses from thermal expansion mismatch leading to actual or increased risk of mechanical failure. Applications at high operating temperature induce large destructive thermal residual stresses leading to actual increased risk of mechanical failure.

Many joining techniques exist but only a few are appropriate for ceramics to metal joining. Microwave technology is suitable for ceramics only, not for metals.

Preferred methods for joining dissimilar materials include diffusion bonding, brazing, mechanical joints.

Stresses are a fundamental problem in joining of ceramics to metals due to thermal expansion mismatch and may result in tensile stress concentration in the ceramic
Consequence may include

- debonding of the joint
- fracture in the ceramic
- limited maximum load

There is a need to characterize and understand residual stress distribution in ceramic-metal systems in developing low stress joining methods.

Before selecting a joining process for a ceramic - metal system additional issues have to be addressed: chemical reaction, microstructure change and mechanical and physical properties.

Non destructive testing, techniques should be used for inspection and evaluation of a ceramic- to- metal joints integrity without affecting future usefulness and serviceability of the joint.

The finite element method is an outstanding tool to estimate and optimise the effects of these modifications. By variation of the parameters of the FEM model one can easily investigate several joint geometries within a short time.

Chapter 2

Brazing Ceramics to Metals

2.1 Introduction

This chapter will be devoted to brazing ceramics to metals with particular reference to joining silicon nitride (and its derivatives) to stainless steels and similar high melting point metals. Fundamentals and techniques of brazing ceramics to metals will be addressed, and advantages and limitation of the technology discussed. An additional purpose of this chapter will be to review recent work in this area of joining.

Brazing is very well suited to the production of ceramic to metal joints and seals. Despite the existence of a wide range of approaches to joining ceramics to metals, including some which are still under development, brazing remains the dominant method used in industry.

The brazing process is suitable for mass production and where large and complex assemblies must be joined in a single operation or where in most cases, many small parts must be joined economically and reliably.

Joining ceramic to metal by brazing presents many advantages. Joints can be brazed for a wide range of service conditions by selection of the appropriate filler metal for the specific ceramic and metal to be joined. In applications where the two parts to be joined exhibit little or no difference of thermal expansion coefficient, large complex assemblies can be brazed in a near stress-free or stress-free condition. A common case is where two joint members of different thicknesses can be brazed to each other, and this is particularly useful when joining large surface areas or when additional members must be joined to a partially completed structure.

The technology of joining ceramics to metals began in the early 1930s and since then extensive research efforts have been directed to developing procedures for producing reliable ceramic to metal joints. The aim was to establish a joining technology based on sound fundamental principles, proven procedures and a good understanding of the various reactions that can take place during joining. In 1940 a first attempt was made to join ceramics to metal using the active metal brazing method. Fine titanium powder (300 mesh) suspended in a suitable binder was painted on the area to be joined, dried, and then the ceramic and metal parts were joined with a silver-based filler metal placed directly in contact with the titanium particles. The system was heated from room temperature to 900°C then to 1000°C in vacuum. When the silver braze filler metal melted, it associated with titanium to form a silver-titanium alloy that bonded strongly to the metal and the ceramic.

2.2 Liquid phase joining

Liquid phase joining might be considered to include many techniques including soldering, glass sealing, brazing and the use of adhesives.

Brazing is recognized as a liquid phase process particularly well suited to preparing joints and seals, and has been used for many years as a reliable technique in joining ceramics-to-ceramics and ceramics-to-metals.

2.2.1 Mechanisms and parameters for adhesion and joining

Most of the work produced on joining ceramics to metal is empirical in nature describing observations by many investigators who have joined a specific ceramic to a specific metal under a specific set of experimental conditions. They generally report on microstructure and the resultant mechanical properties of these specific joint systems.

The large number of variables involved in and the complexity of ceramic structure provide significant difficulties in the development of a satisfactory predictive theory of ceramic to metal bonding. Excellent general reviews of ceramic to metal joining have been produced by Schwartz[2, 52] and Suganuma[77], while extensive backgrounds and examples are presented in texts by Nicholas[1] and by Reimanis et al[78] and by Schwartz[2]. Morrell[3] provides extensive lists of available braze compositions.

The principle variables involved in the production of strong brazed metal–to-ceramic joints are temperature, bonding time, pressure, brazing atmosphere and surface character.

- Temperature: Must be high enough to raise the temperature of the braze material at least to its liquidus temperature but typically 10° to 20° C above it to allow molten braze to spread and flow utilizing capillarity. However it should not be so high as to allow its chemical composition to alter through selective elemental evaporative loss (especially in vacuum brazing) or, by excessive diffusion and intermediate compound formation at and just below the surface which can potentially weaken the joint. Where such interfacial reactions accompany formation of third phases, the growth of the reaction layer is usually restricted by diffusion of a certain element in the reaction layer. The thickness X of a reaction layer may be expressed by the following equation[28, 64].

  $$X^2 = A\, t \exp(-Q/RT)$$

  A: a constant

  Q: activation energy of reaction

  R: gas constant

  t: reaction layer thickness

  T: reaction temperature

  This expression shows that a reaction layer grows at a linear function of the square root of reaction time and is exponentially related to temperature.

- Time: The relationship between diffusion layer thickness and time has been stated above with joint weakening resulting from excessive opportunity or intermetallic compound formation and coarsening. Inadequate time can limit the degree of melt spread and joint filling. Figure 2.1, adapted from Suganuma[20] illustrates the effect that brazing time can have on joint strength.

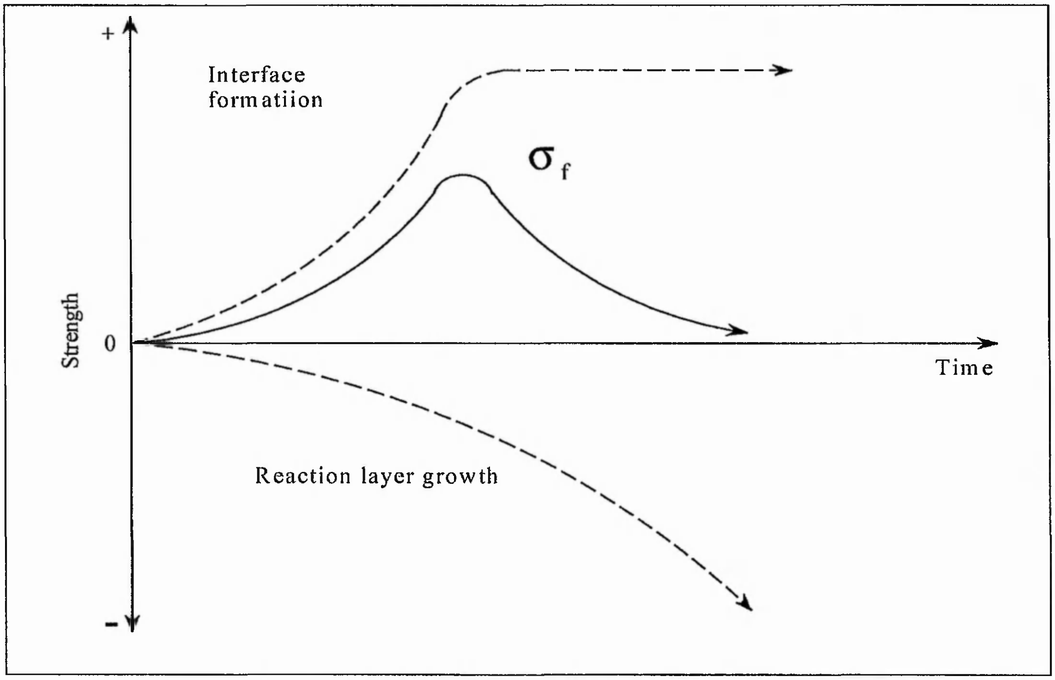

Figure 2.1: Typical curve of joint strength as a function of bonding time. Fracture strength of reacted interface is the sum of two factors, i.e., the interface formation, which increases strength with increasing bonding time and will saturate at some time and the reaction layer growth which decreases strength (adapted from Suganuma[15])

- Pressure: Pressure is less important in liquid phase joining than in solid state joining where early plastic deformation of contacting asperities is followed by creep deformation and diffusion to maximise interfacial contact. Pressure however affects the thickness and uniformity of a braze layer. Only relatively low pressures are necessary in brazing.

- Brazing atmosphere: Whilst protective atmosphere may not be required when joining oxide ceramics to noble metals, the use of vacuum is imperative in active metal brazing to prevent the selective loss of that braze's reactive metal ingredient.

- Surface character. Whilst high levels of flatness are necessary in solid state bonding in order to minimise the time needed to maximise interfacial contact through temperature and pressure, surface roughness (within reason) is no bar to the effective production of strong brazed metal to ceramic joints when the thickness and uniformity of the braze layer is around the optimum.

Chemical alteration of surfaces occurs in the active metal brazing process for ceramics where titanium or another reactive metal constituent within the braze is induced to diffuse into the ceramic surface with the result of facilitating the wetting and spreading of the braze. Ion implantation as well as other surface pre-treatments will also alter the wetting characteristics of surfaces and, sometimes the residual stress pattern within finished joints. Fundamental studies of interfaces between ceramics and metals have been the subject of much investigation over many years. International conferences on ceramic - ceramic and ceramic - metal joining[13, 79] generally include such fundamental contributions. Typically Rűhle and Mader[6] illustrated the structure of alumina to niobium diffusion bonds using high-resolution electron microscopy.

The work conducted by the present author however follows that more 'applied' and empirical approach.

There follows below a brief description of the theory of liquid phase bonding of ceramics to metals.

2.2.2 Wetting and spreading of braze during ceramic to metal bonding

Bonding between ceramic and metal results from mechanical and chemical interaction between the two materials. Chemical reactions may lead to the formation of new compounds at the interface or the creation of weak adhesion links resulting from the formation of secondary bonding forces

A theoretical assumption for the perfect lattice predicts a typical material strength of up to 100GPa. This exceeds by far the observed strength of most materials resulting largely from the presence of lattice imperfections. Examples of high strength have been observed in "nearly perfect" lattices[2]. Secondary bonding forces in general are considered to be rather weak. However, some investigators predict that bond strengths up to 10 GPa can be developed from secondary bond[2]. These secondary bonding forces, often described as Van der Waals forces, result from the asymmetry of charges in atoms and molecules.

Mechanical forces present at ceramic to metal interfaces originate from the interlocking of surface roughness and asperities. Poor interactions are usually due to lack of complete contact between ceramic and metal. Complete contact may be inhibited by inhomogeneities at the surfaces of either material, including surface roughness and the presence of contaminants that contribute to lower bonding strengths.

Chemical bonding and minimal stress differentials at the interface constitute basic requirements for strong joints. All researchers recognize that, for successful joining of ceramics to metals it is desirable to minimise the thermal expansion mismatch between the ceramic and the metal. What is less clear is the exact effect on interfacial residual stress patterns of compositional and microstructural gradients formed during the joining process.

It is well established that two phases can form an acceptable chemical bond if they reach a stable chemical thermodynamic equilibrium at their interface whether or not the bulk phases are at equilibrium, providing they are also compatible physically[80].

A properly mated solid/liquid interface can be formed and recognized easily if the liquid wets and spreads, penetrating fully any irregularities at the solid surface. The second, more important requirement is the presence of a stable chemical equilibrium at the interface. In general this requirement is achieved by reactions, since invariably they form equilibrium phases.

2.2.3 Wetting and adherence

Figure 2.2 shows a molten braze filler metal drop on a ceramic surface. The shape of the drop under gravity is determined by the interacting forces of solid-liquid energy (γ_{SL}) at the interface, liquid surface tension (γ_{LV}) and solid-vapour interfacial energy (γ_{SY}). The balance of interfacial tensions at equilibrium is represented by Young's equation:

$$\gamma_{SL} = \gamma_{SV} - \gamma_{LV} \cos\theta \qquad (1)$$

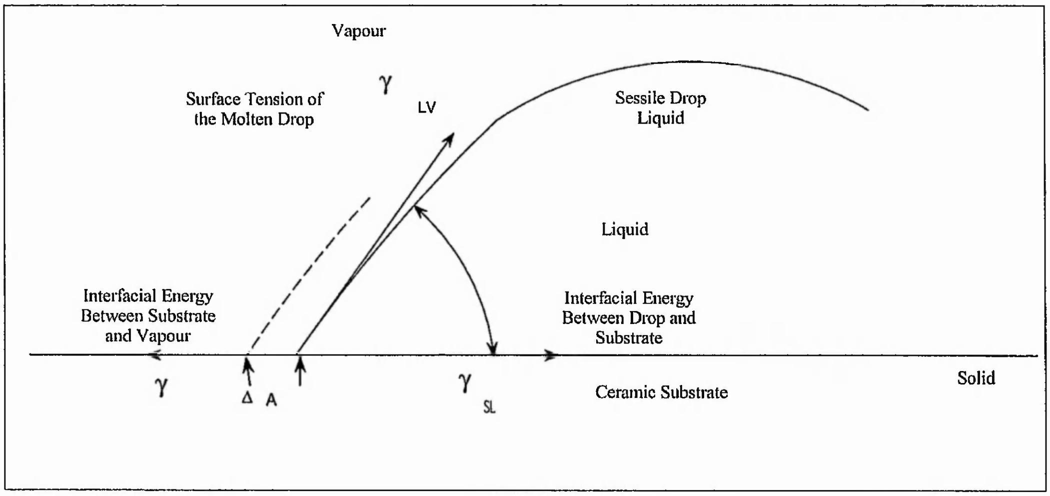

Figure 2.2: Surface energy forces acting on a sessile drop [2]

The angle between the solid surface of the ceramic and the tangent line to the liquid surface at the contact angle θ may vary from 0 to 180°. If γ_{SL} is high, the liquid tends to form a ball having a small interface area. If γ_{SV} is very high, the drop tends to spread. The effect of liquid-vapour surface tension is not easy to understand. If the liquid surface energy is decreased, the contact angle decreases thus wetting is increased ($\theta < 90°$), but it increases for initially non-wetting drops ($\theta > 90°$), as illustrated in Figure 2.2 and Figure 2.5

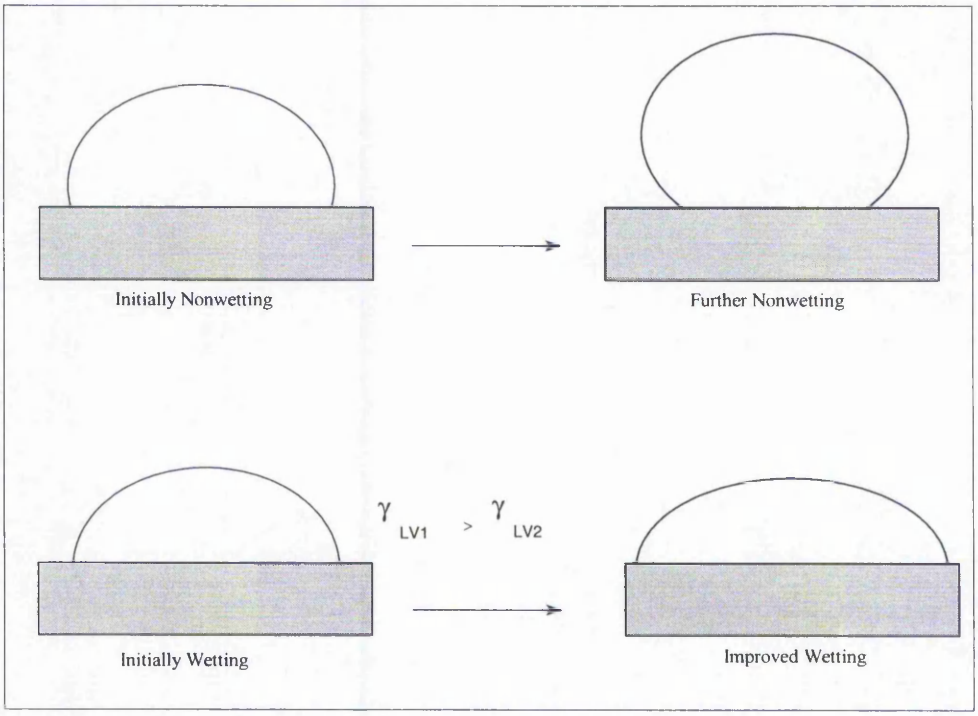

Figure 2.3: Effect on contact angle of decreasing liquid surface tension (γ_{LV}) in the case of an initially non wetting drop (above) and initially wetting drop (below)

In the equation above it can be seen that θ is greater than 90° when γ_{SL} is larger than γ_{SV}, as shown at left in Figure 2.3, and the liquid drop tends to spread.

The figure also shows that if the contact angle is less than 90° the reverse is true, the drop of molten braze flatten and wets the ceramic. The smaller θ is, the more Cos θ approaches unity and liquid spreads over the solid surface.

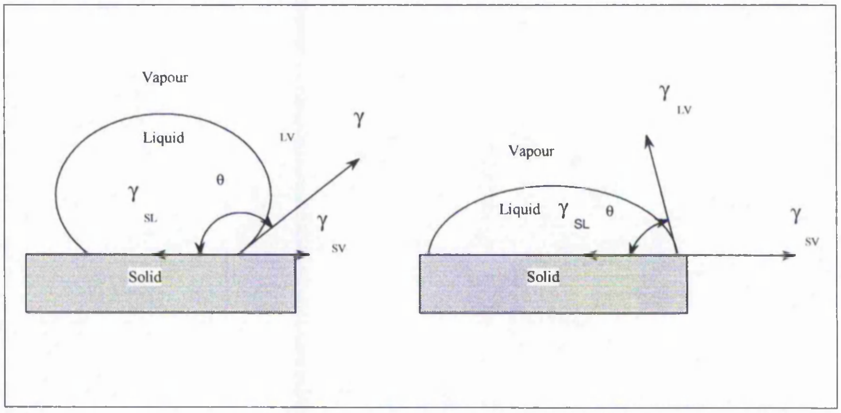

Figure 2.4: Sessile drops and interfacial energies

These considerations show the importance of surface energies in brazing. If the brazing filler metal is to form a joint, it must wet the solid materials. The surface-energy balance must be such that the contact angle is less than 90°. The energy equation shows that if θ is to be less than 90° ($\cos\theta>0$), γ_{Sv} must be greater than γ_{SL}. From a practical brazing standpoint, a contact angle of about 70° has been found to be satisfactory [Figure 2.4] [2].

The associated adhesive energy or work of adhesion (WA) between the sessile drop and substrate that represents the free energy change for separation of a unit area of interface into a liquid and a solid surface is expressed by the Dupre equation $WA = \gamma_{Sv} + \gamma_{Lv} - \gamma_{SL}$ or it can be combined with the Young equation as $WA = \gamma_{Lv}(1 + \cos\theta)$.

Some indication of the adherence of the drop to the substrate is given by the work of adhesion, but it does not necessarily predict the adherence of the solidified drop.

Schwartz[2] reviews the techniques for metallising a ceramic surface in order to promote molten metal-solid oxide wetting and bonding. The most widely used processes [1-3, 6] employ molybdenum and manganese as a metalizing film, traditionally applied over alumina and aluminosilicate substrates. He also reviews the electroless plating and vapour deposition processes for metallizing ceramics

The second most common process is titanium hydride activation. Titanium hydride powder is applied before vacuum brazing and dissociates between 350 - 550°C to form a wettable titanium coating.

2.3 Ceramic/Metal brazing

2.3.1 Processing

In its simple form a braze filler metal is melted between two components; the liquid wets the surfaces and on solidification a joint is formed. Wetting in this context implies a contact angle of less than 90° between the molten braze and the substrate as presented in Figure 2.5. However, the joining of ceramics by brazing is not simple, as many ceramic materials are difficult to wet with liquid metals, indeed some ceramics may be used as crucibles to contain molten metals. Most engineering ceramics, including zirconia, silicon carbide, alumina, silicon nitride, beryllia, and the sialons are not wetted by silver, gold or copper, the basic constituents of many brazing alloys.

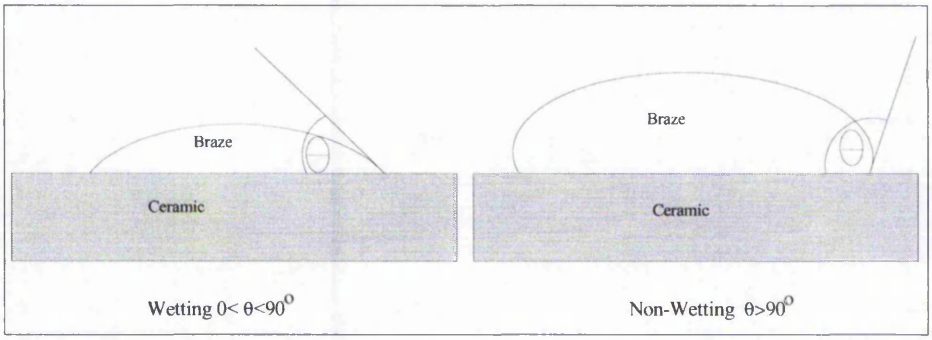

Figure 2.5: Conditions for wetting

A necessary step therefore in many brazing operations is to promote wetting of ceramic surfaces by the filler material. This may be achieved by first metallising the ceramic surface prior to using conventional braze compositions as with the molybdenum-manganese process, or through the use of specialised 'active metal' braze alloys[2].

For a joint to form between ceramics and metals it is important that a chemical reaction takes place between the two partners to promote wetting of the ceramic surface by the metal.

The non-wettability of ceramics by metals is due to their high free energy compared to metals and this limits the number of chemical reactions that might take place. Ceramics show high binding energies due to their ionic and covalent bond types, which lead to the need for higher free energies in the transition zones exceeding those of the parent partners.

Due to the broad range of free energies a strong difference in the wettability of the ceramics can be obtained. It can be easily seen that only a very reactive partner is able to start a chemical reaction with a ceramic like Al_2O_3, while the decomposition of an oxide like NiO takes place at low temperature without requiring high free energies.

Mixed oxides compounds and intermetallic phases possess high free energy, which enable them to react with ceramics.

Six basic scenarios of chemical reactions between ceramics and metals can be distinguished

Scenario 1: Often observed in active brazed joints with a reactive metallic partner such as Ti, Zr or Hf. One or more interlayers are formed depending on the joining parameters and the ambient atmospheric condition.

Scenario 2: This take place in active brazed joints formed between SiC or Si_3N_4 ceramics and transition metallic partners such as Fe, Ni or Co. The chemical reaction consists of the formation of many intermetallic phases i.e. silicides with high free energies and the emission of a gas.

Scenario 3: This scenario is similar to the previous one, with an additional reaction of the gaseous part of the ceramic with the partner metal. The gaseous mixtures react to form an additional oxide, carbide or nitride, which forms, in many cases an interlayer between the parent ceramic and the newly formed intermetallic compounds.

Scenario 4: Concerns dissolution of the ceramic at high temperatures and the solution of both ceramic elements in the partner metal.

Scenario 5: This scenario[2] is based on the application of either a metal, which oxidises during the joining process, or a direct application of a low melting oxide as a filler between ceramics and metals. The oxidation of metal in a wet environment during the metallising process is one of the two basic reactions of this joining technology. The direct application of low melting glass filler materials is used for joining by brazing with this filler material. In both cases the low melting oxides form mixed oxides like spinels, which show higher free energies than the parent ceramic did.

Scenario 6: This scenario illustrates the case[78] where an oxide with a low free energy is painted on the ceramic surface and heat treated in wet N_2/H_2 atmospheres. Under these environmental conditions the metal oxide is reduced to metal, while the partner ceramic remains in its original state.

2.3.2 Pre-metallisation followed by conventional brazing

To overcome the problem of the non-wettability of ceramics by most liquid metals during the process of ceramic to metal joining, a technique has been adopted of pre-metallisation prior to joining. Direct contact between most liquid metals or brazes and advanced ceramics, such as carbide or nitride ceramics, zirconia or sialons, cannot be established due to the difference in atomic structure of the two materials. Coating the ceramic material before the brazing process solves the problem for most dissimilar systems.

This method goes back to the early 1930's when Siemens developed the tungsten- or molybdenum-manganese metallisation process for joining alumina.

The process of pre-metallisation is usually achieved in three steps. Initially the ceramic is coated with a mixture of glass, manganese and molybdenum powders including their oxides, (15-25µm thick). The ceramic is then heated to 1800°C to promote the reaction between metal, oxide and ceramic. The final step consists of plating the modified ceramic surface with nickel or copper in vacuum. The ceramic is then ready for conventional brazing.

2.4 Direct brazing using special brazes.

2.4.1 Active metal brazing

In active metal brazing a metal component is added to the braze alloy to react with the ceramic and render it wettable by changing its chemical surface composition and forming surface and near-surface grains of one or more products, usually containing titanium. This has been observed[34] to occur experimentally using a liquid metal which contains an element that forms a more stable oxide (or nitride) than the oxide (or nitride) ceramic on which the liquid metal is held. The introduction of titanium to various braze alloy compositions results in increased reactivity and considerable improvement in wetting behaviour [81], and forms the basis of a range of commercially available brazes which wet silicon carbide, alumina, and other ceramics such as sialons and silicon nitride.

The number of commercially available metal brazes has slowly expanded. The longest established active metal braze is the 72% silver-28% copper eutectic to which 1.25-5% titanium is added to produce cored wires or sheets. Morrell[3], the Wesgo* company and Schwartz[2] report that other active metal brazes are also available, such as 27Cu-9.5 In-1.25Ti, balance Ag.

***Wesgo, Inc. Technical Ceramics and Brazing Alloys, 477 Harbor By, Belmont, CA 94002**

In Japan active metal brazes are used in the production of ceramic turbocharger rotors. It is important however to note that the temperature of use (~295°C), is well below the melting temperature of the braze (~900°C).

2.5 Problems with brazing ceramics to metals

2.5.1 Reaction layer formation

The strength and integrity of a joint in a ceramic-metal system is not only affected by the amount of residual stresses induced after cooling, as mentioned earlier, but also by the formation of a reaction layer [64, 67, 68], between the two materials. Reactive metal components in the braze cause dissociation on the ceramic surface through chemical reactions. At a certain stage of the brazing process these chemical reactions promote the formation of a few micrometers thick layers which consist of intermetallic compounds with similar structures to that of the parent metal. These can therefore be wetted by the braze matrix. When joints are exposed to high temperatures for long periods of times during the brazing process the reaction layers formed will increase in thickness, and this will lead to a degradation of the bond strengths of the newly formed particles present in local stress concentrations in the microstructure resulting from differences in temperature between them and the modified surrounding or metal microstructure. Failure by interfacial stresses is unavoidable [82].

2.6 Review of recent work in the area of brazing ceramics to metals

Tinsley [7] and Reimanis [78] provided reviews of work in the area of brazing ceramics to metals in 1996 and 1997 respectively.

More recent work by Lugscheider and Buschke[83] demonstrated the use of a new filler material based on Ni-Hf, containing Cr, Co, Mo and Ta to improve brazing of ceramics to metals. Their task consisted of joining steels and advanced ceramics. They found that the use of Ni-Hf based alloys (with B and Si to reduce melting points) had some advantages over the use of conventional Ni-based alloy. By reducing the melting point, the formation of brittle phase was avoided and diffusion treatment was no longer necessary. They stated that the melting temperature of components like Co or Ta became less than 1200°C and that the wetting behaviour of the new filler metal on different ceramics was good.

Dorn et al[42] investigated the strength improvement of Si_3N_4 to X5NiCo (Kovar) joint by brazing, using copper foil at high vacuum. AgCuInTi was used to metallize the ceramic partner prior to joining. Attention was particularly made to the effects of foil thickness (0.1, 0.3, 0.5 and 1.0mm), brazing time (5, 10 and 15 minutes) and brazing temperature (1090°C, 1100°C and 1110°C) on the joint strength. The 4-point bending test was used at different testing temperatures (room temperature, 400°C, 600°C) to evaluate the mechanical properties of the joints. It was found that pre-metallized brazements had better bending strength in comparison to that of direct brazements.

Klose et al[84] studied the interface behaviour during active brazing of the SiC ceramics to X5NiCo29 18 steel using AgCu27Ti3 as active filler alloy. The aim of their study was to describe the interface behaviour during active brazing of these materials. The authors have shown that titanium contained in the filler alloy caused chemical reactions within the steel at the steel-filler alloy interface. Subsequently, reaction phases grew and a layered reaction zone was formed analogous to the process at the interface on the ceramic side. However, the penetration of the molten filler alloy through the reaction layer caused a peeling off process. The reaction layers were floated into the molten filler metal and transformed to a needle like structure during the cooling period. The remaining steel was affected by the filler alloy up to a depth of 10 μm.

Batfalsky [85] investigated the lowering of the fracture strength, caused by induced thermal stresses in ceramic-metal systems, resulting from coefficient of thermal expansion mismatch. He stated that the critical tensile stresses could be reduced by stress relaxation following ion implementation. Batfalsky showed that a SiC-AgTi-SiC joint brazed at 1000°C, implanted with (1, 2.4, and 4.8) MeV C+- ions, presented a value of about 21% higher four-point bending strength and about two points higher indentation fracture toughness. The quality of active metal brazed ceramic joints is dependent on the structure and thickness of the reaction layer resulting from chemical interactions between the reactive agent in the braze and the ceramic.

In their paper, "Interfacial reactions between active filler metals and high performance ceramics" Lugscheider et al[86] studied the chemical interactions during the brazing process first using theoretical thermodynamic calculations and secondly by analyzing experimentally the interface region of several active brazed ceramic joints using light microscopy, SEM and x-ray diffraction. Their theoretical investigations revealed that in the case of non-oxide ceramics, such as SiC and Si_3N_4, the formation of active metal-carbides and nitrides respectively have the most favorable thermodynamic conditions. X-ray diffraction analysis of active metal brazed non-oxide ceramics showed that the reaction layers did not consist of carbides and nitrides only but of silicides as well.

Active metal-oxide interactions are of a much more complex chemistry than active metal-carbide or nitride interactions, because active metals, especially titanium, can form a family of oxides, the stoichoimetry and stability of which depend on temperature and activity level.

Torvund et al[87] investigated the brazing of alumina to AISI 304 austenitic steel using Ag-Ti and Sn-Ag-Ti active brazing alloys in vacuum (3.10^{-5} mbar). They showed that the maximum bending strength of the systems was of 108 MPa using Ag-Ti and 124 MPa using Sn-Ag-Ti active braze. They also reported that rapid cooling from the brazing temperature significantly reduced the joint strength. The two systems were compared and it was found that although the fracture strength was more or less similar for the two brazing metals, their fracture behaviour was different. In the case of Sn-Ag-Ti the fracture took place along the alumina/filler metal interface (probably lower residual stresses), while for the Ag-Ti alloy, fracture occurred in the ceramic body, indicating that the bond strength is controlled by residual tensile stresses induced by thermal expansion mismatch.

Ilto and Kato[88] looked into the annealing problem of steel during brazing to ceramics and discussed the relevance of solving such problem. Industrial applications were given as examples.

Weise et al[89] presented a comprehensive review of industrial applications of active metal brazing of ceramics to metals as a reliable technique for joining. Their illustration covered the electric industry, tool industry, and vacuum technology.

Hegner et al[90] presented a process of using active brazing foil (Zr63 Ni22 Ti15) produced by rapid quenching from melt to joint Al_2O_3 used for a pressure sensor running in a large scale production environment.

Naka et al[91] determined experimentally, the parameters for brazing silicon carbide to metals. They found that the growth rates of the interfacial reaction zones decreased in the sequence of SiC / Ti, SiC/ Cr, SiC/ Nb and SiC/Ta. Thus the reactivity of metals versus SiC decreased in the order of Ti, Cr, Nb and Ta.

Ven der Sluis[92] successfully joined a sialon ceramic with a 25mm x 10mm joint cross section area using Ag-Cu-Ti (67.1%, 26.5%, 6.4%) braze to stainless steel and using a temperature of 920°C for 10 minutes under dead load. He also joined numerous ceramics to various metals of rectangular section (35mm x 27mm x 1mm). He used a variety of brazes with different chemical composition in order to evaluate the joint properties of active brazed metal-to-ceramic systems at room temperature by tensile testing directly after brazing and after thermal cycling from300°C to 500°C.

Santacreu et al[93] have used Ticusil to join silicon nitride ceramic to carbon steel. The optimum joining temperature was of 940°C for 5 minutes. The joint area was of 10mm x 10mm.

Tillman et al [39] produced joints between Si_3N_4- Si_3N_4, SiC-SiC and Si_3N_4-stainless steel using brazing to investigate stability and reaction layer formation in non-oxide ceramic joints. These authors used several filler metals with different Ti content. They demonstrated that the matrix composition of titanium bearing filler metals affected the ceramic wetting characteristics and the reaction layer kinetics. They showed that during fabrication of brazed joints with precious metal-containing filler metals at 1250°C. Si_3N_4 decomposed preventing sound joints from forming. They also showed that pre-metallising Si_3N_4 with an Ag Cu In Ti filler metal resulted in the formation of a reaction layer which led to the fabrication of sound brazed joints at 1250°C. However these researchers were not successful in producing SiC brazed joints with CuTi filler metals because SiC decomposed resulting in very weak joints.

Ferro and Derby [94] in their study of SiC/SiC joints using aluminium as a braze showed that sound joints can be produced, providing long holding times and very slow cooling temperatures were observed. They explained the mechanism of bonding and gave reasons for the formation of strong joints when joining siliconized silicon carbide to itself. Four-point bend strengths were used to assess the joint, and strengths over 200MPa were obtained at a testing temperature of 700°C. The authors also explained how and where fracture occurs in the system describing the propagation crack plane on each side of the ceramic-braze interface.

Lee[95] presented a general review of brazing using different compositions. They investigated the active brazing of SiC by copper-based alloys and the effects of various active elements such as titanium, vanadium, niobium and chromium on the wetting, microstructure and bond strength. The bend strengths of different systems were measured and compared.

Nakamura and Shigematsu[96] studied the autogenous active metal brazing of Si_3N_4 reinforced with carbon fibre. The braze used was72Ag-26Cu-2Ti. The joining interfaces were inspected by SEM and analysed by energy dispersive spectroscopy. Two good joints were produced with strengths of 159MPa and 107 MPa in bending The pull-out process of fibres from the matrix and the reasons for the large scatter in the strength of joints, were discussed. It was concluded that the fibre pullout behaviour could be related to fibre distribution density at the joining interface.

Ramsey and Lewis[97] studied the effects of varying titanium concentration when active metal brazing sialon ceramics. They proved using 4-point bend strength tests that the fracture strength decreased from 300MPa with 5% Ti concentration to 75MPa with 15% Ti concentration.

The remainder of this review focuses on the very relevant work conducted by Kussmaul and Munz[98] and by Foley and Andrews[68], for their work relates closely to the present study. Kussmaul and Munz reported tensile strengths between 50MPa and 145MPa for their 10mm diameter single dome-interfaced metal to ceramic joints without ductile interlayers, (admittedly from a population of 44 tests showing a relatively high Weibull modulus between 4 and 4.5). However these were obtained using a system (Alumina to nickel alloy Ni42) where the C.T.E mismatch was very low indeed, falling from 1.17 to 0.69 during cooling after brazing. These authors do not explain how they managed to precision machine the full concave and convex hemispherical profiles onto their alumina, for, as an electrical insulator any featheredge cannot have been machined by EDM. The profile must therefore have been produced either by direct sintering, which process is unlikely to produce the necessary precision directly, or by conventional machining. The latter inevitably subjects the ceramic to significant forces, possibly introducing grinding cracks and surely exposes any featheredge to the risk of fracture from these forces The strength of the alumina alone was determined as 373MPa by 4- point bending.

Notably, Kussmaul and Munz state that ceramic to metal joint failure due to residual stresses on cooling cannot be avoided by only changing the interface geometry when CTE mismatch is large, which they define as being greater then that between alumina and Ck45 (a medium carbon steel) whose mismatch ratio falls from only 1.71 to 1.37 after cooling.

For flat-interfaced 10mm diameter alumina-Ni42 joints with interlayer they obtained tensile strengths lying between 100MPa and 129MPa. They noted that the weakest joints were those in which fracture had initiated at the ceramic surface a little distance from the interface. They suggest that the initiation site might be local microcracking of the alumina induced by titanium from the braze.

They also performed 4-point bend strength tests on Alumina-Ni42 brazed butt and truncated cone-interfaced joints. Whereas the butt joint strength was 106 MPa, those interpenetrating profiled joints in which the ceramic member was concave had a lower strength of 60.4 MPa compared to their higher strength of 183MPa when convex. They attributed the 60.4 MPa value to the presence of pre-cracked zones but did not state whether these resulted from machining.

As well as conducting an extensive programme of conventional ceramic–to-metal brazing tests (reviewed below), Foley and Andrews[68] introduced novel interlayer materials which they felt would be superior to solid metal interlayers in the particular case of joining large interfacial joint areas or for materials with widely different C.T.E. values. They recognized that the capacity of solid ductile metal interlayers to absorb the large induced thermal stresses generated in large area joints, or in those exhibiting large C.T.E. mismatch may be limited. They successfully joined Si_3N_4 to a nickel-based superalloy through a flat 50mm x 50mm interface to demonstrate shear strengths of around 20 MPa based on the nominal area of the ceramic. This was achieved through the use of a low stiffness expanded metal interlayer which actually joined the two members over only 10% of the available joint area.

Their extensive conventional programme investigated joints between the ceramics: sintered Si_3N_4, Syalon 201, hot pressed silicon carbide and reaction bonded silicon carbide and the metals: ductile cast iron, 12% Cr stainless steel, 29% Ni, 17% Cr-Fe low expansion alloy (Nilo-K) and three nickel-based superalloys.

Some joints contained solid single interlayers Cu, Mo, Nb or Ni, or duplex interlayers Cu-Mo or Mo-Cu and some did not. A titanium activated braze was used throughout.

Their strongest joints, when tested at room temperature in shear over a joint cross-sectional area of 12mm by 12mm were of strength 120 MPa for Si_3N_4 bonded without interlayer to Nilo-K, however the C.T.E. ratio was about unity. Their Syalon 201 to Nilo-K, Syalon 201 to cast iron and Syalon 201 to 12 CrFe joints had significantly higher C.T.E. mismatch so required a copper interlayer and exhibited reduced strengths of 60MPa, 38 MPa and 48MPa respectively.

When tested in tension at room temperature they found that Syalon 201 to Nilo-K joints containing 2mm thick copper interlayers had a strength of 35MPa for specimens of cross-sectional area 4mm x 3mm.

When tested in 4 point bending, also across a 4mm x 3mm joint cross-section, their Syalon 201-to-Nilo-K joints showed a higher room temperature strength of 110MPa. With this small section, joint integrity could be achieved without the need for a metal interlayer. The highest 4-point bend strengths of 300MPa were found in Si_3N_4 – to- Nilo K joints, this value falling to 200 MPa at 500°C. The length of these 4mm x 3mm sectioned specimens was 50mm with the central ceramic element measuring 6mm.

2.7 Conclusions

Active metal brazing has been recognized by industry and many researchers in the field of ceramic-metal joining as the most promising technique for ceramic-metal joining. For this reason and because the proposed programme built on work by Tinsley who also used it, the present author has used it in his own experimental programme.

Chapter 3

Problems affecting ceramic-metal joint production and possible solutions to these problems

3.1 Introduction

Joining ceramics to metals is not an easy task because of several problems arising from differences in physical and chemical differences between the two materials.

The joint strength and bond energy in a ceramic-metal system are largely influenced by the physical properties of the mating materials. Joints manufactured at a high joining temperature will experience induced thermal stresses on cooling resulting from coefficient of thermal expansion (C.T.E) mismatch. Stress concentration usually occurs at sharp edges and corners, however the magnitude of the stress concentration is critically dependent on the exact geometry of the interface in the ceramic-metal system. Usually a large difference in thermal expansion coefficients leads to lower joint strength.

3.2 Difficulties accompanying the joining of ceramics to metals

3.2.1 Coefficient of thermal expansion mismatch

Most of the problems when joining ceramics to metals arise from differences in coefficient of thermal expansion [1, 2, 99, 100] Most metals expand and contract more than ceramics, inducing stresses in the joint, leading to poor joint strength and frequent cracking in the ceramic member. Repeated thermal cycling in service further compounds the problem. In most cases these residual stresses are sufficient to initiate cracks in the ceramics at the interface[2, 6, 25] between the ceramic and the metal, causing the ceramic to break. In a few commercial cases ceramics and metals are satisfactorily joined. A good example of this can be found in a nickel-based alloy, which has been successfully joined to an alumina substrate in the electronic components of a commercial satellite[66].

Highly demanding service conditions, such as for ceramic-metal joints to operate in extreme environments involve rapid heating to elevated temperature followed by fast cooling rate [101, 102] putting the systems into a dynamic thermal mismatch situation where the metal gains or loses temperature faster than the ceramic. Designing such joint systems requires much care in selecting suitable materials with appropriate properties to meet the needs of advanced applications in respect to efficiency, reliability and safety.

3.2.2 Interfacial Chemical reactions

During the process of joining ceramics to metals, chemical reactions at the interface often lead to the formation of an intermediate reaction layer. The difference in molar volume between materials to be bonded and the intermediate compound formed can increase the residual stress level. Moreover, brittle intermetallic compounds can be formed which also contribute in the fracture of the joint, where slow crack growth can occur under the action of stress, usually lower than the critical stress intensity factor. The size of the crack grows until it reaches a critical size and fractures the joint.

3.2.3 Experimental factors to be taken into consideration

a) Optimum temperature
b) Optimum time
c) Optimum heating and cooling rates
d) Quality of vacuum where appropriate
e) Pressure where required
f) Surface condition and roughness

3.2.4 Influence of interface shape geometry on thermally induced stress

Even when an expansion coefficient match at the joint has been realized at the test temperature, stress concentration occurs at edges and corners upon mechanically loading the joint [20]. This is due to the difference in Young's Modulus and Poissons ratio of the mating materials. This effect is often neglected but will become a determining factor in the absence of residual stress.

3.3 Solutions to problems arising from joining ceramics to metals

In some systems it is possible to manufacture metal-ceramic joints without the need to reduce the residual stress induced in the ceramic [103-105]. Although the joints in these particular systems do not fail on cooling, strengths on the other hand are drastically reduced. A current way of preventing residual stresses in the ceramic is to control the joining process itself. This means a low cooling rate should be employed to allow some stress relaxation. In the majority of cases however, this is insufficient and a strain accommodating interlayer (**Figure 3.1**) has to be inserted between the two materials.

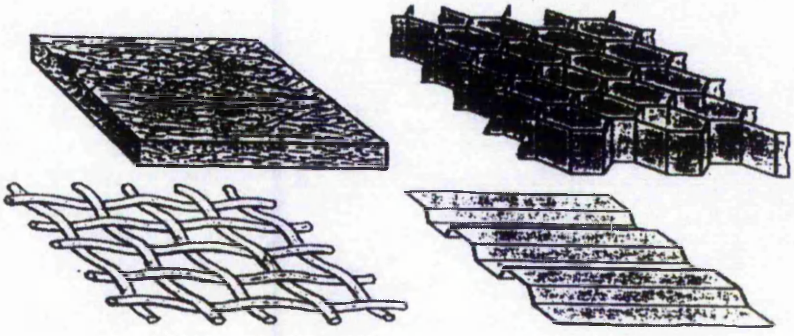

Figure 3.1: Interlayer configuration

3.3.1 Reduction of the thermally induced stresses

3.3.1.1 Existing methods for reducing residual stress

The majority of the published work has focused on the reduction of induced residual stress generated in metal-ceramic joining with planar interfaces by the insertion of strain accommodating interlayers. The interlayers deform accommodating the difference in C.T.E between the two materials reducing the induced stress.

3.3.1.2 Joining process control

Careful control of the joining process, using a low cooling rate allows some stress relaxation.

3.3.2 Using strain-accommodating interlayers in ceramic-metal systems

Various methods have been developed for ceramic-metal systems to accommodate thermal expansion mismatch, and these are:

3.3.2.1 Soft metal interlayer

A layer of metal of thickness about 2mm or less is inserted between the ceramic and metal. The layer is selected to have a low yield stress and small Young's modulus. Soft metal interlayers[106, 107] help reduce stresses in two steps, first they expand with rising temperature increasing the surface contact area between ceramics and metals to accommodate surface mismatch. Secondly, by deforming plastically, they absorb induced thermal stresses on cooling.

Many metals are suitable for this purpose, including copper, aluminium and nickel. It is sometimes recommended to use more then one layer at a time, as a single layer is likely to suffer from fatigue in thermal cycling applications.

3.3.2.2 Composite interlayers

These layers[105, 108] consist of a combination of two or more metals. The soft metal layer with a low C.T.E for example Kovar is joined to the ceramic part, then to another metal with a higher C.T.E. typically Molybdenum. In theory many layers with different properties could be used until they reach the properties of the mating metal partner, typically steel. The laminate interlayer lowers the thermal stress introduced by the high C.T.E metal as the Kovar reduces the effect from the ceramic. The interlayer also improves resistance to rapid temperature changes since the soft metal does not have to deform as quickly as a single interlayer since the movement is restricted by the ceramic and the hard metal with a lower coefficient of thermal expansion.

3.3.2.3 Functionally Graded interlayers

These interlayers are the result of the development of "powder-graded-seal" into "composite interlayer" then into functionally graded interlayers. They usually consist of more than 2 layers made from material with different physical properties, to produce a gradually changing coefficient of thermal expansion between ceramic and metal. This method however has some limitations, because the application of such interlayers is a complicated procedure.

The strength of the joint produced by this method is as strong as the weakest joint between the various graded layers between the ceramic and metal. If during service a mismatch occurs between any interlayers of the graded compound, the whole joint could fail.

Suganuma[104] et al showed in their paper " Joining Si_3N_4 to 405 Steel with Soft Metal Interlayer" that by inserting either Fe or Nb layer in the Si_3N_4/405 steel system improved the interfacial bonding strength. Adding tungsten as a second interlayer in the system led to a tensile strength greater than 50MPa

Xian and Si[105] also found the use of a composite interlayer produced stronger metal ceramic joints in comparison to a single interlayer. These authors obtained a joint strength of 280 MPa using 4-point bend test on a 40% Cr steel/Ag57Cu38Ti5/β /braze/sialon system.

Another method for attachment[51] of ceramics to metals has been used which utilizes a low-modulus insulating fiber metal layer between the ceramic and metal. The low modulus interlayer compensates for the difference in expansion mismatch by distorting to a stress-free geometry.

The change in thermal expansion coefficient between ceramic and metal can be minimised by placing a number of layers between the metal and ceramic. The difference in CTE between each layer should be minimised to minimise the interfacial stresses. The graded CTE technique[2, 52] reduces the mismatch by incorporating layers of different composition and closely matched values; the interfacial stress is minimised if the layers are designed accordingly. However, a large number of layers are desirable to minimise the mismatch. Furthermore, imposing a temperature gradient through the thickness of the ceramic will cause stresses within it, since it is not able to distort.

This method of attachment replaces the intermediate layers in the graded interlayer technique with a single compliant layer having a modulus of elasticity considerably lower in comparison to the one of the metal or the ceramic. The compliant layer is actually a mesh of sintered metal fibers. These compliant layers have much more strength at a given density than sintered powder metal and have a high elastic range (approximately 2% elongation). Modulus of elasticity lies between 70 and 1050 MPa.

The compliant interlayer[2] approach lends itself to a number of compositions. Various wire alloys have been used such as nickels, Hastelloy X, Inconel 600, FeCrAlSi, and FeCrAlY alloys. However, for optimum oxidation hot corrosion resistance, FeCrAlY and FeCrAlSi alloys have been used. Variation in alloy and density of the interlayers can permit variation in elastic modulus and thermal conductivity for design trade-off.

3.3.3 Surface preparation prior to joining

Preparation to reduce roughness of the surfaces to be joined has a beneficial influence on the properties of joints, especially strength.

In diffusion bonding, rougher surfaces require higher temperatures and pressures to mate properly, and in this situation the ceramic near the interface will present a damaged layer with deep scratches, suffering defects and high residual stresses. Rough surfaces can present some advantages as they might present particularly during diffusion bonding an anchoring effect that promotes strength by mechanical interlocking at an interface.

Suganuma [15] showed that that a rougher bond face made joints weaker. This is because the roughly ground bond face had a damaged layer and it remained in the joint even after joining treatment. The fracture of the joints usually took place in the damaged layers along the joining interface. Thus, a roughly ground bond face might weaken the ceramic/metal brazed joint if the damaged layer remains in the joint. Kinds of grinding or polishing methods also have important influence on surface roughness. To make a specific surface roughness during preparation is one of the prerequisites for the metal and ceramic interfaces as shown in [Figure 3.2].

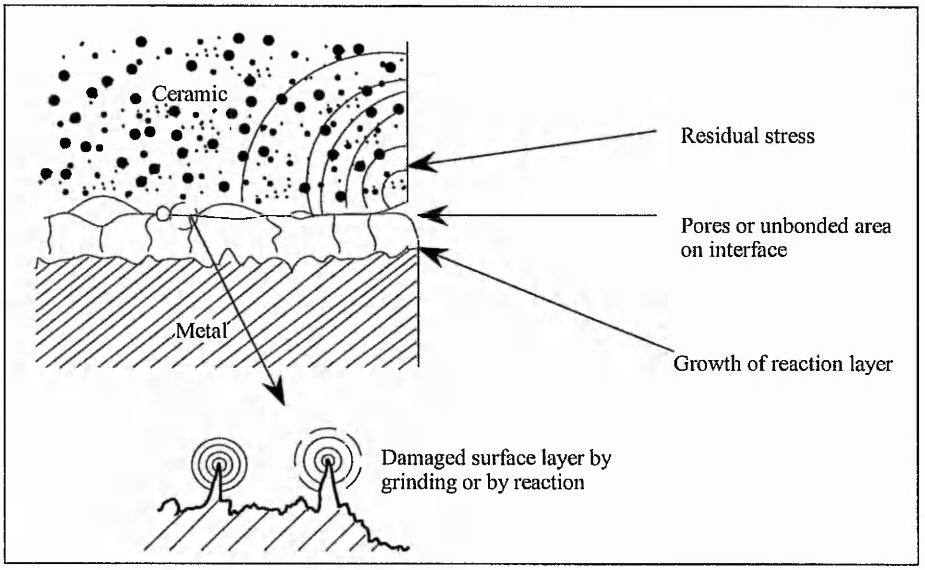

Figure 3.2: Illustration of the factors that might influence the reliability for ceramic/metal joints

The weakening effect mentioned previously is closely related to the stress corrosion effect in the presence of water in a testing atmosphere. It is well known that silicon nitride is sometimes weakened in a moist atmosphere due to stress corrosion[104].

The presence of water is reported [15] to promote stress corrosion in ceramic/metal joints. They state that most structural ceramics such as alumina, silicon nitride, silicon carbide and zirconia are damaged by humidity even at room temperature. The effect of moisture on strength in ceramic -metal systems should be taken into account, where it is known that water degrades the strength.

3.3.4 Geometry optimisation of the mating surfaces between metals and ceramics

In the present work the author used two methods to investigate stress reduction in a Syalon 501(conductive ceramic)-AISI 321 stainless steel system. The first method investigated the effect of using a 2mm thick-curved copper interlayer in the ceramic-metal system. The aim of this method was to reduce or eliminate the resulting residual tensile stress acting on the Syalon 501. The second method studied the effect of changing the size of the test samples from 10mm dome, to 20mm dome flat to 30mm dome flat samples.

Consideration of thermal expansion mismatch is often not necessary when using soft solders or soft metal components. However, as the temperature capability of a joint is raised by using refractory metals and higher brazing temperatures, not only is there a greater mismatch on cooling to ambient temperature but there is also a lesser ability to relax stresses. It is therefore desirable to try to match the thermal expansions of ceramic and metal over the temperature range from ambient to the brazing temperature and to ensure that the ceramic component's interfacial profile is free of thin or delicate sections.

It is desirable to place the ceramic in slight compression[2, 7] by allowing the metal to clamp down on it by relative thermal contraction from the brazing temperature, as in a disc seal.

3.4 Discussion

Joining ceramics to metals for high temperature applications exposes these materials to extremely high thermal variations. Ceramics have a relatively small thermal expansion coefficient compared to commonly used metals, a good example being silicon nitride with a coefficient of thermal expansion of about 3 x 10^{-6} $°C^{-1}$ and steel with one of more than 14 x 10^{-6} $°C^{-1}$. This difference in thermal expansion coefficient can cause great damage to a joint, as large residual stresses are induced during cooling of the joint from high joining temperatures typically 920°C to room temperature due to coefficients of thermal expansion mismatch. Therefore the reduction of thermally induced stresses is important in minimising the risk of failure in ceramic to metal systems. Many researchers have addressed this problem and different solutions have been proposed to overcome the problem.

Along the interface of a ceramics -metal joint the residual stresses are not uniformly distributed. The stresses are greater closer to the interface near the edge of the joint. The most harmful effect is caused by the tensile component of the residual stress at the interface or in the ceramic, and that maximum tensile stress generally occurs at or near the free edge. In most cases the tensile stress acts almost perpendicular to the interface, and usually the actual interfacial strength measured by tensile or bend tests is greatly reduced. In cases where the interfacial bond strength is large enough, fracture will be initiated in the ceramic component where the maximum tensile stress occurs.

In general the magnitude of the residual stress depends on the shape and size of the interface. Shapes with sharp corners are prone to stress concentration and larger joints experience larger residual stresses.

Joints with larger CTE mismatch are weakened, but sometimes from a same batch of sample joints some specimens are stronger then others. This can be explained by the differing distribution of internal flaws, which not only weaken the joints but also produce a wide scatter of the data.

In order to minimise or eliminate the harmful effect that thermal expansion mismatch has on ceramic -metal system it is necessary to reduce the tensile component of the residual stress in the ceramic or at an interface because ceramics are very weak in tension. By contrast metals' tensile stresses can be accommodated by elastic and plastic deformation.

In his theoretical modeling work Tinsley[7, 8] made brief reference to 1, 2 and 3 mm thick single annealed copper interlayers and predicted the resultant reduction in residual stress they could provide, but only in 10mm diameter joints with flat interface. However he did not actually produce, nor mechanically test any copper-bearing metal - to- ceramic joints. Neither did he model, manufacture or test any metal - to- ceramic joints containing curved (i.e. non-planar) copper interlayers. It was a primary objective of the current research programme to contrast the mechanical strengths that can be achieved in Syalon 501/ AISI321 joints with non-flat interfaces and diameters between 10mm and 30mm, both by theoretical modeling; and by actually manufacturing and testing such joints, both with and without copper interlayers.

3.5 Conclusions

Since most metals and their alloys have a coefficient of thermal expansion greater than most ceramics, rigid joints between ceramics and metals become residually stressed on cooling.

The magnitude of residual stresses produced in a joint depend on:

a. The thermal expansion mismatch between ceramic, brazes and metal.
b. The relative thickness of ceramic and metal, and the geometry of the joint including the number and character of any metal interlayers and any non-planar character of the interface.
c. The mechanical properties of both metal and braze, in particular, their ability to relax stresses by deformation of soft metal.
d. The brazing temperature
e. Any dynamic cooling effect

The strength of the joint depends on:

a. Any pre-existing joint residual stresses.
b. The properties of metal, braze material and ceramic including its variability resulting from inherent defect location and character.
c. The integrity of interfaces.
d. Porosity at, or any unbonded areas of, the interface

Joint quality, including the adherence of any pre-metallized metallized layer on a ceramic depends on a large number of practical variables:

a. The type of ceramic and its surface finish
b. The metallising process
c. The type of chemical bond.
d. The particle size of the metal powder and its composition (it may contain a number of components, including metals, reducible metal oxides, glasses, carbides, and hydrides).

e. The thickness of the coating.
f. The heating and cooling cycle and the atmosphere used to make the bond.

From the points above it should be clear that much care is required to make a successful ceramic-to-metal joint. Even small changes in geometry, surface condition or processing might ruin an otherwise successful design.

Chapter 4

Modelling of Ceramic-Metal systems using Finite Element Analysis

4.1 Introduction

This research programme was concerned mainly with investigating geometry, size and shape's effects on ceramic-metal brazed joints' strength, and seeking possible ways to reduce the thermally induced residual stresses. It was a direct continuation of the work carried out in the author's laboratory by Tinsley [7], who demonstrated the benefit of using a 5mm radius dome-shaped interface on reducing residual stresses by up to 70% in a directly joined sialon-stainless steel joint.

The model of the ceramic-metal interface may be produced using advanced CAD packages (e.g. Pro-Engineer 20), either in 2D or 3D then exported into FEA software (e.g. ANSYS 5.5) [73] where it is given geometrical attributes such as 2D or 3D symmetry or axi-symmetry. The model is then given finite element attributes such as type of elements to be used, number of elements, number of nodes, lines and key points, type of mesh and region where high density meshes are necessary for more details and accuracy. Once all geometrical attributes have been satisfied, material properties such as Young's modulus of elasticity, coefficient of thermal expansion, and Poisson's ratio are assigned to each element.

The user can then easily control the shape and the density of the mesh across the model by altering elements' aspect ratios. This is very important, especially in the case of ceramic-metal interfaces where a region of high concentrated stresses occurs at the interface near the free edge between the ceramic and the metal. In this particular region of the model the more dense the mesh is, the more accurate the results will be. In reality, the singularity[75] does not exist. The values of unrealistically high stresses obtained from FEA calculations are not acceptable. Therefore the use of a very dense mesh in those areas of singularity[74, 76], contributes significantly in reducing them to a point where they can be treated as very small with no major effect on the results and the rest of the model. FEA results can be obtained in various output formats ranging from plots or listings of figures to graphs and contour plots.

4.2 Solid modelling

The Initial Graphics Exchange Specification (IGES) is a neutral standard format used to exchange geometric models between various CAD and CAE systems. ANSYS IGES import capability is quite powerful, but in some cases, because the filter can import partial files, only certain volumes can be imported. The default option is very useful because it has access to an enhanced geometry database. It was designed to convert IGES files without user intervention. The conversion includes automatic merging and the creation of volumes to prepare the models for meshing.

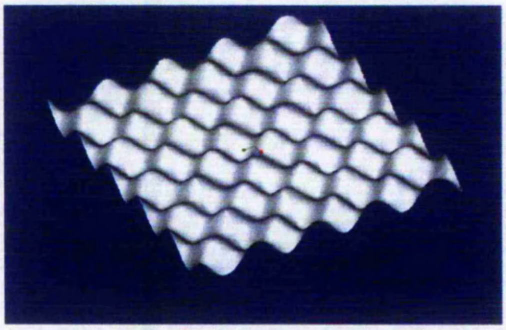

Figure 4.1: Repeated 3-D sine wave pattern produced by the author using Pro-Engineer

In real life, ceramic/metal joints are three-dimensional and present, in many cases an axi-symmetric configuration, which can be of a great advantage when modelling for a F.E.A application. In those particular cases of axi-symmetry, only one plane needs to be modelled in order to obtain a full analysis for the whole model. This reduces considerably computer resources needed, the complexity of the analysis and, most importantly processing time.

In some situations, joint configurations[30] are not axi-symmetric and a 3-D model has to be used for the FEA application (e.g. interface with repeated sine wave pattern, Figure 4.1). In this case more computer resources and a longer processing time are necessary.

4.3 Meshing the solid model

Before meshing the model, and even before building it, it is important to consider whether a free mesh or a mapped mesh is appropriate for the analysis. A free mesh has no restrictions in terms of element shapes, and has no specified pattern applied to it. Compared to a free mesh, a mapped mesh is restricted in terms of the element shape it contains and the pattern of the mesh.

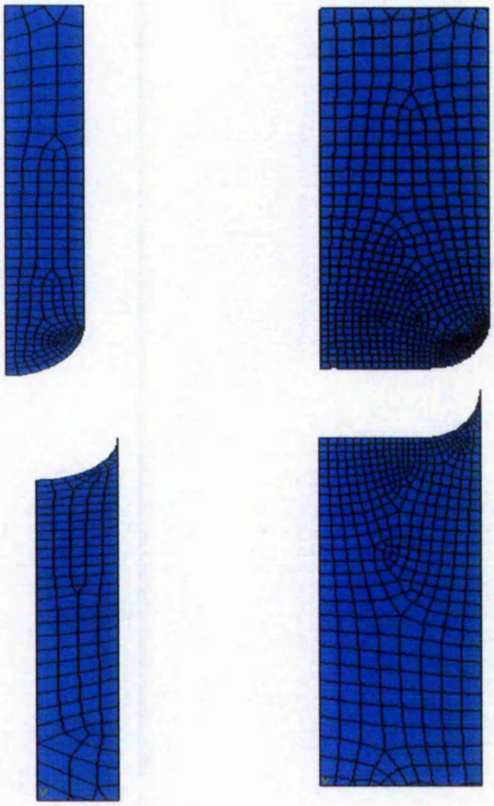

Figure 4.2: Meshing of 1/2 axi-symmetric models

A mapped area mesh contains either only quadrilateral or only triangular elements, while a mapped volume mesh contains only hexahedron elements. In addition, a mapped mesh typically has a regular pattern, with obvious rows of elements. To use a mapped mesh, the designer must consider a series of fairly regular volumes and areas.

Once the design of the ceramic/metal system is satisfactory, a further stage in the process is carried out in which the model is divided into small elements. Each element will later contribute in generating results for the analysis. The size and shape of elements are of great importance as they have a direct influence on the accuracy of the results. Small elements imply more calculation and accuracy, while larger ones less calculation and less accuracy. The ensemble of elements forms a mesh.

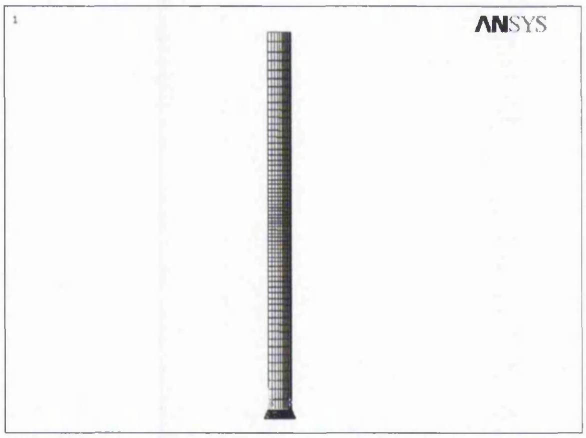

Figure 4.3: Mesh used in the thermo-elastic analysis. The model has been restrained at the bottom to prevent rigid body motion

Regions with small elements are represented by a fine mesh and are always located on areas of interest i.e. at and near the interface of a ceramic/metal joint where residual stresses are expected to peak after complete cooling.

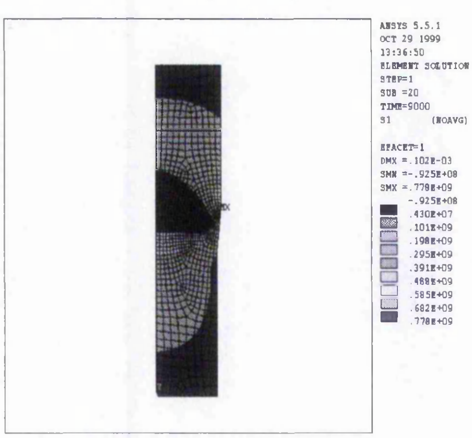

Figure 4.4: Mesh of Ceramic / Metal system (Ceramic top)

Coarse meshes with larger elements are usually used in areas of less importance in order to reduce unnecessary calculation time and save computer resources.

4.4 Analysis of a Ceramic-Metal system

4.4.1 Elastic Analysis

Early F.E.A. investigations concerning ceramic-metal systems used mainly linear analysis where ceramics, soft metal interlayers and metals were regarded as deforming elastically. In practice, if thermally induced stresses exceed the yield strength of the material, permanent plastic deformation is produced. The use of non-linear analysis is more appropriate for such systems.

A good example is illustrated by the work carried out by Suganuma and Elssner[109] in modelling an axi-symmetric Si_3N_4/Steel joint, using a linear analysis. The results revealed a maximum **principal** induced stress of 1600MPa. The same analysis was repeated using a non-linear analysis, predicting a lower maximum principal stress of 1200MPa.

Although elastic analyses are totally acceptable for ceramic-ceramic systems, they are clearly not appropriate for systems containing metal members. Using elastic analysis for metal systems predicts unrealistically high levels of thermal stress.

4.4.2 Thermoelastic-Plastic Analysis

For a thermoelastic-plastic analysis to be performed by ANSYS 5.5.1, the full Newton-Raphson[73] option has to be selected. The stress-strain curve of AISI321 stainless steel is used in the model. It was found that in the majority of published work, the application of the strain hardening was simplified by using classical bilinear hardening[110, 111]. The material properties are specified as a bilinear curve starting at the origin with positive stress and strain ratios.

4.5 The Effect of Material Data on Finite Element

4.5.1 Finite Element Analysis predictions

Many ceramics researchers were concerned by the accuracy of the results obtained from FEA analyses [112] and therefore many attempts were made to compare experimental measurements of residual stress with those obtained from FEA studies. Suganuma[28] has shown using strain gauges that with the increase of the cylinder radius of the test specimen, the joining-induced residual stresses rise sharply. This is in direct contradiction with the work published by Foley [113] who showed using F.E.A. that increasing the radius should lower the induced residual stresses. He believed that any discrepancy may be due to the size of the mesh used in the analyses. Koguchi et al[110] used the indentation fracture method to measure stresses in metal-ceramic joints and obtained a good correlation between the experimental results and those of their finite element analysis. Kim and Na[111]also obtained good agreement between their F.E.A. calculations and those of experimental X- Ray diffraction measurements. Although there was a discrepancy in the magnitude of the forces involved, between the two methods, the general trend was the same.

4.5.2 Verification of previous work

During the early stages of this project an attempt was made by the present author to confirm Tinsley's findings. This was achieved by reproducing some of his work using a more recent version of ANSYS (5.5.1 instead of 5.0). Moreover, whereas his work was based on the simple cooling from 1103K to room temperature, the present author has followed Suganuma's[77] method in applying a temperature difference of -810K, allowing for the joint being cooled from 1103K to 293K.

An example of a predicted thermal profile generated by cooling of a ceramic-metal joint is shown in [Appendix N] as an ANSYS plot. The model is based on the dimensions, physical arrangements and materials of construction (tooling, etc) used originally by Tinsley[7] and proposed for use in the production of joints in the present work.

Models used from Tinsley's work

1- Two flat cylinders (Syalon101/AISI321 steel). In this particular case only the analysis was linear.

2- Two cylinders, one with a convex (5mm-apex height) shape representing the Syalon101 ceramic, the second cylinder with a concave shape representing the AISI 321 stainless steel

Type of interface	Ceramic -metal system	Metal-ceramic system
Flat faces	Ceramic top, Metal bottom	
5mm-radius dome without interlayer	Ceramic Convex, Metal Concave	Metal Convex, Ceramic Concave

Table4.1: Summary of the principal analyses carried out by Tinsley

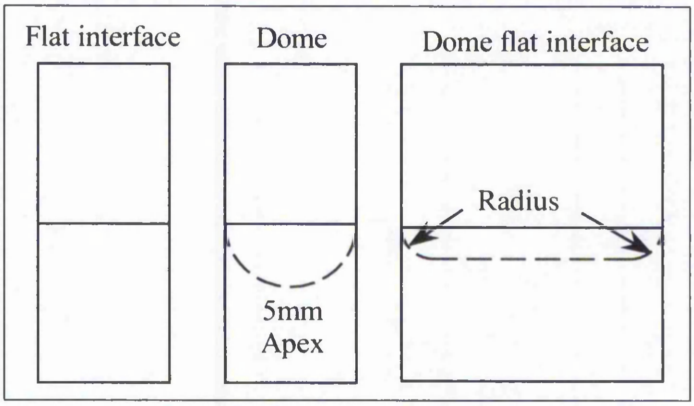

Figure 4.5: Type of interface considered

5mm radius dome with a 2mm copper interlayer, - a first extension of Tinsley's work

The first logical step was to investigate the influence of a 2mm thick, copper interlayer on reducing the thermally induced stresses in the system (5mm-radius dome) during cooling.

Dome-flat model with or without interlayer (Syalon 101 / AISI321 steel), - a second extension of Tinsley's work

In order to study the joint interface diameter size effect on the residual stresses, a new geometry consisting of a flat surface contained between two 5mm-radius half domes was introduced. For ease of reference the systems are called 'dome flat'. All the systems used in this work are modelled with the top half corresponding to a convex ceramic and the bottom half corresponding to a concave metal, unless stated otherwise.

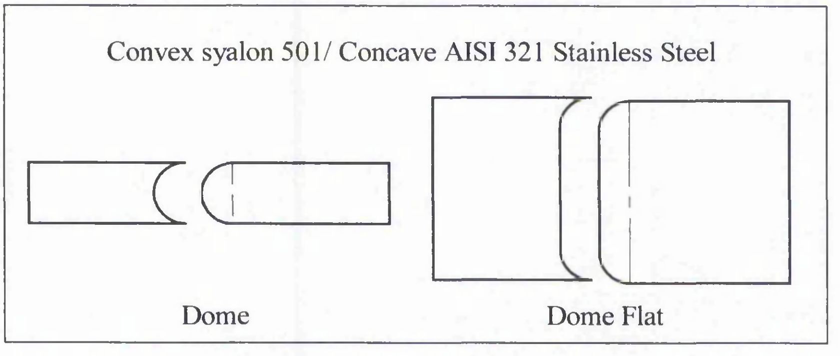

Figure 4.6: Interface configuration used

In extending Tinsley's work the current author has introduced the following models

Type of interface between ceramic and metal (for 10, 20 and 30mm Ø joints)	Ceramic with convex shape ceramic -metal system	Ceramic with concave shape metal-ceramic system
5mm-radius dome, 2mm Cu interlayer Syalon 101/Cu/AISI321 stainless steel	Ceramic Convex Metal Concave	Metal Convex Ceramic Concave
5mm-rad dome flat, no Cu interlayer Syalon 101/AISI321 stainless steel	Ceramic Convex Metal Concave	Metal Convex Ceramic Concave
5mm-rad dome flat, 2mm Cu interlayer Syalon 101/Cu/AISI321 stainless steel	Ceramic Convex Metal Concave	Metal Convex Ceramic Concave

Table4.2: Proposed extension to Tinsley's investigations using Syalon101, with and without copper (Cu) interlayer.

Types of interface: 20mm and 30mm diameter	Ceramic with convex shape
Dome flat, no Cu interlayer-Syalon 501/AISI321stainless steel	Ceramic Convex/Metal Concave

Table4.3: Proposed Extension to Tinsley's Investigations using Syalon 501

4.6 Review of work carried out in the area of Finite Element Analysis in the field of brazing ceramics to metals

In their investigation Maier et al[114] compared results from finite element analyses conducted to evaluate stresses and quality of active metal brazed ceramic-metal joints to those from experiments using X-ray stress analysis, holographic interferometry (HIA) and fracture stress analysis. They have shown that good accordance could be achieved in areas with regular stress-strain fields. Close to the interface's peripheral edge such comparisons were more difficult due to the extreme localised values of stress and strain at this position of singularity. Their investigations were concentrated mainly on the fracture probability of the ceramic component.

Wielage et al[74] conducted a study using finite element analysis to calculate thermally induced residual stresses in brazed metal-ceramic joints. The significance of plastic flow on the residual thermal stress state in such systems was shown. They used elastic-plastic material behaviour and the dependency of the material properties on the temperature in their FEM models to show the stress reducing effect of thermal expansion by using soft metal interlayers. They also proposed other options to reduce the stresses such as ductile interlayers, reinforced brazing alloys, increasing the brazing filler thickness and interface geometry modifications.

Nagasawa et al[76] investigated the thermal residual stress distribution developed during the cooling process after bonding of a cylindrical dissimilar materials joint (Ni-Sialon). Considering a stress gradient λ' on the ceramics side to be useful for the estimation of cooling effect, a relation between λ' and the mean cooling rate was characterised by a logarithmic form. Their conclusions were that λ' could be affected by the mean cooling rate and also by the side length of the joint.

Schreieck et al[115] compared results from finite element-residual stress calculations done on cemented carbide plates jointed by brazing to steel bodies, with results from X-ray stress analyses. A good agreement between the two results was reached. Small differences found near the edges were explained as non-homogeneous cooling in these areas due to the shielding gas flow in the brazing process. Neglecting the radius at the short edges of the cemented carbide plate in the FE-model was found to be the cause of differences between measured and calculated residual stresses in that area. The authors showed that even the quantitative numerical analyses of the maximum residual stress near the brazing gap was difficult, because the real formation of the brazing gap and the wetting behaviour at the edges was different from the idealised assumptions made during the FE-analyses. The FE residual stress calculated allowed the explanation of the failure behaviour of the joints under cyclic loading.

Steffens et al[116] used finite element analysis to investigate interface design variations including a butt-step configuration, oblique and insert joint, in brazed metal - ceramic systems. Four-point-bending tests showed that oblique joints possessed the highest strengths. They stated that for evaluation of the quality of brazed seams, the absolute strength is not sufficient and that using additional strength values expressing the relation to the strength of the joined materials would be more appropriate. They referred to the quotient of the joint strength to the ceramic base material strength and gave the example of the composite Al_2O_3-AgCu27Ti3-X5Ni29Co18 reaching a best ratio of about 0.9. The authors stated also that the thermal expansion coefficient of the metallic joint partner was adjusted to the ceramic one, and that in the case where it was not adjusted the resulting ratio would be very low.

Pintschovius et al[112] studied the influence of various interface geometries on residual stresses in brazed ceramic-metal joints. They also compared the strength of welded and non-welded joints. They found that 4-point-bending tests gave the highest strength values of truncated cone joints. This confirmed the FE-calculations conducted previously which predicted high local tensile stresses in ceramic at the edges of the ceramic-filler metal interface. Al_2O_3 - Ni42 brazed butt joints were subjected to tensile testing, and exhibited two types of fracture surface, depending on whether the ceramic surface near the edges was effectively joined or not. Higher strength values were obtained for cases where the edges were not joined together.

Kivilahti and Kouhia [100] used a finite-element model to evaluate thermal stresses in the AlN/ Ag-Cu /Ti system. The authors incorporated in their model, temperature dependent work hardening and creep induced stress relaxation. The materials characterisation was based on incremental constitutive equations, where the strain rate was decomposed into elastic, plastic, creep and thermal parts. The plastic behaviour was modelled using the J2-flow theory and the creep deformation was based on a power law. The authors stated that the simulation could predict reasonably well the effects of the brazing parameters and thicknesses of Ti sheets on the magnitude and distribution of thermal stresses. Good joints could be obtained only if the braze reacted with the parent materials, and the cooling rate to room temperature was low enough for the formation of soft, non lamellar eutectic structure to allows a more ready relaxation of thermal stresses through plastic and creep deformation. The paper showed good correlations between SEM and the FEM calculations.

Rabin and Williamson[107] used finite element modelling to investigate the role of interlayers on residual stresses in ceramic-metal joining to offer broad guidelines for selecting ceramic-metal joining techniques and suitable joint interlayer materials. They modelled simple axisymmetric Al_2O_3-Ni specimens using elastic-plastic temperature dependent properties. Residual stresses and strains were calculated for various interlayer types, and the stresses responsible for causing joint failures were compared to those for the direct bonding (no interlayers) case. The authors concluded that in some cases, composite and graded interlayers can result in local stresses higher than for direct bonding, where plasticity plays a significant role in limiting peak stresses. Significant reductions in the critical stresses were only predicted for low yield strength, ductile interlayers, or for interlayers having non-linear composition profiles exhibiting gradual changes in properties adjacent to the ceramic. The authors stated also that brazing is attractive because it is practical, cost effective and has demonstrated the potential for achieving high bond strengths in a number of technologically important ceramic-metal systems.

4.7 Results from present study: Finite element predictions

4.7.1 Flat interface

Figure 4.7 represents the 10mm diameter Syalon 101 ceramic member. The peak stress S1 obtained from the analysis is 1470MPa, which is clearly higher than the tensile strength of the ceramic with a value of approximately 500MPa. This result agrees with Tinsley's for the similar analysis (Elastic-linear).

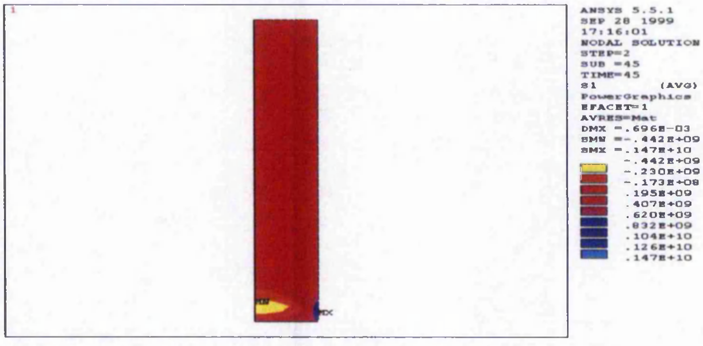

Figure 4.7: Principal stress S1 of ceramic member after cooling

Figure 4.8 shows Stress Equivalent Von-Mises stress (SEQV) for the flat interface of AISI 321 steel member. This result also compares favourably with Tinsley's result.

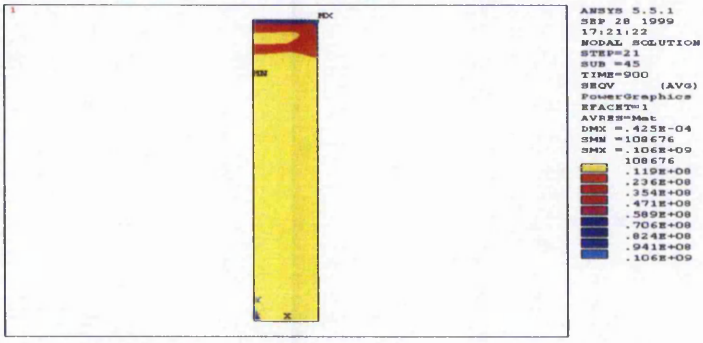

Figure 4.8: Von Mises stress contour map of steel member after complete cooling

From the above results it is clear that flat interface configurations generate high stresses at the free edge of the joint, which are greater than the tensile strength of the ceramic and therefore flat interface systems are not recommended

4.7.2 Convex Syalon 101 with 5mm-radius dome, no interlayer

Figure 4.9 shows the area of concentration of peak principal stress (S1), which is located at the free edge of the ceramic-metal joint. The value of the stress is evaluated after only 135s of cooling. The value of 37.4MPa is still relatively low.

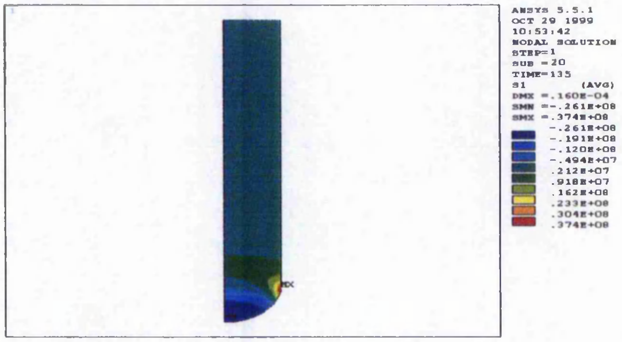

Figure 4.9: Principal stress S1 generated after 135s of cooling

Figure 4.10 gives the value of the principal stress S1 after complete cooling. The value of the stress calculated in this case is of 224MPa and is only slightly higher than the 204MPa peak stress evaluated by Tinsley[7] from his simpler analysis.

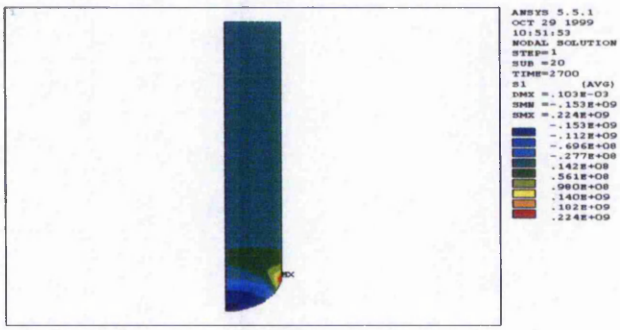

Figure 4.10: Principal stress S1 generated after 2700s of cooling

4.7.3 Convex Syalon 101 with 5mm-radius dome and copper interlayer

We can see from this result that using a 2mm Cu soft metal interlayer predicts a further 14.3% reduction of the principal peak stress. The value obtained is only 192MPa.

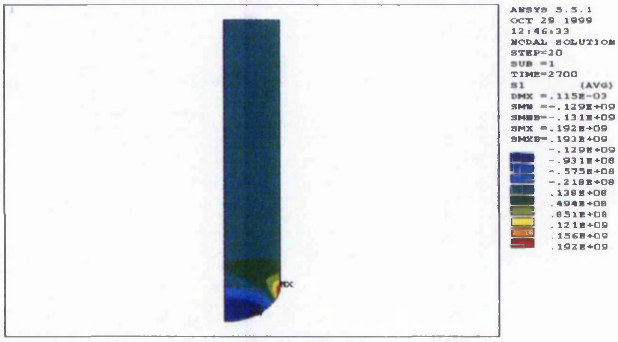

Figure 4.11: Principal stress S1 generated after 2700s of cooling

4.7.4 Convex Syalon 101 dome-flat model, no Cu interlayer 20mm

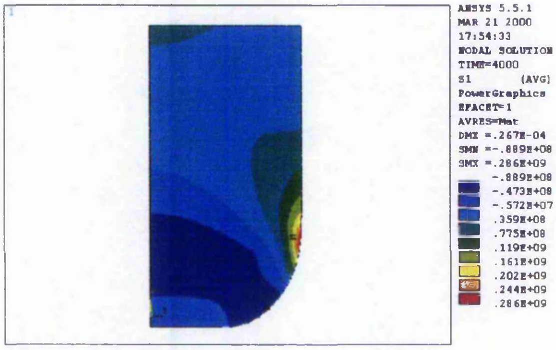

Figure 4.12: Principal stress S1 generated after full 4000s cooling (20mm)

Figure 4.12 shows the area of concentration of peak principal stress (S1) located at the free edge of the 20mm diameter ceramic-metal joint. The stress reached a value of 286 MPa after complete cooling.

4.7.5 Convex Syalon 101 dome-flat model, 2mm copper interlayer 20mm

Figure 4.13 shows the area of concentration of peak principal stress (S1) located at the free edge of the 20mm diameter ceramic-metal joint containing a 2mm thick copper interlayer. The stress reached a further reduced value of 266 MPa after complete cooling.

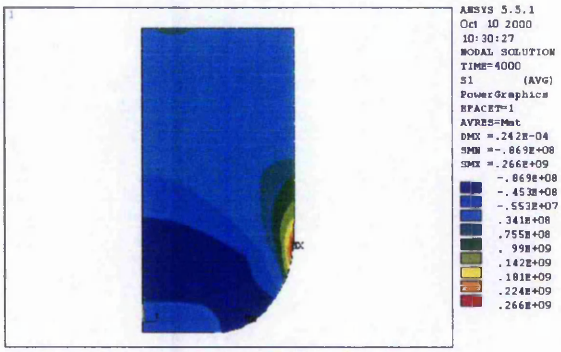

Figure 4.13: Principal stress S1 generated after full 4000s cooling(20mm)

4.7.6 Convex Syalon 501 dome-flat model, no Cu interlayer 20mm

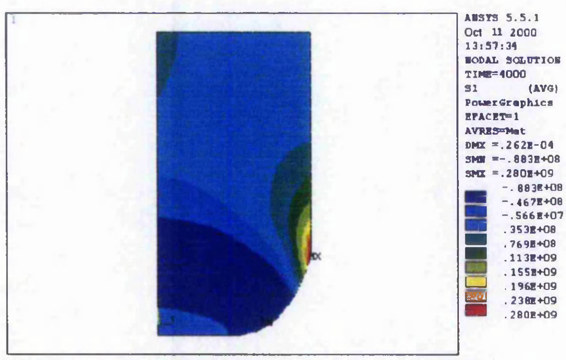

Figure 4.14: Principal stress, S1 generated after 4000s cooling (20mm)

Fig 4.14 shows the area of concentration of peak principal stress (S1) located at the free edge of the ceramic-metal system. The predicted peak principal stress in this case reached a value of 280 MPa after complete cooling. The increase in stress is linked to a drop in temperature with time resulting in contraction mismatch between the metal and the ceramic.

4.7.7 Convex Syalon 501 dome-flat model with Cu interlayer 20mm

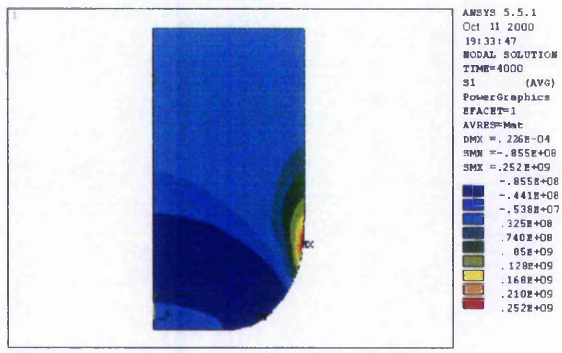

Figure 4.15: Principal stress, S1 generated after 4000s cooling (20mm)

Figure 4.15 shows the peak principal stress (S1) located at the free edge of the ceramic-metal system containing a 2mm thick copper interlayer. The peak principal stress has a reduced magnitude of 252MPa after complete cooling.

4.7.8 Convex Syalon 101 dome-flat model, 30mm no interlayer

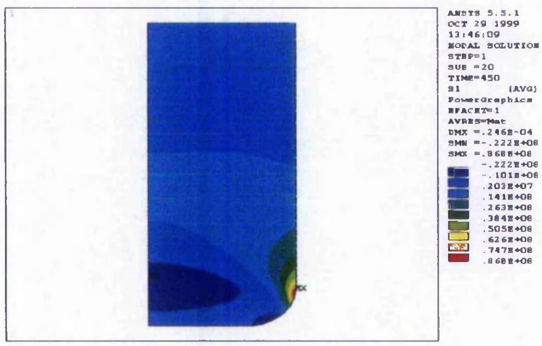

Figure 4.16: Principal stress S1 generated after 450s of cooling

After initial cooling for 450s the peak principal stress showed a value of 86.8MPa, still relatively low.

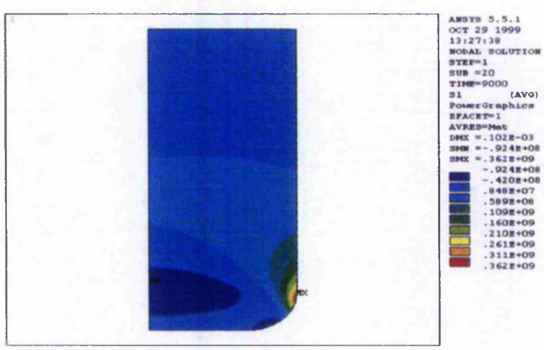

Figure 4.17: Principal stress, S1 generated after full 9000s cooling (30mm)

After complete cooling over 9000s the predicted stress had risen to 362MPa. The large increase in stress is again linked to a drop in temperature with time compounding thermal contraction mismatch stress.

4.7.9 Convex Syalon 101 dome-flat model, 30mm with 2mm copper interlayer

Fig 4.18 shows the value of the stress at an early phase of cooling, (450s) giving a value of 67.4MPa

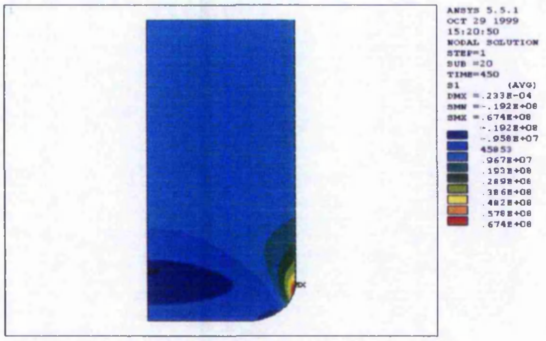

Figure 4.18: Principal stress S1 generated after 450s of cooling (30mm)

Fig 4.19 shows that by introducing a 2mm Cu interlayer into the system gives once more a substantial reduction of the peak residual stress. The value obtained was 329MPa representing a further reduction of 9.1% attributable to the copper interlayer.

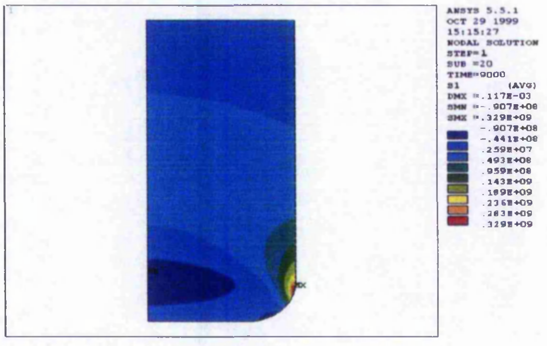

Figure 4.19: Principal stress S1 generated after full 9000s cooling (30mm)

4.7.10 Mating steel part of convex Syalon 101 dome flat, no interlayer

Fig 4.20 shows values of principal stress in the mating steel member after 450s of cooling of a dome-flat Syalon 101/AISI 321, no interlayer system.

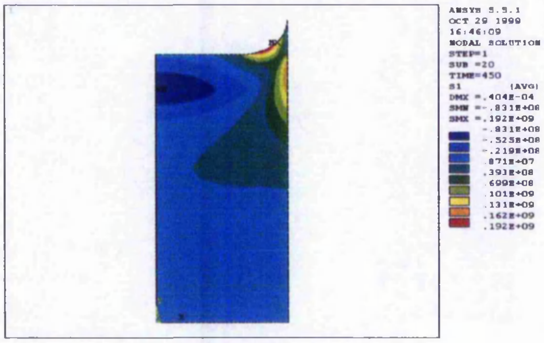

Figure 4.20: Principal stress S1 generated after 450s of cooling (30mm)

The S1 value obtained of 192MPa is higher than the 86.8MPa obtained for the ceramic member of the same system as shown in Figure 4.16. This is a combined result of the interaction of the complementary surfaces and the stress relaxation occurring within the thermoelastic metal member.

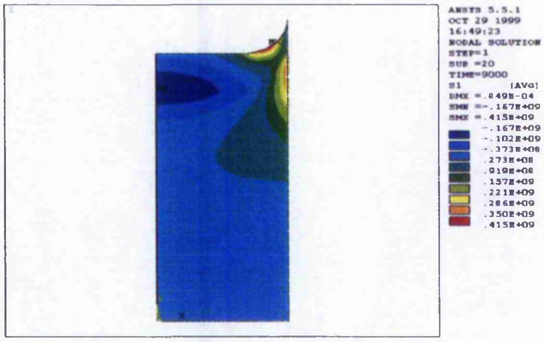

Figure 4.21: Principal stress S1 generated after full 9000s cooling (30mm)

Fig 4.21 shows a value of 415MPa for the peak stress after complete cooling. Once more the value obtained is higher than the one for a convex ceramic interface.

4.7.11 Convex dome-flat model without interlayer (Syalon 501 / AISI321 steel)

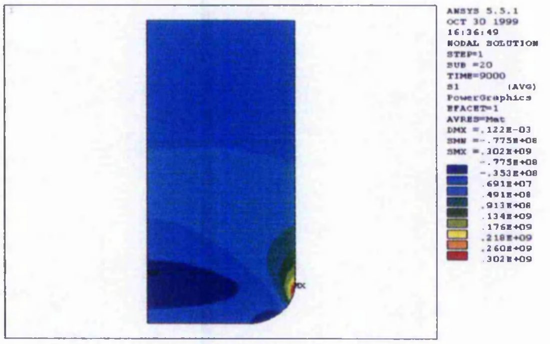

Figure 4.22: Principal stress S1 generated after full 9000s cooling(30mm)

After complete cooling the peak residual stress calculated is of 302MPa, which is slightly less than the one calculated for an identical interface shape, but with Syalon 101. This is due to the fact that Syalon 501 has a larger coefficient of thermal expansion.

4.7.12 Summary of results from finite element study of Syalon/AISI 321 joints

In Table 4.4 is presented a summary of the predicted maximum (MX) and minimum (MN) stress values in Syalon 101 for convex Syalon 101/concave AISI 321 dome and dome-flat joints after full cooling. Values in brackets were computed for Syalon 501/ AISI 321 joints and are included for comparison.

Joint type	Predicted MX values (MPa)	Predicted MN values (MPa)
10 mm dome without copper	+204 +224*, (+192)*	-153 -279* (-259)*
10 mm dome with copper	+192	-129

20 mm dome-flat without copper	+286 (+280)	-88.9 (- 88.3)
20 mm dome-flat with copper	+266 (+252)	-86.9 (- 85.5)
30 mm dome-flat without copper	+362 (+302)	-92.4 (-77.5)
30 mm dome-flat with copper	+329	-90.7

Table 4.4: Summary of predicted maximum (MX) and minimum (MN) stress values for convex Syalon 101/concave AISI 321 dome and dome-flat joints after full cooling.

* Data taken from Tinsley[7]

Convention: Positive values represent tensile stresses

Negative values represent compressive stresses

4.8 Discussion

The process of combining ceramics to metals requires full interface joining of the two[1-3]. It was established in Chapter 1 that metals and ceramics have very different physical properties, making joining very difficult but not impossible. This justifies the need for more research in this field. The point of principal difficulty results from differences in coefficient of thermal expansion for the metal and ceramic within the joint inducing thermal stresses during fabrication and in service, leading to ceramic fracture.

As the need for critical ceramic structural components increases, reliability becomes a significant issue. Ensuring reliable performance means being able to predict with a high degree of certainty whether a component will fail under typical operating conditions. This requires an accurate description of the stresses likely to be encountered in service, as well as knowledge of the mechanical properties and flaw distribution of the ceramic component.

Finite element analysis (FEA) techniques significantly improve prediction of service stresses in components with complex shapes and loading geometries. Using the new version of ANSYS 5.5.1 gave stress values close to the ones presented by Tinsley[7].

Inserting a 2mm copper interlayer into a 5mm-radius dome system reduced further the thermally induced stresses.

The use of the new geometry consisting of dome-flat interfaces showed that larger ceramic-metal systems should be produceable without excessive free-edge stress generation. It is clear however from the FEA conducted that the stresses do increase with joint size.

Whilst exact values of the stresses predicted should not be considered to be 100% accurate on account of quoted material property values' variation, unforeseen environmental conditions arising during service and the modelling parameters used, nevertheless the trends, nature (tensile or compressive) and locations of regions of concentration of stresses are believed to be correct. Moreover, this work has established, using an approach at least as sophisticated as any previously reported (by attention to the dynamic nature of cooling and to detailed modelling of the specimens' environment on cooling), that interfacial stresses increase progressively as cooling proceeds. This approach of monitoring stresses on cooling could be a useful aid in promoting action to reduce the build up of stresses in joints.

ANSYS is a useful modelling tool to investigate a design before experimentation, in this case areas of high stress concentration after cooling from a high joining temperature to room temperature. Compression and tension zones were clearly identified. It was found that most of the stress concentration occurred at the free edge of the ceramic-to-metal interface. This information was useful in confirming the value of the featheredge system in deforming whilst absorbing stresses, so helping the ceramic to cope with excessive strain produced by the mismatch with the metal component.

It is proposed that this investigation is an original application of FEA to complex non–planar interlayered metal-to-ceramic joints, while incorporating the effect of varying diameter.

Mechanical testing is necessary to predict true service behavior. Testing does not guarantee specific component performance, but it is critical in assessing new materials, ranking materials for a specific application, and attempting to predict failure conditions.

There follows in Chapter 5 a description of an experimental programme in which an attempt was made to validate the predictions obtained from Chapter 4.

4.9 Conclusions

In order to gain maximum accuracy in of the FEA analysis of an axis-symmetric thermoelastic-plastic modelled ceramic to metal joint, appropriate steps were taken to refine the mesh size in areas around the free edge and the interface of the ceramic and metal, to minimise the errors created by the presence of singularity in those regions. The errors were contained in only a few elements in each material lying adjacent to the free edge at the intersection of the two materials. The inaccuracy, if not contained and removed from the mesh would have led to misrepresentative results.

Even by eliminating the unreliable data from the model, by refining the mesh as described above, the use of a pure elastic assumption for both metal and ceramic was unrealistic, as the stress level reached much higher values in the metal than its actual yield stress.

The results of the analysis based on a thermoelastic-plastic model with the use of a bilinear curve, described by Young's modulus and a plastic modulus, predicted lower levels of stress in the ceramic to metal system.

Two factors affecting stress generation were investigated in both an active metal brazed Syalon 501- AISI 321 stainless steel joint and a Syalon 501-copper- AISI 321 stainless steel joint. The first examined the effect of a soft, shaped metal interlayer (copper) on reducing the level of thermal stresses in such systems and the second, the effect of size change from 10mm through 20mm to 30mm diameter.

Principal stresses obtained from a linear elastic analysis of a flat interface were very high and not commercially acceptable. Tinsley's value of 1940MPa found using an early version of the software was determined as 1470MPa in the present study using ANSYS5.5.1.

Principal stresses S1 obtained from joining 5mm-radius Syalon 101/AISI321without interlayer produced values matching those found by Tinsley. The 8.9% difference in value obtained is probably due to the different version of the software and to the mesh size used.

The use of concave metal interfaces and convex ceramic interfaces in the model showed a lower residual stress than that present in a reciprocal system, and this confirmed the work of Tinsley[7]. A decrease in strength was noted with the increase in joint size. Elimination of the singularity from the model by design, using dome and dome-flat interfaces was beneficial for the joint integrity, as it would otherwise promote crack propagation, interface debonding or yielding.

Tinsley did not model the effect of a copper interlayer on a 5mm-radius domed Syalon 101/AISI321system. The current author has investigated this and established that a further reduction in principal stresses of about 14.3% can be obtained. This is clearly a result of the compliant interlayer deforming plastically to absorb a proportion of the joining stresses.

A 20mm diameter Syalon 101 convex dome-flat interface showed a rise in peak principal stress to 286MPa for samples without a soft Cu interlayer while the rise in peak principal stress was to 266MPa for the same ceramic with the insertion of a 2mm Cu cup between the Syalon 101 and the AISI321 stainless steel. This represented a reduction of 7.0 % in thermally induced stress. (Figure 4.12 & 4.13)

Syalon 501 convex dome-flat ceramic showed a peak stress of 280MPa without copper interlayer and a peak principal stress of 252MPa with the use of copper. This is a further 5.26% reduction in thermal stresses between Syalon 101 and AISI 321 stainless steel. The difference in the thermal expansion coefficient between Syalon 101 and Syalon 501 explains the difference in peak principal stresses at the free edge between the ceramic and the metal. (Figure 4.13 & 4.15)

Thirty millimetre diameter ceramic convex dome-flat configurations showed a noticeable increase in peak principal stresses after complete cooling, in comparison with stresses obtained for 5mm-radius dome configurations. The increase from 224MPa to 362MPa in stress values clearly indicates a joint area effect on the predicted magnitude of principal stresses.

In his investigations Tinsley[7] showed that the convex configuration for the ceramic generated lower stresses in comparison to a concave configuration. This is confirmed in the present study, which **also shows it to be true for dome-flat interfaces**.

In previous work, the use of a soft metal interlayer helped in most situations to reduce stresses. This still applies for the current work where the use of a 2mm copper interlayer predicted a further reduction of 9.1% in peak tensile stresses in the case of the 30mm Syalon 101 system.

Ceramics with higher expansion coefficients generate lower residual stresses, and this was confirmed by the model of a Syalon 501 convex dome-flat ceramic (Figure: 4.22) which reduced stresses further by 16.6% over values for Syalon 101 (Figure: 4.17) where their respective expansion coefficients were 5.6 x $10^{-6}$and 3.04 x 10^{-6}. Thus, ANSYS predicted values of 362MPa were determined for Syalon 101 compared with 302MPa for Syalon 501 after 9000s of cooling to room temperature.

Chapter 5

Experimental programme

5.1 Introduction:

The theoretical study considered in the previous chapter can only be validated by an experimental evaluation of ceramic to metal joints under real testing conditions. In this chapter, procedures for manufacturing and testing of joints with different interface geometries between Syalon 501 conductive ceramic and stainless steel will be described. Syalon 501 is commercially available and suitable for electrical discharge machining (EDM).

The finite element analysis study conducted in the previous chapter predicted that by varying the interface geometry between ceramic and metal from a flat surface to either a dome with a 5mm-apex height or to a dome-flat configuration for larger samples, a noticeable reduction in thermally induced residual stresses should result. This is promising in that it points to a way of reducing stress levels in ceramic-to-metal joint systems through adopting improved interface geometry design.

Since active-metal brazing has been shown in Chapter 2 to be an established and reliable joining technique by many researchers and in previous work within the author's laboratory by Tinsley[7], it was the obvious route to follow to manufacture reliable ceramic to metal joints.

The difference in material properties between stainless steel and Syalon 501 ceramic, and in particular the mismatch in coefficient of thermal expansion, makes these two materials very hard to join because of very high values of thermally induced residual stresses. To get around the problem in practice a series of designs was implemented to keep the residual tensile stresses lower then the strength of the ceramic material. To achieve this the interface design between the steel and the ceramic was varied from 5mm apex domes to 5mm radius dome-flat configurations. The concept of curved interfaces was introduced by Tinsley[7] after the flat interfaced joints he produced proved very weak and non-reliable.

The manufacturing element of the experimental programme therefore consisted of joining double- convex faced Syalon 501 ceramic samples to two stainless steel bars, each with mating concave ends. Joints were manufactured with a range of diameters, with one group of each diameter incorporating a soft metal interlayer at each metal-ceramic interface, while the other group had no interlayers.

To be consistent with the earlier work by Tinsley[7], successful joints were tested in tension to evaluate their strengths.

5.2 Programme of experimental tests

The planning of the experimental programme had to address 4 main requirements in investigating the effect of increasing joint cross sectional area whilst seeking a potential generally applicable, industrially based methodology for manufacturing ceramic to metal joints.

These four requirements comprised:

1. Selection of appropriate materials for metal- to- ceramic joint production and of an appropriate joining method. (See section 5.4 below)
2. Identification of appropriate processing variables and investigation of their roles in facilitating the extension of existing metal-to-ceramic joining technology through an experimental programme of joint production and evaluation. (See section 5.8.4.1)
3. Establishing a technique for manufacturing copper EDM electrodes of complex forms to generate mating metal and ceramic joint interface profiles that might be

generally applicable for all electrically conductive ceramic-to-metal joint systems. (See section 5.5 below).

4 Investigation of contrasting industrial methods for the manufacture of complex metallic interlayers that might again be considered for direct industrial application in the manufacture of ceramic-to-metal joints that contain a metallic interlayer. (See section 5.8 below)

Even before addressing these four requirements, however there follows below an account of the equipment used by the author for the actual joining and testing programme, including changes that had to be effected to existing equipment.

5.3 Equipment used for joining and testing

5.3.1 High temperature annealing facilities

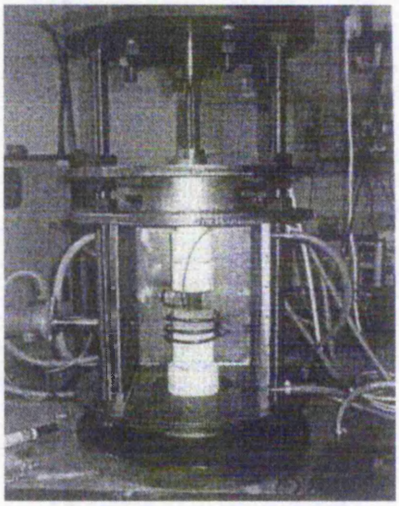

Figure5.1: Heat treatment facility

5.3.1.1 Heat treatment of stainless steel AISI 321

Two facilities were used to anneal AISI 321 stainless steel samples. The first facility comprised an argon-flushed induction heated hot press which, for its normal use in hot pressing ceramic blanks used graphite tooling when working up to 1800ºC. After machining, the 10mm diameter AISI 321 steel members for the joints were annealed at 1050°C for 30min in the heated enclosure of this unit created by retracting fully the upper tooling. This removed the residual stresses created within the steel during bar production and machining to profile.

The remaining AISI 321 steel members having diameters 20mm and 30mm were annealed more conventionally at the same temperature for the same time in an air filled furnace after packing them inside a sealed steel box filled with cast iron turnings to ensure a non oxidising environment. A conventional electric muffle furnace with adequate temperature capability was used. The samples were soaked at a temperature of 1050°C for 30 minutes..

Vickers hardness measurements performed on the stainless steel samples before and after annealing are presented in Appendix [J]

5.3.1.2 Heat treatment of Syalon 501

As ceramic samples had been diamond machined, cut and ground during fabrication. It was thought necessary to heat treat them prior to joining to metal in an attempt to heal or blunt by flow of the glass matrix, any micro-cracks that may have existed, although no major crack was visible after visual examination for those selected to be joined.

When joining Syalon 501 to AISI321 stainless steel Tinsley[7] annealed the ceramic by heating it to a temperature of 1673K for 30 minutes in an inert atmosphere. The present author followed the same procedure.

The induction heated 1800°C hot press described above was used, with up to 5 samples contained within a turned graphite capsule with a tight fitting lid.

The furnace chamber was sealed with fire clay. The chamber was flushed with nitrogen at 8 l/min for 5 minutes, then 2l/min for the remainder of the operation. The samples were heated gradually to 1673 K at a rate of 100K/min.

The annealing temperature was maintained for 30 min then the samples were allowed to cool down to room temperature. The flow of nitrogen was maintained until complete cooling of the samples had occurred, to prevent carbon and the ceramic's titanium nitride from reacting with oxygen from the air.

5.3.1.3 Heat treatment of Cu interlayers

Copper interlayers were annealed in air at 1000K for 30 min. After annealing the copper oxide layer formed was cleaned away in an ultrasonic bath. The hardness value for the copper was 65 HV10kg. This value showed that the annealing operation had worked well by relieving the unwanted stresses accumulated during the machining operations. During heating for brazing at 20°C per minute, the copper was above 1000K for 10 minutes, then held at 1193K for 15minutes before cooling.

The interlayers experienced a further 10minutes before the temperature fell below 1000K. The hardness value of the interlayers might be expected to fall further during this more extreme heating.

5.3.2 Vacuum brazing unit

This research relied heavily on the use of a vacuum brazing unit to join Syalon 501 ceramic to AISI 321 Stainless Steel. The high vacuum induction-brazing unit was able to operate at a temperature up to 1000°C, while maintaining a vacuum at 920°C of 1×10^{-3} mbar during brazing. When cold the system could be evacuated to a 1×10^{-5} mbar. The unit comprised a fused quartz envelope tube of internal diameter 108mm, which enclosed the heating cell, susceptor, anvils, and brazing jig, all manufactured from graphite.

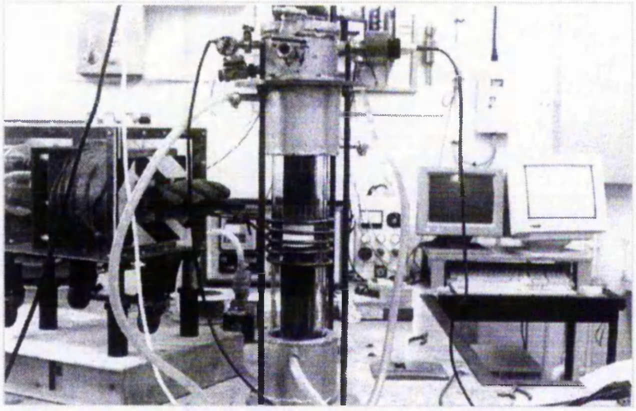

Figure 5.2: Vacuum furnace used for brazing Syalon 501 and AISI 321 stainless steel

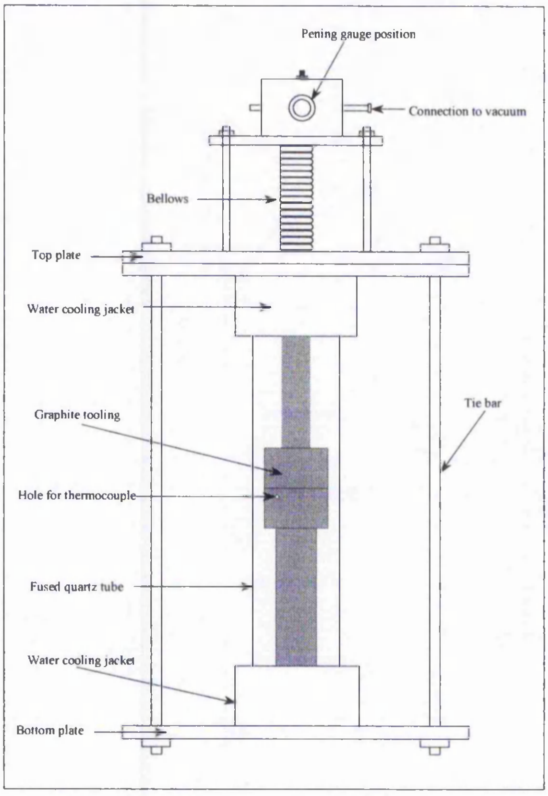

Figure5.3: Line drawing of the vacuum furnace

The two ends were water-cooled. A five-turn copper coil surrounded the quartz tube and transferred power to the graphite susceptor from a 15KW solid state induction generator Ψ

Ψ Radyne type 15 TQ 50, Wokingham, UK

The system provided the option for applying dead loads under vacuum by means of a stainless steel bellows to joints pre-assembled for brazing. The temperature was monitored and controlled by the use of a microcomputer. A second chromel-alumel thermocouple provided independent confirmation of the temperature adjacent to the brazing site.

5.3.3 Carbon tooling

The tooling system for the vacuum brazing unit was made secure by using an aligning system of pegs and holes. This prevented the tooling from moving or falling over and touching the furnace tube wall. The diameters of the carbon susceptor and anvils were selected to create more room in the unit.

In order to accommodate 10mm, 20mm and 30mm joint samples, the present author introduced modifications to the design of the carbon tooling.

The base susceptor was the same for all three types, but three alternative inner sleeves were introduced to accommodate changes in specimen diameter Figure 5.4(c).

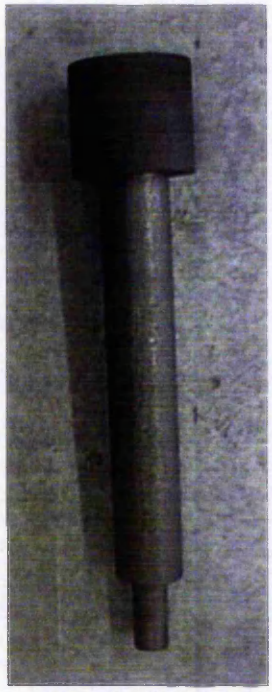

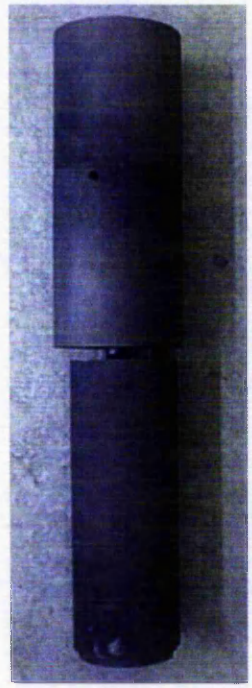

(a) Graphite extension **(b) Main graphite column**

(c) Split graphite brazing fixture

Figure5.4: Graphite tooling

Ceramic and steel constituent parts of each joint had to be joined in excellent alignment with one another. Poor alignment would have resulted in a bending moment during tensile testing and generated misrepresentative results.

Great care was taken during the manufacture of the carbon tooling to ensure close tolerances during machining and sliding fits where appropriate.

A horizontally split susceptor was made to house the ceramic, metal, copper and braze, while a reamed hole through the center of the restrained, vertically split brazing fixture held the joint members in alignment with one another. This graphite fixture was made in two halves for easy assembly and easy disassembly after joining of the steel/Ticusil/copper/Ticusil/ceramic/Ticusil/copper/Ticusil/ steel system.

Along the inner surface of this split carbon sleeve around the joints, a small volume of graphite was removed to prevent any excess braze sticking to the susceptor. A through-hole of 2mm diameter was drilled in the main carbon susceptor to allow a type K thermocouple to be mounted between the 2 metal-ceramic interfaces for accurate temperature measurement and control.

5.3.4 Tensile testing apparatus

The tensile testing of the samples was performed using a 2 tonne capacity multi-ranged motorised screw-driven tensile machine (Tensometer 20) with a digital display of force and extension. The applied tensile force and any resulting crosshead movements during test were recorded automatically on a 2D plotter and the breaking load recorded. Using the values of the breaking load obtained and the projected cross-sectional areas of each specimen the strength of the weakest of the 2 interfaces simultaneously under test was calculated.

To be consistent with the earlier research conducted by Tinsley[7], tensile testing was the preferred method to assess ceramic-metal joints' strengths. It was expected that the mean peak strength for curved interfaces should increase with the use of novel interfaces, since lower residual stresses were predicted in these models.

*Tensometer 20 from Monsanto, UK

5.3.5 Vickers hardness testing facility and Leitz Miniload microhardness testing facility

Standard Vickers hardness tests were conducted on copper interlayers and on the stainless steel member of each joint to check that they were fully annealed before assembly and brazing.

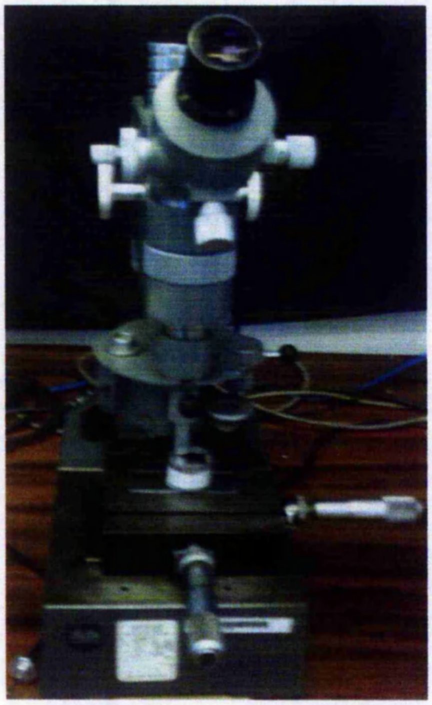

Figure5.5: Leitz Miniload microhardness testing facility

5.3.6 EDM machine and machining parameters

In this research EDM was used firstly to shape Syalon 501 cylinders into double domed (10mm), or double domed-flat (20mm, 30mm) samples. To achieve the required profiles, three EDM machining stages were conducted, starting with a roughing operation, then a semi-finishing operation and finally a finishing operation. In cases where copper interlayers were not used, the ceramic constituent part of each proposed joint was generally used briefly as an EDM electrode to 'burn' it into the AISI 321 steel member after the finishing EDM operation, to achieve a better mating of the interfaces.

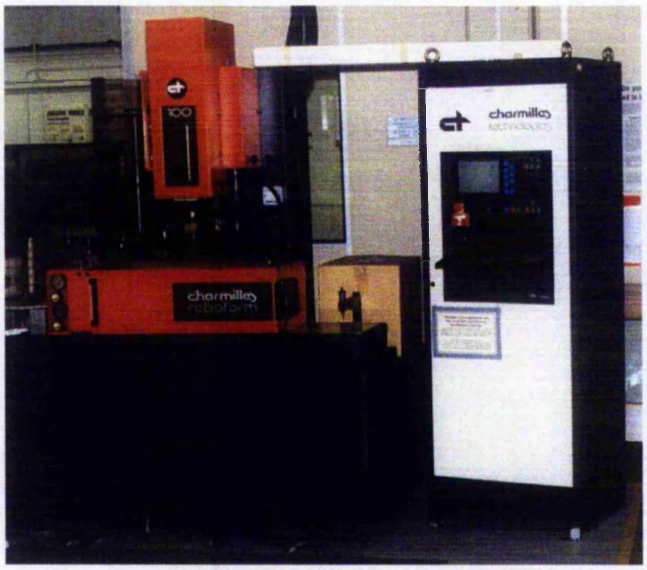

Figure5.6: EDM machine used

Secondly, the EDM machine was used to section finished ceramic/metal and ceramic/copper/metal joints for inspection and evaluation purposes. This approach had the advantage of being non-contact and therefore unable to introduce any post-testing damage. This was because no additional stresses were introduced when cutting through the successive interfaces of ceramic, soft copper interlayer and austenitic stainless steel.

The machine used was a Charmilles Roboform 100. The optimum parameters for EDM machining had to be carefully specified. They depended on the electrode being used, the material to be machined and the surface finish required. Most of the parameters used in this investigation were derived from the work done in the author 's laboratory by Mordecai [117], Trueman[118] and Tinsley[7].

Since the Syalon 501 ceramic samples were to be joined to AISI 321 stainless steel using active metal brazing, it was essential that the machined surfaces had good surface finish. It was also essential that the machining process did not in any way degrade the strength of the material by cracking it or by inducing additional residual stresses to it. Mordecai [117] showed by using 4-point bend tests that the strength of this ceramic was not decreased by EDM machining compared to that of conventionally diamond lapped samples.

Tinsley[7] using parameters shown in (Table 5.0) produced an average surface finish of 2.82 μm (Ra), which was improved further to 2.2 μm (Ra) after 'bead blasting' to remove the recast layer. Bead blasting is an established technique and is widely used in industry. Tiny glass or plastic beads are fired under compressed air to remove attached unwanted surface 'recast' layers.

Table 5.0: -E.D.M parameters used to machine Syalon 501 using copper electrodes

M	V	P	A	RF	T	B	R	U	SV	PR
7	5	7	7	39	1	8	0	9	73	9

Appendix [M] interprets fully the parameters shown in Table 5.0, however it shows essentially that a current of 7 amps was used in association with a pulse duration of 7 ms and a duty factor of 9%.

Care was taken when using a copper electrode with an inner concave profile, not to trap air in its cavity, which would lead to uneven machining, The level of the dielectric had to be relatively high and above the surface of the ceramic at all times to ensure that the tool's regular retraction did not repeatedly break surface to draw air into the confined space between the work piece and the tool's concave inner surface. The presence of air bubbles would have led to uneven machining especially at the tip of the apex of domed samples due to lack of electrical conductivity.

The EDM was computer numerically controlled and hence precision fabrication was relatively straightforward. Before each machining operation the ceramic samples were precisely located in 3-D space by performing a series of edge finds. This involved moving the electrode slowly towards the work piece while the machine was dry (without dielectric) using a low voltage. Current flowed when the electrode touched the part thereby allowing the machine to make measurements. When this operation was completed the tank was filled with dielectric, the flushing switched on and the copper electrode sunk onto the ceramic sample.

5.4 Material selection for the experimental work

The metal to ceramic joint system selected for practical investigation was Syalon 501 to stainless steel AISI 321.

Syalon 501 is a commercially available sialon and a conductive material and thus appropriate for EDM machining. This system was selected for all the experiments which should ideally be conducted in large numbers to allow for experimental scatter. In practice the availability of time and material allowed 40 double interfaced ceramic to metal jointed samples to be manufactured. Section 6.1 describes how these tests were divided between 10, 20 and 30mm samples and how many joints contained soft copper interlayers.

Syalon 501 satisfied the requirement of being electrically conductive and tolerant to EDM, particularly if any inadvertent arcing occurred during normal smooth machining by multitudes of tiny sparks Moreover its electrical discharge machining parameters had been extensively researched by workers in the author's laboratory including Mordecai[117], Mordecai et al[119], Huddleston and Trueman [120] and Trueman [118] alongside previous joining research by Tinsley[7] which also utilised Syalon 501. Mordecai et[119] also investigated the electrical-discharge machining behavior of silicon carbide-based ceramics while Pitman and Huddleston[121] investigated titanium nitride-bearing zirconia and Put et al[122] investigated zirconium dioxide based ceramics containing conductive networks introduced as discrete particles of the nitride, carbide and carbonitride of titanium. Some of these workers also investigated the electrical-discharge machinability of titanium diboride-bearing zirconia and sialons[120, 123]. The commercial availability and more comprehensively researched machinability of Syalon 501, however were significant reasons for selecting this material in preference to those others.

Notwithstanding this, the coefficient of thermal expansion (CTE) mismatch between the ceramic selected (Syalon 501) and AISI 321 exceeds a ratio of 1:3, so successful joining in this ceramic-metal system would amply verify the validity of the EDM interface shaping-for-joining route for systems with less adverse CTE mismatch. This would apply especially when the ceramic is conductive zirconia, which with 30% by volume content of boride, nitride etc. would yield a CTE ratio against commercial carbon steels that was very close to unity. This would reduce almost to zero the residual stresses induced during cooling from the brazing temperature, or generated during thermal cycling in service, which should make this approach to ceramic to metal joining particularly attractive.

5.4.1 Stainless steel AISI 321

AISI 321 has been used by many researchers as the metal constituent in metal-to-ceramic joining research including Tinsley[7] who uniquely joined it in small diameter to Syalon 501. As an austenitic stainless steel it has several attractive properties for its use in such joints including:

- It suffers no potentially disruptive phase changes upon cooling or heating with no risk, as with martensitic steels where large volume changes can promote cracking.
- It maintains a clean surface during elevated temperature joining and service applications up to modest temperatures or where oxygen is largely excluded. It is easily wetted by active metal brazes during joining in-vacuo.
- Its elastic modulus is relatively low, especially at elevated temperature, which allows some plastic deformation to occur adjacent to metal-to-ceramic joints, especially where, as in the current investigation the stainless steel member is machined down to **an easily deformable** featheredge. Thus during cooling from elevated joining temperatures that deformation will provide a partial stress relieving mechanism for residual stresses and consequently should yield higher residual or 'working' strength in those joints.

5.4.2 Active metal braze

The selection of Ticusil as the specific brazing alloy of choice was firstly its commercial availability and secondly its popularity among researchers including Tinsley[7] in his preliminary work to the present investigation. This choice ensured continuity to be maintained with the earlier investigation and trusted techniques to be employed.

Section 5.4 justified the selection of Syalon 501 and austenitic stainless steel AISI 321 as the ceramic-to-metal combination to be investigated with active metal brazing as the joining method. Following Tinsley[7] the active metal braze selected was Ticusil in the form of 0.05mm thick foil. More information concerning this material is summarised in Table 5.1 below.

Name	Nominal Composition	Liquidus		Solidus	
	Percent %	oC -	oF	oC -	oF
Ticusil	Ti - 4.5 Cu - 26.7 Ag - 68.8	850	1562	830	1526

Table5.1: Properties of Ticusil (*Wesgo, Inc Technical Ceramics and Brazing Alloys, 477 Harbor Boulevard Belmont, CA 94002, USA)

The liquidus and solidus temperatures for Ticusil quoted by the manufacturer are 850°C and 830°C respectively, but no detailed advice appeared to be available from them specifically regarding joining silicon nitride ceramics.

It was found from the literature review reported in Chapter 2, however that previous work was conducted using Ag-Cu-Ti type braze to join sialon type ceramics to steels. Chapter 2 reviewed specifically such work by Ven der Sluis [92] and by Santacreu et al[93].

5.5 Design and manufacture of electrodes for EDM

5.5.1 The Electrical-Discharge Machining of Syalon 501

In order to use the EDM machine, specific electrodes had to be designed and manufactured. The electrodes had to contain negative profiles of the required shape to be produced on the ceramic, in this case, concave geometries with dome or dome-flat profiles.

Commercially pure copper was used to make the electrodes for EDM machining, the reasons for using this material were its availability, ease of machining, relative cheapness and, most importantly its electrical conductivity.

The electrodes were used in three important stages of the process of shaping Syalon 501:

1 Roughing operation

2 Semi-finishing operation

3 Finishing operation

Following the first roughing operation, where the ceramic was transformed from a flat-ended cylinder to one with a roughly domed end, the electrode experienced considerable erosion causing it to lose its original shape. Each electrode therefore had to be re-machined intermittently to progressively produce accurately profiled interfaces comprising 5mm-apex dome or 20mm or 30 mm diameter dome-flat ceramic samples.
The detailed drawings for the electrodes used are presented in Appendix [B].

Casts were made of each machined AISI 321 interface using an acrylic setting compound (Figure 15.23); this specifically had low adhesion and shrinkage properties. The casts were subsequently removed and measured using a shadow-graph in an attempt to ensure dimensions were within acceptable limits. The profiles of the Syalon 501 samples were also checked on the shadow-graph and any misshapen profiles were re-machined

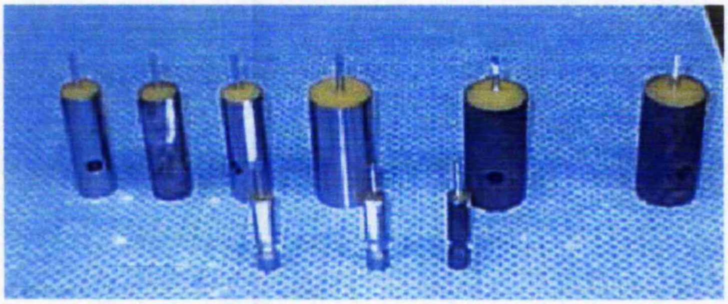

Figure 15.23: Acrylic casts used to measure the curvature of the AISI 321' interface surfaces

5.5.2 Electrode Fabrication

Ball nosed drills were used to machine the desired concave profile on copper cylinders to produce the electrodes. This was a cheap and reliable method, as ball nose cutters are accurately dimensioned, cheap and commercially available in a wide range of sizes. Their use ensures a good machining quality, providing the tool is kept sharp. On the other hand the use of conventional CNC tools would have required special fixtures to hold small components such as 10mm diameter bars. The cutting tools would have been made for conventional lathes with set radii, but the accuracy and reliability would have been in question.

Since the diameter of the smallest ceramic sample used was 10 mm, a 5 mm apex height (hemisphere) was easily obtained in the metal member directly by the use of a 10 mm diameter ball nosed drill.

To allow for machining to proceed on the 44 ceramic test piece's 2 ends without an excessive number of stops for worn EDM electrode reprofiling, 16 cylindrical copper electrodes were made, each having a concave profile machined into one end using the appropriate ball nosed drill. Four were made to machine the 10mm Syalon 501 ceramic samples, 6 for the 20mm diameter samples and 6 for the machining of the 30mm ceramic samples.

5.6 Design and manufacture of test samples

To be consistent with the finite element analysis models 10mm, 20mm and 30mm diameter cylindrical samples were used. The cylindrical shaped samples were beneficial in terms of avoiding edges where stresses might concentrate and also for the manufacture of tooling, as the samples were to be tensile tested and alignment was therefore of concern.

The decision made in this research to assess specimens by tensile testing necessitated the manufacture of double jointed samples so that the steel member could be easily gripped onto the tensile machine. It was anticipated that only one joint would break, the second being available for sectioning for microscopical inspection or microhardness evaluation if required.

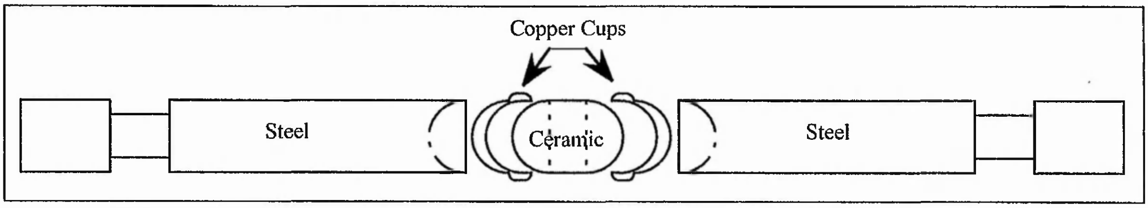

Figure 5.7: Exploded ceramic-to-metal assembly for 10mm samples

5.6.1 Ceramic samples

Each test piece was manufactured from a solid cylindrical rod of the ceramic material, 10mm, 20mm and 30mm in diameter and 15mm or 20mm long.

The EDM machining parameters used to machine the Syalon 501 parts of each joint were reported in section 5.3.6.

Also repeated there were the steps taken to try to ensure accurately machined profiles and interfacial conformity, including the making of acrylic casts from surfaces for measurement at high magnification on a shadow-graph.

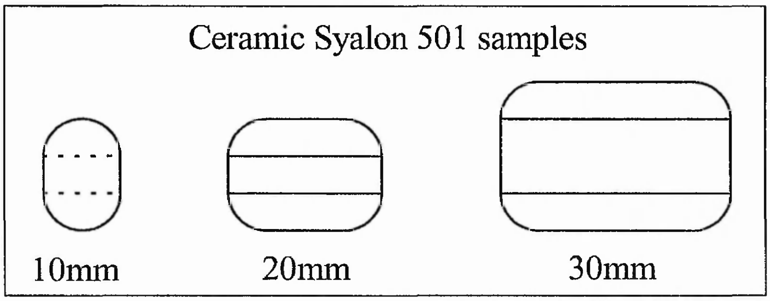

Figure 5.8: Syalon 501 samples after machining into dome and dome-flat Shape shown in elevation view

5.6.2 Manufacture of the stainless steel constituent of each joint

Stainless steel was supplied as machine ground 12mm, 22mm and 32mm diameter bars, which were cut into 65mm lengths and machined conventionally on a lathe to form the

10mm, 20mm and 30mm diameter parts of each joint. The flat steel cylinders were then faced square.

The machining operations to create end profiles comprising 10mm diameter concave domes were carried out on an EMCO Compact 5 CNC station for end profiling.

The faced ends of the bars were centre drilled to a depth of 4mm to ensure centrality. These holes were then opened out by drilling axially with a 3mm slot drill to a depth of 4.5mm then finally machined to a diameter of 10 mm and a depth of 5mm using a ball nose cutter.

The 20mm dome-flat profiles with 5mm radius on the outside and a 10mm central flat area, were again started on a conventional lathe for primary operations then transferred to the EMCO Compact 5 CNC station to achieve the desired final profile.

These bars were again centre drilled to ensure centrality. They were next drilled with a 3mm slot drill to a depth of 2.5mm, then with a 5mm slot drill to the same depth, finishing with a 16mm slot drill to 4.5mm depth. The bars were then transferred to the EMCO Compact 5 CNC station to obtain the desired shape of the 20mm dome-flat concave profile using a milling operation with a 5mm radius ball nose cutter.
In the final operations, not only were the final profiles achieved but also the very fine feather edges were created.

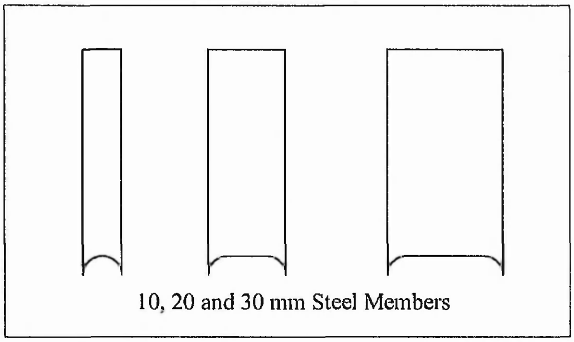

Figure 5.9: The steel members in their finished form, after profiling on the EMCO station

Each of the bars had an 8mm diameter transverse hole drilled through it at a distance of 20mm from the flat non-profiled end of the bar. This hole accommodated the pin securing the specimen into the tensile axis of the tensile testing machine. The 30mm dome-flat profiles with 5mm radius on the outside and a 20mm central flat area, were created on a conventional lathe for primary operations then again transferred to an EMCO Compact 5 CNC station to achieve the desired profile.

Following facing of the ends and centre drilling, the bars were drilled with 3mm slot drill to a depth of 2.5mm then with a 5mm slot drill to the same depth, then with a 16mm slot drill to 4.5mm deep and finally to the required profile on the EMCO Compact 5 CNC station using the 5mm radius ball nose cutter.

It is maintained by the present author that featheredges play an important and original role in joining ceramics to metals in the present investigation. Not only do they deform plastically to allow the metal to accommodate the thermally induced stresses generated during bonding, but also they help to locate and align the ceramic and metal constituents when assembling the parts in the brazing jig.

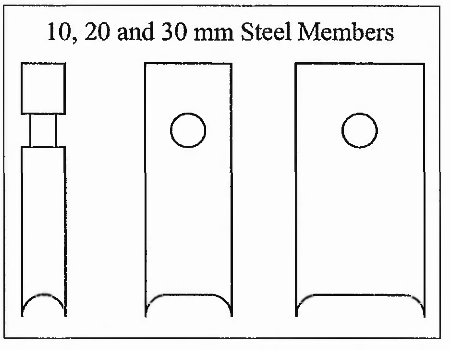

Figure 5.10: The three types of test samples used, including features for tensile testing

As the Syalon 501 samples had already been machined to the desired profile it was decided that these might be used as E.D.M tools, since stainless steel is conductive. 'Burning' the steel member into the ceramic member generally added the benefit of guaranteeing a good match between the two interfaces, ensuring a perfect mating during the brazing operation.

At an early stage in the machining process of the AISI 321 steel members it was noticed that it was physically impossible to machine a perfect 5 mm radius concave hemisphere, or perfect 5mm radius curves for the dome-flat samples in any material since there is a limit to the thickness at which the material will support applied conventional machining loads. The edges in these cases were razor sharp, and the use of an external colette during machining was a near complete solution to prevent the feather edges from 'swaging' out. In cases where the edges were less then perfect, additional thin layers of braze were used.

5.7 Design and manufacture of the drilling jigs

In attempting to ensure perfect alignment during tensile testing it was necessary, among other measures to ensure that the transverse holes that accommodated the pins that secured the steel ends of the joined test pieces to the grips on the tensile testing machine were drilled exactly normal to the specimen's axis of symmetry and exactly on the diameter. To achieve this, two special drilling fixtures had to be manufactured for use on all 20mm and 30mm diameter double-interfaced joint test pieces. Figure 5.11 shows the design of these drilling fixtures that were developed and manufactured by the author. Detailed drawings of the drilling jigs are presented as Appendix [H].

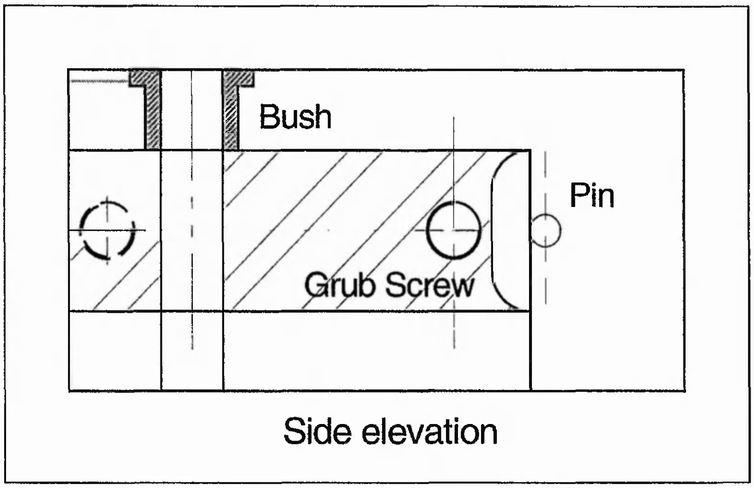

Figure 5.11: Design of drilling jig, used to centrally drill the steel ends of the double-interfaced ceramic-to-metal joint test pieces.

Figure 5.12: Aluminium drilling jigs for 30mm samples

5.8 Design and manufacture of the copper interlayers

The requirement was to make copper interlayers of 2mm thickness which exactly fitted between the two previously machined 10mm hemispheres (or 20mm or 30mm dome-flat profiles) between the convex surfaced ceramic and the concave surfaced stainless steel. Thus the ideal interlayer cross section is shown in Figure 5.13 to be 2mm thick at all points and so terminate in featheredges with parallel vertical sides.

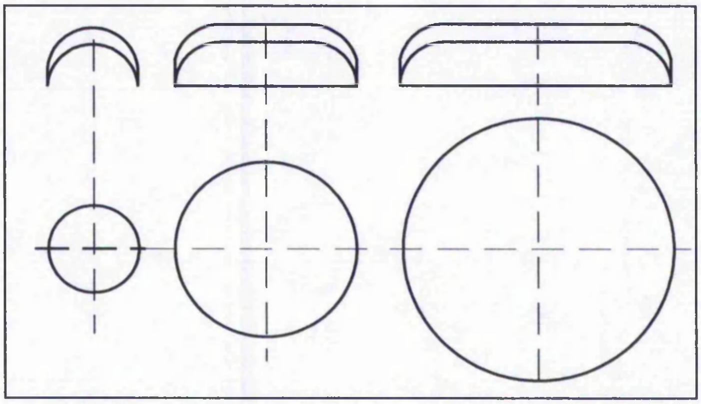

Figure 5.13: Elevation and plan views of ideal copper interlayers for 10mm domes, 20mm and 30mm dome-flat profiles

While it was deemed desirable to obtain as near perfect conformity as possible between ceramic and stainless steel mating profiles in **non** copper-bearing joints by using a final electro discharge machining operation to 'burn' the ceramic (used as an EDM tool) into the curved stainless steel surface, this was not deemed necessary for copper interlayered joints. It was envisaged that the modest bonding pressure used during joining would be sufficient at 920°C ($0.87Tm_{Cu}$) to cause the copper to deform to fully fill the space between the not necessarily perfectly mating ceramic and metal profiles in response to the local high stresses generated at contacting asperities.

5.8.1 Cold and hot copper forming trials

As stated above and in Section 5.2, the fourth aspect of preliminary planning for the experimental programme was to investigate contrasting industrial methods for the manufacture of the necessary soft metal interlayers of complex form.

To shape copper into interlayers suitable for joining stainless steel AISI 321 to Syalon 501 ceramics the following techniques were subjected to preliminary investigation in the order listed:

- cold forming
- hot forming
- die casting
- conventional machining

All four might prove to be capable of producing the desired interlayers where, for example in industry specific machinery and manufacturing expertise might be available, however in the current investigation successful production of a set of suitable interlayers by any of the above techniques would be acceptable.

Figure 5.13 shows the desired finished cross sections for the 10mm, 20mm and 30mm diameter copper interlayers. Two millimetre thick annealed copper sheet was used and discs of diameters 15.71mm, 25.71mm and 35.71mm were blanked from it using a hand operated press. The discs were then annealed at 727°C (1000K) for 30 minutes. The copper discs were presented to the tool sets shown in section in Figure 5.15 that were developed specifically by the author for this operation.

The die and punch used for the 10mm and 30mm samples are presented in Figure 5.14(a, b) and Appendix F contains detailed drawings for die and punches used for 20mm and 30mm samples.

Attempts were first made at room temperature to cold form 5mm copper hemispheres, then 20 and 30 mm dome-flat interlayers by using the punch and die on a fly press. Care was taken to apply the load vertically. Some hemispherical blanks were indeed produced but others were damaged beyond use when attempting to remove them once they had become stuck in the die, even though a pressure sensitive lubricant had been used.

The few interlayers that were produced were found to suffer from severe edge cracking owing to excessive work hardening. In addition the formed blanks were found to be of non uniform thickness, being thinner towards the edge. Other blanks were of incomplete form, having become displaced during forming.

To remove the danger of edge cracking resulting from excessive work hardening it was decided to attempt to produce the required dome and dome-flat forms by hot forming. Here the copper blanks were heated to 750°C in an electric muffle furnace and transferred rapidly to the die. The fly press was again used but it again proved impossible to create formed shapes without edge cracking.

At this point both hot and cold forming trials were discontinued.

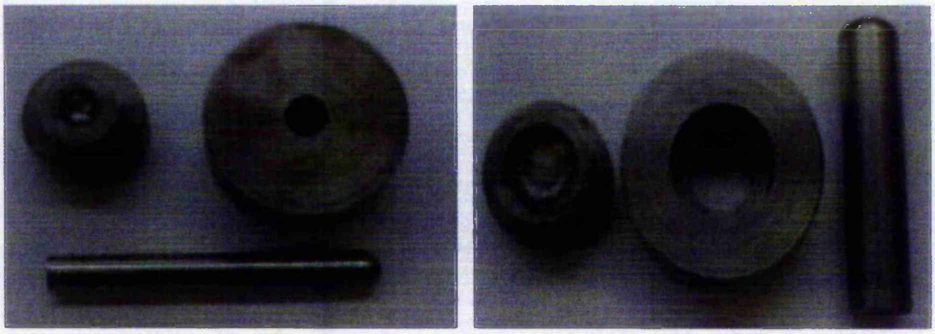

(a) For 10mm Copper discs **(b) For 30mm Copper discs**

Figure 5.14: Punch and die

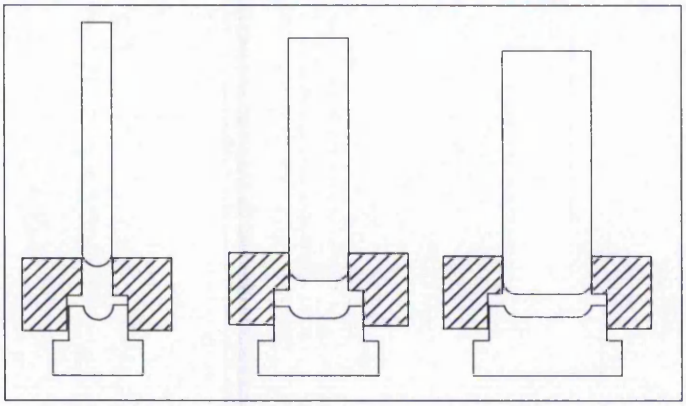

Figure 5.15: Arrangement of die and punch, used in an attempt to blank and simultaneously form the 2mm thick copper interlayers

5.8.2 Shaping of the copper interlayers by casting

Although investment casting was considered and contact was made with a jewellery workshop and with a specialist investment casting company, each expressed doubt that the precise dimensions incorporating the feathered edges required could be obtained. Gravity die casting was therefore selected for the next shaping trials.

A two-cavity prototype die was designed as shown in cross section in Figure 5.16 (a). It was machined from graphite and comprised a central feed sprue, horizontal runners and a single vertical vent rising from the highest point of each cavity. Tight fitting graphite plugs were used as cores to introduce some arbitrary detail to the prototype shape required.

A tight fitting cylindrical slug was placed within the central feed sprue then the temperature of the graphite die containing the copper was raised to 1120°C within an electrically heated muffle furnace. Figure 5.16 (b) shows the form of the solidified casting. Clearly, the convex profile on the frozen sprue indicated poor wetting of graphite by the molten copper. Incomplete filling of both cavities reinforced this point which was further supported by the total absence of copper in the two vents suggesting that the fluidity at the temperatures used may not have been sufficient.

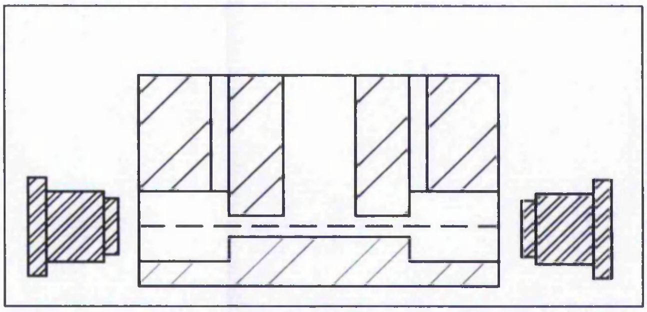

(a) Permanent mould design for casting trial

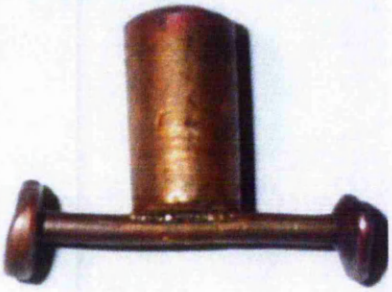

(b) Solidified casting

Figure 5.16: Casting trial

On the positive side, the metal had begun to reproduce some details of the step on the cores' ends and the horizontal 3 mm diameter runners were sound, containing occasional surface depressions, possibly from trapped air or loose debris. The surface finish was smooth and free of oxidation.

A design had been made for a seven cavity industrially inspired seven core split graphite die (see Figure 5.17) to extend the casting trial, however early conventional machining trials, (see section 5.9 (b)) proved successful in providing the forms of interlayers required, so this unit was not manufactured and the casting trials were discontinued.

A greater level of success might have been obtained had facilities for pressure die casting been available.

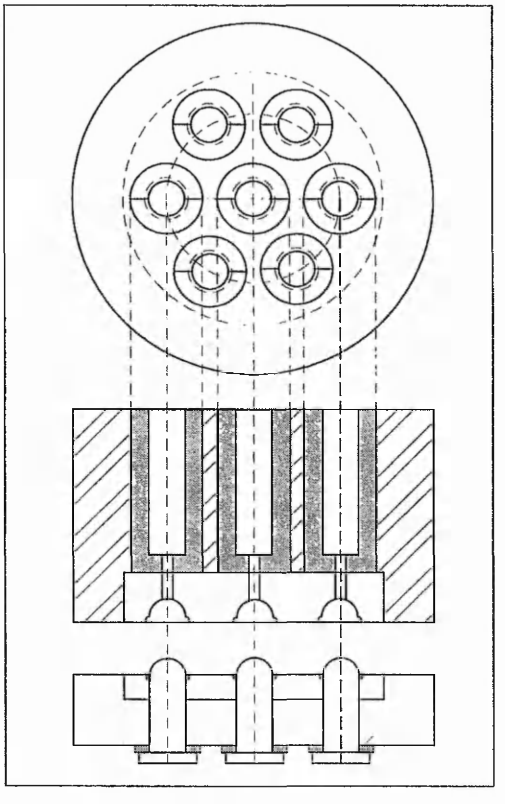

Figure 5.17: Proposed design for gravity die casting of copper cups

5.8.3 Copper shaping using conventional machining

In practice it proved particularly difficult to machine soft copper with feathered edges, so the ideal sections shown in Figure 5.13 were abandoned in favour of those sections shown in Figure 5.18(b) where additional reinforcement was provided. This had the additional benefit of helping slightly to align the constituent parts of the joints more accurately before brazing.

A preferred design for the reinforcement would have been that shown on the left in Figure 5.18(b), for it would have assisted the assembly and perhaps guaranteed even better alignment. This design was rejected however on account of the perceived difficulty in machining the narrow re-entrant.

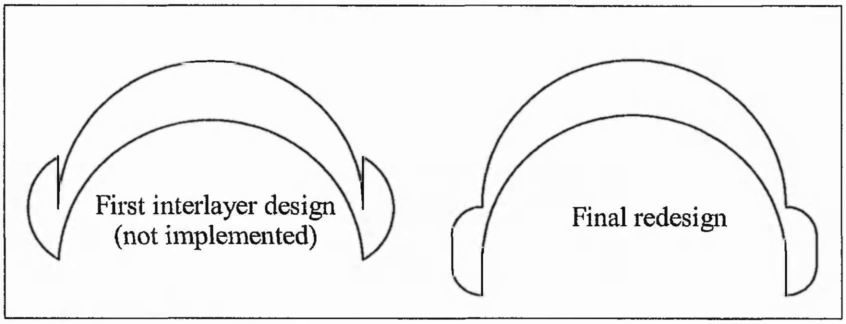

(a) Stages followed in redesigning the 2mm thick copper interlayer

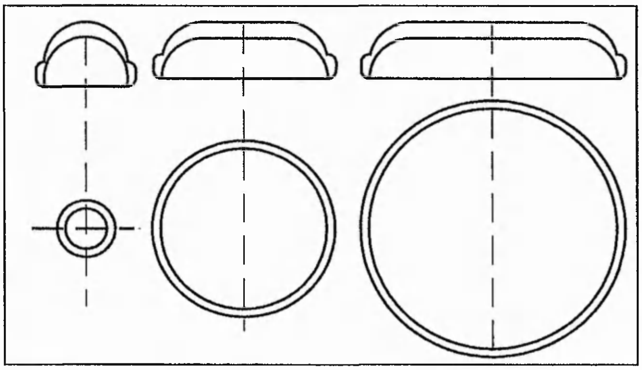

(b) Elevation and plan views of finally adopted design for 10mm domes, 20mm and 30mm dome-flat profiled copper interlayers

Figure 5.18: Development of redesigned copper interlayers

The machining operations to form the profiled copper interlayers are described schematically in Figure 5.19. The 10mm dome, 20mm and 30mm dome-flat interlayers were made from 12.5mm, 22.5mm and 32.5mm diameter bars and each size required the manufacture of a dedicated mandrill.

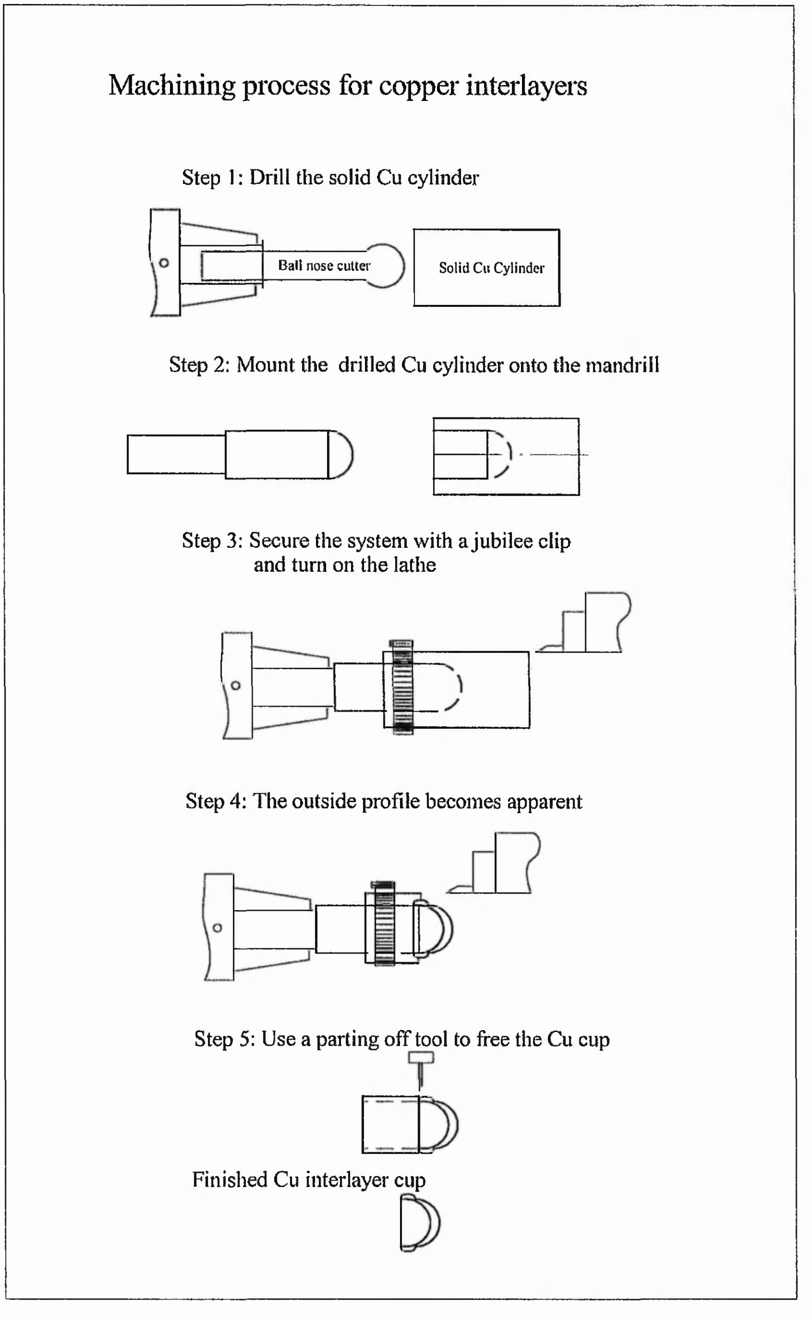

Figure 5.19: Schematic views of manufacturing route developed for 10, 20 and 30mm diameter copper interlayers

Each copper bar was first drilled then finished to final internal profile with a ball nosed cutter, the total depth of 18mm.

The tubular section was split to a depth of 10mm to ensure that the stock could be securely attached to the mandrill using a jubilee clip. With the concave profile complete and perfectly supported, the outer convex profile could be completed with care before the tubular section within the jubilee clip could be parted away from the finished profiled interlayer.

5.9 Bonding procedures

Considering the information and results presented by other researchers, a bonding temperature of 920°C for 15 minutes was chosen for this research investigation. A vacuum of 1x 10^{-3}mbar or better was maintained throughout the brazing operation. For the 20mm and 30mm diameter specimens a dead load of 25N was applied directly onto the preassembled parts being joined through the 50mm diameter bellows, making a combined force from dead load and vacuum pull-down of 221.3N. For the 10mm samples, only the vacuum pull-down force of 196.3 N was used. The heating cycle is presented in Figure 5.20.

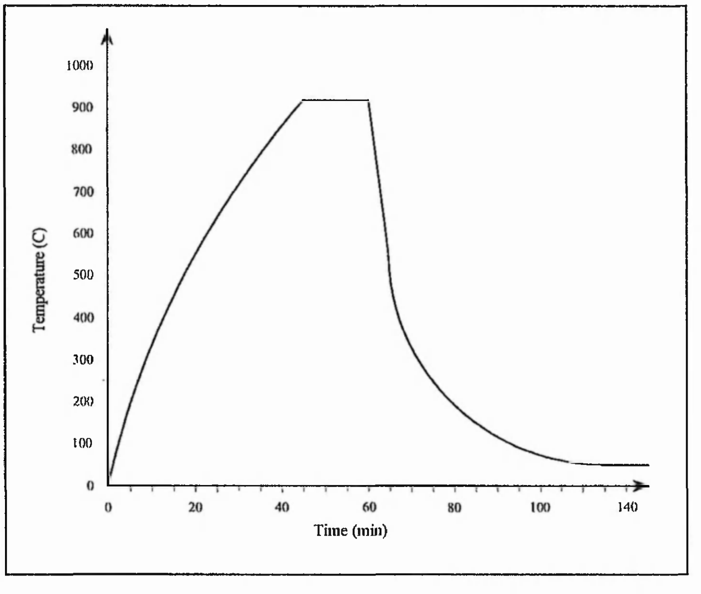

Figure 5.20: Temperature cycle followed during brazing operations

After machining ceramic samples by EDM, their machined surfaces were bead blasted to remove any recast layer but not polished.

Although the finish of the metal interface was not critical the specimens were ground lightly using, 600 then 800-grade emery paper to remove most machining marks. All metal, foil and ceramic parts were then cleaned for 10 minutes in an ultrasonic bath containing inhibisol.

The Ticusil had been cut into discs with diameters 15.71mm, 25.71mm, and 35.71 mm, used respectively for the 10mm, 20mm and 30mm test samples. These disc diameters equated to the interfacial surface areas that were to be covered. To ensure that the entire surface area of the interface was coated with braze, two foils were used per joint, a maximum corresponding braze thickness of 100 μm.

Figure 5.21: Typical system showing steel, ceramic and brazing foil

Braze positioning, was difficult with 5mm dome samples but became relatively easier with increasing sample diameter.

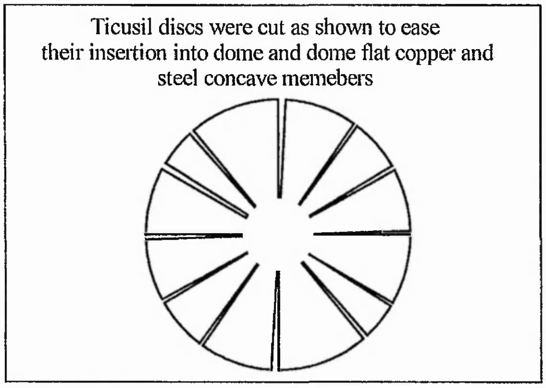

Figure 5.22: Active metal braze discs

Cutting the Ticusil disc into the shape shown in Figure 5.22, helped a great deal in positioning the braze foil within the samples' cavities. This also allowed a better positioning of the joint members as the braze could better assume the contour of the interface while at room temperature.

5.10 Testing and evaluation of joints

5.10.1 Tensile testing

Before the metal-ceramic-metal joints produced by active metal brazing in vacuum were evaluated by tensile testing, appropriate grips and shackles were designed.

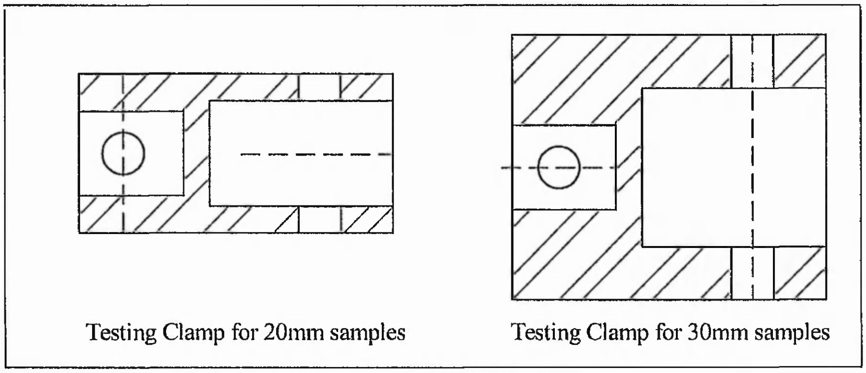

Figure 5.24: Clamp for testing the joints produced

The testing machine used was a motorised Monsanto Tensometer 20 of capacity 2-tonne force. Axiality during testing was ensured through the use of self-aligning pin-jointed couplings. It was necessary to design and manufacture specific tubular and pinned shackles with diameters 20mm and 30mm in order to accommodate the brazed joint test pieces. Figure 5.24 shows the 20mm and 30mm chucks in sectioned view. The full dimensioned drawings to which the chucks were made are presented as Appendix [I].

The best method of attaching the joint to the tensile testing machine was by the use of the existing collet grips. These both had universal joints, which allowed them to self align throughout the test. The mild steel clamps fabricated as shown in Figure 5.24 were used to adapt the machine's collet grips to accept 20mm and 30mm diameter brazed samples. A 'V' block was used to assemble the samples to ensure alignment.

Each brazed joint was then tensile tested using a crosshead speed of 0.5mm/min and the load at breakage was recorded in each case from a digital readout. Force and crosshead measurement were recorded on an x-y plotter

5.10.2 Preparation of sections through fracture surfaces for ceramographic and microhardness examination

All 20mm and 30mm diameter specimens were sectioned perpendicular to the fracture face for ceramographic and microhardness examination. This sectioning was achieved using EDM with a copper sheet electrode used as a sectioning and parting-off tool. Each parted off piece was individually mounted in cold setting compound with alumina powder added first to surround the specimen and preserve its flatness during pregrinding and polishing.

Table 5.1 shows the ceramographic preparation procedure that was used to pre-grind, then polish the sectioned fracture surfaces for examination. Each mounted specimen was ultrasonically cleaned between stages to avoid cross-contamination between the dedicated wheels and polishing discs and cloth used.

Surface	Lubricant Extender	Abrasive Type / Size	Time (min:sec)	Force Per Specimen	Speed (RPM)	Relative Rotation
Ultra-Prep TM	Water	Nickel bond - 40μm Diamond		6Lbs	300	Comp
Ultra-Prep TM	Water	Resin bond - 30μm Diamond	2:00	9Lbs	300	Comp
Ultra-Prep TM	Metadi ® fluid	Metadi® Supreme-6μm	3:30	9Lbs	200	Comp
Trident TM	Mastermet ®	Metadi® Supreme-1μm	4:00	9Lbs	150	Comp
Chemomet ®		Mastermet®	1:00	6Lbs	150	Comp

Table 5.1: Ceramographic preparation procedure recommended by Buehler Ltd., Coventry , UK

5.10.3 Microhardness examination of fractured joints.

Microhardness surveys were conducted on four representative samples. Firstly the 20mm and 30mm diameter Syalon501-AISI321 joints without interlayer,(S3 and S1 respectively) were investigated.

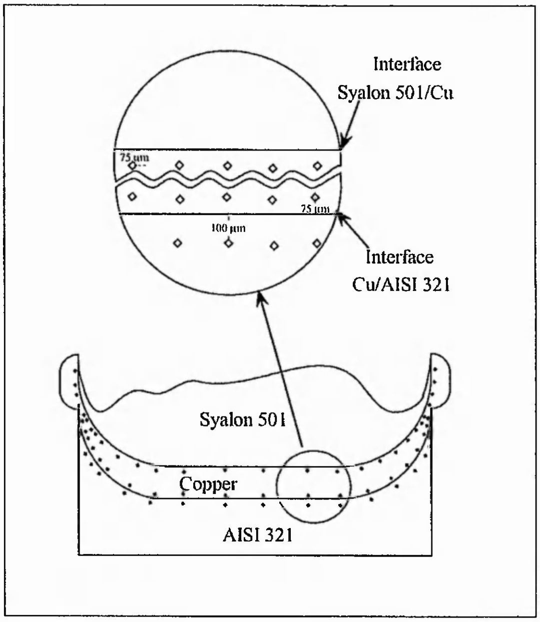

Figure 5.25: Locations of the three microhardness surveys conducted on joints containing copper interlayers

The microhardness surveys were made just 100 ± 10 micrometers inside the stainless steel across the dome –flat profile to determine the extent of differential strain-induced work hardening experienced by the stainless steel.

The second set of surveys was conducted on the 20mm and 30mm diameter samples (S17 and S8) that did contain a 2mm copper interlayer. These surveys again included those conducted 100 ± 10 micrometers inside the stainless steel, again to determine the extent of differential strain-induced work hardening in order to establish whether, and by how much the deformation of the copper interlayer might have shielded the stainless steel from much of the thermally induced strain. In addition, surveys were conducted close to the Cu-AISI321 and the Syalon501-Cu interfaces to assess the levels of work hardening imparted into the copper interlayers, whose function was to shield the ceramic in particular from excessive differential thermal strain-induced stresses and probable fracture. These traverses were conducted within the copper in both cases just 75 ± 10 micrometers from the adjacent interfaces.

A Leitz Miniload microhardness testing machine was used to create the indentation using a 100g load. A digital camera system was mounted on a reflected light microscope and used to view the indentations on a computer screen. This image on the screen could be simulatneously viewed at low magnifications to show the relative positions of microhardness impressions within a group, whilst also allowing accurate measurements of single magnified impressions in a split screen situation.

In all cases the average of three readings were recorded for each indentation. The load used was 100g and the microhardness was recorded as HV100g. Figure 5.25 shows where these microhardness readings were taken.

The results, plotted graphically were used to identify regions where work hardening of the metals took place. These were to be compared with regions of high stress concentration predicted by ANSYS during the theoretical analyses for each model which were presented in Chapter 4.

5.11 Determination of tensile strength, percentage elongation and work hardening ability for annealed copper and AISI 321 stainless steel

In order to characterise both the copper used for interlayers and the AISI 321 stainless steel forming the metal component of the joint, a sample of each was prepared as a tensile testpiece. Appendix [R] shows the specimens to have 20mm^2 and 10mm^2 cross sections respectively.

After machining, the copper test piece was subjected to the same thermal experience as the copper interlayers used, namely an initial anneal at 727°C for 30min, followed immediately by 15min at 920°C before cooling slowly within a sealed steel box. The stainless steel specimen was held at 1050°C for 30min and allowed to cool slowly in a sealed box packed with cat iron drillings. When cool, each test piece was polished carefully, marked up then tensile tested to destruction on a motorised 20KN testing machine using a cross head speed of 0.24mm/s.

After fracture a necked end from each test piece was mounted in cold setting resin and ground down to its centreline using copious flow of cold water on a rotary wheel using abrasive papers.

The microhardness surveys were conducted using 100g and 200g load with special attention paid to the maximum hardness value achieved within the necked region of each testpiece.

The tensile strength and ductility values found for each sample are presented in section 6.3 along with the results of the microhardness surveys.

5.12 Conclusions

An existing furnace brazing facility was upgraded to meet the experimental requirements of this research. The seized bellows system was dismantled and lubricated to ensure efficient transfer of pressure during the brazing operation.

Carbon tooling was redesigned and manufactured. The new design had to accommodate the three sample sizes used. The inner sleeves in each case acted as an alignment device to ensure perfect alignment of the ceramic to metal system during brazing.

The reliable high temperature, high vacuum induction brazing furnace met the experimental requirements needed for the active metal brazing of ceramics to metals. It could operate at a vacuum greater than 10^{-3} mbar and operating temperatures up to 1000°C. It was successfully used to fabricate Syalon 501/Copper/AISI 321 stainless steel joints using a commercially available active metal braze containing Ag, Cu and Ti.

An extensive experimental study was conducted to validate the results predicted by the finite element analysis study conducted in Chapter 4

For profiling the Syalon 501's ends in preparation for brazing, a non-contact method of manufacture was exploited, namely spark erosion or electrical discharge machining (EDM). This took advantage of Syalon 501's electrical conductivity. In addition, this material's 32% per volume of TiN assisted wetting and spreading during brazing and almost doubled the Syalon's thermal expansion coefficient reducing dramatically the differential thermal contraction-induced residual stresses from brazing.

Precision shaping methods for manufacturing curved copper interlayers were reviewed and, after discontinuing casting and hot and cold forming trials, precision machining was adopted.

Some difficulties were encountered during the brazing of metal-to-ceramic joints, but were mainly overcome and many good joints were produced both with, and without copper interlayers. The principal difficulties had been associated with machining ceramic, feather-edged steel and profiled copper interlayers to accurate dimensions and the subsequent alignment of these constituent parts of the double interfaced joints incorporating Ticusil foils.

The experimental programme finally contained 39 tensile tests on double ceramic-to-metal interfaced joints. These tests were divided into 3 main categories. Each category comprised samples of different diameter.

Six joints were fabricated for 10mm samples; in this case all of the joints included copper interlayers as a means of reducing the thermally induced residual stresses. Twenty-two joints were manufactured for 20mm samples, 9 of which did not include copper interlayers while the remaining 13 did. Twelve joints were manufactured for 30mm diameter samples, 4 of which were assembled without copper interlayers, the remaining 8 included them.

Figure 5.26: The stainless steel samples machined ready for joining

Ceramographic preparation was performed on nearly all the fractured tensile test pieces in order to assess the quality of the respective fractured joint to help derive a confidence measure for the tensile strength recorded.

Finally, after characterizing the annealed copper and the annealed stainless steel used, and determining the maximum work hardenability of each by tensile testing, microhardness surveys were conducted in the stainless steel and in the copper interlayers of representative manufactured joints where local thermally induced contraction strains had led to related levels of strain hardening. These microhardness results and their significance in relation to the ANSYS predictions of residual stress induced during joining are presented in Chapter 6.

Chapter 6

Results from Experimental Programme and Discussion

6.1 Introduction

The brazed specimens, each containing 2 or 4 joint interfaces were made using the procedures described in Chapter 5 and were tested to failure in tension. The results of the 5 groups of tensile tests are presented in Tables 6.1 – 6.5. The 5 groups of specimens comprised 20mm and 30mm diameter directly joined samples and 10mm, 20mm and 30mm diameter specimens that contained a dome or dome-flat shaped copper interlayer between each pair of ceramic/stainless steel joints in each test piece. Considerable practical difficulties experienced in the manufacture of all these joints led to a large scatter being observed in the tensile strength results. For this reason a specific review of the tensile performance of **each sample,** as revealed by metallographic / ceramographic examination* is presented in Section 6.2. This review identified those samples that it was felt fell well short of the manufacturing quality standard required, that is, it identified samples which showed defects sufficiently severe as to make their measured strengths unrepresentative. The criteria for rejection included: - non-alignment owing to imperfect assembly, poor wetting and a deficiency of braze materials (particularly when the molten braze had failed to reach the outer periphery of the Syalon/copper interface) and weld lines that had become misshapen through the expulsion of excessive amounts of molten braze.

*For convenience, throughout this chapter, the term 'metallurgical' will be used in connection with the preparation of all metal-to-ceramic joint samples for microscopical examination where metallographic and ceramographic techniques were used.

In the discussion that follows, the tensile testing results that were not disregarded were analysed to determine what trends they revealed and whether those trends could give useful information regarding the possibility of successful design and manufacture of large area ceramic-to-metal joints on an industrial scale.

They should also reveal the level of benefit, if any that 2mm copper interlayers might have on the strength of brazed joints of increasing joint area. In particular, special attention will be paid to the accuracy or otherwise of the ANSYS residual stress predictions made in Chapter 4.

In Section 6.3 the results of microhardness studies conducted on polished sections taken from representative samples of the 4 joint types comprising the 20mm and 30mm diameter joints are presented and their significance discussed.

Finally in Section 6.4 a general discussion is presented which reviews the experimental aspects of the research programme, in particular the practical aspects of joint production, with reference to potential industrial exploitation.

6.2 Metallurgical examination of fractured metal-to-ceramic jointed tensile test samples.

Before presenting a detailed description of the characteristics of each individual fractured tensile test piece, it is proposed to present a more detailed description of just one specimen (the strongest copper-interlayered 20 mm diameter sample, No18) especially with regard to the microstructural aspects relating to the behaviour of the Ticusil braze and the copper interlayer. This will remove the need for much repetition. In samples where no copper interlayer was used, many of the same observations applied but clearly those relating to the role of copper were not seen.

6.2.1 Metallurgical examination of the strongest joint No 18 (Fracture strength 52.58MPa)

The fracture surface exhibited about 14 fracture origins. Figure 6.1 shows the crack profile to be almost symmetrical, the crack from each side dipping then rising sharply.

Figure 6.1:General sectional view of sample No 18

Figure 6.1(a) shows the whole of the stainless steel/copper interface and most of the copper/Syalon interface.

Figure 6.1(a): Detailed sectional view of the whole of the stainless steel/copper interface and most of the copper/Syalon interface. Specimen diameter is 20mm

Figures 6.1 (b) and(c) shows the points of crack initiation on the right and left hand sides to be level with the top of the copper reinforcement and up to one millimeter below that level respectively.

The figure show how the machining accuracy and any plastic deformation required of the copper interlayer had resulted in near-perfect conformity at the two interfaces. The choice of Ticusil (Ag 68.8%, Cu 26.7%, Ti 4.5%) resulted in a little of the copper interlayer being dissolved away at the brazing temperature of 920°C. This had 2 consequences. Firstly it generated a series of cavities, secondly it enhanced the volume of liquid braze available whilst increasing its relative proportion of copper, effectively transforming the liquid from a near-eutectic composition (liquidus 850°C, solidus 830°C) to a hypoeutectic composition (liquidus 920°C, solidus 830°C (or down to 780°C if all the titanium was transferred to the ceramic or stainless steel)).

Figures 6.1(b) and 6.1(c) show respectively the left and right hand sides of the stainless steel feather edge, the machined peripheral 'reinforcement' of the copper interlayer (protruding 1mm proud of the Syalon and stainless steel), the major fracture path and the adjacent minor crack systems.

Figure 6.1(d) shows a close-up view of the Syalon/modified Ticusil interface. Clearly, the braze layer was no longer of 100% eutectic appearance as may have been expected, but showed rounded primary dendrites of copper-rich solid solution set in a matrix of eutectic structure.

The ratio of dendritic to eutectic areas appeared to slightly favour the dendrites. In addition the size of the dendrites appeared to increase towards the top of the copper reinforcement.

The machined dimensions of copper, Syalon and stainless steel coupled with adequate bonding pressure had forced intimate contact to be developed at both the interfaces shown. It should be noted however that a short length of porosity had resulted at the copper/stainless steel interface owing to the dissolution of a little copper in the molten Ticusil. Figure 6.1(e) illustrates this in a magnified view of the left hand edge of the interfaces shown Figure 6.1 (a). Notwithstanding these small voids formed by dissolution in a non-critical area, the appearance of the interfaces in this sample gave confidence regarding the high quality and strength of this joint.

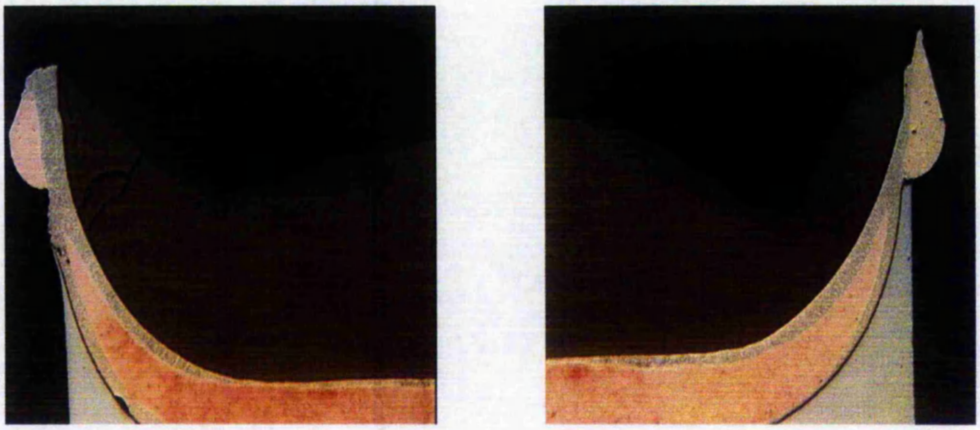

(b) (c)

Figures 6.1(b) & 6.1(c): Left and right-hand sides of the copper-interlayered joint.

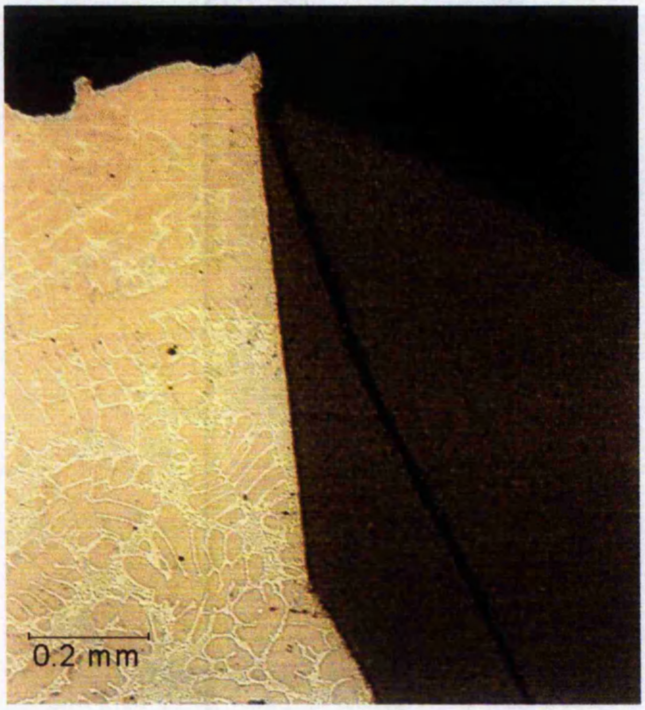

Figure 6.1(d): Close-up of hypoeutectic braze and origin of fracture of Syalon.

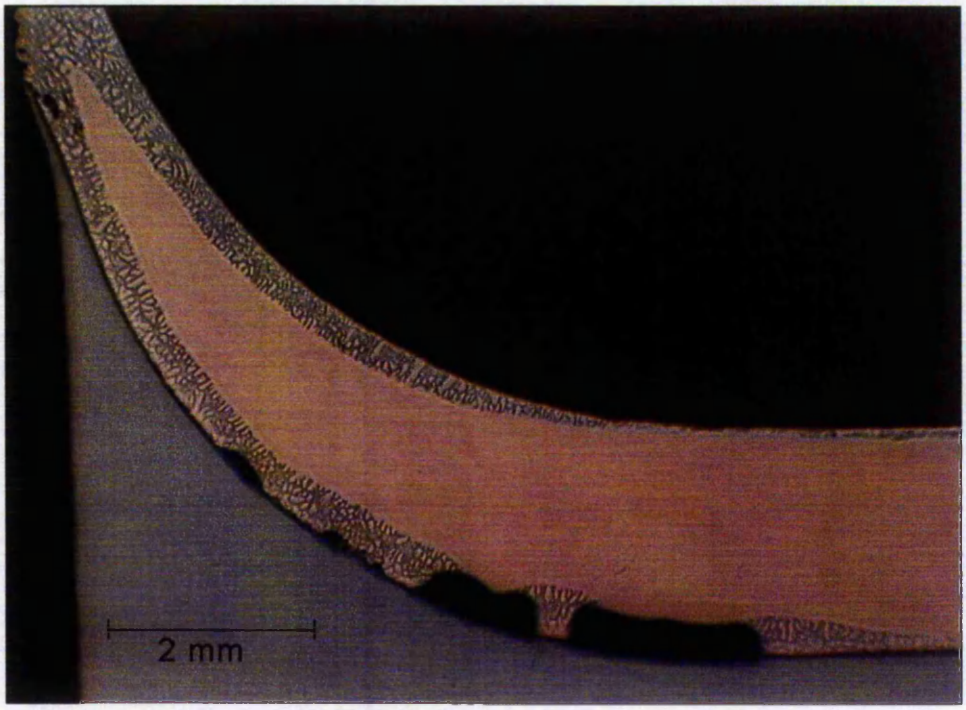

Figure 6.1(e): Magnified view of left hand side of Figure 6.1 (a)

6.2.2 Metallurgical examination of double-interfaced, 10mm diameter samples with copper interlayers.

Specimen 1 Fracture strength 32.47MPa

The alignment of steel and Syalon constituents appeared good, however a small degree of tilting of both copper interlayers was seen. In addition, the critical near-peripheral region of the Syalon/copper interfaces appeared to be slightly incompletely filled. These factors explain the lower than expected strength.

Figure 6. 2: General views of sample No 1 after fracture

Specimen 2 Fracture strength 36.29MPa

The filling of the stainless steel/copper interfaces by Ticusil appeared to be very good while the filling of Syalon /copper interfaces appeared to be satisfactory. However, rotation of one copper interlayer and slight misalignment of the dome-ended Syalon constituent of the joint can be expected to have lowered the strength to 36.29MPa.

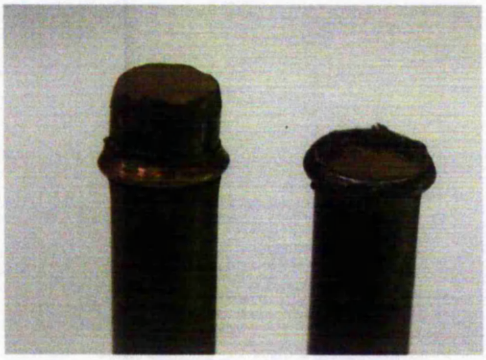

Figure 6. 3: General view of sample No 2 after fracture

Specimen 3 Fracture strength 20.37MPa

The alignment of the five major constituents (2 stainless steel, 2 copper, and Syalon) appeared good, as was the positioning of the two copper interlayers. Although there was again good filling by Ticusil of the stainless steel/copper interfaces, with surplus melt expelled, the Ticusil had again failed to fully fill those critical interfacial regions between Syalon and copper close to the sample's free surface. This appeared to have weakened the joint significantly making this result unrepresentative.

Figure 6. 4: General view of sample No 3 after fracture

Specimen 4 Fracture strength 37.57MPa

This sample showed good alignment of the Syalon and stainless steel but again some tilting of both interlayers was observed.

Figure 6. 5: General view of sample No 4 after fracture

Specimen 5 Fracture strength 12.60MPa

Marked rotation of both copper interlayers had left the Syalon constituent slightly out of alignment with the specimen's main axis. This low strength result was considered to be unrepresentative.

Figure 6. 6: General view of sample No 5 after fracture

Specimen Number	Joint strength (MPa)		Reasons for failure
	Weakest	Strongest	
1	32.47	> 32.47	Slight deficiency of Ticusil at Syalon/Cu interface periphery; slight rotation of both copper cups
2	36.29	> 36.29	Slight misalignment of Syalon component from rotation of one copper cup
3	20.37	> 20.37	Incomplete filling of Syalon/Cu interface periphery
4	37.57	> 37.57	Some tilting of both copper cups otherwise none apparent
5	12.60	> 12.60	Rotation of both copper cups caused the Syalon to be slightly misaligned.
6	2.50	> 2.50	Rotation of both copper cups causing misalignment.
7	R	R	Rejected owing to poor EDM-ed profile (R).
8	R	R	Rejected owing to grinding cracks detected before pre-brazing assembly(R).
9	R	R	Rejected owing to grinding cracks detected before pre-brazing assembly(R).
10	R	R	Rejected owing to grinding cracks detected before pre-brazing assembly (R).

Table 6. 1: Summary of strengths and principal faults in 10mm dome samples with copper interlayers

6.2.3 Metallurgical examination of double-interfaced 20mm diameter samples without copper interlayers.

Specimen 1 Broke on handling, repaired and tested again as Specimen 9, see below.

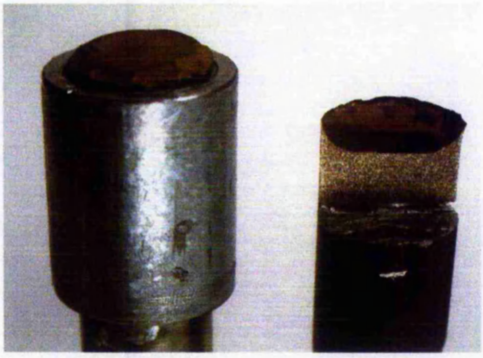

Figure 6. 7: General view of sample No 1 after fracture and sectioning

Specimen 2 Fracture strength 10.82MPa

Unusually, both welds failed simultaneously roughly parallel to the 2 Syalon/copper interfaces, the cracks initiating close to the regions identified as maximum residually stressed regions in the ANSYS analysis. As this was the first sample to be successfully joined by the present author in this study a decision was made to take vertical sections normal to one of the fracture surfaces at positions, 1/2, 1/4 and 1/8 diameter positions. These polished sections are shown in Figures 6.8 (a), (b) and (c). In each section can be seen the excellent conformity achieved by using the EDM-machined ceramic constituent's end as an EDM tool to finish-profile the stainless steel members.

The Ticusil braze appeared to have filled the interfaces satisfactorily, extending as it did to the top of each feather edge.

(a) At position ½ of diameter

(b) At position¼ of diameter

(c) At position 1/8 of diameter

Figure 6.8 (a), (b), (c): Sectional views at 1/2, 1/4 and 1/8 diameter of sample No1

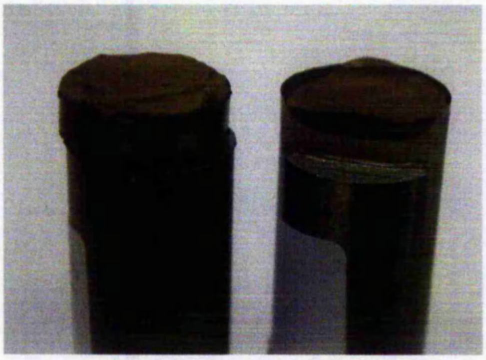

Figure 6.8 (d): General view of sample No 2 after fracture

The low strength observed is believed to result from the control computer crashing as the cooling phase commenced. This necessitated manual control of the induction heater power supply. Before this procedure could be fully implemented, the specimen had experienced a period of excessively fast cooling.

Specimen 3 Fracture strength 18.46MPa

Perfect conformity was again visible as shown in Figure 6.9. Ticusil had wet both constituents and spread effectively across the whole interface. The fracture face exhibited approximately 8 fracture origins around the perimeter. The fracture surface cross-section showed that cracks propagated radially inwards, dipping significantly towards the area of maximum predicted residual compressive stress before veering away upwards on the left hand side and less sharply on the right. A minor crack on the left-hand side (shown here containing polishing compound) terminated after a short distance.

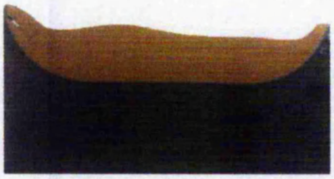

Figure 6. 9: General sectional view of sample No 3 (20mm)

Specimen 4 Fracture strength 6.68 MPa

This specimen failed prematurely during tensile testing. Figure 6.10 shows in general view that two thirds of the fracture surface which, though effectively coated with Ticusil, was unbonded. This must indicate that there was incomplete contact between ceramic and stainless steel. Even the remaining third of the surface that had fractured through the ceramic appeared also to have a trace of void behind part of it. The low fracture strength was therefore explained.

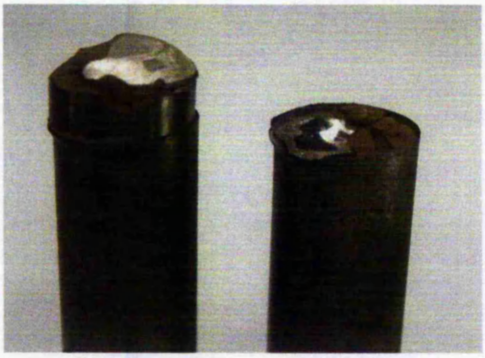

Figure 6. 10: General view of sample No 4 after fracture

Specimen 5 Fracture strength 2.38MPa

The polished section (Figure 6. 11 (b)) shows the fracture surface profile to comprise a crack initiating at each featheredge before dipping downwards then rising again. The section again shows the perfect conformity achieved between the stainless steel and the Syalon at the joint interface. On the section shown the Ticusil appeared to fill the interfacial gap, extending outwards to the perimeter. This situation did not pertain at all points around the perimeter however as some peripheral regions appeared to be free of Ticusil, probably accounting for the unacceptably low strength.

Figure 6. 11 (a): General view of sample No 5 after sectioning

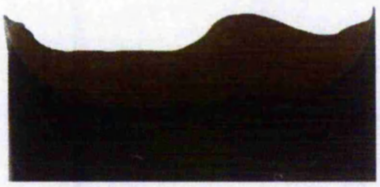

Figure 6. 11 (b): Sectional view of sample No 5

Specimen 6 Fracture strength 1.30MPa

This sample originally broke on handling. By 'repairing' this fracture by sleeving with a close-fitting thick-walled aluminum tube and copious use of epoxy adhesive it was possible to re-tensile test the sample to determine the strength of the previously unbroken joint. The patent weakness of the remaining interface was explained by the fracture surface showing traces of the original machined profile, with some machining marks still visible on the stainless steel which was covered by silvery Ticusil. Clearly, effective bonding of this interface had not been achieved, the fracture resembling Specimen 4.

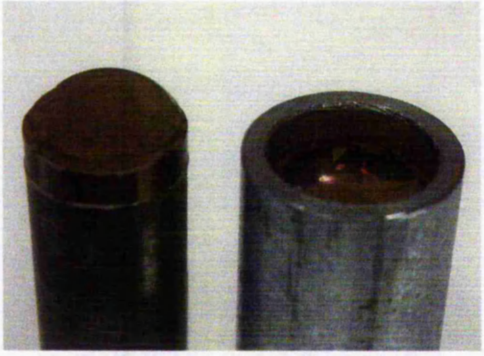

Figure 6. 12: General views of sample No 6 after fracture

Specimen 7 Fracture strength 25.49 MPa

This was the strongest specimen in this group and again showed the effectiveness of using the shaped Syalon's end as an EDM tool for finish-machining the adjacent stainless steel member and producing perfect interfacial conformity (Figure 6.13). This figure also shows the same crack profile that appeared in many of the strongest specimens, that is, cracks initiating at the top surface of the feather edge when the critical peripheral region of the Syalon/stainless steel interface was completely filled with Ticusil. They again tended to travel initially downwards from the featheredge towards the compression zone before veering away and merging near the centerline.

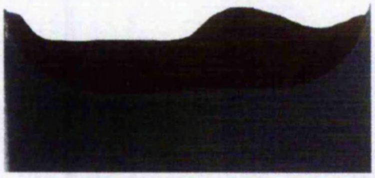

Figure 6.13: General sectional view of sample No 7 (20mm)

Specimen 8 Fracture strength 16.55MPa

This poor result was explained by reference to Figure 6.14 which shows that the 20mm diameter x 15mm high ceramic member had rotated approximately 5 degrees, resulting in up to 75% of the interfacial area comprising a void up to 1mm wide, that was inadequately filled by Ticusil. The Ticusil appeared however to have been drawn as far as the feather edges to give good bonding at these most critical positions. The relatively high, but unacceptable strength was due to those good regions of joint that represented only about 20% of the area.

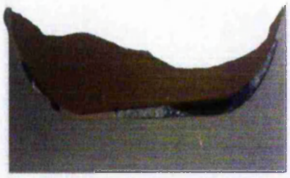

Figure 6. 14: General sectional view of sample No 8 (20mm)

Specimen 9 Fracture strength 1.59MPa

This sample was the repaired Specimen 1. The repair was effected in the same manner and for the same reason as in 20 mm diameter Specimen 6. Figure 6.15 shows that the joint appeared to be imperfectly assembled owing to rotation of the Syalon member out of alignment by 3 or 4 degrees to generate a gap, up to 0.7 mm wide and about 9mm long. The Ticusil did appear however to have flowed to the top of the featheredges though the specimen still appeared to be very weak. The fracture appeared to have initiated from about 8 points around the perimeter of the interface. Like Specimen 2 this sample had experienced a period of uncontrolled rapid cooling (estimated to be about 60°C/min), this time resulting from a power failure. This strength value was deemed to be unrepresentative.

Figure 6. 15: General sectional view of sample No 9 (20mm)

Specimen Number	Joint strength (MPa)		Reasons for failure
	weakest	strongest	
1	BOH*	See No 9	Rapid cooling
2	10.82	> 10.82	Rapid cooling
3	18.46	> 18.46	None apparent
4	6.68	> 6.68	Inadequate pressure gave only 30% interfacial contact
5	2.38	> 2.38	A little incomplete filling of interface at periphery
6	1.30	> 1.30	Inadequate wetting and spreading except at periphery
7	25.49	> 25.49	None apparent
8	16.55	> 16.55	Misalignment; poor conformity; very large void at the interface, but bonded around periphery
9	See No 1	1.59	Rapid cooling

Table 6. 2: Summary of strengths and principal faults in 20mm dome-flat samples without copper

BOH* = Broke on handling

6.2.4 Metallurgical examination of double-interfaced 20mm diameter samples with copper interlayers.

Specimen 10 Fracture strength 34.69 MPa

The fracture surface exhibited about 12 fracture origins spaced approximately evenly around the perimeter. The specimen showed that slight rotation of both copper interlayers had occurred. Figure 6.16. shows that two major crack deflections had occurred during tensile fracture. The cracks originating from each side propagated from the top level of the Ticusil which was situated 1.5 – 2mm below the top rim of the copper reinforcement section of the soft metal interlayer. The figure shows some deficiency of Ticusil in the non-critical central section of the interface.

Figure 6. 16: General sectional view of sample No 10 (20mm)

Specimen 11 Fracture strength 30.08 MPa

Unusually, this specimen fractured simultaneously at both joints. The two fracture surfaces appeared to show 11 and 12 fracture origins respectively. Figure 6.17 shows that incomplete filling of the peripheral Syalon/copper interface had occurred at one point on the left of the figure to a depth of 6mm below the top of the copper reinforcement. This major defect can be assumed to have lowered the sample's strength significantly.

Figure 6. 17: General sectional view of sample No 11 (20mm)

Specimen 12 Fracture strength 42.65 MPa

The fracture surface exhibited about 14 crack initiation sites. Figure 6.18 (b) revealed that the Ticusil filled both interfaces very well indeed, with the excess expelled all round the perimeter of the fractured joint. This was supported by the absence of any gaps at the interface due to rotation of the interlayer or to non-conformity between stainless steel, copper and Syalon. The fracture face showed a fracture path, which initiated, as required from near the top of the copper reinforcement. The major crack from one side dipped slightly towards a compressive region before moving upwards and away while that from the other side dipped then continued approximately horizontally before merging with the crack approaching from the other side. The appearance of the fractured specimen suggests that this joint may have approached its full strength potential.

(a),

(b)

Figure 6.18 (a), (b): General sectional view of sample No 12

Specimen 13 Fracture strength 4.32 MPa

The alignment exhibited by the Syalon and copper components of the double-jointed specimen appeared less than perfect. The machined dimensions of the copper interlayer situated adjacent to the fracture surface appeared to be incorrect as it did not sit properly in the machined recess within the stainless steel. A large gap, up to 1.5mm wide and about 14mm diameter resulted at the stainless steel copper interface.

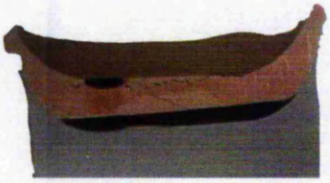

Figure 6. 19: General sectional view of sample No 13 (20mm)

The fracture surface profile was almost horizontal, that is, cracks showed very little deflection. Within the copper interlayer a hot tear appeared between the copper and the adjacent copper-diluted Ticusil. This specimen's result was unacceptable, as it was not representative of what can be achieved with correct bonding conditions.

Specimen 14 Fracture strength 6.78 MPa

The fracture surface appeared to show about 10 points of crack initiation and the fracture surface profile was almost horizontal. The specimen exhibited slight non-alignment which was again due to the rotation of one of the copper interlayers. Ticusil, however appeared to have filled the critical near-featheredge areas and the fracture origins were close to the top of the copper reinforcement.

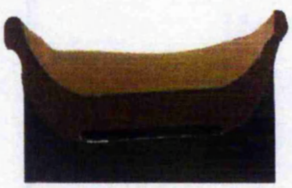

Figure 6. 20: General sectional view of sample No 14 (20mm)

The low strength was presumed to be the result of the slight misalignment, the large central void shown in the figure 6. 20 appearing to play no part in the fracture.

Specimen 15 Fracture strength 5.72 MPa

The fracture surface appeared to show about 11 points of crack initiation. Good conformity was shown between the ceramic, copper and stainless steel surfaces with fracture initiating below but close to the top of the copper reinforcement. The specimen also exhibited slight misalignment. Uniquely, the specimen failed almost diagonally across the ceramic member.

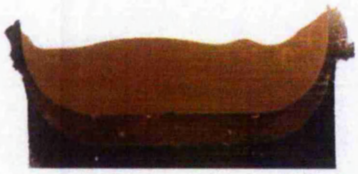

Figure 6. 21: General sectional view of sample No 15 (20mm)

This result can again be discounted as being non-representative on account of the misalignment.

Specimen 16 Fracture strength 29.23MPa

Figure 6.22 shows that the copper interlayer was incorrectly seated and appeared to have rotated by about 5-10 degrees. The copper reinforcement region on the right-hand side was resting 1mm above the level of the steel's featheredge, suggesting that inadequate pressure was used or that the dimensions of the copper were incorrect. Ticusil had filled the Syalon/copper interface completely however.

Figure 6. 22: General sectional view of sample No 16 (20mm)

Secondary cracks meeting the Syalon /copper interface were stopped, probably by localized plastic deformation at crack tips, that is dislocation activity in the copper or Ticusil.

Specimen 17 Fracture strength 29.28 MPa

The fracture surface exhibited about 15 fracture origins. Ticusil had excellently filled the whole interface and appeared therefore not to have allowed the formation of a notch. Figure 6.23 shows the fracture surface to be symmetrical with the fracture on both sides starting level with the top of the copper reinforcement, then dipping down before finally rising to merge cleanly at the specimen's centre line.

Figure 6.23: General sectional view of sample No 17 (20mm)

As with a number of the sectioned specimens examined under the microscope, this specimen showed some minor cracks leaving the main crack and branching before terminating at the copper or Ticusil interface where they were stopped probably by localized plastic deformation and energy absorption in one or both of the latter.

Specimen 18 Fracture strength 52.58 MPa (Also reviewed in Section 6.2.1)

The fracture surface exhibited about 14 fracture origins Figure 6.1 shows the crack profile to be almost symmetrical, the crack from each side dipping then rising sharply. The machined dimensions of copper, Syalon and stainless steel coupled with adequate bonding pressure had forced intimate contact to be developed at both the interfaces shown. It should be noticed however that a short length of porosity had resulted at the copper/stainless steel interface owing to the dissolution of a little copper in the molten Ticusil.

Figure 6.1: General sectional view of sample No 18 (20mm)

The figure shows the points of crack initiation on the right and left hand sides to be level with the top of the copper reinforcement and up to one millimeter below that level respectively. Notwithstanding the small voids formed by dissolution in a non-critical area, the appearance of the interfaces in this sample gave confidence regarding the high quality and strength of this joint.

Specimen 19 Fracture strength 11.65 MPa

The fracture surface exhibited only about 6 fracture origins and the crack profile was almost flat. All the fracture origins were on that side of the specimen which showed an excessively large gap at the Syalon/copper interface around much of the interface perimeter. This gap between Syalon and copper (not shown fully in Figure 6.24) extended over approximately one third of that interface. This gap was not able to be filled as the amount of available molten Ticusil was insufficient, even after the liquid's volume was increased by a little dissolution of copper from the solid interlayer.

Figure 6.24: General sectional view of sample No 19 (20mm)

The stress intensity factor of this 'notch', supplemented slightly by the reduced interfacial area effect explains the unrepresentative low strength of this sample.

Specimen 20 Fracture strength 25.14 MPa

The fracture surface exhibited about 21 fracture origins spaced equally around the perimeter and the fracture surface was almost flat. The Syalon member was seen to have been rotated out of alignment by one of the shaped copper interlayers on which it sat.

There appeared to be sufficient Ticusil in the critical peripheral areas around the featheredge in both the Syalon/copper and the copper /stainless steel interfaces.

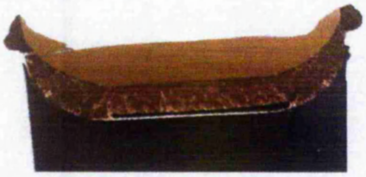

Figure 6. 25: General sectional view of sample No 20 (20mm)

Figure 6.25 shows the central parts of the copper /stainless steel interface to be incompletely filled. This figure also shows that, uniquely, a crack had passed through the copper interlayer at its narrowest point. It was felt that the tensile strength of 25.14MPa might be unrepresentative owing to the specimen's misalignment.

Specimen 21 Fracture strength 30.08 MPa

The fracture surface exhibited about 15 fracture origins distributed almost uniformly around the perimeter. Alignment within the specimen appeared good. Figure 6.26 shows the fracture path to pass 2- 3mm below the top of the copper reinforcement and to show little sign of deflection. Study of the fractured parts revealed that the fracture started level with the top of the Ticusil, where the latter had not spread to the top of the reinforcement.

Figure 6. 26: General sectional view of sample No 21 (20mm)

A little dissolution of copper at the Syalon/copper interface well away from the perimeter had neither affected the strength nor contributed to the fracture. The fact that this sample fractured about 2mm below the top level of reinforcement identifies this position as being very close to the point of maximum residual stress as indicated on the ANSYS plot. It had been more common in the samples tested to find the strongest ones broke at a level 2-3mm higher inside the ceramic, i.e. level with the top of the copper reinforcement but 2mm along the parallel part of the ceramic member's length.

Specimen 22 Fracture strength 25.27MPa

The fracture surface exhibited about 7 fracture origins. While wetting and spreading were good on one side of Syalon/copper interface they were relatively poor at the diametrically opposite position where a 3-4mm length of the curved profile remained unwetted. Figure 6.27 shows how this resulted in an asymmetric fracture surface.

Figure 6. 27: General sectional view of sample No 22 (20mm)

Specimen Number	Joint strength (MPa)		Reasons for failure
	weakest	strongest	
10	34.69	> 34.69	Deficiency of Ticusil at interface periphery
11	16.23	> 16.23	Slight misalignment and copper reinforcement misshapen by globules
12	42.65	> 42.65	None apparent
13	4.32	> 4.32	Misalignment and poor interface conformity
14	6.78	> 6.78	Slight misalignment and misshapen copper reinforcement
15	5.72	> 5.72	Slight misalignment and misshapen copper reinforcement
16	29.23	> 29.23	Slight misalignment
17	29.28	> 29.28	Slightly misshaped copper reinforcement otherwise none apparent
18	52.58	> 52.58	None apparent
19	11.65	> 11.65	Incomplete filling of Syalon/Cu interface at periphery.
20	25.14	> 25.14	Slight misalignment
21	30.08	> 30.08	Incomplete filling of Syalon/Cu interface at periphery.
22	25.27	> 25.27	Incomplete wetting and spreading of Ticusil at part of Syalon/Cu interface periphery

Table 6. 3: Summary of strengths and principal faults in 20mm dome-flat samples with copper

6.2.5 Metallurgical examination of double-interfaced 30mm diameter samples without copper interlayers.

Good alignment during assembly was easier to achieve with this group of samples because, not only were there no copper interlayers to rotate or fit badly, but the 20mm diameter flat-based areas allowed easier perpendicular stacking.

Specimen 1 Fracture strength 3.74 MPa

This fracture surface exhibited only about 4 fracture origins. Like the 20mm diameter copper-interlayered sample Number 11, this sample also fractured diagonally across the ceramic component. Figure 6.28 shows the fracture on the right hand side to have passed through the parallel-sided part of the sample about 3mm above the featheredge. On the other side the crack ran level with the featheredge.

The figure shows a section in which relatively poor peripheral interface conformity appeared well compensated for by ample filling by Ticusil, excepting a 3mm length of porosity set back 2.5mm from one side. One 5mm long crack started at this pore. It rose slightly before being brought to rest, presumably by local compression.

Figure 6.28: General sectional view of sample No 1 (30mm)

A more general study of the fractured pieces, however showed that the principal source of weakness lay at the other interface where a poor conformity existed over about one third of the interface area where a 0.5 mm gap had remained unfilled owing to insufficient availability of Ticusil. This poorly bonded area at the weaker interface must explain this specimen's low strength. The other interface can be assumed to have been significantly stronger.

Specimen 2 Fracture strength 0.17MPa

Uniquely, the fracture surface revealed an extensive unbonded area extending well down the curved surface to 6mm below the tip of the featheredge. The cause appeared to be a serious deficiency of Ticusil to fill the gap. A study of the fracture surface suggested that this might constitute the only fracture origin.

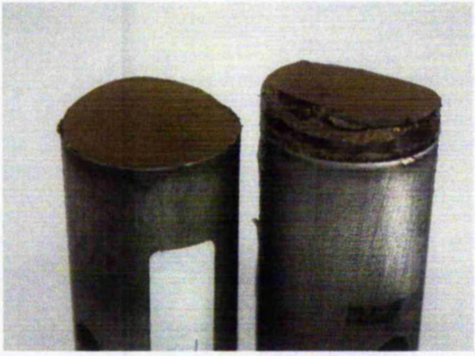

Figure 6.29: General sectional view of sample No 2 (30mm)

Alternatively, the initial fracture origin may have been located diametrically opposite to this region and might have been a small manufacturing defect in the ceramic. Obviously little importance should be placed on the very low indicated strength of this sample.

Specimen 3 Fracture strength 16.76 MPa

The sample showed a small amount (1-2degrees) of misalignment of the Syalon component with respect to the stainless steel. The fracture surface appeared to show about 4 fracture origins. Figure 6.30 shows the most striking feature to be the existence of an extremely large area (about two third of the total) of unbonded Syalon/stainless steel interface, notwithstanding the excellent level of wetting and spreading on both surfaces by the molten Ticusil. Remarkably, the depth of penetration achieved by a paper 'feeler gauge' was 21mm from the top of the exposed featheredge. The total diametric unbonded distance measured along the ceramic surface was calculated to be 35.7mm.

Only the lower interface in Figure 6.30 therefore appeared to be well bonded, its perimeter appearing clean with an attractive miniature and shiny Ticusil fillet running all around it. The other was bonded over only one third of the interface plus a contribution from a superficial joint at the extreme periphery of the unbonded region.

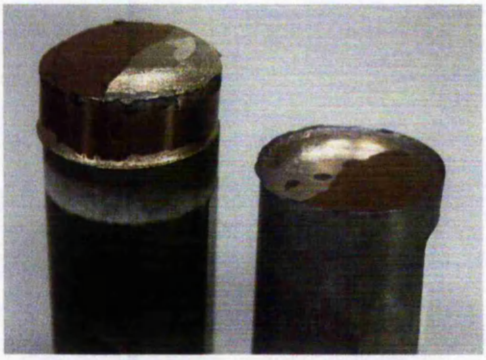

Figure 6.30: General sectional view of sample No 3 (30mm)

Specimen Number	Joint strength (MPa)		Reasons for failure
	weakest	strongest	
1	3.74	> 3.74	Poor conformity as not burnt in
2	0.17	> 0.17	Poor conformity and large cavity at Syalon/Cu interface
3	16.76	> 16.76	Poor conformity and large cavity at Syalon/Cu interface

Table 6. 4: Summary of strengths and principal faults in 30mm dome-flat samples without copper

6.2.6 Metallurgical examination of double-interfaced 30mm diameter samples with copper interlayers.

Specimen 4 Fracture strength 2.87 MPa

The fracture surface of this weak specimen exhibited only about 4 fracture origins located close to each other. These fracture origins appeared to be set back by up to 3mm from the normal top of the copper reinforcement. The expulsion of a significant volume of molten Ticusil, probably diluted by dissolved copper had broadened the copper reinforcement at this point by up to 3 mm. This explains why the fracture originated on the surface of the parallel section of the ceramic some distance from the weld. Figure 6.31 shows that excellent conformity was achieved at the Syalon/copper and copper /stainless steel interfaces. This indicated that machining accuracy was good, that bonding pressure was adequate and that any necessary plastic deformation required in the copper had been achieved. The figure shows a surface fracture profile that dips and rises only slightly. On the left-hand side fracture appeared to originate level with the top of the copper reinforcement, but on the other side passed about 1mm below that position.

Figure 6. 31: General sectional view of sample No 4 (30mm)

Two secondary cracks on each side terminated in the Syalon/copper interface and another ran nearly parallel to and up to 2mm away from the central 22mm of the interface in a manner first illustrated by Suganuma[15]. The copper interlayer contained two spherical cavities of 2mm diameter; these in turn were associated with areas of partial melting. The misshapen form of the copper reinforcement is likely to be the cause of the unrepresentatively low strength of this sample.

Specimen 5: Retained in unbroken form

Specimen 6 Fracture strength 1.05MPa

The fracture surface revealed about 23 fracture origins distributed evenly around the perimeter. The Syalon/copper interface exhibited incomplete wetting and spreading of the molten Ticusil and a gap was seen between the Syalon and copper that extended over most of the curved area of the interface. Two interesting features were observed within the copper interlayer. Firstly, much of the copper reinforcement at the end of the copper/stainless steel interface had been carried away by molten Ticusil, though the copper at the copper/Syalon interface had not been affected. Secondly a continuous narrow region of porosity ran within the copper, parallel to nearly all of the copper/stainless steel interface and touched it occasionally. It resembled a hot tear.

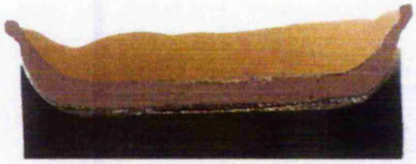

Figure 6.32: General sectional view of sample No 6 (30mm)

Figure 6.32 shows this defect and also proved that the copper/stainless steel interface had experienced shear at about 900°C with the steel contracting slightly more then the copper, This does not necessarily indicate that the thermal expansion coefficient of steel is greater than that for copper,(for it is not), but that the dynamic effect of cooling (the steel cooling faster than the copper and adjacent low thermal conductivity Syalon), must have given that same effect.

The poor wetting and spreading by Ticusil, and the incomplete filling of the Syalon /copper interface made the recorded strength of 1.05 MPa unrepresentative.

Specimen 7 Fracture strength 1.06 MPa

The fracture surface showed about 13 fracture origins distributed around the perimeter. The principal fracture origin however appeared to coincide with an area of enhanced reinforcement caused by excessive localised expulsion of molten Ticusil (probably containing dissolved copper). The alignment of stainless steel, Syalon and one copper interlayer appeared good though there was slight rotation of the second copper interlayer within the unbroken joint. Interfacial conformities were excellent throughout, however one 2mm long cavity had formed in the copper at the Syalon/copper interface as a result of dissolution by molten Ticusil.

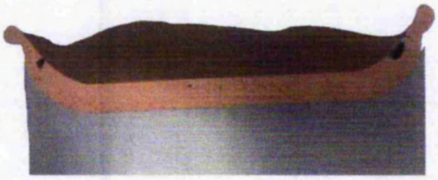

Figure 6.33: General sectional view of sample No 7 (30mm)

Figure 6.33 shows that while fracture passed through the Syalon level with the top of copper reinforcement on the left, it passed 3mm lower on the right, very close to the cavity described above within the copper. There was some dissolution of the copper reinforcement adjacent to the fracture origin and more adjacent to the unbroken interface. As with Specimen 6 the strength value of 1.06MPa recorded for Specimen 7 was considered to be unrepresentative.

Specimen 8 Fracture strength 8.78MPa

The fracture surface showed about 8 fracture origins, the largest forming a crack front that traversed about 80% of the specimen's cross section. This major crack surface exhibited river markings emanating from a fracture origin on the as-ground parallel-sided part of the specimen, almost mid-way between the two joints, that is about 2mm away from the nearest copper reinforcement and coincided with the location of the lower end of a 2mm long globule of surplus Ticusil that was expelled from the Syalon/copper interface of the 'unbroken' adjacent joint. The local stress concentration thus created was the most likely reason for fracture initiation at this point. Alternatively it is conceivable that a small manufacturing defect may have been exposed by the centreless grinding or this surface, or that a surface crack might have been generated by the grinding itself, however neither type of defect had been detected when the samples were examined prior to assembly for joining. One cavity 1.5mm long x 1.5 mm wide was situated within the copper close to the periphery of the Syalon/copper interface seen on the left side of Figure 6.34. The cavity was caused by the localised dissolution of the copper by molten Ticusil. This cavity may have influenced the formation of a localised and relatively complex system of cracks observed within the adjacent Syalon. Figure 6.34 shows that, on the right-hand side the fracture path passed from the top of the copper reinforcement before dipping down then rising sharply before meeting the essentially horizontal major crack referred to above. This right-hand fracture origin was one of about 6 located closely together and diametrically opposite to the major crack's origin. These right-hand side origins were all located level with the top of the copper reinforcement.

Unfortunately, a 10mm long by 2mm wide region of unbonded peripheral Syalon/copper interface was situated next to these 6 closely grouped initiation sites, effectively increasing the number of sites to 7.

Figure 6. 34: General sectional view of sample No 8 (30mm)

The good alignment and excellent interfacial conformity would, had it not been for the premature failure, have allowed a greater strength then 8.78 MPa to have been recorded.

Specimen 9 Fracture strength 0.72MPa

The fracture surface showed about 25 fracture origins situated evenly around the periphery. The fracture path shown in section in Figure 6.35 was almost horizontal with limited deflection or branching. This fracture path passed about 4mm below the top of the Syalon's radiused surface on the left, and about 1mm below the top of the copper reinforcement on the right. The Ticusil had clearly failed to fill the Syalon/copper interface in the critical peripheral region. Conformity between the two interfaces illustrated was not good, the copper interlayer slightly tilted and the copper/steel interface only half filled.

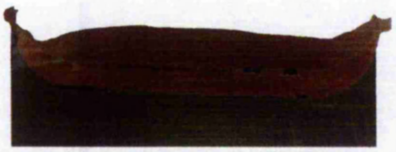

Figure 6.35: General sectional view of sample No 9 (30mm)

A 13mm long hot tear was visible just inside the copper but did not reach the critical peripheral region. The unbroken interface also appeared to be very slightly tilted and, unusually, had a considerably greater misshapen external appearance (resulting from extensive melt expulsion) than the weaker interface.

The principal cause of weakness in this sample was believed to be the incomplete filling of the Syalon/copper interface around its perimeter

Specimen 10 Fracture strength 6.22MPa

The fracture surface showed about 5 fracture origins situated close to each other, the largest single crack front radiating out smoothly to cover about 90% of the fracture face. An excess of molten Ticusil had been expelled from the most misshapen of the 2 Syalon/copper interfaces to form globular outcrops at these points of crack initiation. The copper reinforcement at the unbroken joint was more uniform and less seriously attacked by expelled braze, but was slightly tilted. Figure 6.36 shows the cracks from left and right-hand sides again to have dipped before rising to merge at the centreline. Regions of copper dissolution were again found at the two ends of the 20mm flat section of the interlayer.

Figure 6.36: General sectional view of sample No 10 (30mm)

Although the interfaces shown in the Figure 6.36 exhibited excellent conformity and the Ticusil appeared to have filled the critical peripheral regions of the Syalon/copper interface, it was considered that the strength of this sample had been reduced somewhat by the large localised expulsion of Ticusil misshaping the joint's external profile. This created localised stress concentrations and, conceivably, microstructural changes in the surface of the overrun Syalon.

Specimen 11 Fracture strength 12.78 MPa

The fracture surface showed about 11 fracture origins situated evenly around the periphery of the joint whose copper reinforcement had been most seriously attacked by molten Ticusil. A hot tear or 'melt-assisted shear fracture' was seen to run through the copper, parallel to and about 0.5mm away from the Syalon/copper interface, though it had not contributed to the sample's fracture. Whilst there was generally excellent interfacial conformity, a region of copper of significant size had been removed by Ticusil dissolution from the Syalon/copper interface near to the specimen's periphery. This may have contributed, along with the extensive melt expulsion and the dissolution of reinforcement referred to above, to reduce the strength of this (strongest) sample.

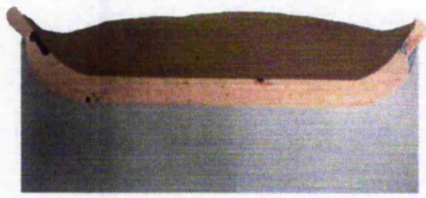

Figure 6.37(a): General sectional view of sample No 11 (30mm)

An additional factor is likely to be the 15mm length by 2mm wide area at the periphery that appeared not to have been wetted. Had a greater quality been attached to the sample, a higher joint strength should have been possible.

Specimen Number	Joint strength (MPa)		Reasons for failure
	weakest	strongest	
4	2.87	> 2.87	Globules on attacked copper reinforcement
5	–	–	Retained in unbroken form
6	1.05	> 1.05	Incomplete wetting, spreading of braze; large cavity at Syalon/Cu interface
7	1.06	> 1.06	Globules on attacked copper reinforcement
8	8.78	> 8.78	Surface defect; globules on copper reinforcement; small unbonded region;
9	0.72	> 0.72	Incomplete filling of Syalon/Cu interface at periphery owing to voids above/below interlayer
10	6.22	> 6.22	Globules on attacked copper reinforcement
11	12.78	> 12.78	Globules on copper reinforcement; small unbonded region

Table 6. 5: Summary of strengths and principal faults in 30mm dome-flat samples with copper

6.2.7 Summary of experimental peak and average tensile strengths for 5 joint types after rejection of values deemed unrepresentative.

The largest proportion of successful tensile tests conducted were those for the 20mm diameter joint samples, both with and without copper interlayers. Somewhat less confidence therefore attaches to the 30 mm diameter samples, and less again to the 10mm ones. On the basis of the detailed review of each individual test (reported in sections 6.22-6.25) it is possible to quote in Table 6.6 the strength values indicated by the experimental programme.

Joint type	Peak recorded value (2 interfaces a, b) MPa	Group average for joints without apparent brazing faults (2 interfaces a, b) MPa	Comments
30mm without copper	(a) 16.76 (b) > 16.76	-	No samples free of brazing faults
30mm with copper	(a) 12.78 (b) > 12.78	-	No samples free of brazing faults
20mm without copper	(a) 25.49 (b) >25.49	(a) 21.97 (b) >21.97	-
20mm with copper	(a) 52.58 (b) >52.58	(a) 47.62 (b) > 47.62	-
10mm with copper	(a) 37.57 (b) >37.57	(a) 36.93 (b) >36.93	Showed slight misalignment

Table 6.6: Peak and average tensile strength

Weibull strength distribution plots for 20mm diameter dome-flat joints, without and with copper interlayers are presented in **Figures (6.37(b), 6.37(c))**. These two joint types contained the largest populations of 13 and 8 specimens respectively.

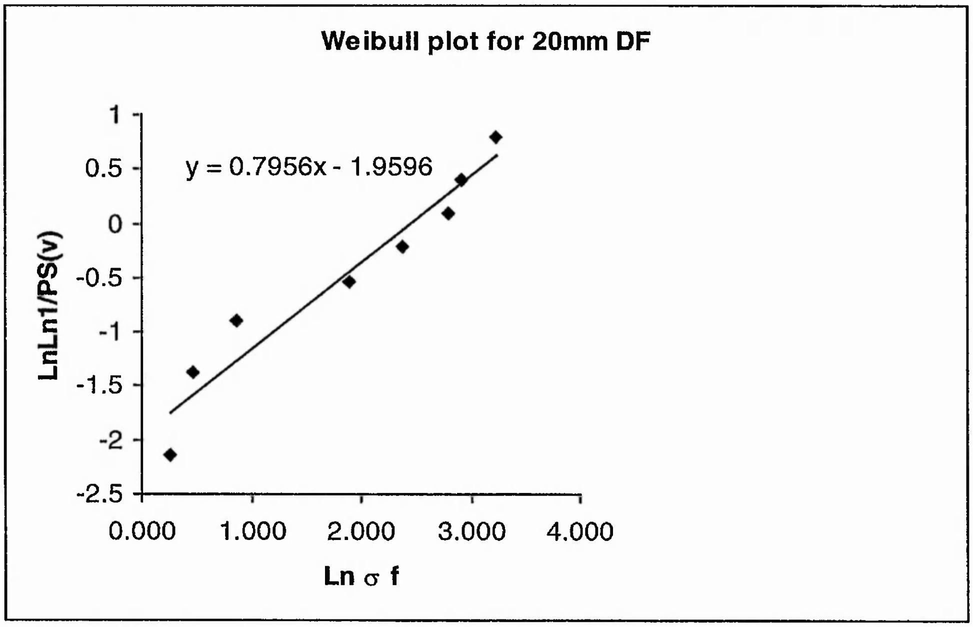

Figure6.37 (b): Weibull strength distribution plot for 20mm diameter dome-flat joints without interlayers

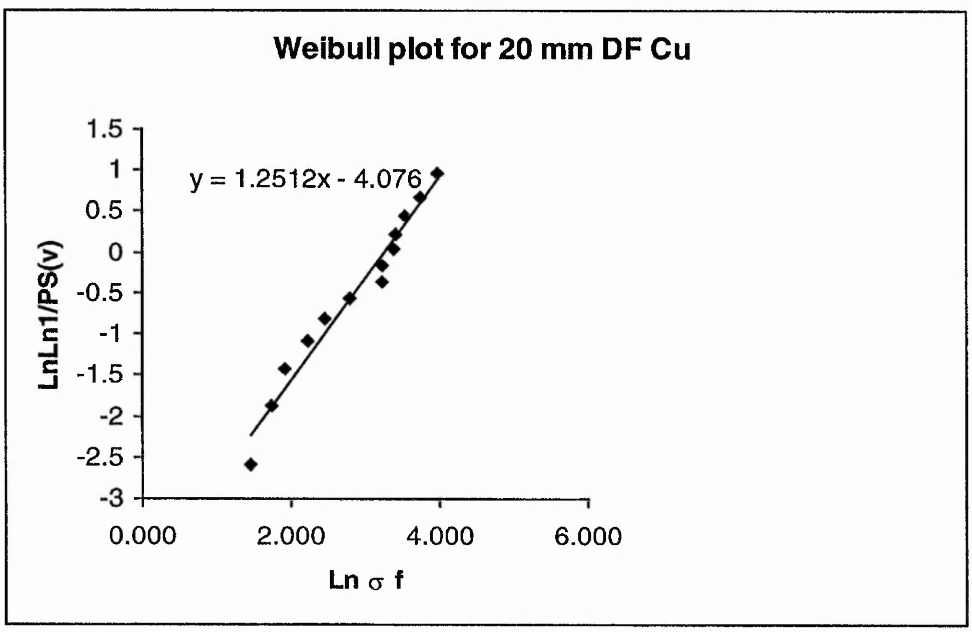

Figure 6.37 (c): Weibull strength distribution plot for 20mm diameter dome-flat joints containing interlayers

6.3 Characterisation of the copper and stainless steel and results of the microhardness testing surveys

The tensile strength and the ductility values found for the full-simulation annealed copper and stainless steel used in the metal-to-ceramic joints are presented below.

	ASTM standard	Experimental value
T.S. MPa. (max)	517/723	602
% elongation (min)	35/45	63.4%

Table 6.3.7: Tensile properties of AISI 321 after annealing at 1050°C for 30 minutes

	BS. 2874 C101 Rod	Experimental value
T.S. (MPa)max	260	191
% elongation (min)	32%	32.7%

Table 6.3.8: Tensile properties of annealed copper (experienced same thermal history as copper interlayers)

The results of the microhardness survey conducted around the necked region of the copper are presented in Appendix [S]. They revealed peak values up to 169 HV100g. The average peak hardness value of 165 ± 9 HV100g was recorded for comparison purposes, for when viewing results of the microhardness surveys conducted on the copper interlayers for the 4 representative joint types.

Appendix [S] also shows the results of the microhardness survey conducted within the necked region on the polished section of the fractured stainless steel test piece. The maximum value of work hardening achievable by this material was recorded as 520 ± 5 HV100g.

All microhardness values were taken using the 100g or 200g loads on the indenter, with corrections made by reference to the calibration conducted using a certified test block supplied for the Leitz Miniload microhardness tester.

The graphs were used to identify regions where work hardening of the metal had taken place, its magnitude being dependent on the levels of differential thermal strain-induced stress generated at each point examined.

Figures 6.38, 6.39(a-c), 6.40 and 6.41(a-c) show graphs of microhardness plotted against distance from the free surface along each of the interfaces under investigation for the samples: 30mm diameter without copper and with copper, and 20 mm diameter without copper and with copper, in that order.

These 'strain hardening maps' were expected to relate directly to the predicted thermally induced stress patterns developed by the author using ANSYS software during the theoretical analysis for each joint type in Chapter 4.

6.3.1 Microhardness conducted on 30mm sample without Cu interlayer

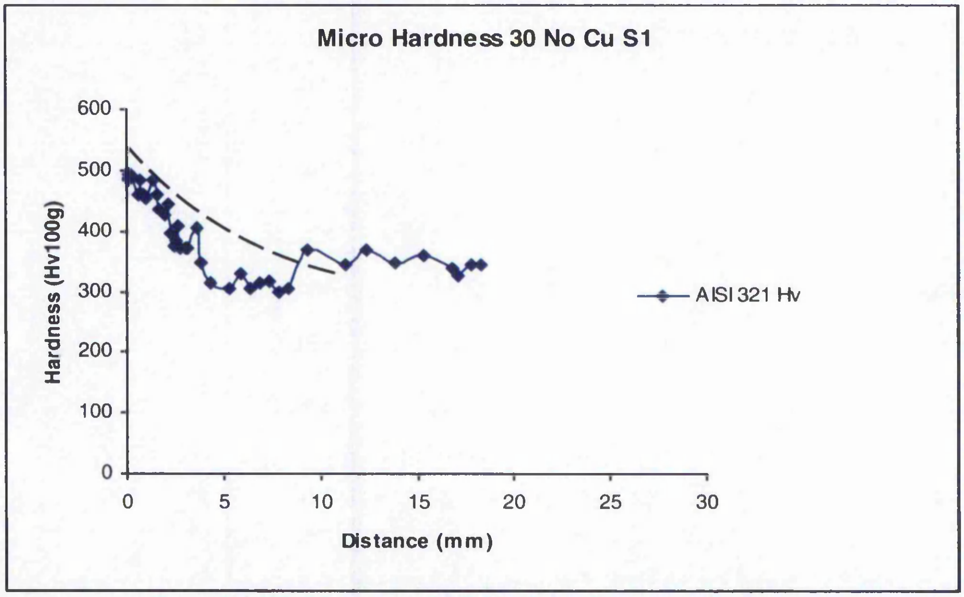

Figure 6.38: Microhardnesses survey along interface for 30mm diameter sample without Cu interlayer: traverse within stainless steel adjacent to AISI 321/Cu interface. The dashed line has been superimposed to indicate where the peripheral part of the graph might have been, had the thick Ticusil layer not been present to act as a deformable interlayer.

6.3.2 Microhardness conducted on 30mm sample with Cu interlayer

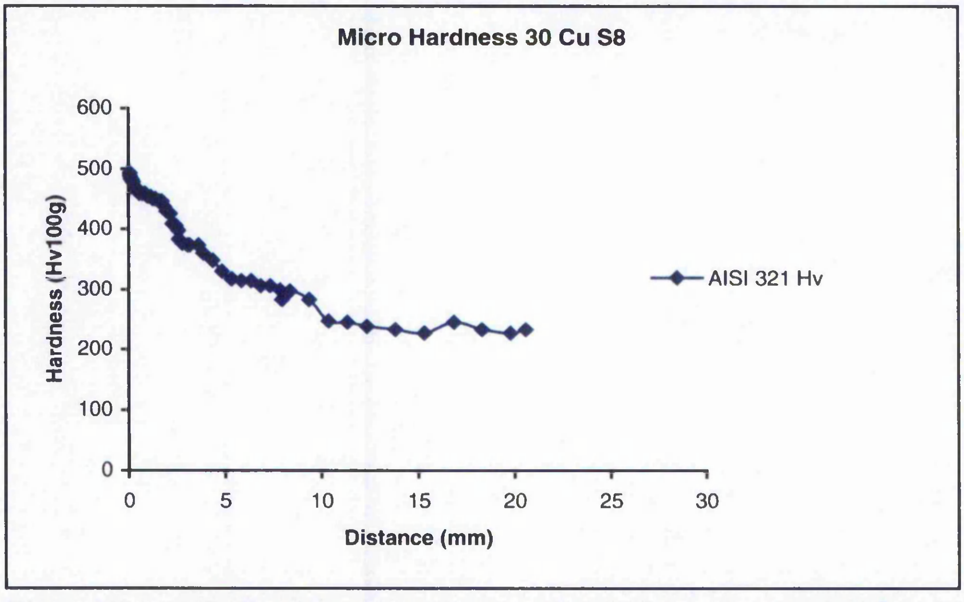

Figure 6.39 (a): Microhardness survey along interface for 30mm diameter sample with 2mm Cu interlayer: traverse within stainless steel adjacent to AISI 321/Cu interface.

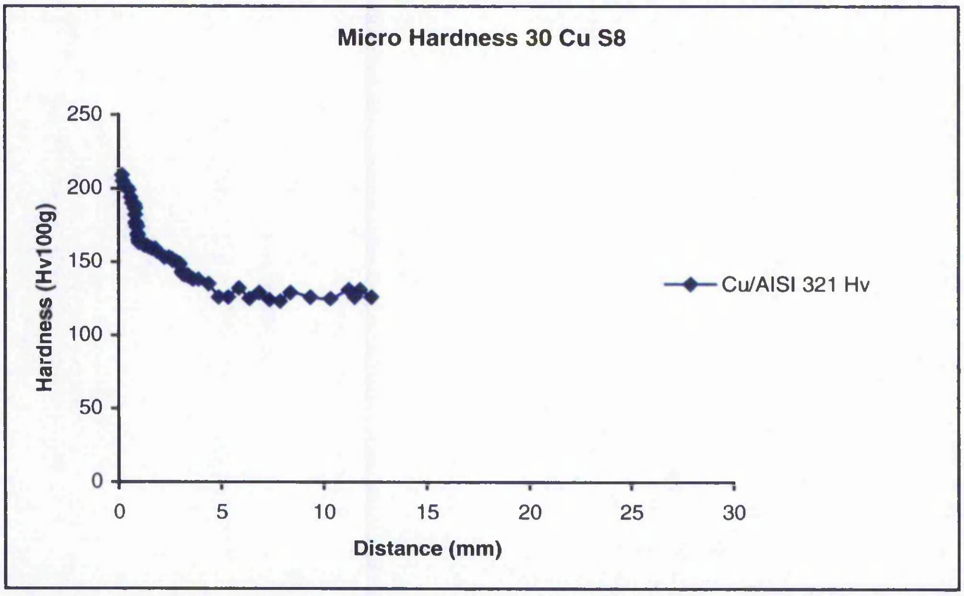

Figure 6.39(b): Microhardness survey along interface for 30mm diameter sample with 2mm Cu interlayer: traverse within copper adjacent to Cu/AISI 321 interface.

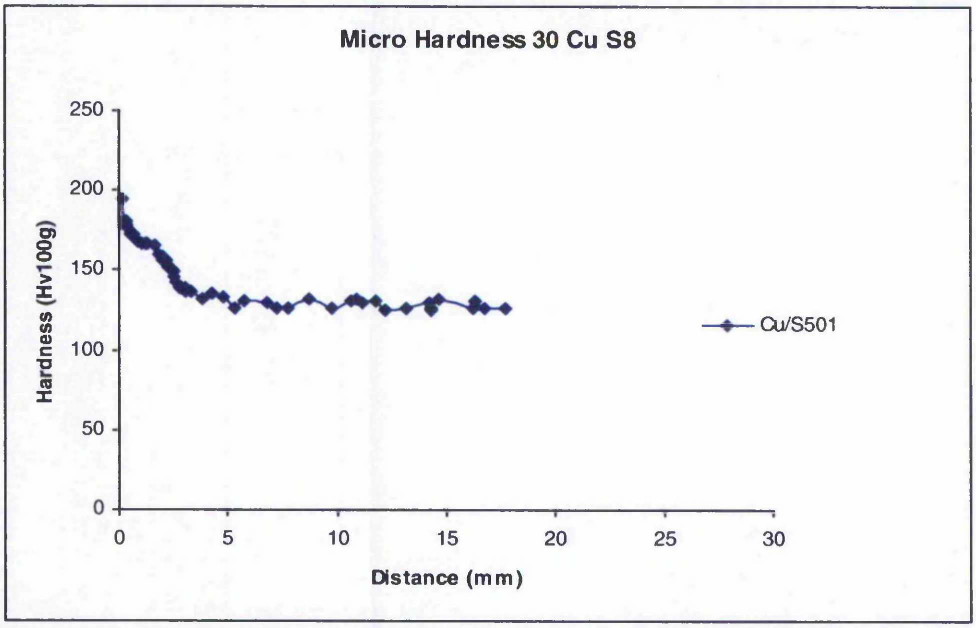

Figure 6.39(c): Microhardness survey along interface for 30mm diamter sample with 2mm Cu interlayer: traverse within copper adjacent to Cu/Syalon501 interface.

6.3.3 Microhardness conducted on 20mm sample without Cu interlayer

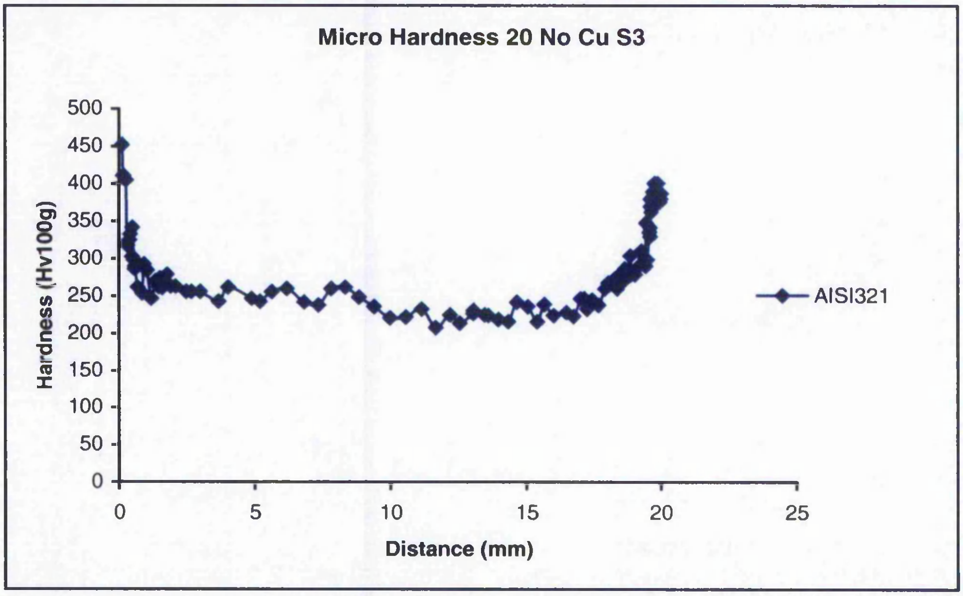

Figure 6.40: Microhardness survey along the interface for 20mm diameter sample without Cu interlayer: traverse within stainless steel adjacent to AISI321/Cu interface.

6.3.4 Microhardness conducted on 20mm sample with Cu interlayer

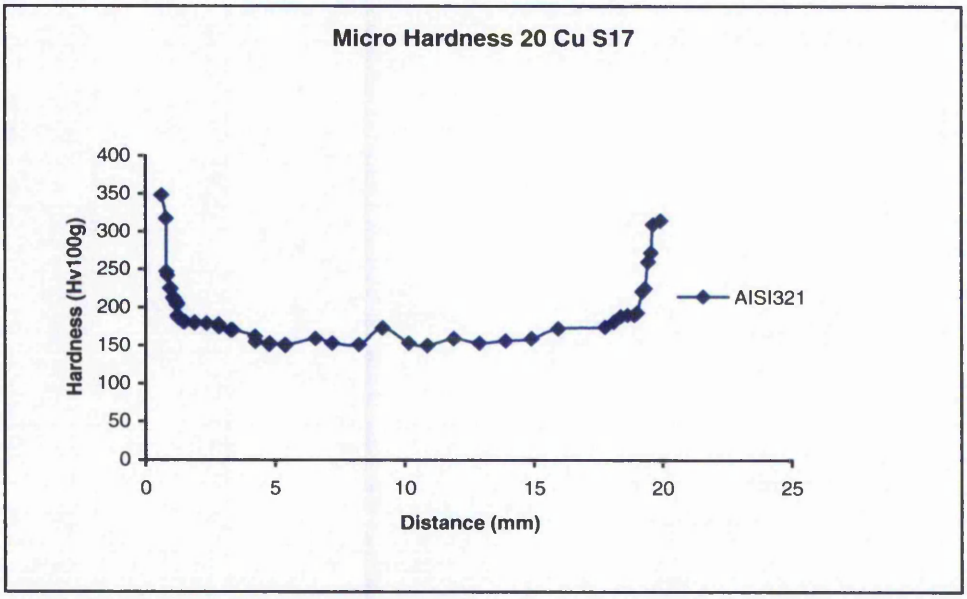

Figure 6.41 (a) Microhardness survey along interface for 20mm diameter sample with 2mm Cu interlayer: traverse within stainless steel adjacent to AISI 321/Cu interface.

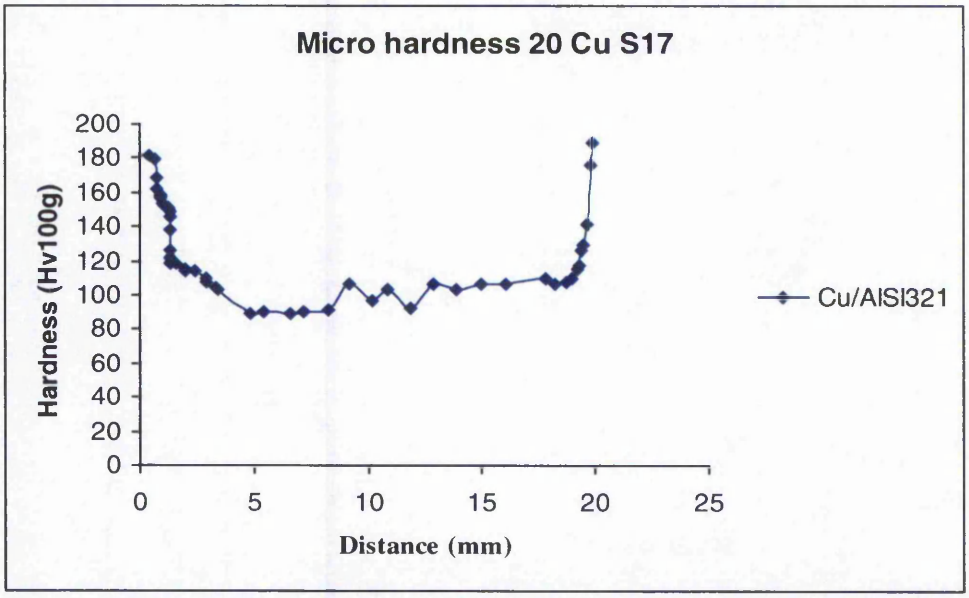

Figure 6.41 (b): Microhardness survey along interface for 20mm diameter sample with 2mm Cu interlayer: traverse within Cu adjacent to Cu/AISI321 interface.

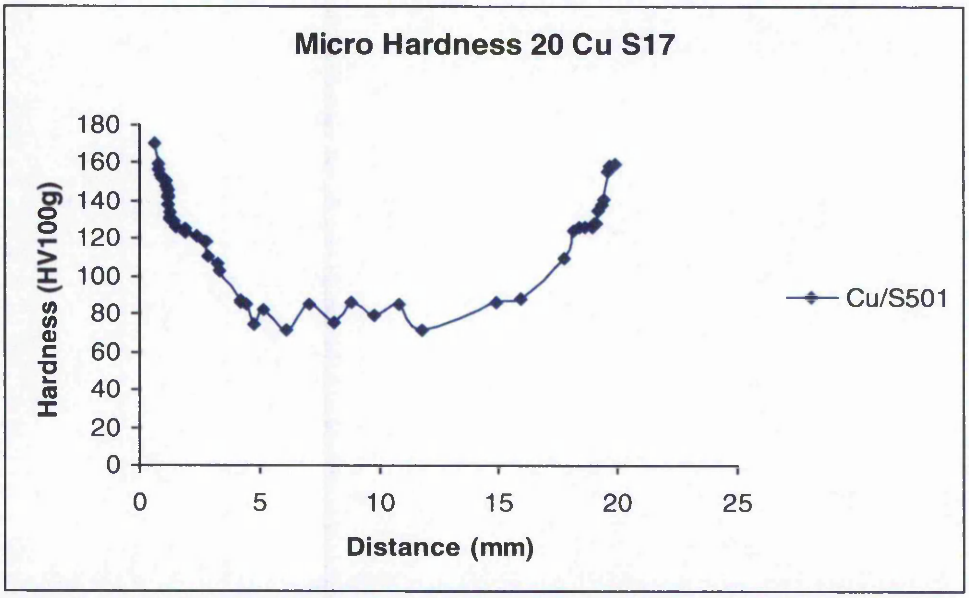

Figure 6.41 (c) Microhardness survey along interface for 20mm diameter sample with 2mm Cu interlayer: traverse within copper adjacent to Cu/Syalon 501 interface.

In Table 6.7 the peak microhardness values exhibited at or near the peripheral edge of each of the four joint type's interfaces is presented. It also presents the minimum microhardness values representative of the central 'flat' part of each dome-flat interface. This information is presented for all three traverse positions i.e. for 100 ± 10 micrometers inside the stainless steel for 75 ± 10 micrometers above the copper- AISI 321 interface and for 75 ±10 micrometers below the Syalon501 - Cu interface.

Joint type	30mm No Cu HV 100g	30mm Cu HV 100g	20mm No Cu HV 100g	20mm Cu HV 100g	10mm No Cu * HV 100g
Peak hardness at featheredge AISI 321	[94%] 489[a] (220%)	[93%] 485[c] (217%)	[78%] 408[i] (167%)	[62%] 322[k] (110%)	[49%] 253[q] (46%)
Peak hardness at interface periphery AISI 321- Cu	-	[99%] 209[d] (386%)	-	[82%] 181[l] (321%)	-
Peak hardness at interface periphery Cu- Syalon501	-	[90%] 194[e] (351%)	-	[70%] 161[m] (274%)	-
Average hardness across central section of interface: AISI 321	[64%] 333[b] (118%)	[46%] 237[f] (55%)	[45%] 234[j] (53%)	[32%] 163[n] (7%)	[39%] 200[r] (16%)
Average hardness across central section of interface: AISI 321 – Cu	-	[52%] 131[g] (205%)	-	[32%] 98[o] (127%)	-
Average hardness across central section of interface: Cu- Syalon501	-	[47%] 123[h] (186%)	-	[23%] 84[p] (95%)	-

*** Data obtained by Shipstone in Khene et al[124]**

Table 6.7: Summary of peak peripheral and minimum centerline values extracted from microhardness surveys conducted adjacent to ceramic/metal interface and metal/metal interfaces in 4 representative joint types (Figures in round brackets show local percentage hardening experienced by stainless steel and copper interlayers and in square brackets show local microhardness as a proportion of the maximum work hardening available)

Notes

Hardness of annealed 30mm diameter AISI321 = 143 HV10Kg
Hardness of annealed 20mm diameter AISI321 = 139 HV10Kg (153 HV100g)
Hardness of annealed 10mm diameter AISI321 = 158 HV10Kg (173 HV100g)

Hardness of annealed 20mm and 30mm copper interlayers after exposure to temperatures simulating the bonding cycle = 38.6 HV10Kg (43.0HV100g)

(a) Peak hardness at featheredge between 0-0.24 mm from periphery was reduced by 0.5-mm thick layer of Ticusil (taking up poor peripheral interfacial conformity and acting as interlayer to relax stresses locally Figures 6.28 and 6.38)

(b) Average flat interface hardness between distances from periphery of 5-20mm

(c) Average values from left and right hand side featheredges between 0-0.24mm from periphery. (It was 489 HV100g between 0 – 0.10mm from periphery.)

(d) Average values from left and right hand side featheredges between 0-0.20mm from periphery

(e) Average values from left and right hand side featheredges between 0-0.20mm from periphery

(f) Average flat interface hardness between distances from periphery of 10-20mm

(g) Average flat interface hardness between distances from periphery of 5-12.5mm

(h) Average flat interface hardness between distances from periphery of 5-18mm

(i) Average peak hardness at left and right hand side peripheries (average of top 2 values from each side)

(j) Average flat interface hardness between distances from periphery of 5-15mm

(k) Average values from left and right hand side featheredges between 0-0.58mm from periphery

(l) Average values from left and right hand side featheredges between 0-0.42mm from periphery

(m) Average values from left and right hand side featheredges between 0-0.59mm from periphery

(n) Average flat interface hardness between distances from periphery of 5-15mm

(o) Average flat interface hardness between distances from periphery of 5-15mm

(p) Average flat interface hardness between distances from periphery of 5-15mm

(q) Average values from left and right hand side featheredges between 0-0.20mm from periphery

(r) Average flat interface hardness between distances from periphery of 4-6mm

6.4 Discussion

6.4.1 Experimental and manufacturing aspects of joint production

During the heating cycle the 30mm diameter metal joint members expanded more than anticipated causing the carbon susceptor to fracture. The problem was solved by sleeving the fractured part with two stout precision machined and tight fitting graphite rings. The graphite rings performed well and no further expansion problems occurred.

During development work preceding the production of brazed samples 1-40, the clearance between the joint members and the split carbon brazing jig was insufficient to allow for the steel member's expansion during heating. Irrespective of the joining pressure applied, this prevented the ceramic and steel joint members from making intimate contact with one another across the interface during joining, rendering them useless for tensile testing.

This was resolved by very slightly widening the hole at the top of the carbon susceptor. It was only necessary for the top member to remain free during the test.

Keeping the brazing foil in place during assembly and ensuring it covered all the interface area was an extremely delicate and difficult operation.

In some cases the braze foil moved to one side during assembly causing incomplete filling of some interfaces to the periphery on one side, whilst expelling molten braze from the opposite side. By contrast, the increased volume of Ticusil foil used in joining most of the 30mm diameter samples may be interpreted, in retrospect as having been counter productive, being subsequently identified as having produced globules of molten braze that were expelled under pressure during the joining process. It is proposed that these globules close to the sensitive peripheral region of joint interfaces constituted both a physical stress concentration (due for their producing a local, abrupt change of cross section) and probably a 'metallurgical notch' resulting from any diffusion of titanium atoms from the molten globule into the underlying Syalon to cause local microstructural change (i.e. formation of titanium silicides and nitrides). Figure 6.42 shows the proposed effect.

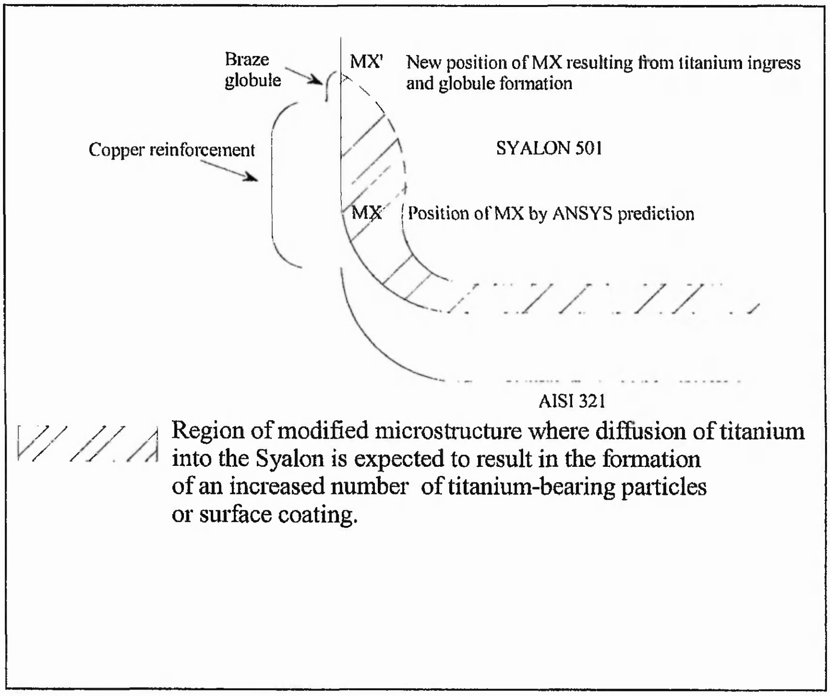

Figure 6.42: Proposed effect of surface globule of expelled surplus Ticusil on microstructure and on position of maximum tensile stress (MX) for dome-flat interface.

All seriously defective brazed joints were identified in Sections 6.2.2 - 6.2.6 and those joints' strengths were deemed unrepresentative.

The additional important elements of manufacturing procedure necessary to ensure strong Syalon 501/AISI321 joints were found in this research to include the following:

- Attention to quality of electroconductive ceramic supplied
- Interfacial conformities before brazing
- Prevention of hot tears at interfaces
- Control of brazing temperature and time

The two issues regarding **quality of the electroconductive ceramic** supplied were

- microstructural homogeneity
- internal, and especially surface integrity

A uniform dispersion of fine electroconductive particles was essential. Their function was to provide an electrical conductive path throughout the material to guarantee that easy EDM-ing occurred. This latter was found troublesome by Tinsley[7] and was attributed to density segregation-out of the small heavy particles of TiN prior to cold pressing and consolidation by sintering. This problem was not experienced by the present author.

The discovery of extensive longitudinal grinding cracks in three of the 10mm diameter diamond ground blanks supplied by the manufacturer limited the maximum number of double-interfaced 10mm diameter joints that could be attempted to just 7.

The production of excellent **conformity between mating interfaces** was reliant on the precision of machining of the concave profile (including the delicate featheredges of the stainless steel) and the convex profiles EDM-ed onto the Syalon 501. The former objective was achieved by established metal machining techniques that included supporting the featheredges against the machining forces. Accurate profiling of the ceramic by EDM however was difficult. Whilst the problem can be reduced by rotating the tool relative to the workpiece and by using successively finer cuts with freshly profiled tools, tool wear will generally result in some departure from the profile required. It was found desirable therefore to make the final machining operation a "burning-in" one where the finish-profiled Syalon component was used briefly as an EDM tool against the concave steel member. Thus, as long as no subsequent relative rotation between the two mated components resulted, the next time that those parts met, with braze foil rather than liquid dielectric between them, perfect conformity was assured.

Regarding the very high levels of hardening measured in the peripheral regions of the copper interlayers (up to 209HV100g) in the 30mm diameter joints, compared with the annealed value of 43 HV100g, it appears unlikely that even extreme work hardening of a annealed value of 43 HV100g, it appears unlikely that even extreme work hardening of a pure metal could more than quadruple its annealed value of hardness. It is more likely therefore that a significant level of alloy hardening had occurred within those surface regions of the copper interlayers in which the microhardness surveys were conducted (i.e. 75± 10μm inside each face of the interlayer).

Examination of Figure 6.1 (a – e) revealed that this was indeed the case, with some of the surface copper having dissolved within the Ticusil brazes placed above and below it, before the enhanced liquid volume froze to give a hypoeutectic structure of copper solid solution within a local matrix of fine eutectic. Furthermore, reference to the Cu-Ti thermal equilibrium diagram[55] shows that up to 7.3 atomic percent Ti can be taken into solid solution by copper, thereby further contributing to the hardness observed. Additionally, a continuous film of TiN was observed between the Ticusil and the Syalon, which will have resulted from a reaction between Ti and Syalon.

Further evidence that the microstructure modification was responsible for the unexpectedly high hardness in the copper interlayers was provided by the tensile test conducted on a sample of the copper after it had been exposed to the full simulated thermal history of the interlayers used in joining. The peak hardness adjacent to the tensile test piece's fracture face measured to be 164 HV100g [Appendix S]. While there is no doubt that the differential strain within the dome part of the interfaces did indeed harden the copper, the resultant hardness value would have been expected to lie in the range 43 – 164 HV100g and probably towards the lower end. It can only be assumed therefore that the values of hardness reported in the copper at its periphery will contain of the order of 100 HV100g points attributable to the alloy hardening referred to above, i.e. a maximum hardness of 209HV100g in the 30mm diameter joints.

Reference to Figure 6.1(a – e) shows however that the radial depth within the copper to which this Ticusil-induced dissolution and freezing occurred was limited primarily to the curved outer sections of each interface. This suggests that lower temperatures, and perhaps poorer access for the liquid to attack the copper interlayer, existed in the flat area of the joints and as such, the hardnesses reported there up to 131HV100g may be less significantly affected by the alloying referred to above.

Though much has been made above of the 'damage' done to the copper-interlayer by the molten Ticusil, the dissolution of the surface copper, accompanied by melt-flow, was a major reason for the attainment of **excellent conformity**, (sometimes at the expense of introducing some modest interfacial porosity, though generally in non-critical positions), with capillary action very commonly in evidence in ensuring that the all-important peripheral regions were fully filled with (modified) braze.

Hot tears were seen running just within the copper in 4 of the brazed specimens. In specimen 13 (20mm diameter) and in specimens 9 and 11 (30mm diameter) the tear ran close to the copper-Syalon 501 interface, while in specimen 6 (30mm diameter) it ran close to the AISI 321-copper interface. In no case did these tears extend beyond the flat part of the interface, so remained in the non-critical part of the joint. They most likely resulted from shear stresses generated at the interfaces from the differential contraction of Syalon against copper and of copper against AISI 321. They were sometimes associated with local solidification shrinkage resulting from a local deficit in braze volume.

It is proposed that they formed not simply due to the static thermal expansion mismatch across the interface, but also due to the dynamics of cooling which might promote more rapid cooling on one side of an interface than on the other.

The other reason for the greater work hardening being observed in the copper at the AISI 321/copper interface, even though the copper and steel have relatively little mismatch in CTE, is proposed to be due to this interface falling to a temperature below the copper's recrystallisation temperature before the Syalon 501/copper interface, which is situated slightly closer to the high temperature end of the cooling gradient. This would have allowed recrystallisation, with its continual softening effect to proceed for longer at the Syalon 501/Cu interface.

Finally, other researchers' recommendations that close control of brazing **temperature and time** are essential to maximise the strength of joints are confirmed. Whilst others have shown that excessive temperatures and times can lead to the formation of coarse, weakening reaction products, it has been shown in this research that above the melting temperature of the braze there is also an increasing quantity of dissolution of any soluble interlayer or reinforcement as well as a general increase in dangerous differential thermal contraction stresses.

Regarding the production of closely conforming and profiled interlayers, this research has shown that careful machining can be used, but, where adequate industrial facilities exist that are capable of making these items to accurate dimensions and high integrity, such as by pressure die casting or powder metallurgy, these manufacturing routes should be attempted if possible.

This research has shown that by using painstaking care, excellent and relatively strong joints can be produced up to 20 mm and 30 mm in diameter in a relatively unfavourable metal/ceramic combination.

Through the production of a number of poorly formed and weak joints, but by learning from these mistakes, enough information has been presented here to allow those identified pitfalls to be avoided and for joints to be produced, ideally with high consistency to avoid the formation of seriously compromised joints and so produce joints of high individual and group average strength.

6.4.2 Microhardness surveys

Whilst locally raised values of hardness within the upper and lower surfaces of the copper interlayers resulted partly from their dissolution and freezing after interaction with molten Ticusil and probable solution of titanium, equally titanium accompanied by carbon and nitrogen[49] from the brazing environment may have contributed to the stainless steel interfacial hardening. As all 10mm, 20mm and 30mm diameter joints experienced the same brazing temperature and time, the 'alloy hardening' proportion of all the measured microhardness values should have been approximately the same. If increased values were present, it is proposed that, at temperatures as low as 920°C this could be relatively small. It is proposed that alloy hardening is unable to explain fully the very large hardness differential seen in joints of different diameter and in every sample between peripheral and joint central areas. In all the surveys conducted any scatter was attributed primarily to small variations in distance of the indentation from the interface under examination. Proximity to any subcutaneous microporosity within the frozen modified braze would have tended to give larger impressions.

The eight representative sets of peak peripheral and minimum centre line microhardness values shown in Table 6.7 proved conclusively that the magnitudes of differential strain-induced work hardening (complemented by an approximately constant alloy hardening contribution) increased with increasing specimen diameter. Values for stainless steel were raised in two cases from 153 HV100g (20mm diameter joints) to values approaching 520 HV100g. Similarly, for copper values were raised from 43 HV100g to values that exceeded the maximum for fully work hardened pure copper. These maxima, of 165 Hv100g and 520 Hv100g for pure copper and for stainless steel respectively, had been determined experimentally from two independent tensile tests conducted on test pieces that have been subjected to the same full thermal histories as those experienced by the copper interlayers and stainless steel.

The percentage values in square brackets in Table 6.7 showed how effective the 2mm copper interlayer was in shielding the stainless steel's periphery from undue work hardening. Thus, in some 30mm diameter copper interlayered joints, the copper itself at the AISI 321 – Cu interface had reached that part of the 99% copper's hardening which was attributable to work hardening (i.e. excluding the approximately constant (recurring value) complementary part due to alloying) in restraining the adjacent stainless steel featheredge. It can be expected that its low yield strength and high ductility will have had a similar induced stress shielding (' stress absorption') effect to protect the Syalon 501's periphery from reaching its tensile strength during cooling from brazing. The lower levels of work hardening experienced in the copper interlayer adjacent to the Syalon is misleading. The differential strain at this interface, at any moment in the dynamic cooling sequence was probably higher at this interface however it is proposed that, the fact that this interface remained above the recrystallisation temperature for longer than the cooler AISI 321/Cu interface meant that the build up of work hardening progressed for a longer periods at that cooler interface.

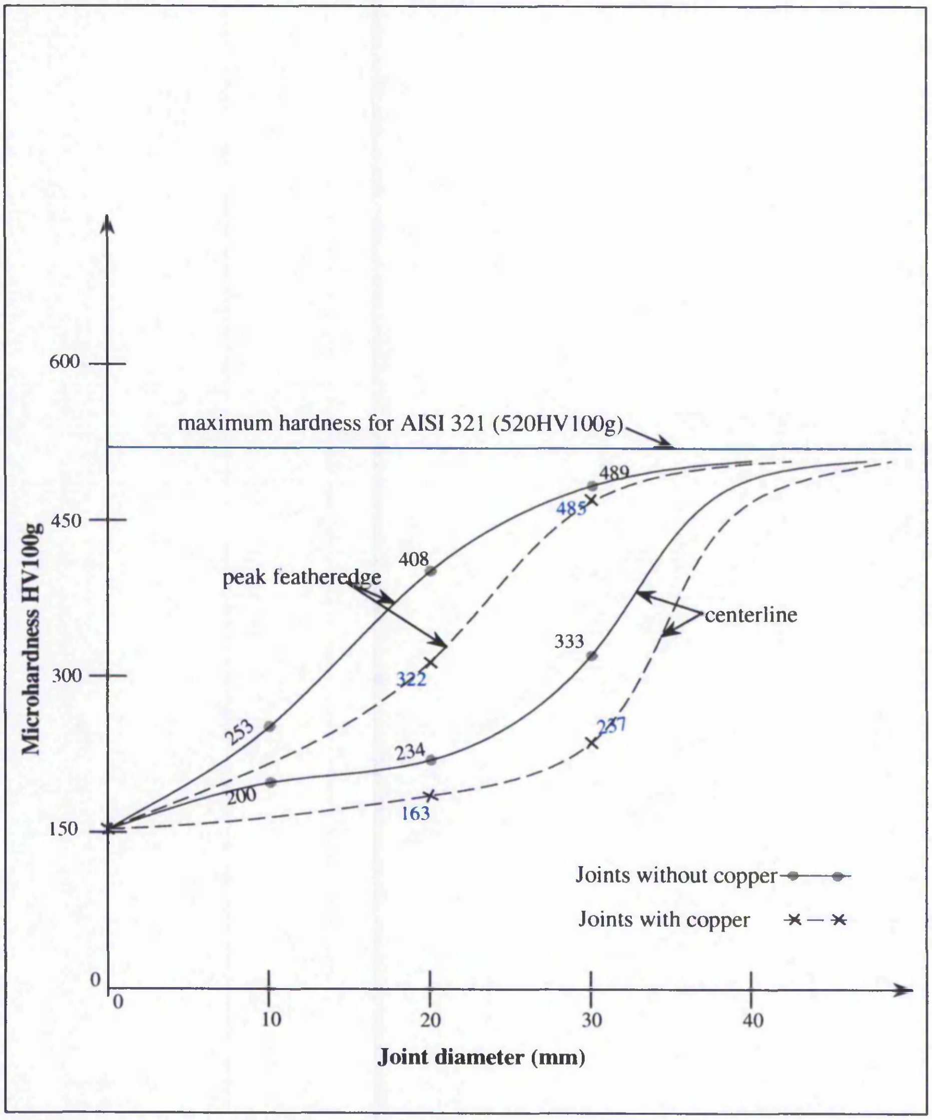

Figure 6.43: Peak (featheredge) and minimum (centreline) hardness values for AISI 321 in joints with, and without 2mm copper interlayer

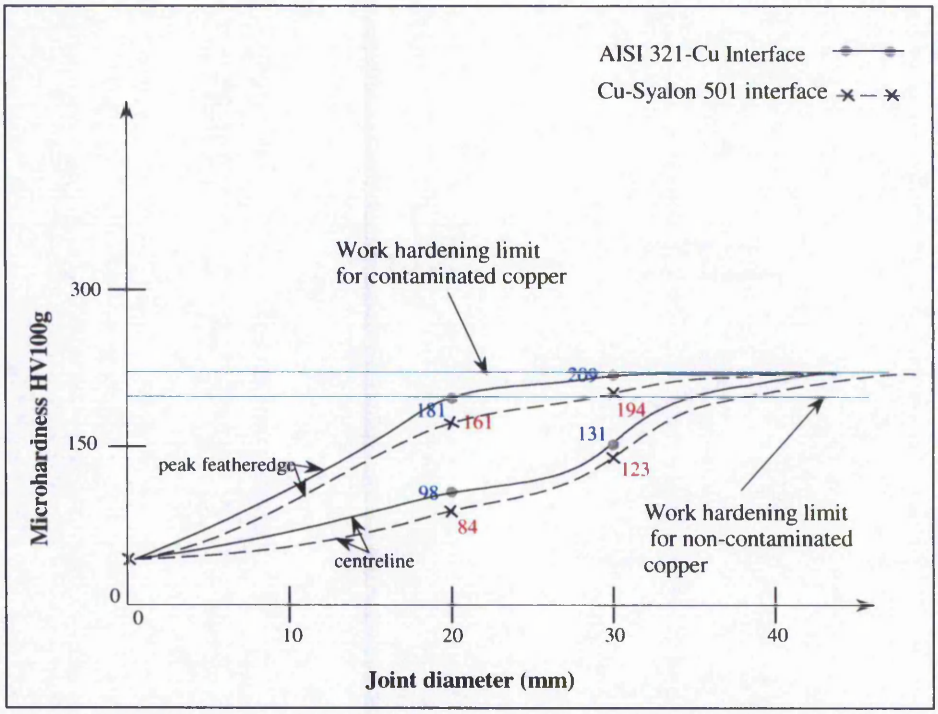

Figure 6.44: Peak (peripheral) and minimum (centreline) hardness values for copper interlayers' interfaces (note copper hardness raised by up to 45HV100g by 'contamination')

In contrast to the not unexpected increases in work hardening recorded from within steel featheredge and peripheral copper regions particularly, the hardness differential across the width of each copper interlayer was not marked, suggesting a relatively uniform take-up of plastic strain across the interlayer rather then simply a superficial effect associated with each interface. This hardness differential across the interlayers decreased from 12.4% and 16.7% at joint periphery and centreline respectively for 20mm samples to 7.7% and 6.5% at joint periphery and centreline respectively for 30mm samples. As discussed above, the harder values were always found at the AISI 321/Cu interface. These differentials, decreasing with increased work hardening experienced with increasing joint diameter, appear to indicate the existence of a limiting diameter of only slightly higher then 30mm that might be joined successfully in the Syalon 501/AISI 321 system under the dynamic cooling regime used and with the assistance of featheredges. That is, the capacity of the 2mm copper interlayer to absorb interfacial stresses appeared to be approaching exhaustion.

The very high values of microhardness generated within the stainless steel featheredges indicate that, at 30mm diameter this material is also reaching its stress absorption limit.

Thus the copper interlayers have had a dramatic effect in reducing the hardness and residual stress induced into the stainless steel and, by inference into the ceramic also. This bears out the predictions of the finite element analyses conducted and reported in Chapter 4.

In Table 6.7 the percentage values shown in square brackets as falling from 99% to 24% for the percentage achievement of work hardening supported by an approximately constant alloy hardening contribution inside the copper at the Syalon 501-Cu and Cu-AISI 321 interfaces appears to indicate the order of take-up of stresses within the ceramic/Cu/AISI 321 system. This same order was shown by the different rates of take-up of work hardening at each interface in Figure 6.44, with the copper at the periphery of the AISI 321 /Cu interface being the first to absorb differential interfacial stresses and strains, followed closely by the Syalon 501/Cu interface at a point 2mm below it. This was followed, rather later by the Cu/AISI 321 interface in the flat part of the dome-flat interface and, shortly after this by the copper at the central region of the Syalon 501/Cu interface.

Figure 6.43 also confirms the beneficial effect of the copper interlayer in absorbing differential thermal strain to shield the stainless steel. Its effect on supporting the stress relaxing ability of the stainless steel featheredges is shown by the displacement of the full line curves to higher diameter positions. Thus the effect the 2 mm copper interlayer was to add about 5mm to the diameter of the joint that did not contain copper for it to result in the same degree of stress in the stainless steel's periphery whilst probably shielding the ceramic to the same extent.

The factor which appears to have received little or no attention in the published literature is the opportunity that must exist in pure, relatively low melting point metals used as interlayers (such as the copper in the present study), to recrystallise during cooling at temperatures perhaps as low as 0.5Tm, where Tm is the melting temperature in Kelvin. Any such extended range of retained softness will naturally reduce the levels of residual stress generated.

In summary, the progression of hardening in stainless steel and in copper interlayers within joints of increasing diameter, both with and without copper interlayers is presented graphically in Figure 6.43 in relation to those peak and joint centerline levels of work/alloy hardening determined by the present author. Graphs of this type could be applied to any ceramic-to-metal joint system, with or without interlayers, to show the maximum limits to be imposed on the diameters that can be joined as dictated by the capacity of both the stainless steel (featheredges particularly) and the interlayers to absorb the differential thermal strain-induced stresses produced for that system.

If the criterion for the maximum diameter of joint that could be made, while still retaining joint integrity (though negligible strength), were to be defined by a peak microhardness attributed purely to work hardening in stainless steel of 490 HV100g (being 94% of capacity) and of 350 HV100g at the centreline, this would be read from Figure 6.43 as relating to a copperless joint of 30 mm diameter or a 2mm copper interlayered joint of about 35 mm diameter.

Thus, it is proposed that as soon as the capacity of the stainless steel (and, when present the soft metallic interlayer) to absorb thermally induced stresses by lattice strains is lost, the subsequent increases of stress, now carried over fully to the ceramic, will cause its tensile strength at the peak stress position (MX in the FEA models) to be exceeded, causing fracture to result through the ceramic.

6.4.3 Tensile tests

All the joints that failed on testing broke in the ceramic with the fracture initiating at or near the free edge adjacent to the metal-ceramic interface, the relevant stress concentration usually being associated with either

- Joint interface periphery being incompletely filled with braze
- Misshapen joint line through the presence of expelled globule of surplus braze or through localised dissolution of copper reinforcement
- The ' metallurgical notch' effect of abrupt changes in microstructure, especially on a free surface
- Misalignment

The results for tensile strength in relation to joint diameter were presented in Table 6.6 and showed the trend of decreasing joint strength with increasing joint diameter.

Generally the joint strength did decrease with increasing diameter as predicted by the finite element analyses conducted in Chapter 4. For **20mm diameter samples**, systems containing copper interlayers showed an improvement in strength in comparison with those without copper interlayers. Peak and group average strengths were found to be 52.6 MPa and 47.6 MPa compared to 25.5 MPa and 22.0 MPa respectively.

Against expectation, the joint strength for **10mm diameter samples** did not increase when a copper interlayer was incorporated, however it did show more consistent strength values averaging at 36.9 MPa. Because misalignment was the apparent cause of this group's low results, on account of the considerable difficulty experienced in assembling the 9 small constituent parts of each joint stacked vertically through their shiny hemispherical faces, this small group produced a strength of only 37.6MPa in its strongest specimen. This complexity, leading ultimately to an unacceptable misalignment is believed to account for the contrasting findings reported by Wilkes[29] who studied ten similar 10mm diameter joints made **without** copper interlayer (i.e. with only 5 constituent parts). These showed considerable inconsistency and a wide range of strengths above 3.4 MPa, averaging at 56.6MPa and with two strongest values of 112.6 MPa and 173.7 MPa.

In defence of the whole body of tensile strength values obtained from the 40 tests, where that body contained some particularly low values, the decision to produce double-interfaced AISI 321/ Syalon 501/ AISI 321 joints was always going to result in the fracture of just one joint, possibly at a stress below 1.0MPa. This joint becomes sacrificed probably long before the other joint, probably excellently produced and with a fracture strength possibly two orders of magnitude higher. This superior joint's strength value however can never be revealed. Because the 10mm diameter joint group finally comprised only 6 specimens, it was not a major focus of this research which was to seek to determine the potential of the 'dome' and 'dome-flat ' joining technique in terms of the maximum joint diameters that can be made reliably.

Regarding the 30mm joint samples, again the number of specimens in each group was small (7 and 3 for those containing and not containing copper interlayers respectively). As it was unknown whether such large diameters would be joinable at all when the FEA predicted levels of tensile stress at joined peripheries up to 302 MPa in joints without interlayers, the fact that all the 30mm diameter joints were formed successfully, albeit with small residual strengths was welcomed.

The manufacturer of Syalon 501 did not provide exact tensile strength values for this material, but specified for Syalon 101, the value of '450MPa, minimum acceptable 400MPa'. It is understood that these approximate values were obtained from small polished test pieces with 4mm diameter. The same strength values have been adopted in the finite element analysis and shall be used again in the discussion on pages 181-184.

Reasons for the very low strengths of the 30mm joints ($\geq$ 12.8 MPa and $\geq$ 16.8 MPa peak strengths for samples with and without copper interlayers respectively) can be listed as follows:

- The magnitude of thermally induced residual tensile stresses over such a large interface.
- The Weibull factor of large ceramic sections being statistically weaker than smaller ones
- An 'effective Weibull factor' of large joint areas being statistically more prone to brazing defects.

In addition, of course these joints were likely to show the same defects as other groups, i.e. misalignment, misshapen interface, metallurgical notch and any incomplete filling by Ticusil of peripheral regions of any joint's pair of Syalon/stainless steel or copper /AISI 321 and Syalon 501/copper interfaces as referred to above.

In addressing the variability seen in joints' strengths, there follows here an explanation of the low group averages recorded in Table 6.7.

Firstly, it is noted from the Syalon 501 data sheet (Appendix R) that the manufacturer's value for the Weibull modulus of this material lies in the range 8-14, compared with 11 for Syalon 101.

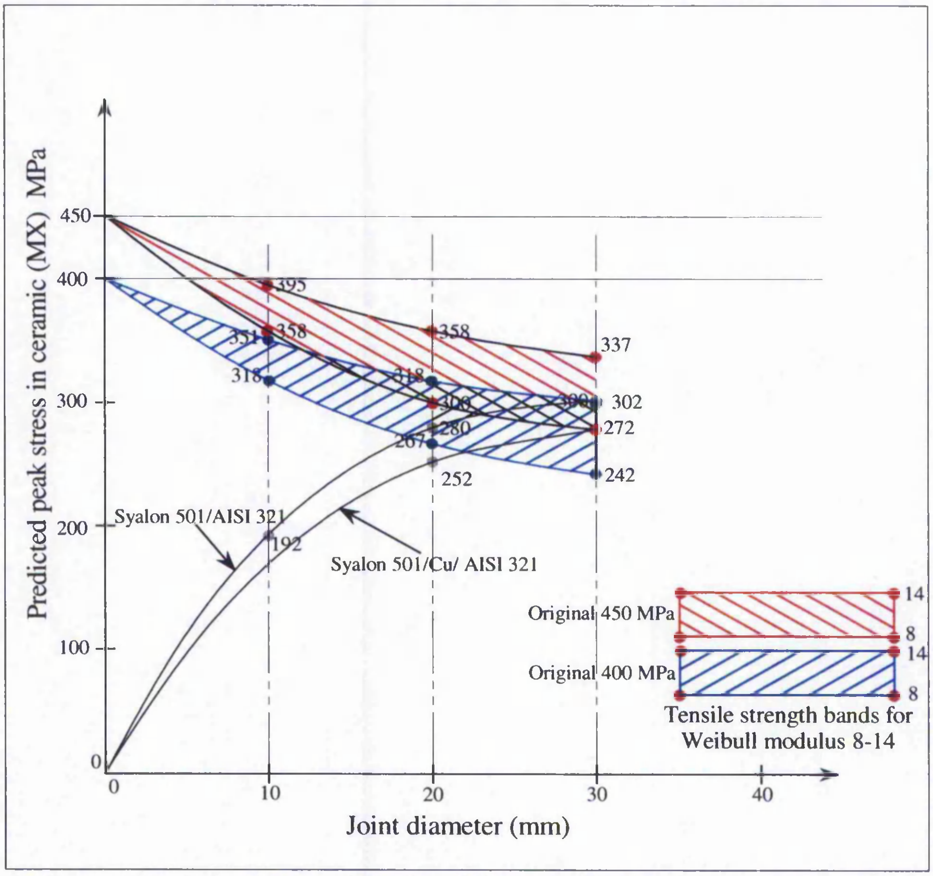

Figure 6.45: Effect of increasing joint diameter on FEA-predicted peak induced tensile stresses and on predicted tensile strength of Syalon 501

It is noted that the variability in joints' strengths within each of the 5 groups tested is large. This variability begins with the variability in the diamond ground ceramic cylinders provided by the manufacturer, characterized by the Weibull modulus range stated above. However a substantial variability is likely to have originated in the final joint strength by (i) any defects associated with the bulk volume of braze and braze-affected zones. This may be considered constant inside each of the 5 groups of results. This factor reduces the effective Weibull modulus value, m to the reduced value m′, and (ii) any variation in processing conditions, for example applied force, brazing temperature and time and any Ticusil deficiency or excessive use causing m′ to fall even further to a new lower value m″.

The experimentally determined values of m″ for 20mm joints with copper (13 specimens) and for 20mm joints without copper (8 specimens) were determined in figures 37(a) and 37(c) to be 1.25 and 0.796 respectively.

Figure 6.45 shows how the predicted maximum induced tensile stress values (MX) determined in Chapter 4, approached the 400 – 450MPa band as joint diameter increased, leaving an ever decreasing residual tensile strength available for load bearing purposes. The position of this band however must be adjusted to allow for the size effect of the ceramic under test. These modified bands representing decreasing predicted strengths for both the reference values 400MPa and 450MPa are shown for Weibull modulus values of 8 and 14.

On the assumption of a 400-450MPa reference tensile strength for a 4mm diameter cylindrical section being extrapolated to larger cylindrical volumes of the same height, and using the manufacturer's values for $8 \leq m \leq 14$, where derived on 4mm diameter polished test pieces, it can easily be shown using the well known expression [125]

$$\frac{\sigma_{V1}}{\sigma_{V2}} = \left(\frac{V_2}{V_1}\right)^{\frac{1}{m}}$$

relating tensile strength (σ) to volume (V) under test, that the reduced values listed in Table 6.8 will result for 10mm, 20mm and 30mm diameter cylinders:

Ceramic diameter	Predicted tensile strength*
10mm diameter	318-351MPa (on the basis of a 400MPa reference strength) 358-395MPa (on the basis of a 450MPa reference strength)
20mm diameter	267-318 MPa (on the basis of a 400MPa reference strength) 300-358MPa (on the basis of a 450MPa reference strength)
30mm diameter	242-300MPa (on the basis of a 400MPa reference strength) 272-337MPa (on the basis of a 450MPa reference strength)

Table 6.8: Predicted tensile strengths of Syalon 501 after application of a size correction factor *(Appendix [P] shows these calculations)

This diagrammatic representation of the shrinking load bearing capacity with increasing specimen diameter supports the widely accepted view that the use of large monolithic ceramics in tension imposes large limitations, as here where a 30mm Syalon 501 member in tension is clearly at very severe risk.

By reference to the 400-450MPa tensile strength bands and the FEA predicted stresses for 30mm diameter joints with and without copper, it can be seen simplistically in Figure 6.45 that the maximum residual strengths that these joints might retain, even if not weakened by the brazing process (i.e. are perfectly formed, though thermally stressed joints) these values would only be –30 MPa and 0 MPa on the basis of a nominal 4mm diameter Syalon 501 specimen's strength of 400MPa and with $8 \leq m \leq 14$, or of 0 and 65MPa against a nominal of 450MPa, again with $8 \leq m \leq 14$, respectively.

Alternatively Figure 6.45 shows that a peak residual tensile stress of 272MPa on a Syalon 501/AISI 321 joint could exactly balance out the predicted tensile strength of a 30mm diameter Syalon 501 cylinder in an ideal joint containing no brazing faults where the nominal tensile strength of a 4mm diameter Syalon 501 reference test piece was 425MPa with 'm' approximately 10.

Consistency between the 20mm diameter joint and the 30mm diameter joint group averages, both with and without copper interlayers can be shown by again applying equation 1, using as reference the Weibull modulus values 1.25 and 0.796 obtained from the 20mm diameter tensile test results, these being the two largest populations from among the 5, and considered therefore to be the most accurate.

Thus whereas a group average of 47.62MPa existed for the 20mm diameter copper-bearing joints, this predicts a value for the 30mm diameter copper-bearing joints of 24.89 MPa. Similarly, the strength value for 20mm diameter joints without copper is reduced in 30mm diameter joints without copper from 21.96MPa to 7.9MPa. The actual values for 30mm diameter joints were close to these predicted values. Although no 30mm diameter joints were free of joining defects however, peak values of ≥12.8MPa and ≥16.76MPa respectively fell within the range of experimental error and again clearly showed how close these two large diameter joint systems were to their maximum diameters.

In practice, however not one specimen from any of the five groups produced, fractured in cooling from the brazing operation. One 20mm diameter specimen broke during setting up for tensile testing, so might conceivably have contained small cracks generated by the excessive cooling rates that this joint was known to have experienced. Thus the dynamics of cooling, which clearly contributed to excessive interfacial stress generation in this case, may have created a situation where insufficient opportunity was presented to the stress dissipation mechanisms provided by the slender featheredges and the extended (curved) peripheral regions introduced to remove the stress singularity, to perform their function.

It is suggested that, because the steel featheredges and both interfaces of the copper interlayer were allowed to work harden to just within their full potential in the remainder of the joints tested, that the pattern of cooling rates across the two interfaces must, fortunately, have approached the optimum for maximum dissipation of thermally induced brazing stresses.

More impressive is the fact that all joined samples were left for several days and, in some cases weeks before tensile testing, which gave ample opportunity for any cracks produced during cooling to propagate either partially or fully across the section of the joints before testing.

It has been clearly shown by the FEA and in the experimental investigation that strengths above 40 MPa can be obtained in 20mm diameter brazed joints with copper interlayer in the 501/AISI 321 system. This result contrasts favourably with Kussmaul and Munz[98] who were unable to join Al_2O_3 - Ck45 carbon steel at only 10mm diameter and with a mismatch of only 1.7:1 being only half the value 3.4:1 for the Syalon 501/AISI 321 system joined successfully in the current investigation.

Whilst they did achieve tensile strengths between 50 – 150 MPa for 10mm hemispherical and truncated cone interfaced joints for the Al_2O_3 –Ni42 superalloy system, this strength range was identical to that obtained for their simple flat faced butt joints in this system, which is only to be expected for a system in which the CTE ratio deviates hardly at all from unity.

The results from the present investigation compare favourably also with those of Foley and Andrews[68] whose single flat interfaced 12mm diameter joints containing 2mm copper interlayers tested in tension yielded values up to 120MPa, though only between Si_3N_4 and Nilo-K where the CTE ratio was again almost unity. They showed average tensile strength values of 38 MPa and 48 MPa for joints of only 12mm diameter between Syalon 201 with cast iron with 12 CrFe respectively with CTE mismatch ratios up to 3.5.

Clearly, even with the attractive residual strengths shown in the present investigation, there is still scope for improving on the manufacturing techniques to raise the level of group average values up to, or above those highest individual values for joint strengths already obtained.

The author believes that the approach used in Figure 6.45 for presenting, albeit simplistically the proportions of a ceramic's potential strength (as measured under ideal condition on typically small test pieces), that may be assigned to (i) strength-reducing residual stresses, (ii) the size reduction effect on strength, and (iii) the residual proportion of the strength available for load-carrying in service applications, may be original. It should be noted however that the apparent working stress range available should be treated with the usual caution applied in design, that is that a factor of safety be applied to cover service stress overloads and, ideally a factor to allow for imperfect brazing manufacture.

The approach provides a ready source of design information and for comparing likely operating stress ranges for specified ceramics in relation to their load bearing diameter within a single metal to ceramic system, both when and when not containing interlayers.

Furthermore, where lower CTE mismatch values apply as in Si_3N_4- Nilo-K, the proportion assigned to peak residual tensile stress will be much lower in relation to that fixed proportion lost to the size effect, leaving a wider operating range available for the ceramic-to-metal joint, or to the safe use of a wider range of commercially faster cooling rates without compromising the width of the working stress range too much.

This is summarised in Figure 6.46 which shows that, while in high CTE mismatch joints the maximum applied stress in use may be limited by the tensile residual stresses generated by cooling, by contrast, where the CTE mismatch is small, then it is the strength reduction factor that will predominate as larger diameter joints are manufactured.

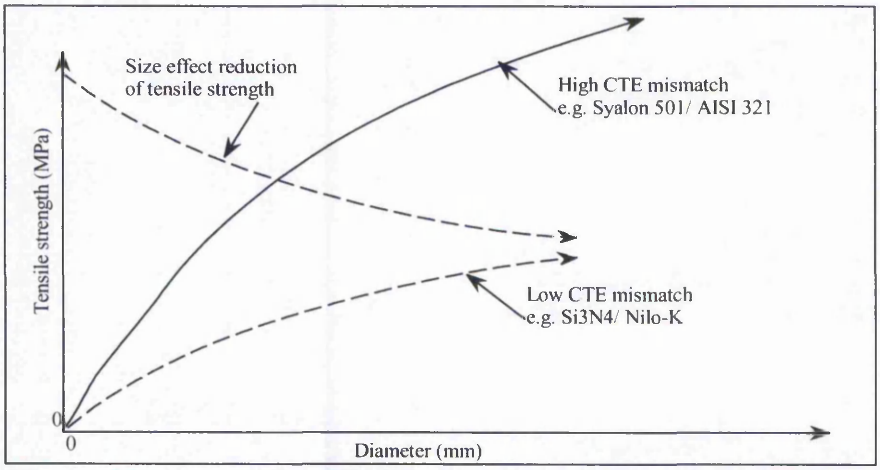

Figure 6.46: Comparative operational tensile stress ranges for metal-to-ceramic joints of increasing diameter, with high and low CTE mismatch

Methods for widening the available working stress band therefore comprise

(i) use of higher strength ceramic, with higher Weibull modulus

(ii) use of a low CTE mismatch system.

(iii) taking steps to reduce the maximum induced tensile stress value by imposing slow cooling with optimum cooling rates across individual interfaces to give maximum opportunity for each of the stress dissipation mechanisms available to the featheredges and interlayers to be used to full potential.

6.5 Conclusions

The conclusions for this chapter are incorporated into the general conclusions presented on the pages immediately following under section 7.1

Chapter 7

Conclusion and Recommendations for Further Work.

7.1 General Conclusions

This research has proved that removal of the excessive stress concentration associated with the peripheral region of simple flat interfaced joints, has allowed useful joints to be manufactured with dome or dome-flat interface geometries in diameters up to 30mm in the Syalon 501/AISI 321 system despite a very unfavourable thermal expansion mismatch ratio. These joints are believed to be the largest and the strongest of their type recorded. It has proved the advantage to be gained in reducing stresses in metal/ceramic joints by careful design of interfaces and interlayers, and by the use of dome and dome-flat interfacial geometries in particular.

The FEA modelling generated data that were considered very satisfactory in indicating the residual stress levels induced by differential-thermal stresses in the dynamic situation of cooling. Confirmation of these values was provided by the good agreement with experimentally determined strengths for 20mm and 30mm diameter joints made both with and without copper interlayers. All 10mm, 20mm and 30mm diameter joints retained their structural integrity on cooling.

Electrical discharge machining on its own proved capable of generating perfect conformity at the Syalon 501- AISI 321 interface, particularly when the convex shaped end of the prepared Syalon member was used as a finish-machining tool on the mating stainless steel member to guarantee conformity.

It is proposed that the emergence of new ceramics containing internal electrically conductive pathways provided either by interconnecting particles or by conductive coatings on contacting reinforcing fibres[126, 127] makes these materials an excellent choice for use in joints containing profiled interfaces. Generally conductive particles, while increasing the electrical discharge machinability of the dispersion-containing ceramic, also provide the additional benefit of increasing, the thermal expansion coefficient of the composite to match more closely that of the metal to which it is joined, thus reducing differential thermal mismatch strains and potential disruptive residual stresses.

Techniques were developed for the accurate machining of complex interlayers designed for the dome and dome-flat interfaced joints.

In addition, a design for producing precision cast or sintered metal interlayers was proposed which could be applicable for the mass production of interlayers for joints.

The use of Ticusil as the active metal braze of choice combined with pure copper for the shaped interlayers led to superficial dissolution of these interlayers which was unforeseen, however this turned out to have an advantageous effect in helping to ensure perfect interfacial conformities. Using such a 'semi-soluble' interlayer would result in any deviation to higher brazing temperatures producing an increased volume of liquid, ensuring a generous capillary flow of molten braze to joint's critical peripheral regions, however excessive temperatures were avoided in this research for they result in higher levels of residual tensile stress in a joint.

The use of copper interlayers within joints generally raised their strengths and always resulted in more consistency being achieved in tensile tests on metal-ceramic joints. Modes of failure of joints were attributed to:

- Misalignment
- Lack of active braze, particularly in peripheral regions
- excess of braze leading to the formation of surface globules
- hot tears

- excessive cooling rates

The additional band of copper reinforcement surrounding each machined interlayer was introduced as a practical contingency to facilitate precision manufacture of interlayers by machining. It is not believed to have altered the system's stress pattern significantly. If anything, it enhanced joint strength by carrying the position of maximum induced tensile stress, identified on the joint stress maps created by the FEA, up onto the parallel side of the specimen (ie beyond the position on the model where the curved surface of the dome or dome-flat met the parallel section of the ceramic member). Microhardness measurements taken along the length of the copper reinforcement band found it to be of uniform value, at the maximum level shown at the joint periphery.

The author has introduced the simplistic graphical concept of showing the working stress level for a metal-ceramic (or ceramic-cermet) joint system as lying between the falling strength value resulting from the ceramic's increasing diameter and the value, increasing with joint diameter, of the thermally induced stresses as predicted by FEA.

It has been shown, for lower CTE mismatch systems, that diameters in excess of 30mm can be joined, where the limiting factor on joint strength may be determined more by the decreasing strength attributable to increased joint size and modest Weibull modulus, than by the restrictive effects of induced differential thermal strains from joining.

This working band was shown to increase for a greater joint diameter with the use of stronger ceramic with a higher Weibull modulus and by choice of a low CTE mismatch system. In addition the reduction of induced stresses was shown to be achieved by the use of appropriate interlayers and by manipulation of the dynamic cooling effect for joints, to allow each stress relief mechanism incorporated into the joint's design to perform to its full potential. Finally, attention to producing the highest quality of brazing increased the factor of safety pertaining in use.

Microhardness tests proved invaluable in monitoring the differential thermal stress-induced strain within copper interlayers, proving that in 30mm diameter joints with the particular dynamic cooling pattern that was used, these strains had reached higher values compared to 20mm joints and even higher values compared to 10mm joints (the alloy hardening contribution being assumed to be approximately constant for corresponding points between periphery and joint centre line for 10, 20 and 30mm diameters samples). It is proposed that, in 30mm diameter joints, the featheredged peripheral regions of the stainless steel members and the adjacent parts of copper interlayers were virtually at the limit of their strain absorbing capacity. These microhardness tests have identified the sequence in which the hardening occurred in the thermal stress-relaxing design features comprising the stainless steel featheredges and the copper interlayers.

Increased complexity introduced within dome-interfaced joints comprising AISI 321/ Ticusil/ copper/ Syalon 501/Ticusil/copper/Ticusil/AISI 321 led to assembly difficulties. The use of dome -flats restricted the chance of rotation between members during assembly and loading for brazing. It is proposed that better results could have been obtained for 10mm diameter joints had dome-flat interfaces been used. Single-, and particularly double-domed interfaces are not recommended especially where multiple interfaces are involved.

The strongest joints produced in this research were characterized by freedom from defects in the starting ceramic, by good alignment along the tensile axis, by complete filling of all interfaces up to joints' peripheries, but not by the use of excess Ticusil such that any excess would be expelled to form stress-raising globules on surfaces external to the joint. In addition, interlayers had to be machined to precise form, cooling rates kept low and fracture paths initiated on the parallel section above the joint's initial curvature and level with the top of the copper reinforcement.

7.2 Recommendations for Further Work

The dome and novel dome-flat interfaces designed, made and tested in this research have been uniquely referred to by the present author as a special type of functionally graded interface[124]. This is because the peaks at the metals' (and interlayers') peripheries broaden progressively in relation to apex height until the metal proportion measured perpendicularly to the test piece axis has progressed smoothly without discontinuities from 0 to 100% at the centreline for a dome interface or from 0% to 75% then abruptly to 100% at the end of the curved interface and beginning of the flat section for a 20mm diameter dome-flat interface. For a 30mm dome-flat interface these proportions become 0% to 55.5% followed by the abrupt transition to 100%. The ceramic proportion in this case progresses smoothly from 100% to 44.4% before jumping to 0%.

Appendix [P] shows ways in which the flat part of the dome-flat interface might be redesigned in such a way as to reduce the magnitude of the discontinuities described above for 20mm and 30mm diameter dome-flat joints. The additional FEA work outlined in Appendix [P] was conducted early in this research but discontinued, in part owing to practical difficulties experienced in machining the EDM tools for some of these more complex profiles, (in particular the 3-D repeated sine wave pattern).

It is recommended that these profiles be investigated through a more detailed FEA study, supported by joints production and testing to investigate whether, by designing a degree of interpenetration between the ceramic and the metal in the central (previously flat) parts of the interfaces, that these central areas might absorb a higher proportion of induced stresses. It might then reduce to some extent the excessive peak tensile stresses and levels of featheredge work hardening at peripheries of joints produced, both with and without deformable interlayers.

This modification of the central section of the interface might alternatively be modified by the incorporation of ceramic (or metal) pegs to dowel the interfaces of metal and ceramic together before the application of brazing foils, punched out to allow these dowel's to pass through them during joint assembly. Electrical discharge machining of these holes would be very easy. In addition to further investigation of modified interface profiles it is proposed that the emerging conductive ceramics be evaluated in metal-to-ceramic joints, in particular zirconia-TiB_2 and zirconia-TiN to steels.

References

[1] Nicholas, M. G., *"Joining of ceramics"*. The Institute of Ceramics, Chapman and Hall, 1990

[2] Schwartz, M.M., *"Ceramic joining"*, ASM International, 1990

[3] Morrell, R., *"Handbook of properties of technical and engineering ceramics"* Pt.2, Data reviews Section 1,High-alumina ceramics, HMSO, 1987

[4] Janczak-Rusch, J., Zigerlig, B., Klotz, H, Elsener, R., Brem, F., and Kübler, J *"Joining of Si3N4/TiN Ceramics with Steel Components Using Particle Reinforced Active Brazing"*, 6th International Conference on Joining Ceramics, Glass and Metal, Munich Publ. DVS, 30 Sept 2002

[5] Indacochea, J.E. and Tillmann, W., *"Joining Techniques in Advanced Ceramics"*, in Proc. 5th Int. Conf. 'Joining Ceramics, Glass and Metal', DVS-Berichte Band 184, May 17-19, pp 29 –33, 1997

[6] Ruhle, M. and Mader, W., *"Structure and Chemistry of Metal/Ceramic Interfaces"*, Designing Interfaces for Technological Applications, Elsevier Applied Science, 1988

[7] Tinsley, N.D., *"The Reduction of Residual Stress Generated in Metal-Ceramic Joining"*, PhD Thesis, Nottingham Trent University, 1996

[8] Tinsley, N.D., Huddleston, J. and Lacey, M.R., *"The Reduction of Residual Stress Generated in Metal-Ceramic Joining"*, Materials and Manufacturing Processes, **13**, No 4, pp 491-504, 1998

[9] Lee. K.-Y, Case. E.D. and Reinhard. D. "Microwave Joining and Repair of Ceramics and Ceramic Composites" Ceramic Eng. and Sci. Proceedings, Am.Ceram. Soc. **18**, Issue 4, pp 543-550, 1997

[10] Zheng, J., Unal, O., and Akinc, M., "*Green State Joining of SiC using Polycarbosilane*" J. Am. Ceram. Soc., **83**, No 7, pp1687-1692, 2000.

[11] Zheng, J., and Akinc, M., "*Green State Joining of SiC without Applied Pressure*" J. Am. Ceram. Soc, **84**, No. 11, pp 2479 - 2483, 2001

[12] Unal, O., Sordelet, D. J., Bernard, D., and Akinc, M., "*Strength Measurement of Thick Brittle Coatings on Metals*", Ceramic Engineering and Science Proceedings. **4**, pp 283-292, 1998

[13] Peteves, S.D., Ceccone G., Paulasto ,M., Stamos, V. and Yvon, P."*Joining Silicon Nitride to Itself and to Metals*" Overview, JOM, **48**, No 1, pp 48-52, 1996

[14] Santella, M.L., "*A Review of Techniques for Joining Advanced Ceramics*", Ceramic Bulletin, **71**, No 6, pp 9 47-954, 1992

[15] Suganuma, K., "*Recent Advances in Joining Technology of Ceramics to Metals*", ISIJ International, **30**, No12, pp1046-1058, 1990

[16] Elssner, G. and Petzow, G. "*Metal-Ceramic Joining*", ISIJ International, **30**, No12, pp 1011-1032, 1990

[17] Grunling, W and Linssen, G "*Ceramic-to-metal joints*" in Proc. 5th Int. Conf. 'Joining Ceramics, Glass and Metal', DVS-Berichte Band 184, May 17-19, pp 222-221, 1997

[18] Lange, H., Dogigli, M. and Bickel, M., "*Ceramic fasteners for high temperature applications*", ibid, pp 55-58, 1997

[19] Weiss, R. and Sassani, F., "*Strength of Friction Welded Ceramic/Metal Joints*", Journal of Material Science and Technology, **14**, No. 6, pp 554-560, 1998

[20] Suthoff, B., *"The Processes of bonding by the friction welding"*, in Proc. 4th Int. Conf. Joining Ceramics, Glass and Metal', Konigswinter, May 17-19, Ed. Krappitz H and Schaeffer, H. A., Publ. Verlag der Deutschen Glastechnischen Gesellschaft, pp 272-278, 1993

[21] Greitman, M. J. and Weiss, R., *"Advances in Friction Welding and Ultrasonic Welding of Ceramics to Metals"*, Ceramic Transactions, Ceramic Joining, Edit. Ivar. E. Reimanis, Charles. H and Antoni P. Tomsia, Publ. The American Ceramic Society, **77**, pp 165-176, 1997

[22] Broring Vegla, K., and Vereinigte Glaswerke G., *"Adhesive bonding of automotive and architectural glass",* in Proc. 4th Int. Conf.'Joining Ceramics, Glass and Metal', Konigswinter, May 17-19, Ed. Krappitz H and Schaeffer, H. A. Publ. Verlag der Deutschen Glastechnischen Gesellschaft, pp 356-363, 1993

[23] Lemus, J. and Drew, R.A. L., *"Diffusion bonding of silicon nitride to titanium"*. British Ceramic Transactions, **99**, No 5, pp 200 - 205, 2000

[24] Morozumi, S., Kikichi, M., Saito, K., and Mukaiyama, S. I., "*Diffusion Bonding of Niobium and Y2O3-Stabilised ZrO2 or HfO2*", ISIJ International, **30**, No.12, pp 1066-1070, 1990

[25] Naka, M., Shibayanagi, T. and Miyake, H., *"Phase Reaction of Diffusion Bonded Interface between TiAl and SiC"*, Proc. 5th Int. Conf. on Brazing, High Temperature Brazing and Diffusion Bonding , Aachen, Germany, pp310-313, 1998

[26] Derby, B. and Quin, C.D., "*Interface Reactions During the Diffusion Bonding of ZrO_2 to Ni and Ni-Cr alloys*", in Proc. 3th Int. Conf.'Joining Ceramics, Glass and Metal', Aachen, May 17-19, pp 54-57, 1992

[27] Stoop, B. and Ouden, G., *"Diffusion Bonding of Silicon Nitride to Austenitic Stainless Steel without Interlayers"*, Metallurgical Transactions, **24A**, pp 1835-1843, 1993

[28] Derby, B. and Wallach, E., "*Theoretical-Model for Diffusion Bonding*", Metal Science, **16**, No.1, pp 49-56, 1982

[29] Wilkes, J., "*Ceramic metal joining*" MSc Dissertation, Nottingham Trent University, December 1996

[30] Hill and Wallach, E., "*Modelling Solid State Diffusion Bonding*", Acta Metal, **37**, No.9, pp 2425-2437, 1989

[31] Van Loo, F. J. J. and Kodentsov, A. A., "*Diffusion bonding of Si-containing ceramics to transition metals*" in Proc. 5th Int. Conf. 'Joining Ceramics, Glass and Metal', DVS-Berichte Band 184, May 17-19, pp 60-63, 1997

[32] Tanghe, B., Evrard, O., Meynckens, J.P and Delannay F."*Diffusion bonding between Inconel 600 and alumina*"in "Interfaces in New Materials", Ed. Grange. P and Delmon, B., Publ, Elsevier, London, pp 190-199, 1991

[33] Nicholas, M.G., " *Joining processes - Introduction to Brazing and Diffusion Bonding*", Kluwer Academic Publishers, 1999.

[34] Paulasto, M., and Kivilahti, J., "*Active Brazing of Al2O3 with Ag-Cu-Ti Filler Alloys*", Journal of Materials Research, **13**, No. 2, pp343-352, 1998.

[35] Urai, S., Kimura, I., Maeda, K. and Naka, M., "*Brazing of SiC Using Cu-Sn-Ti*", ibid, pp 314-316, 1998

[36] Tamai, F. and Naka, M., "*Role of Ag and Ti in Brazing of Si3N4 with Cu-Ag-Ti Filler Metals*", ibid, pp 317-319, 1998

[37] Feng, J.C., Yuli, L., Naka M. and Fukai, T., "*Diffusion Bonding of SiC Ceramics with Metals*", Proc. 9th National Conf. on Brazing, Soldering and Diffusion Welding, Yangzhong, China, pp 387-392, 1996

[38] Stephens, J.J., Vianco, P.T., and Hosking, F.M., "*The active metal brazing of TZM-Mo and SiN Ceramics*", JOM, **48**, No 1, pp 54-58, 1996

[39] Tillmann, W., Lugscheider, E., Schlimback, K., Manter C., and Indacochea, J.E., " *Heat-Resistant Active Brazing of Silicon Nitride – Part 1: Mechanical Evaluation of Braze Joints*," Welding Journal, **76**, No 8, pp 300-304, 1997

[40] Eustathopoulos, N., Nicholas, M.G., and Drevet, B., "*Wettability at high Temperatures*", Pergamon, 1999

[41] Naidich, Y., "*Ceramic - Metal interface: adhesion and wettability process in fundamental and practical aspects*", British Ceramic Proceedings, **1**, No 60, pp 315-318, 1999

[42] Dorn, L., El-Ashram, A., Shaker M. and Abd El-Hafez, H., "*Strength improvement of Si_3N_4 - metal joints using alternative braze metal and brazing procedure*", in Proc. 5th Int. Conf. 'Joining Ceramics, Glass and Metal', DVS-Berichte Band 184, May 17-19, pp 154-156, 1997

[43] Baffie and Saint-Antonin, F., "*Joining of aluminium nitride to copper by brazing*", British Ceramic Proceedings**1**,, No 60, pp329-331, 1999

[44] Chaumat, G., Lovato, G. and Lemoine, P., "*Brazing CFC on DS-copper for divertor flat tiles*", in Proc. 4th Int. Conf. 'Joining Ceramics, Glass and Metal', Konigswinter, Ed. Krappitz H and Schaeffer, H. A. Publ. Verlag der Deutschen Glastechnischen Gesellschaft, pp 401-405, May 17-19,1993

[45] Klein, J., "*Processing with Microwaves*", Metals Progress, **1,** No 4, pp 36-39 1985

[46] Palaith, D. and Silberglitt, R., "*Microwave Joining of Ceramics*, " Am. Ceram. Soc.Bull., **68,** No 9, pp 1601 – 1606, 1989

[47] Binner, J.G., Fernie, J.A. and Whittaker, P.A., "An Investigation into Microwave Bonding Mechanisms via a Study of Silicon Carbide and Zirconia", *Journal of Materials Science* , **33**, No12 pp 3023-3029 1998

[48] Unal, O., Anderson, IE and Maghsoodi, S.I., "*Test Method To Measure Shear Strength Of Ceramic Joints At High Temperatures*" J. Am. Ceram. Soc., **80**, No.5, p1281-1284, 1997

[49] Smithells. C. J. "Metals Reference Book" 6th Edition, Edit. Brandes. E.A. Publ., Butterworths pp **11**-151, pp **11**-363, 1983

[50] Lehman, R. L., El-Rahaiby, S. K., and Wachtman, J. B., "*Handbook on Continuous Fiber-Reinforced Ceramic Matrix Composites*", Am. Ceram. Soc., New York p 495, 1995

[51] Cartz, L., "*Nondestructive Testing*", ASM Materials Park, OH:, 1995, Available at <URL: http://www.asm-intl.org

[52] Schwartz, M.M., "*Composite Materials*", Prentice-Hall, 1997

[53] Bray D. E., and McBride, D., "*Nondestructive Testing Techniques*", Publ. Wiley and Sons, 1992

[54] Richerson, D.W., "*Modern Ceramic Engineering*", Publ. Marcel Dekker, 2nd Ed, 1992

[55] Hansen, M. "*Constitution Of Binary Alloys*" 2nd ed. McGraw Hill, pp 643-646,1958

[56] Netzelmann, U., "*Non destructive testing of ceramic-metal joints by high-frequency ultrasound techniques*" in Proc. 4th Int. Conf.'Joining Ceramics, Glass and Metal', Konigswinter, Ed. Krappitz H and Schaeffer, H. A. Publ. Verlag der Deutschen Glastechnischen Gesellschaft, pp 168-175, May 17-19, 1993

[57] ASM Handbook, *"Non destructive Evaluation and Quality Control"* ASM Materials Park, OH:, **17**, p. 231, 1992

[58] ASNT *Handbook: Nondestructive Testing,* 2nd ed., ASNT,1985

[59] Kim, J. and Liaw., P. K., *"The Nondestructive Evaluation of Advanced Ceramics and Ceramic-Matrix Composites"* JOM-e,. **50**, No. 11, 1998. Available at <URL:http://www.tms.org/pubs/journals/JOM/9811

[60] Ekinci, S. and Bilge A.N., "*British Journal of NDT",* **33** , No 9, pp 450-452, 1991

[61] Pollinger, J., "*Current Usage And Needs Assessment Of NDE For Structural Ceramic Component Applications*" Nondestructive Evaluation of Ceramics, Ceramic Transactions, Ed. Christopher Schilling, J. N. Gray, R. Gerhardt, and T. Watkins, Publ. The American Ceramic Society, **89**, pp116-119, 1997

[62] Nagasawa, S., Fukuzawa, Y., Takahashi, H.,Yamada, Nagaoka, T., Sakuta, H., and Tateno, M., "*Analysis of cooling effects on residual stress distribution on joined cylindrical dissimilar materials",* in Proc. 5th Int. Conf. 'Joining Ceramics, Glass and Metal', DVS-Berichte Band 184, May 17-19, pp 120-121, 1997

[63] Gao, M., and Bao, F., "*Brazing of Silicon Nitride With Cu-Based Filler Metals Mechanism and Residual Stress in its joints"*, Materials Science Forum, pp 399-404. 1995

[64] Nakao, Y., Nishimoto, K., and Saida, K., "*Reaction Layer Formation in Nitride Ceramics (Si_3N_4 and AlN) to Metal Joints Bonded with Active Filler Metals"*, ISIJ International, **30**, No 12, pp 1142-1150, 1991

[65] Klomp, J. T., "Surfaces and Interfaces of Ceramic Materials", ed. L.C. Dufour, C. Monty, and G. Petot-Evras, Nato ASI series Kluwer, pp 375-377, 1989

[66] Electronics, "*Satellites Use Alloy to Bond Ceramics, Metal*", Nickel, **11**, No4, pp 8-9, 1995

[67] Indacochea, J.E., Tillmann, W., Lugscheider, E., and Xu, R., "*Kinetics and Microstructural Aspects of the Reaction Layer at Ceramic/Metal Braze Joints*", Journal Materials Science, **31**, pp445, 1996.

[68] Foley, A.G. and Andrews, D. A., "*Joining Metals to Ceramics using Active Metal Brazing*", in Proc. 2nd European Colloquium, 'Designing Ceramic Interfaces II', Petten, Ed Peteves, S. D., Publ. Commission of the European Communities, pp 411-427, November 11-13, 1993

[69] Yoshino, Y. and Shibatta, T., "*Structure and Bond Strength of a Copper-Alumina Interface*", J. Am. Ceram. Soc, **74**, No 10, pp 2756-2760, 1992

[70] Rabin, B.H., Williamson, R.L., Watkins, T.R, Wang, X. L, Hubbard, C.R., and Spooner, S., "*Characterization of Residual Stresses in Graded Ceramic-Metal Structures: A Comparison of Diffraction Experiments and FEM Calculations*", Proceedings of the 3rd Int. Symposium on Structural and Functional Gradient Materials, Ceramic Transactions, Am. Ceram. Soc., pp 209-14, 1995.

[71] Bossi R. H., and Georgeson, G.E., "*Materials Evaluation*", **53**, pp 1198-1203, 1995,

[72] Kovalev, S., Miranzo, P.and Osendi, M. I., "*Finite element simulations of thermal residual stresses in joining ceramics with thin metal layers*". J. Am. Ceram. Soc., **81,** No 1, pp42-48, 1998

[73] ANSYS5.5.1 Manual - *Structural Guide*. 000646. First Edition. Swanson Analysis Systems Inc. P. O. BOX 65, Johnson Road, Houston, PA, U.S.A.

[74] Wielage B., and Schuler, H., "*Simulation of thermal residual stresses in brazed metal-ceramic joints using the Finite Element Method*" in Proc. 5th Int. Conf. 'Joining Ceramics, Glass and Metal', DVS-Berichte Band 184, May 17-19, pp 114-116, 1997

[75] Sckuhr, M. A., Bruckner-Foit, A., Munz, D., and Yang, Y., "*Stresses near the singular point of a two materials joint considering elastic-plastic material behaviour*" ibid, pp 117-119, 1997

[76] Nagasawa, S., Fukuzawa, Y., Takahashi, H.K, Yamada, Nagaoka, T.K, Sakuta H., and Tateno, M., "*Analysis of cooling effects on residual stress distribution on joined cylindrical dissimilar materials*" ibid, pp 120-121, 1997

[77] Suganuma K. and Okamoto, T., "*Interlayer Bonding Methods For Ceramic / Metal Systems With Thermal Expansions Mismatches*", Journal of Material Science, **22** , 1031-1034, 1985

[78] Fernie. J. A. "*Joining Ceramic Materials*" in Ceramic Joining, Ceramic Transactions, Eds. Reimanis, I. E. Henegar C. H and Tomsia, A. P. Publ. American Ceramic Society, **77**, pp 3-14, 1997

[79] Agathopoulos, S., Moretto, P., Peteves, S.D., Emiliano, J.V. and Correia, R.N., "*Brazing of Zirconia to Ti and Ti6AlV*", ibid., pp 75-82, 1997

[80] Intrater, J., "*Review of Some Processes for Ceramic-To-Metal Joining*", Materials and Manufacturing Processes, **8**, No 3, pp 353-373, 1993

[81] Naka, M., "Interfacial structure of SiC/metal joint brazed with Ni-Ti alloys" in Proc. 4th Int. Conf.'Joining Ceramics, Glass and Metal', Konigswinter, May 17-19, Ed. Krappitz H and Schaeffer, H. A. Publ. Verlag der Deutschen Glastechnischen Gesellschaft, pp 85-91, 1993

[82] Naka, T. Fukai, El-Sayed, M.H., Feng, J.C. and Schuster, J.C. "*Bonding and Interfacial Structure of Ceramic/Metal*", Proc, 5th Inter. Conf. on Brazing, High Temperature Brazing and Diffusion Bonding, Aachen, Germany, pp85-87, 1998

[83] Lugscheider E. and Buschke, I., "*New Ni-Hf based filler metals for high temperature joining of innovative materials*" in Proc. 5th Int. Conf. 'Joining Ceramics, Glass and Metal', DVS-Berichte Band 184, May 17-19, pp 132-133, 1997

[84] Klose, H., Podlesak, H., and Wielage, B., "*Reaction layer formation on the metal side of active brazed metal-ceramic joints*", in Proc. 5th Int. Conf. 'Joining Ceramics, Glass and Metal', DVS-Berichte Band 184, May 17-19, pp 170-172, 1997

[85] Batfalsky, P., "*Ion implantation influence on the stress state in high temperature brazed metal-to-ceramic joints*", in Proc. 4th Int. Conf.'Joining Ceramics, Glass and Metal', Konigswinter, Ed. Krappitz H and Schaeffer, H. A, Publ. Verlag der Deutschen Glastechnischen Gesellschaft, May 17-19, pp 36-43, 1993

[86] Lugscheider, E., Tillmann, W. and Broich, U., "*Interfacial reactions between active filler metals and high performance ceramics*", ibid, pp 125-136, 1993

[87] Torvund, T., Akselsen, O., Grong, M., and Ulvensoen, O., "*Vacuum brazing of alumina to AISI 304 austenitic stainless steel*",ibid, pp 256-263, 1993

[88] Ilto, M. and Kato, N. "*Brazing ceramics to metals and related application*" ibid, pp 321-330, 1993

[89] Weise, W., Degussa, H. "*Industrial applications of active metal brazed ceramic parts*", ibid, pp 331-340, 1993

[90] Hegner, F. Klahn, T. Schmidt, E. Reimann, P. Messmer, S. Breitenstein, Guntherodt, H., and Endress, H.J., "*Active brazing foil prepared by rapid quenching from the melt and its application to join ceramics for pressure sensors*", ibid ,pp 348-355, 1993

[91] Naka, M., Feng, J C and Schuster, J. C., "*Interfacial reactions and diffusions between silicon base and metals*", Ceramic Joining, Ceramic Transactions, Edit. Reimanis, I. E. Henegar C. H and Tomsia, A. P. Publ. The American Ceramic Society, **77**, pp 127-136, 1997

[92] Van der Sluis, H.H., "*Active metal brazing of Technical Ceramics, High Temperature Brazing and Diffusion*", Welding, Lectures and Posters of the 3rd International Conference presented by the German Welding Society (DVS) in Aachen, pp 68-72, November 24-26, 1992

[93] Santacreu, P., Koutny, J. L., Bienvenu, Y., Bartout, J.D., and Colin, C., "*Reactivity of ternary Ag-Cu-Ti in the brazing of silicon nitride to a construction steel*", High Temperature Brazing and Diffusion Welding, Lectures and Posters of the 3rd International Conference presented by the German Welding Society (DVS) in Aachen, pp 239-242, November 24-26, 1992

[94] Ferro, A. C., and Derby, B., "*Liquid phase bonding of siliconized silicon carbide*",Journal of Materials Science, **30**, No 24, pp 6119-6135, 1995

[95] Lee, H. K., "*A study of the wetting, microstructure and bond strength in brazing SiC, BY cU-x (x=Ti, V, Nb, Cr) alloys*", Journal of Materials Science, **31,** No 13, pp 4133, 1996

[96] Nakamura, M., and Shigematsu, I., "*Joining of Carbon fibre-reinforced silicon nitride composites with 72Ag-26Cu-2Ti filler metal*", Journal of Materials Science, **31,** No 17, pp 4629-4634, 1996

[97] Ramsey, M.J. and Lewis, M. H, "*Interfacial Reaction Mechanisms in Syalon*

Ceramic Bonding", Material Science and Engineering, **71**, pp 113-122, 1985

[98] Kussmaul, R., and Munz, D., "*Residual stresses in brazed ceramic-metal joints of various interface geometries and their mechanical behaviour*" in Proc. 4th Int. Conf.'Joining Ceramics, Glass and Metal', Konigswinter, Ed. Krappitz H and Schaeffer, H. A. Publ. Verlag der Deutschen Glastechnischen Gesellschaft,pp 152-159, May 17-19, 1993

[99] Doyama, M., Somiya, S. and Chang, R.P.H., "*Metal-Ceramic Joints*" Conference Proceedings in Advanced Ceramics, Tokyo, Japan, MRS International, **8**, 1998

[100] Kivilahti, J. K and Kouhia, R. "*Effect of plastic and creep deformations on thermal stress in brazed AIN-metal joints*", The Processes of bonding by the friction welding, in Proc. 4th Int. Conf. Joining Ceramics, Glass and Metal', Konigswinter, Ed. Krappitz H and Schaeffer, H. A. Publ. Verlag der Deutschen Glastechnischen Gesellschaft, pp 160-167, May 17-19, 1993

[101] Maeda, M., Igarashi, O., Shibayanagi, T. and Naka, M., "*Relation Between Interfacial Structure and strength of Solid State Diffusion Bonded V/Si3N4 Joints*", Proc. Inter. Symp. on Environment-Conscious Innovative Materials Processing with Advanced Energy Sources, Kyoto, Japan, pp 589-594, 1998

[102] Üstündag, E., "*Metal-Ceramic Composites for Hostile Environment Applications,*" Advances in Ceramic Matrix Composites III, Edit. Bansal, N. P. and Singh, J. P, Ceram. Trans., **74**, pp 595- 597, 1996

[103] Yu, H. Y, "*Residual Stresses in Ceramic-Interlayer-Metal Joints*", J. Am. Ceram Soc, **76**, No.7, pp 1661-1664, 1993

[104] Suganuma, K., Okamoto, T., Miyamoto, Y., Shimada, M., and Koizumi M., "*Joining Si3N4 to 405 Steel with Soft Metal Interlayer*", Material Science and

Technology, **2**, pp 1156-1161, 1986

[105] Xian, A. P., and Si, Z.Y., "*Interlayer Design For Joining Pressure-Less Sintered Sialon Ceramic And 40Cr Steel Brazing With Ag57Cu38Ti5 Filler Metal*", Journal of Materials Science, **27**, pp 1560-1566, 1992

[106] Jacquemin, J.P., Juve. D., Treheux. D., Miranzo, P., and Oscendi, M. I., "*Joining Of Si_3N_4 Using Al And Ni Interlayers*", Interfacial Science in Ceramic Joining, Kluwer Academic Publishers, 1998.

[107] Rabin, B. H., and Williamson, R. L., "*The effect of interlayer Properties on Residual Stresses in Ceramic-Metal Joining*", Ceramic Joining, Ceramic Transactions, Ed. Reimanis, I. E. Henegar C. H and Tomsia, A. P. Publ. The American Ceramic Society, **77**, pp 137-148, 1997

[108] Rabin, B.H., Williamson, R.L., Bruck, H.A., Wang, X.L., Watkins, T.R., Feng, Y.Z. and Clark, D.R. "*Residual Strains in an Al2O3-Ni Joint Bonded with a Composite Interlayer: Experimental Measurements and FEM Analysis*", J. Amer. Ceram. Soc. **81**, No 6, pp 1541-1549,1998

[109] Suga T., and Elssner, G., "*Characterisation of Strength of Ceramic-Metal Joints*", Proceedings of The Material Research Society International Meeting On Advanced Materials, **8**, pp 99-104, 1988

[110] Koguchi, H., Hino, T., Kikuchi Y., and Yada, T., "*Residual Stress Analysis of Joints of Ceramics and Metals*", Experimental Mechanics, **34**, No.2, pp 116-124, 1994

[111] Kim W. B., and Na, S. J., "*A Study of the Residual Stress Reduction Method Through the Mechanical Loading Cycle in Metal- to-Ceramic Brazed Joints*", Proceeding of the Institution of Mechanical Engineers Part-B-Journal of Engineering Manufacture, **209**, No.1, pp 53-62, 1995

[112] Pintschovius, L., Pyka, N., Kussmaul, R., Munz, D., Eigenmann, B. and Scholtes, B., "*Experimental and Theoretical Investigation of the Residual Stress*

Distribution in Brazed Ceramic-Steel Components", Material Science and Engineering, **177**, pp 55-61, 1994

[113] Foley A. G. and. Winters C. G, "*The use of Finite Element Methods in the Design of Ceramic –to-Metal Joints*", British Ceramic Proceedings, **48,** pp 107-122, 1991

[114] Maier H. R., Magin, M. Kruhoffer, W and Schmitz, F., "*Reliability analysis of active brazed ceramic-metal-joints",* in Proc. 5th Int. Conf. 'Joining Ceramics, Glass and Metal', DVS-Berichte Band 184, May 17-19, pp 110-113, 1997

[115] Schreieck, B., Eigenmann, B., and Lohe, D., "*Residual stresses and failure of brazed joints of cemented carbide and steel similar to cutting tools",* in Proc. 5th Int. Conf. 'Joining Ceramics, Glass and Metal', DVS-Berichte Band 184, pp140-144, May 17-19, 1997

[116] Steffens, H. D., Wielage, B., Wilden, J., Mohwald, K., Meininghaus, T. and Nolle, A., "*Investigations on production, design and calculation of joined composites*", in Proc. 5th Int. Conf. 'Joining Ceramics, Glass and Metal', DVS-Berichte Band 184, May 17-19, pp 192-194, , 1997

[117] Moredecai, N. L., "*Mechanisms of Material Removal in Advanced Ceramics Processed by Electrical Discharge Machining (E.D.M)*", PhD. Thesis, The Nottingham Trent University, 1994

[118] Trueman C. S. " The Electrical Discharge Machining of Ceramics", PhD thesis, The Nottingham Trent University, 1997

[119] Mordecai N L , Trueman C S and Huddleston J., "*A Die Sinking Technology for the Evaluation of Spark Erodable Ceramics"*, Br. Ceram Trans., **95**, No4, pp 157-161, 1996

[120] Huddleston, J. and Trueman, CS, "*Contribution to Ultra Hard Materials For Tribological Application*", (ULTRATRIBO), BRITE –EURAM Project BE96-3356 Final Technical Report, Commission of the European Communities, 1999

[121] Pitman, A. and Huddleston, J., "*Electrical discharge machining of ZrO2/TiN particulate composite*", British Ceramic Transactions , **99**, No 2, pp 77 – 83, 2000

[122] Put, S., Vleugels, J., Van der Biest, O., Trueman C.S., and Huddleston J., "*Die Sink Electrodischarge Machining Of Zirconia Based Composites",* British Ceramic Transaction, **100,** No 5, p 207 –213, 2001

[123] Jones , A.H..,. Trueman C., Dobedoe, R. S., J. Huddleston, and M.H. Lewis "*Production and EDM of Si3N4-TiB2 Ceramic Composites* "British Ceramic Transactions, 100, No 2 pp 49-54, 2001

[124] Khene, K., Trueman, C.S., Tinsley, N.D., Lacey, M.R. and Huddleston, J., "*A Novel Method of Joining Ceramic-Metal Systems to Reduce Thermally Induced Stresses*", Proceedings of 6th International Symposium on Functionally Graded Materials, Estes Park, Colorado, in Ceramic Transactions, Am. Ceram. Soc., **114**, pp 619-626, 2000

[125] Morrell, R., "*Handbook of properties of technical and engineering ceramics Part 1 : An introduction for the engineer and designer"*, Publ. H. M. S. O., 1985

[126] Khene, K., "*The Feasibility of Autogenous Joining of an Advanced Silicon Carbide Fibre-Reinforced Silicon Carbide*" MSc thesis, The Nottingham Trent University, 1997

[127] Pitman, A., "A acoustic emission study of the electrical discharge machining of electro-conductive ceramics" PhD thesis, The Nottingham Trent University, 1998

Appendix A
Carbon tooling

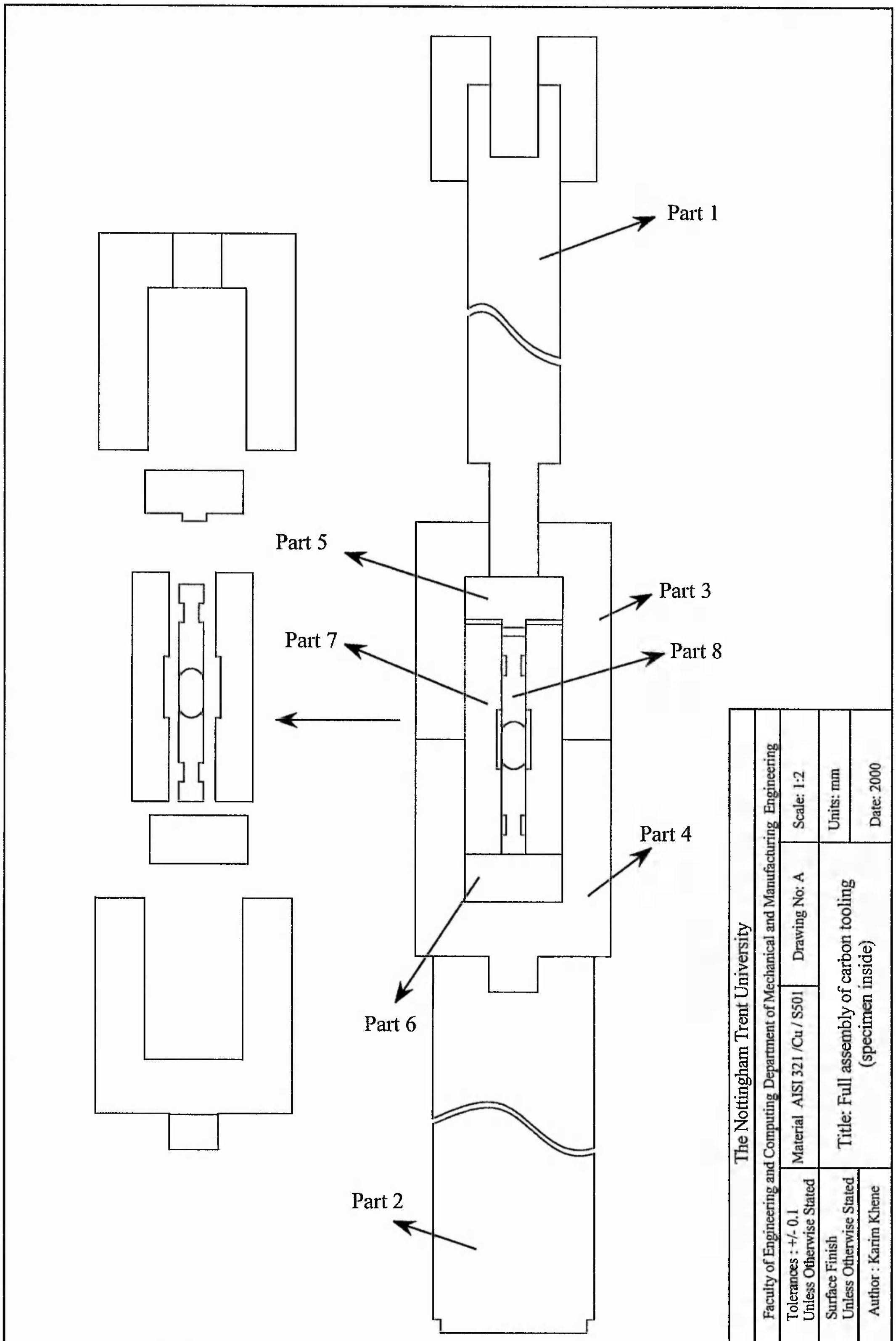
Part 1
Part 5
Part 3
Part 7
Part 8
Part 4
Part 6
Part 2
The Nottingham Trent University
Faculty of Engineering and Computing Department of Mechanical and Manufacturing Engineering
Tolerances : +/- 0.1
Unless Otherwise Stated
Material AISI 321 /Cu / S501
Drawing No: A
Scale: 1:2
Surface Finish
Unless Otherwise Stated
Title: Full assembly of carbon tooling
(specimen inside)
Units: mm
Author : Karim Khene
Date: 2000

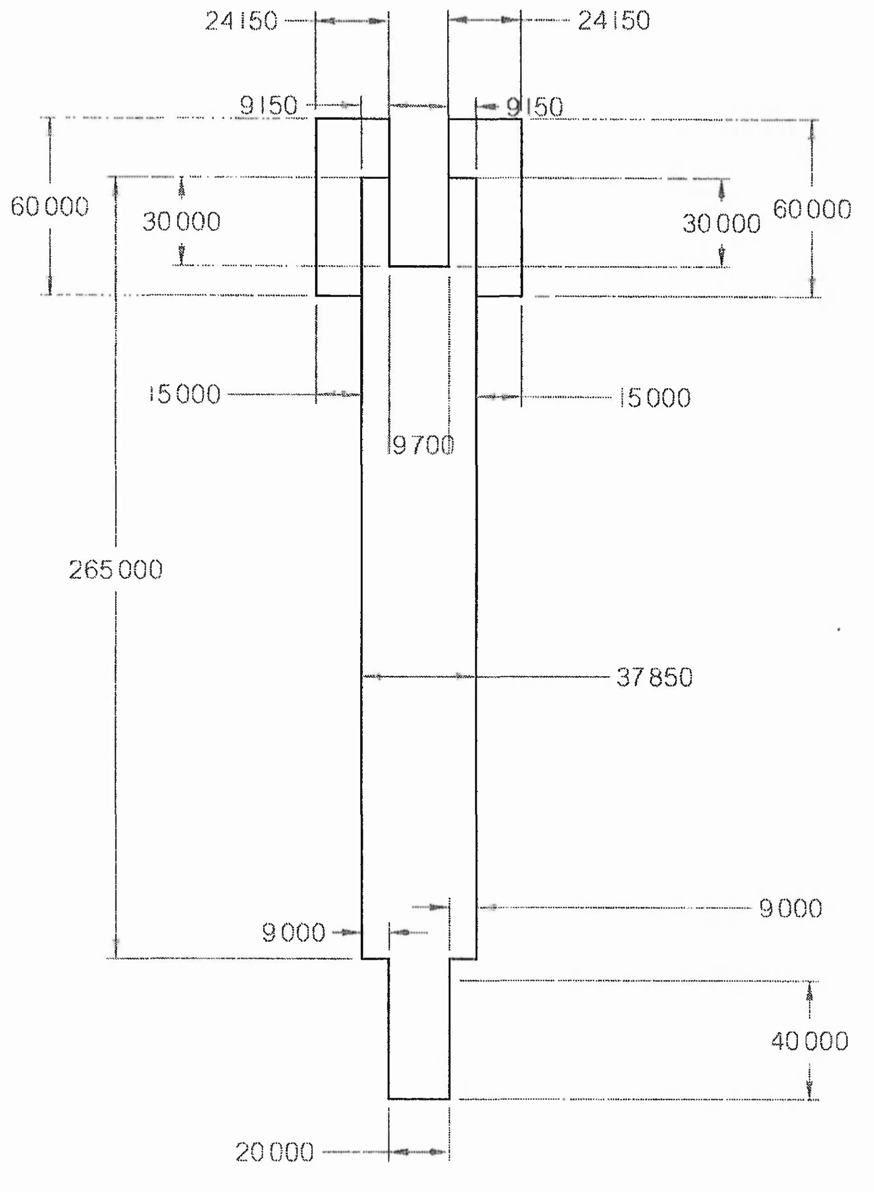

The Nottingham Trent University			
Faculty of Engineering and Computing	Department of Mechanical and Manufacturing Engineering		
Tolerances : +/- 0.1 Unless Otherwise Stated	Material Graphite	Drawing No: A (Part 1)	Scale: 1:2
Surface Finish Unless Otherwise Stated	Title: Top Part of Graphite Column		
Author : Karim Khene	Date: 2000		

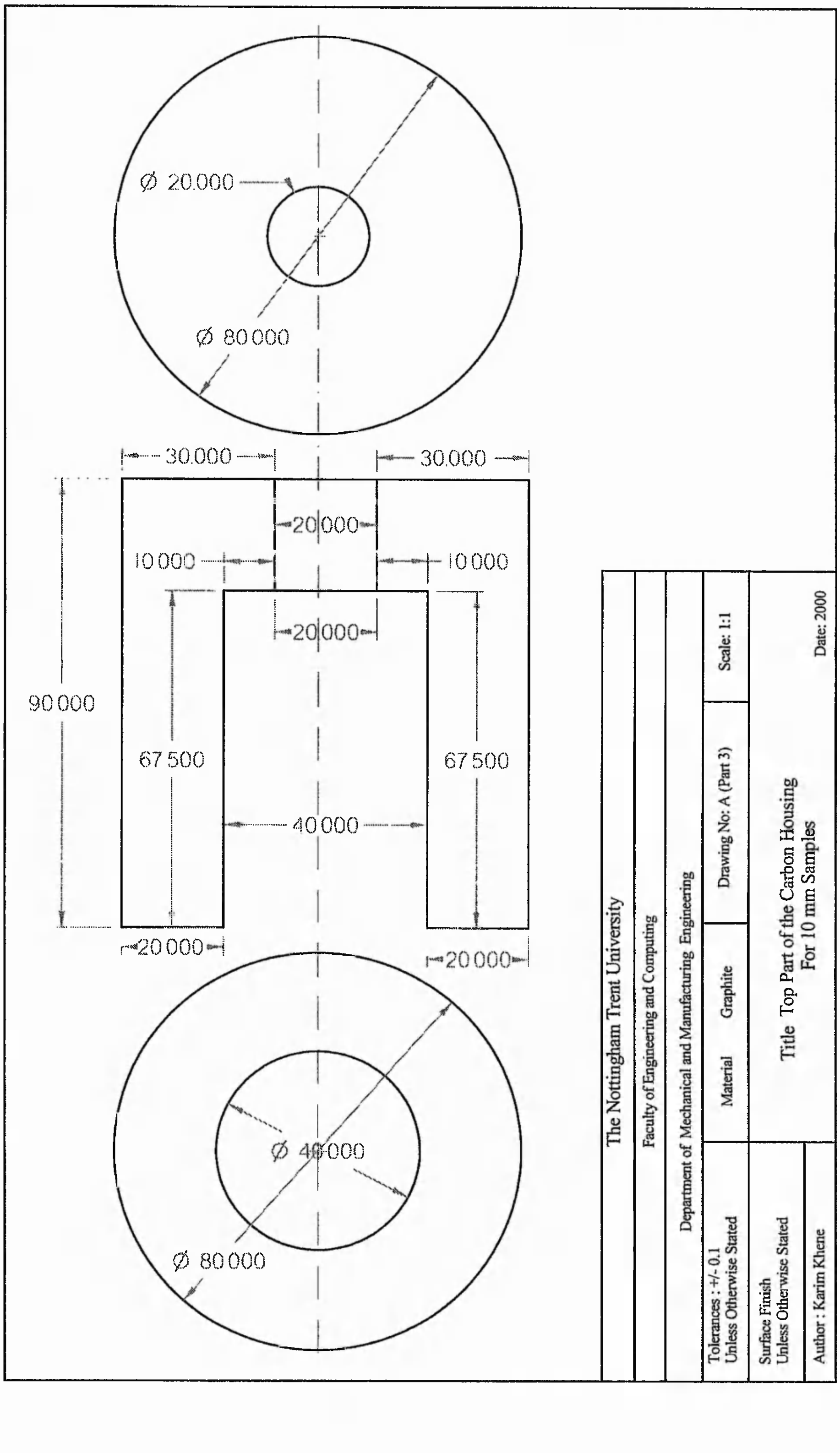
Ø 20.000
Ø 80 000
30.000
30.000
20 000
10 000
10 000
20 000
90 000
67 500
67 500
40 000
20 000
20 000
Ø 40 000
Ø 80 000
The Nottingham Trent University
Faculty of Engineering and Computing
Department of Mechanical and Manufacturing Engineering
Tolerances : +/- 0.1
Unless Otherwise Stated
Material
Graphite
Drawing No: A (Part 3)
Scale: 1:1
Surface Finish
Unless Otherwise Stated
Title Top Part of the Carbon Housing
For 10 mm Samples
Author : Karim Khene
Date: 2000

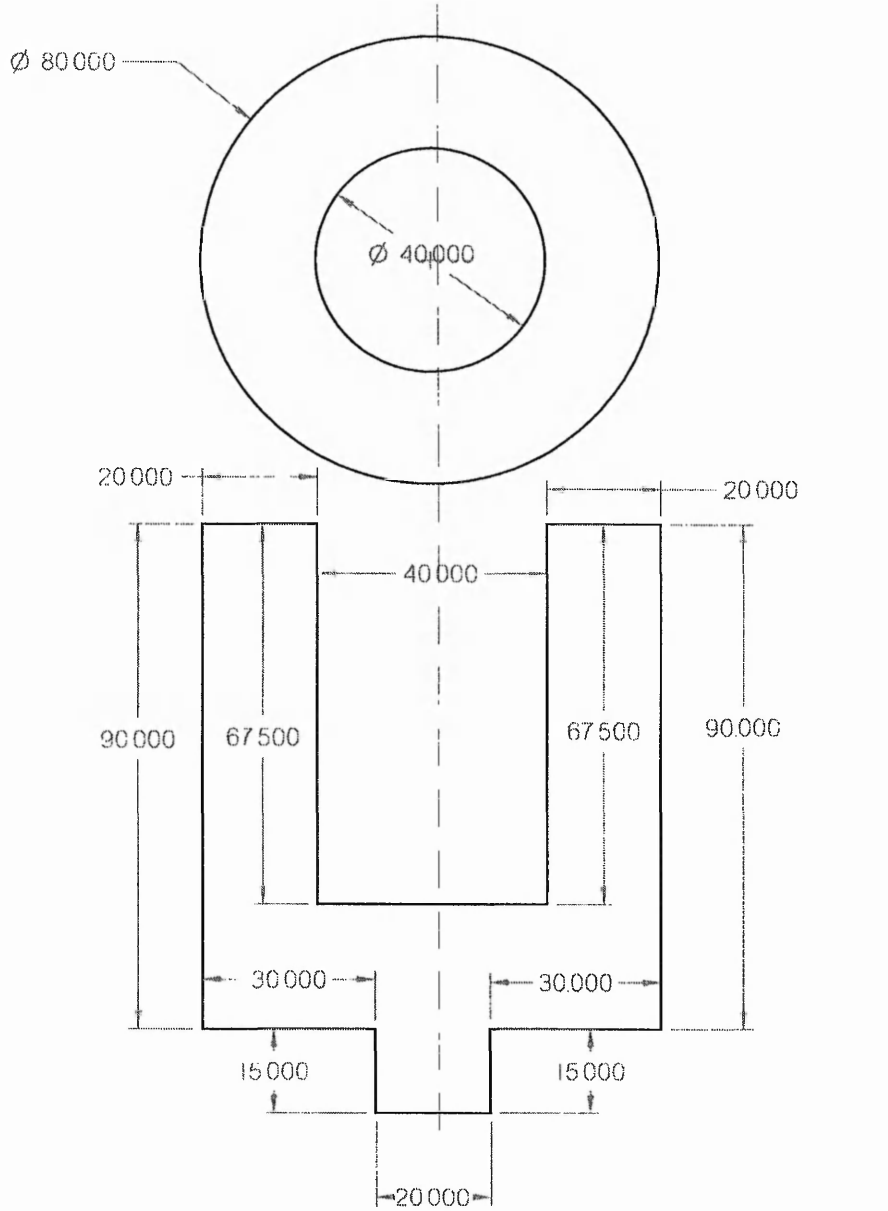

The Nottingham Trent University			
Faculty of Engineering and Computing			
Department of Mechanical and Manufacturing Engineering			
Tolerances : +/- 0.1 Unless Otherwise Stated	Material Graphite	Drawing No: A (Part 4)	Scale: 1:1
Surface Finish Unless Otherwise Stated	Title: Carbon Housing (Bottom of Tooling)		Date: 2000
Author : Karim Khene			

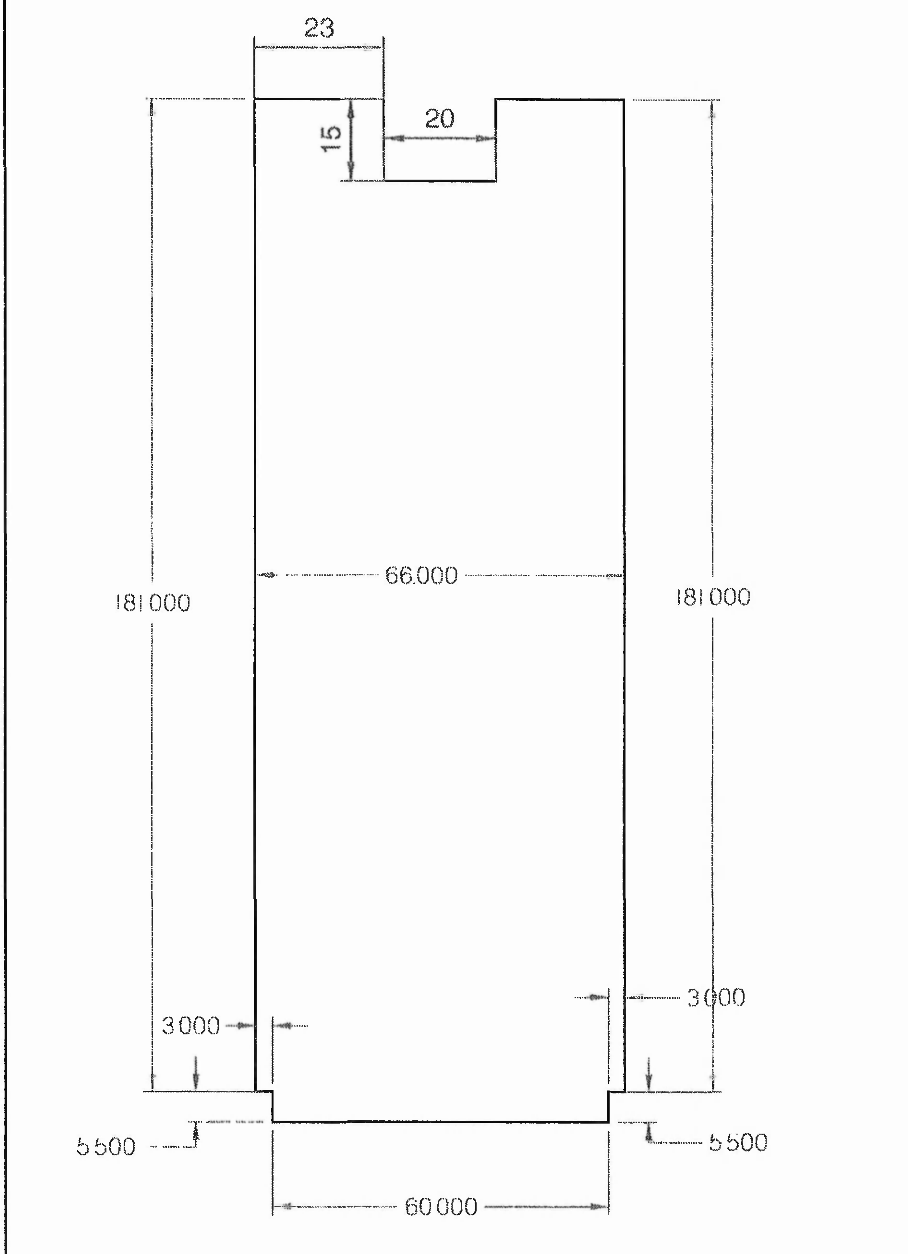

The Nottingham Trent University			
Faculty of Engineering and Computing Department of Mechanical and Manufacturing Engineering			
Tolerances : +/- 0.1 Unless Otherwise Stated	Material Graphite	Drawing No: A Part 2	Scale: 1:1
Surface Finish Unless Otherwise Stated	Title: Bottom part of the graphite column		
Author : Karim Khene	Date: 2000		

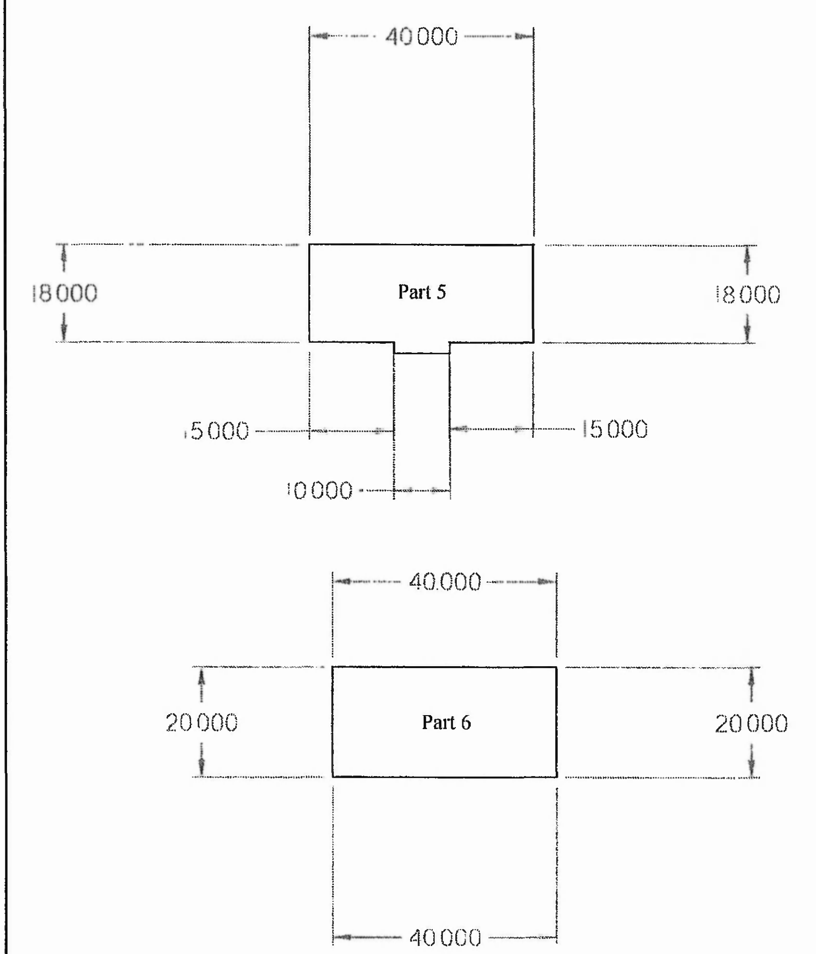

The Nottingham Trent University			
Faculty of Engineering and Computing			
Department of Mechanical and Manufacturing Engineering			
Tolerances : +/- 0.1 Unless Otherwise Stated	Material Graphite	Drawing No: A Part 5 & Part 6	Scale: 1:1
Surface Finish Unless Otherwise Stated	Title: Adjustment Discs		
Author : Karim Khene	Date: 2000		

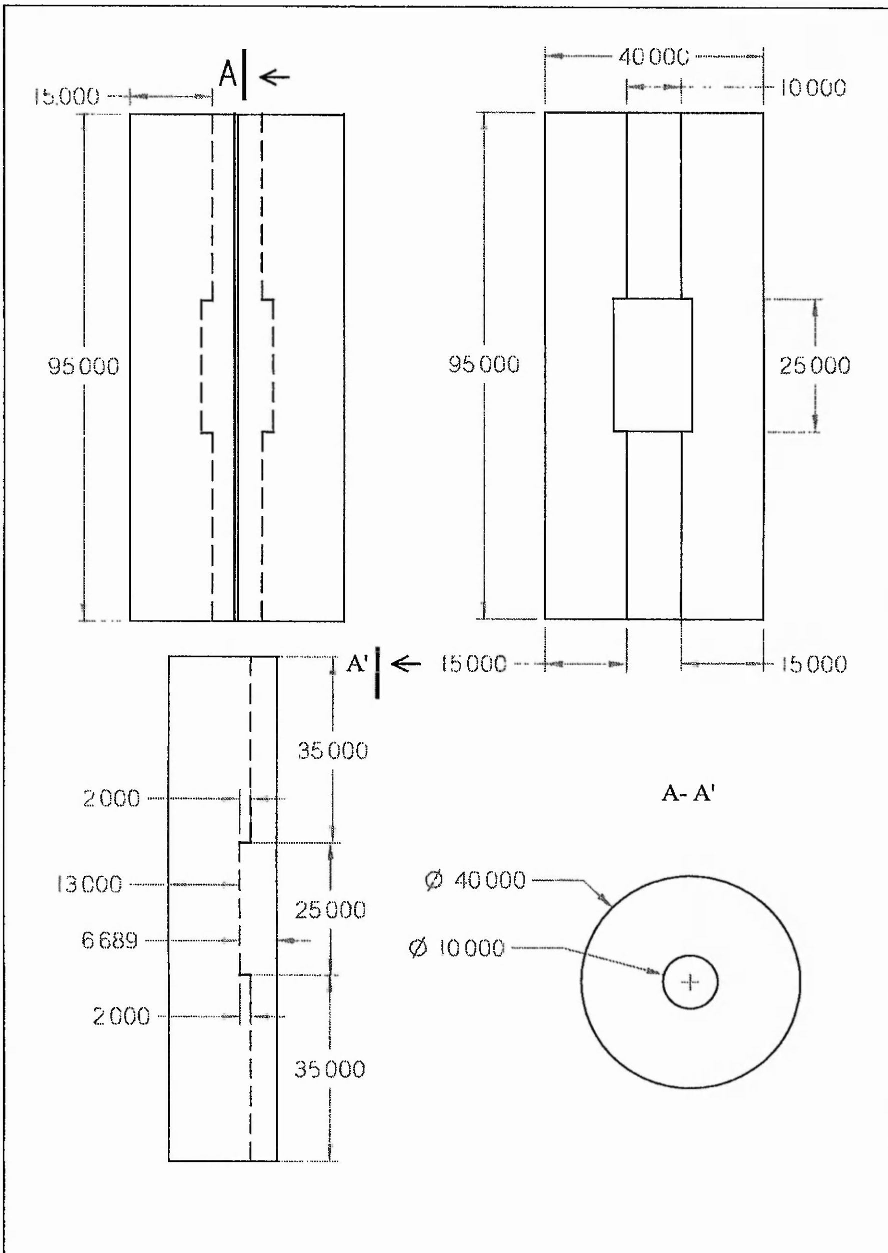

The Nottingham Trent University			
Faculty of Engineering and Computing Department of Mechanical and Manufacturing Engineering			
Tolerances : +/- 0.1 Unless Otherwise Stated	Material Graphite	Drawing No: A Part 7(10mm)	Scale: 1:1
Surface Finish Unless Otherwise Stated	Title: Sleeve Details For 10 mm Samples		Date: 2000
Author : Karim Khene			

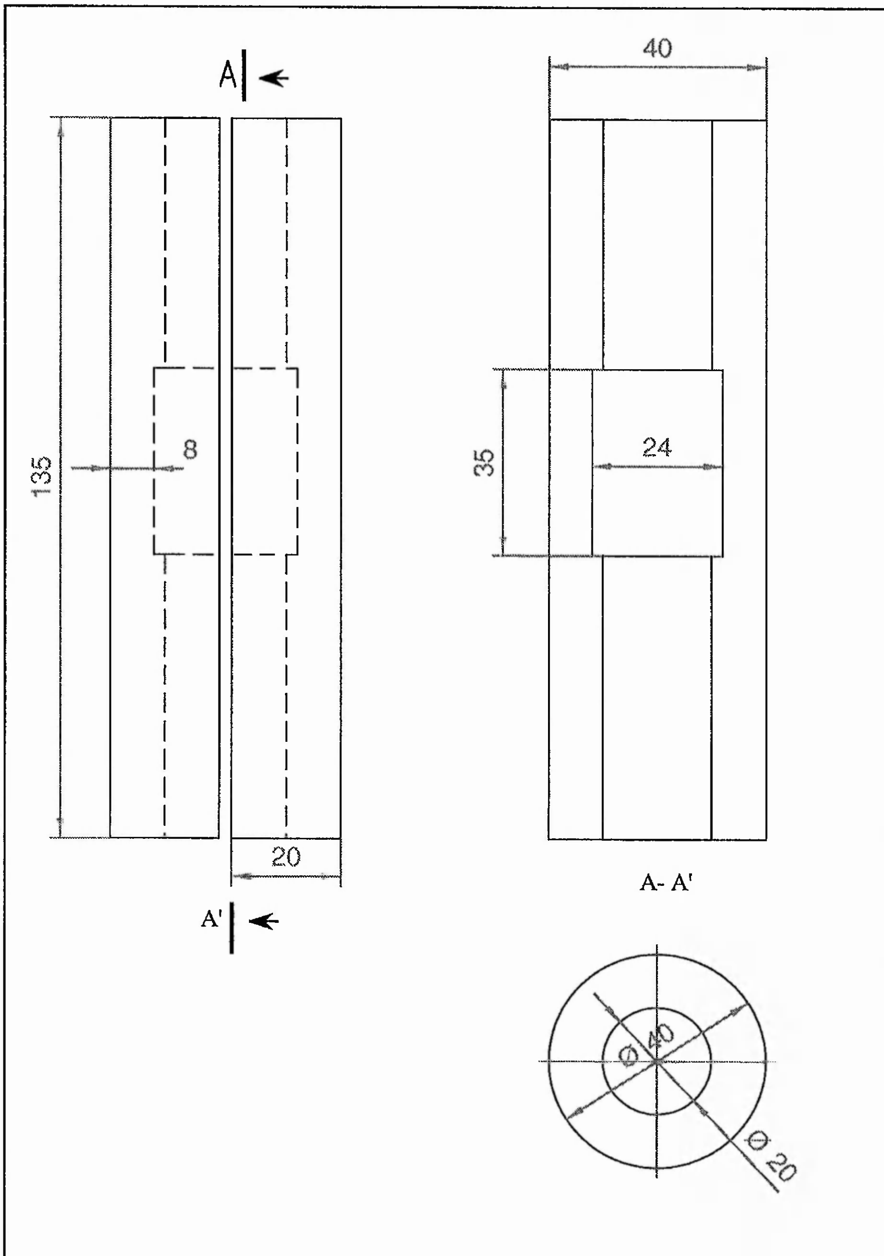

The Nottingham Trent University			
Faculty of Engineering and Computing Department of Mechanical and Manufacturing Engineering			
Tolerances : +/- 0.1 Unless Otherwise Stated	Material Graphite	Drawing No: A Part 7(20mm)	Scale: 1:1
Surface Finish Unless Otherwise Stated	Title: Sleeve Details For 20 mm Samples		
Author : Karim Khene	Date: 2000		

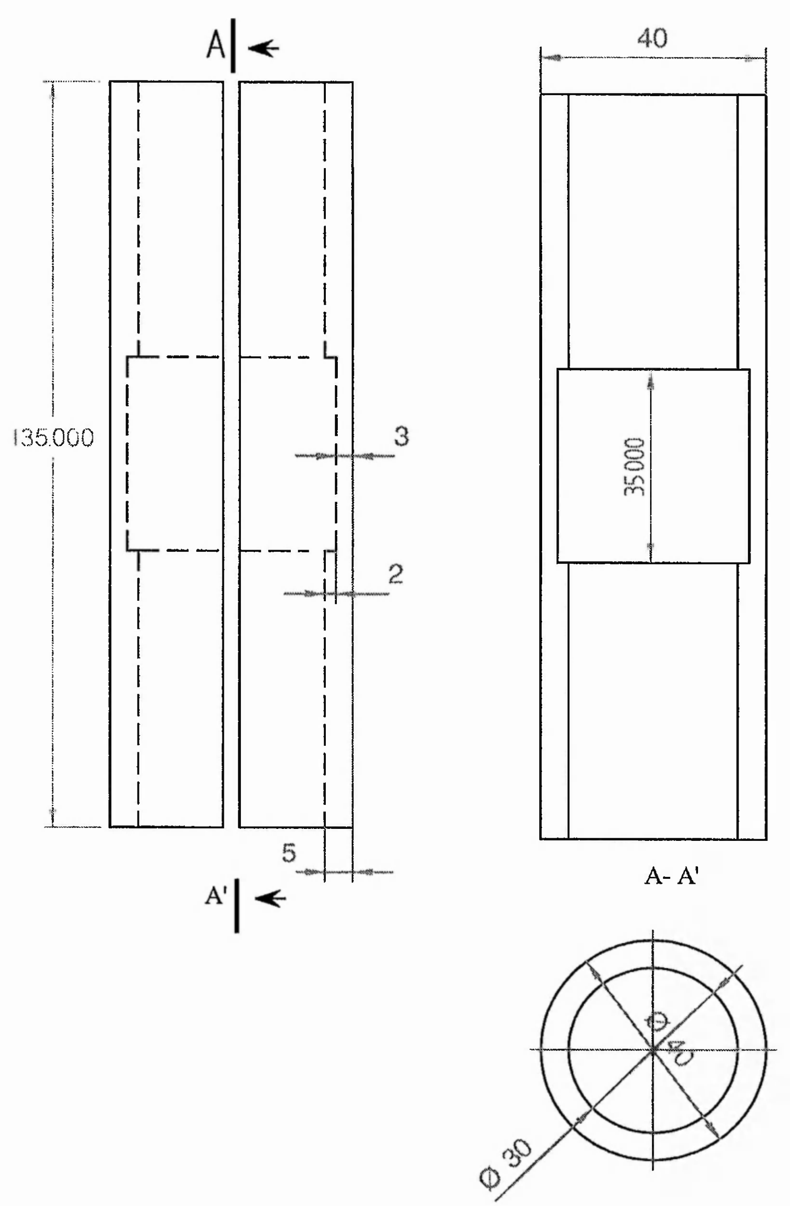

The Nottingham Trent University			
Faculty of Engineering and Computing Department of Mechanical and Manufacturing Engineering			
Tolerances : +/- 0.1 Unless Otherwise Stated	Material Graphite	Drawing No: A Part 7(30mm)	Scale: 1:1
Surface Finish Unless Otherwise Stated	Title:Sleeve Details For 30 mm Samples		
Author : Karim Khene	Date: 2000		

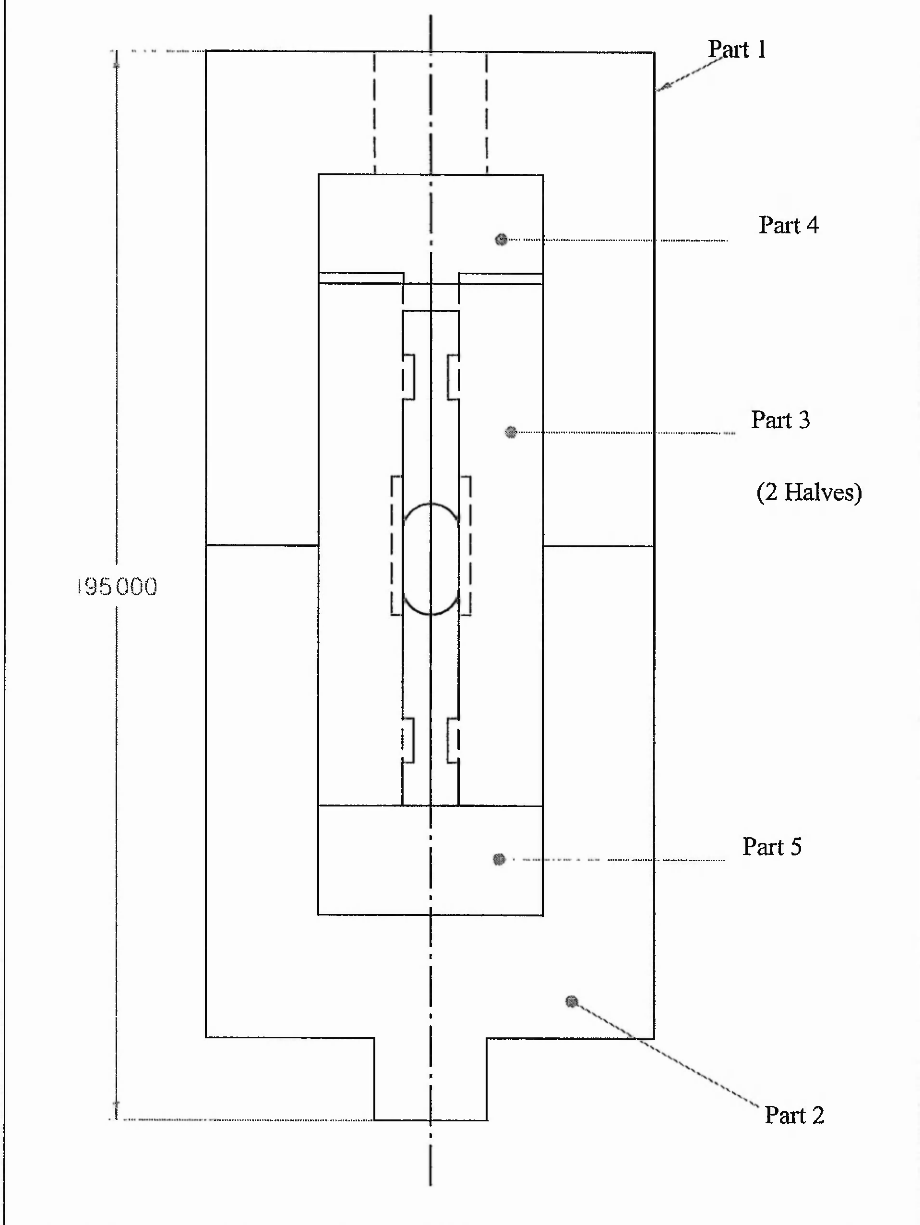

The Nottingham Trent University			
Faculty of Engineering and Computing			
Department of Mechanical and Manufacturing Engineering			
Tolerances : +/- 0.1 Unless Otherwise Stated	Material Graphite/AISI 321/Ticusil / S501	Drawing No: A1(10mm)	Scale:1:1
Surface Finish Unless Otherwise Stated	Title: Full Assembly		
Author : Karim Khene	Date: 2000		

Appendix B

Copper electrodes

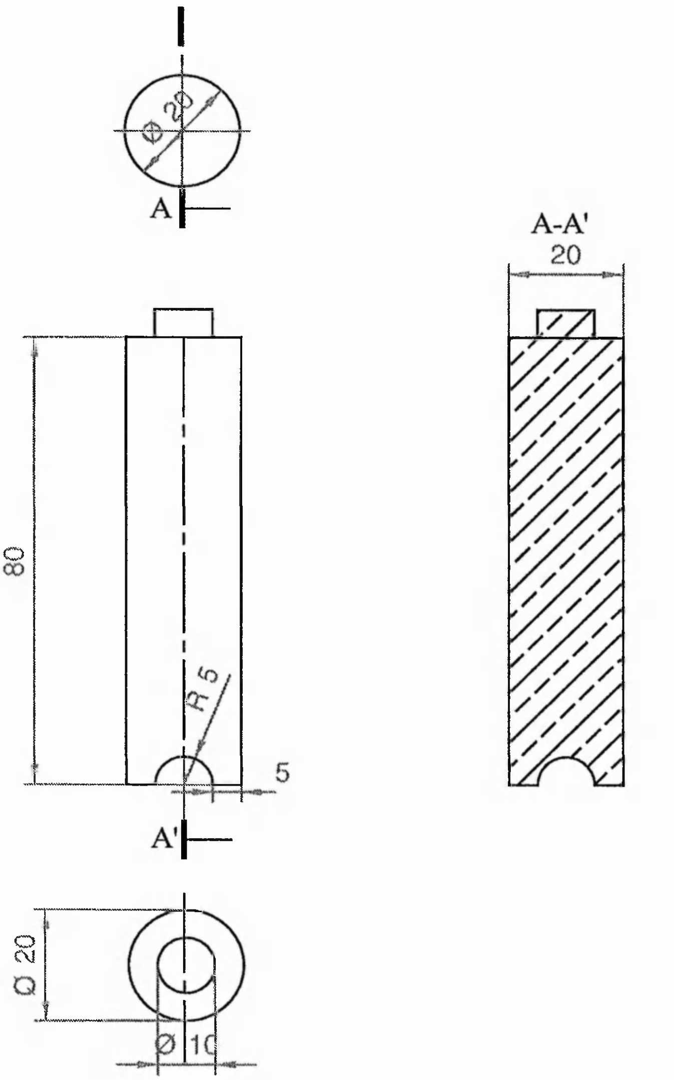

The Nottingham Trent University			
Faculty of Engineering and Computing Department of Mechanical and Manufacturing Engineering			
Tolerances : +/- 0.1 Unless Otherwise Stated	Material Copper	Drawing No: B1	Scale: 1:1
Surface Finish Unless Otherwise Stated	Title: 10 mm Electrode		Units: mm
Author : Karim Khene			Date: 2000

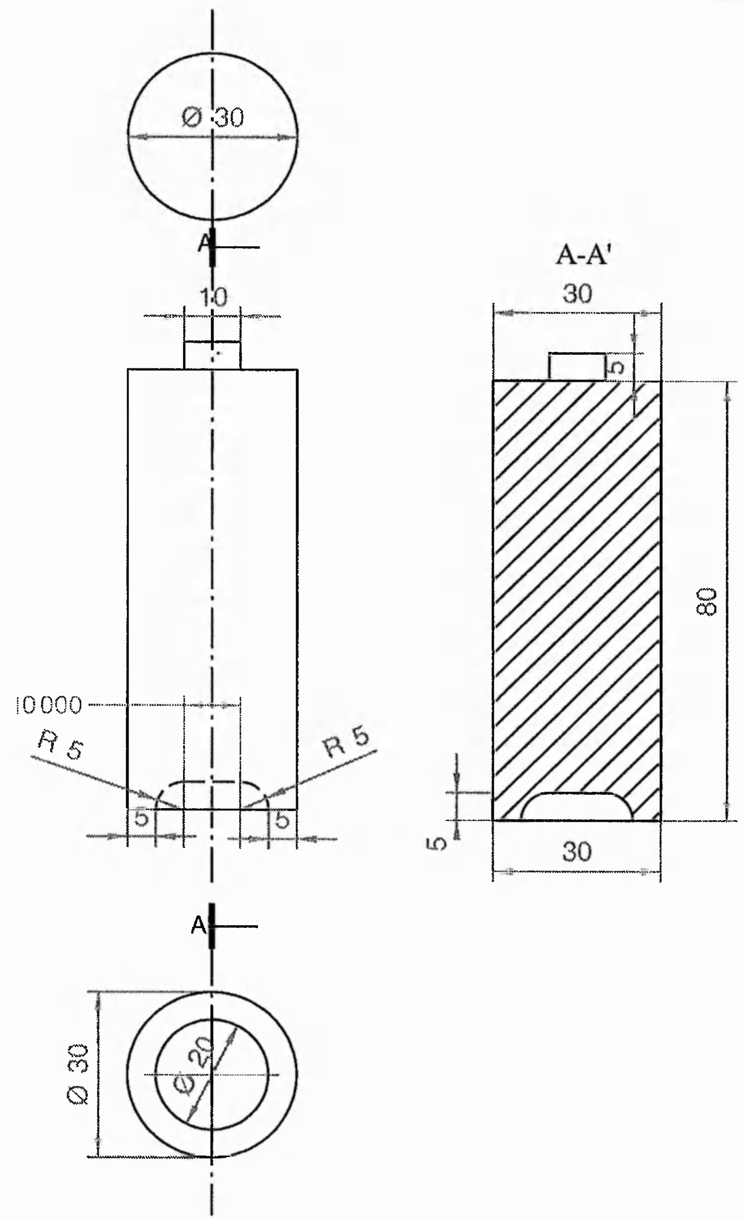

The Nottingham Trent University			
Faculty of Engineering and Computing Department of Mechanical and Manufacturing Engineering			
Tolerances : +/- 0.1 Unless Otherwise Stated	Material Copper	Drawing No: B2	Scale: 1:1
Surface Finish Unless Otherwise Stated	Title: 20 mm Electrode		Units: mm
Author : Karim Khene			Date: 2000

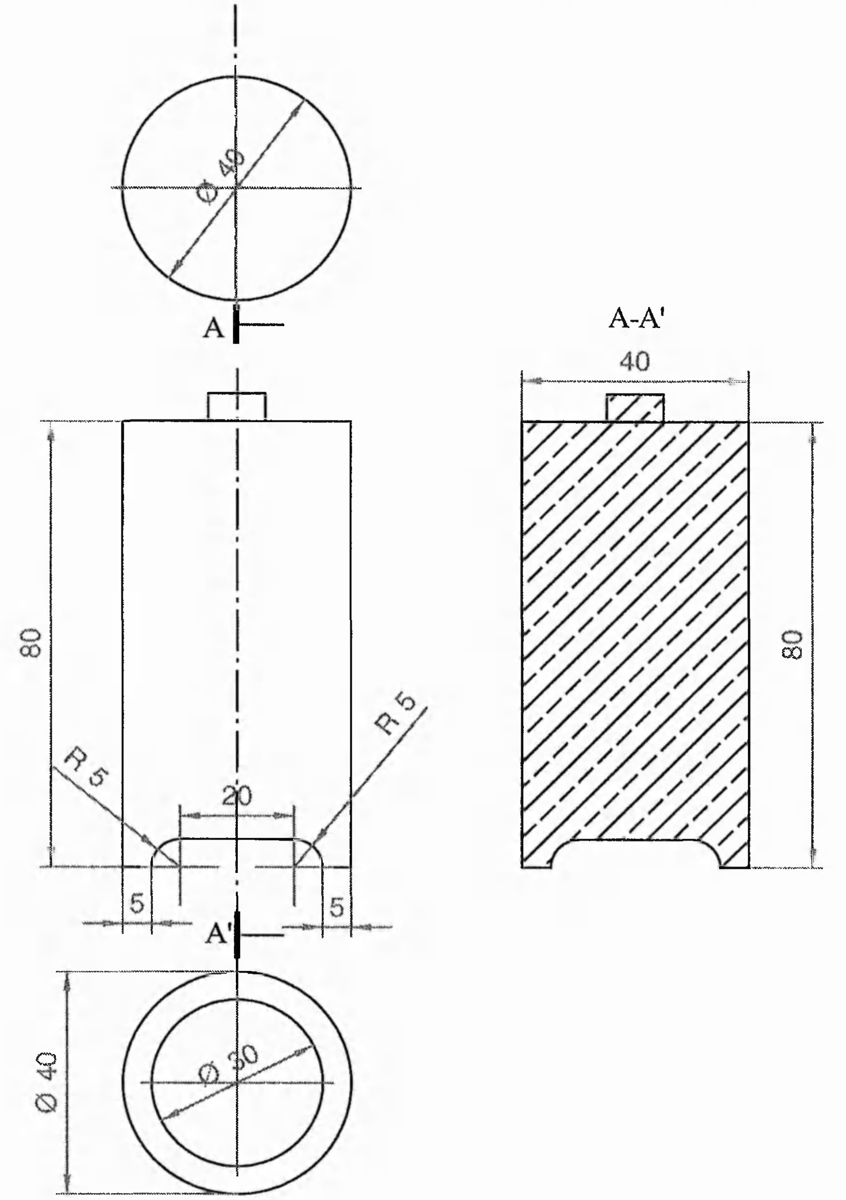

The Nottingham Trent University			
Faculty of Engineering and Computing Department of Mechanical and Manufacturing Engineering			
Tolerances : +/- 0.1 Unless Otherwise Stated	Material Copper	Drawing No: B3	Scale: 1:1
Surface Finish Unless Otherwise Stated	Title: 30 mm Electrode		Units: mm
Author : Karim Khene			Date: 2000

Appendix C

Ceramic samples

Before machining After machining

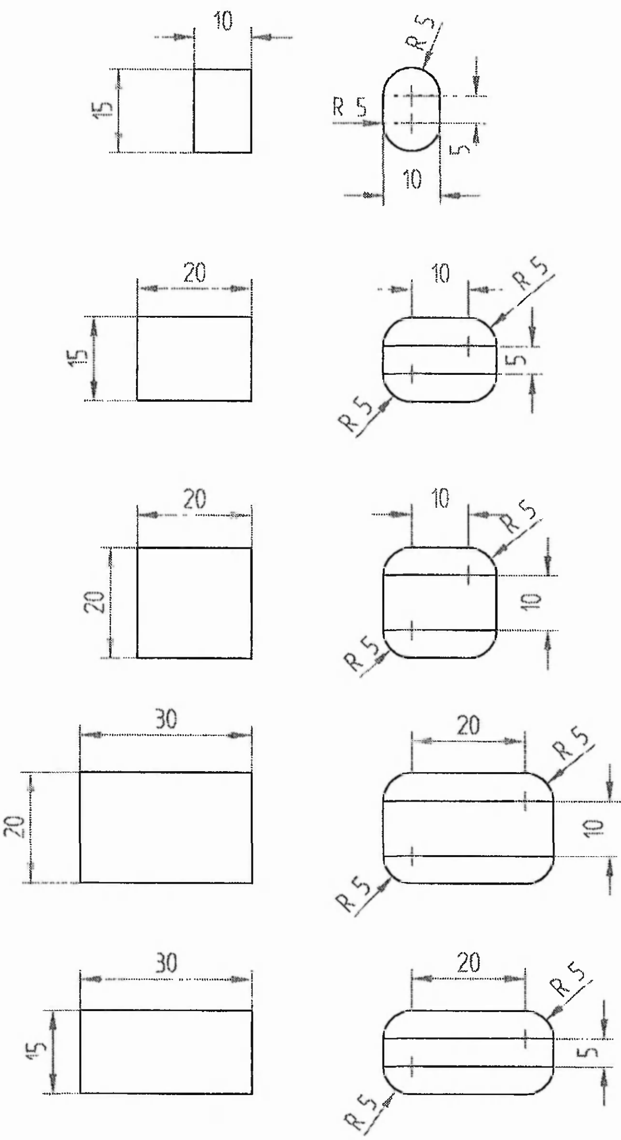

The Nottingham Trent University			
Faculty of Engineering and Computing Department of Mechanical and Manufacturing Engineering			
Tolerances : +/- 0.1 Unless Otherwise Stated	Material Syalon 501	Drawing No: C1	Scale: 1:1
Surface Finish Unless Otherwise Stated	Title Ceramic Samples used for experiments		Units: mm
Author : Karim Khene			Date: 2000

Appendix D

AISI 321 stainless steel members

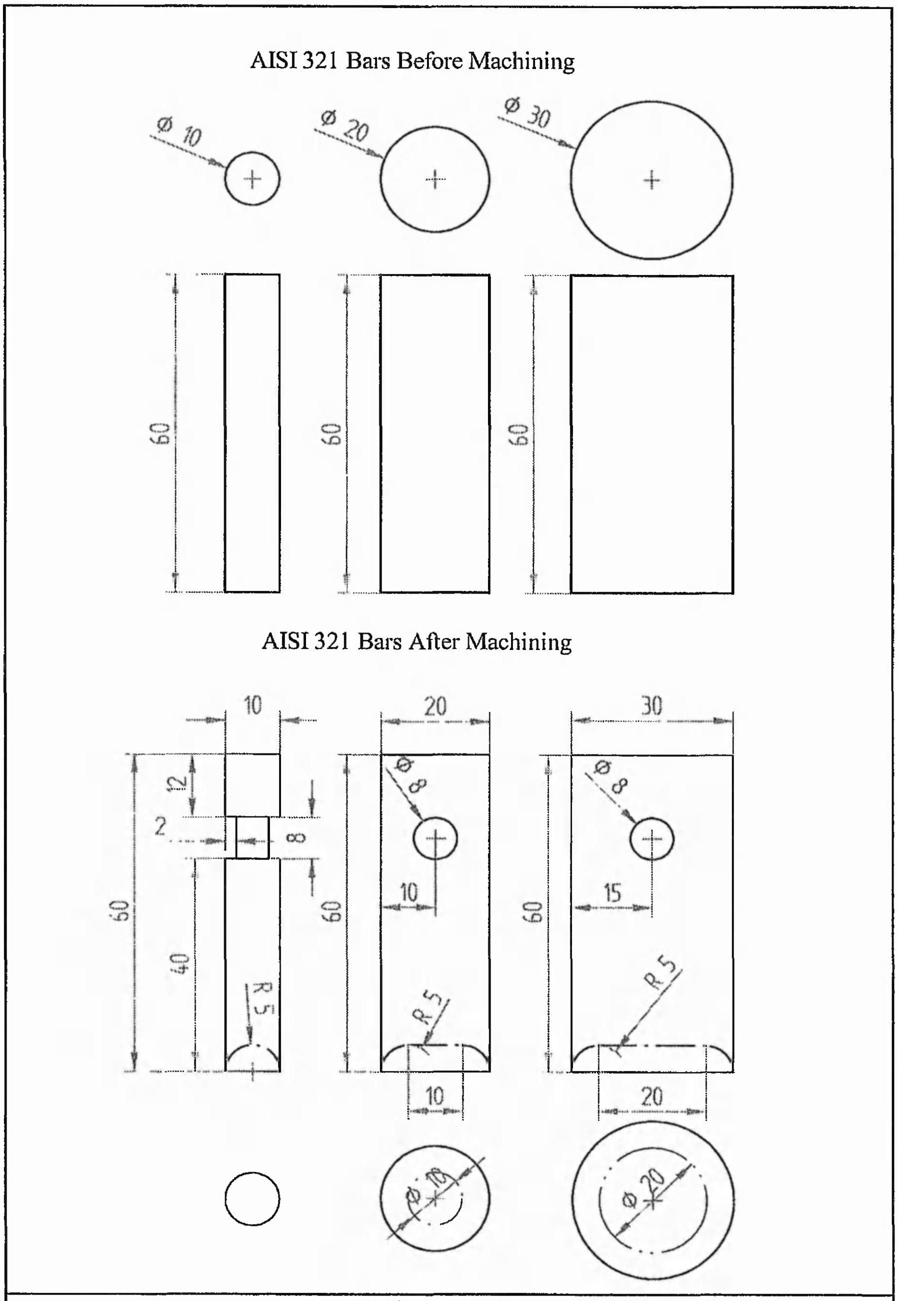

The Nottingham Trent University			
Faculty of Engineering and Computing Department of Mechanical and Manufacturing Engineering			
Tolerances : +/- 0.1 Unless Otherwise Stated	Material AISI 321 Steel	Drawing No: D1	Scale: 1:1
Surface Finish Unless Otherwise Stated	Title Steel members used for experiments		Units: mm
Author : Karim Khene			Date: 2000

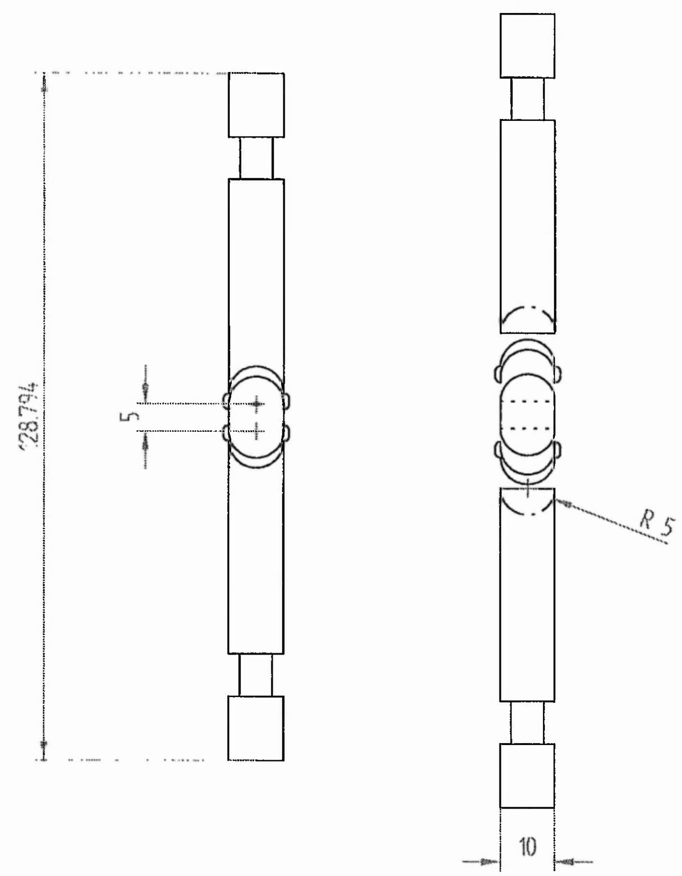

The Nottingham Trent University			
Faculty of Engineering and Computing Department of Mechanical and Manufacturing Engineering			
Tolerances : +/- 0.1 Unless Otherwise Stated	Material AISI 321 /Cu / S501	Drawing No: D2	Scale: 1:1
Surface Finish Unless Otherwise Stated	Title Full assembly (10mm samples)		Units: mm
Author : Karim Khene			Date: 2000

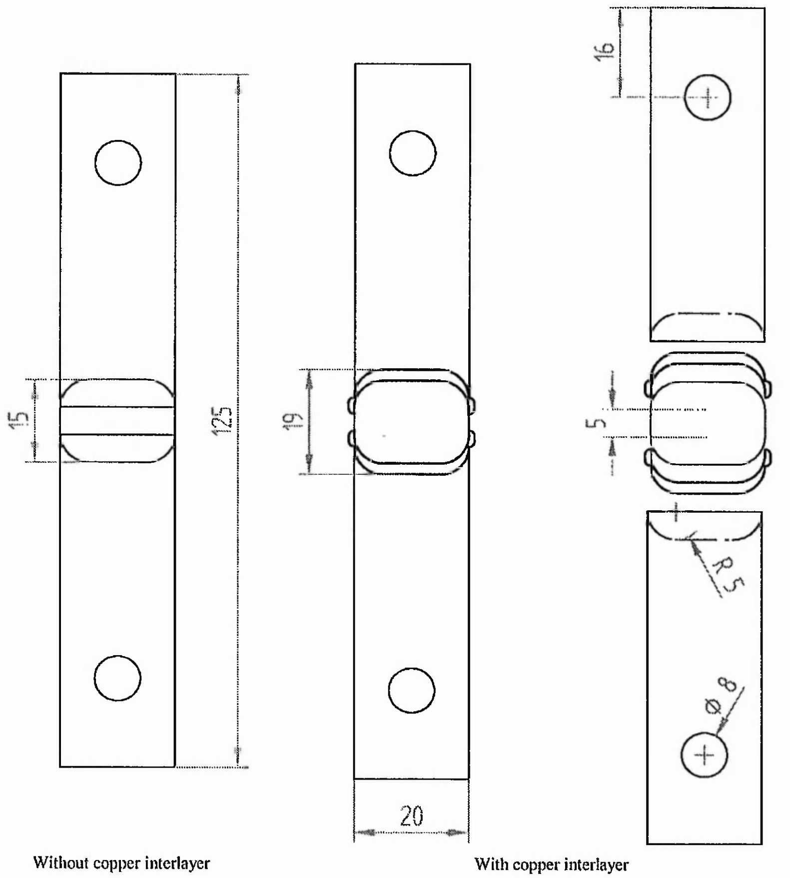

The Nottingham Trent University			
Faculty of Engineering and Computing Department of Mechanical and Manufacturing Engineering			
Tolerances : +/- 0.1 Unless Otherwise Stated	Material AISI 321 /Cu / S501	Drawing No: D3	Scale: 1:1
Surface Finish Unless Otherwise Stated	Title Full assembly (20mm samples)		Units: mm
Author : Karim Khene			Date: 2000

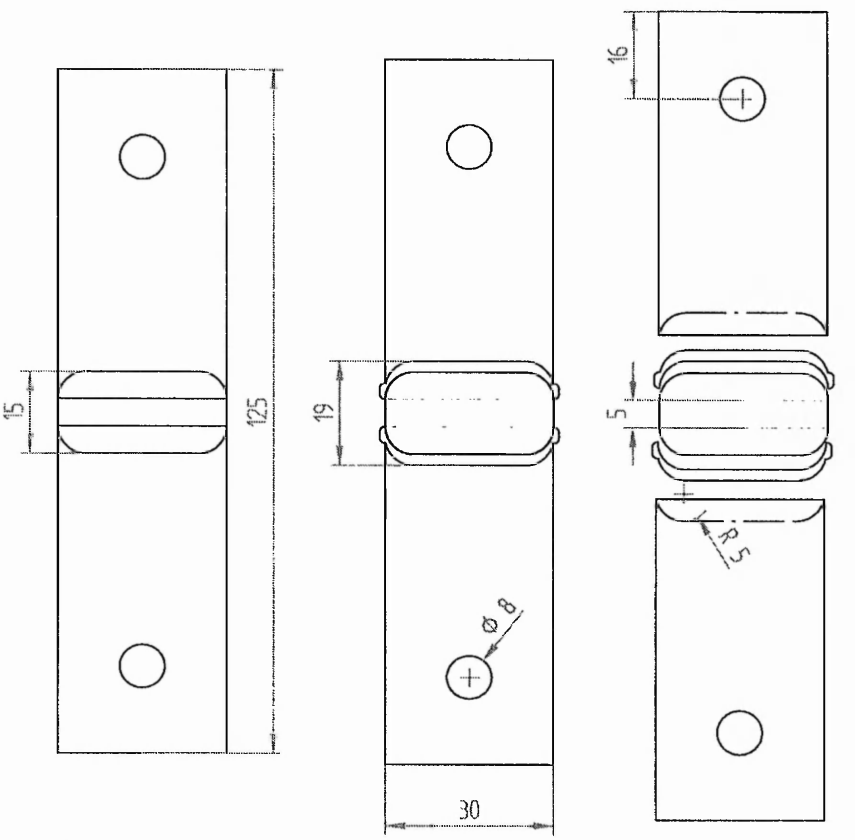

Without copper interlayer

With copper interlayer

The Nottingham Trent University			
Faculty of Engineering and Computing Department of Mechanical and Manufacturing Engineering			
Tolerances : +/- 0.1 Unless Otherwise Stated	Material AISI 321 /Cu / S501	Drawing No: D4	Scale: 1:1
Surface Finish Unless Otherwise Stated	Title Full assembly (30mm samples)		Units: mm
Author : Karim Khene			Date: 2000

Appendix E

2mm copper interlayers cup

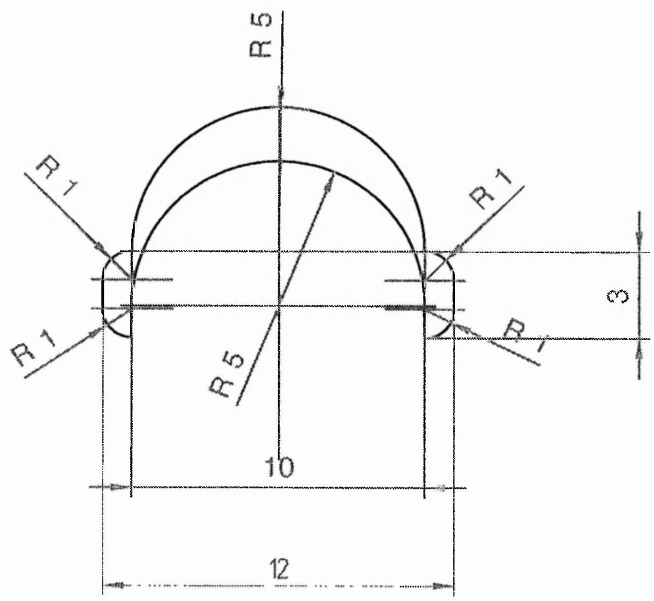

The Nottingham Trent University			
Faculty of Engineering and Computing Department of Mechanical and Manufacturing Engineering			
Tolerances : +/- 0.1 Unless Otherwise Stated	Material: Copper	Drawing No: E1	Scale 5:1
Surface Finish Unless Otherwise Stated	Title: Copper interlayer for 10mm samples		Units: mm
Author : Karim Khene			Date : 2000

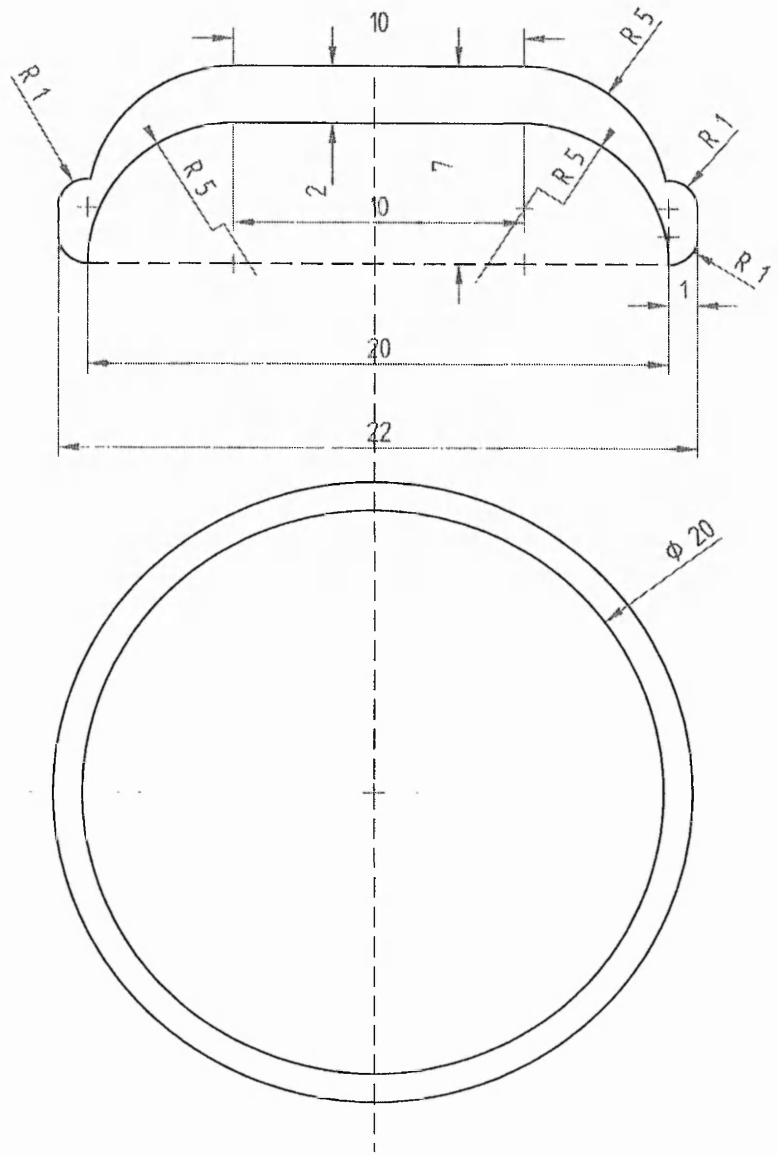

The Nottingham Trent University			
Faculty of Engineering and Computing	Department of Mechanical and Manufacturing Engineering		
Tolerances : +/- 0.1 Unless Otherwise Stated	Material: Copper	Drawing No: E2	Scale 5:1
Surface Finish Unless Otherwise Stated	Title: Copper interlayer for 20mm samples		Units: mm
Author : Karim Khene			Date : 2000

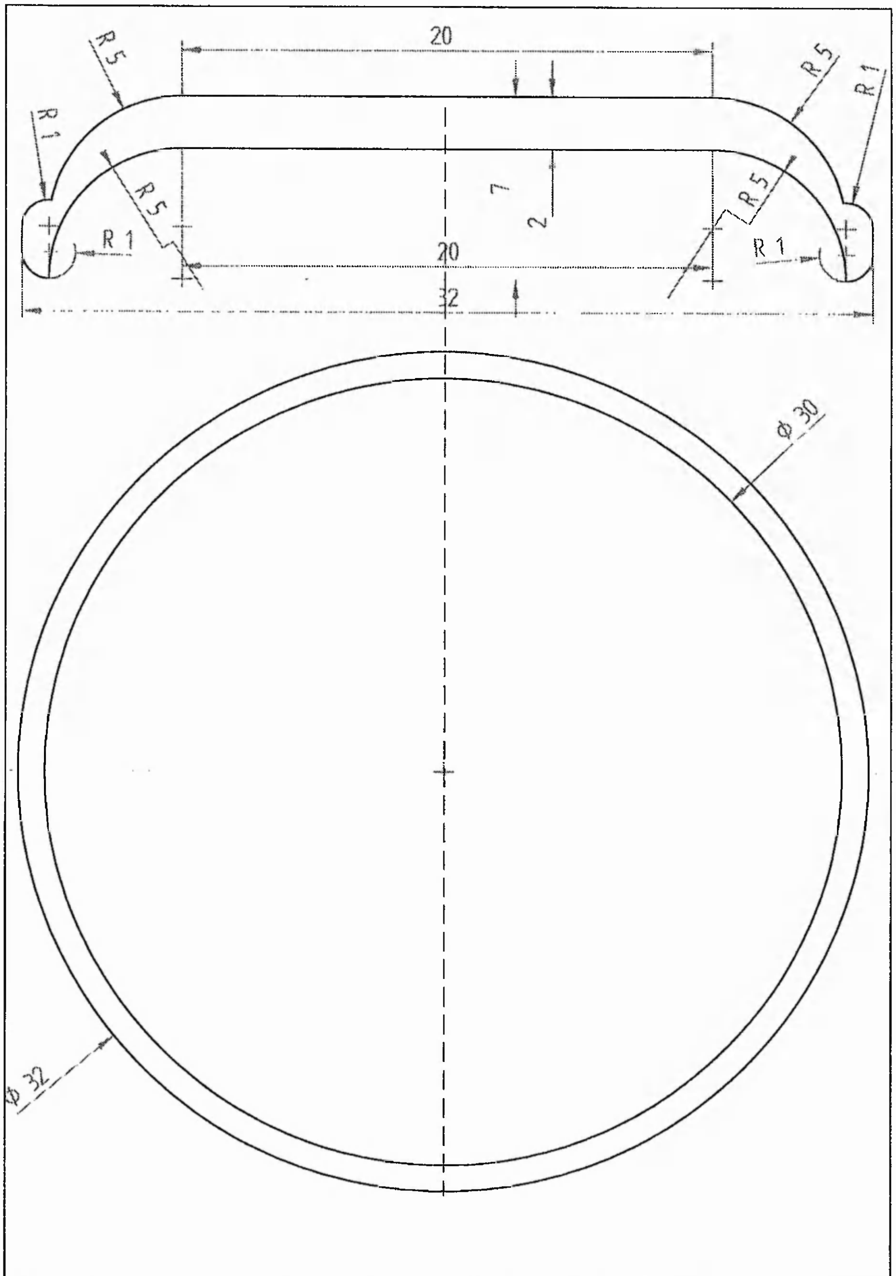

The Nottingham Trent University			
Faculty of Engineering and Computing Department of Mechanical and Manufacturing Engineering			
Tolerances : +/- 0.1 Unless Otherwise Stated	Material: Copper	Drawing No: E3	Scale 5:1
Surface Finish Unless Otherwise Stated	Title: Copper interlayer for 30mm samples		Units: mm
Author : Karim Khene			Date : 2000

Appendix F

Copper forming dies and punches

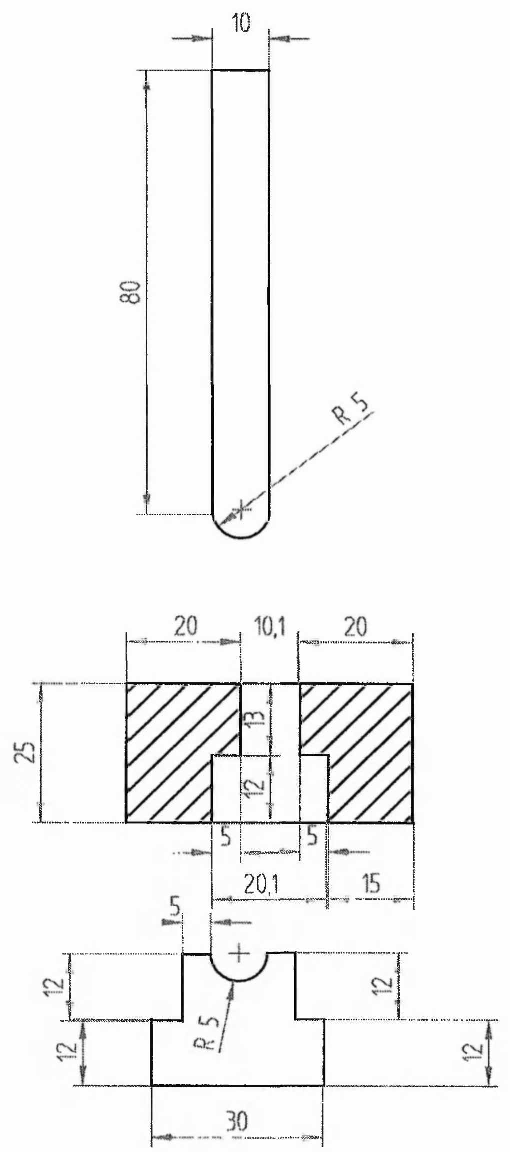

The Nottingham Trent University			
Faculty of Engineering and Computing Department of Mechanical and Manufacturing Engineering			
Tolerances : +/- 0.1 Unless Otherwise Stated	Material Mild Steel	Drawing No: F1	Scale: 1:1
Surface Finish Unless Otherwise Stated	Title: Die and punch 10mm interlayers		Units: mm
Author : Karim Khene			Date: 2000

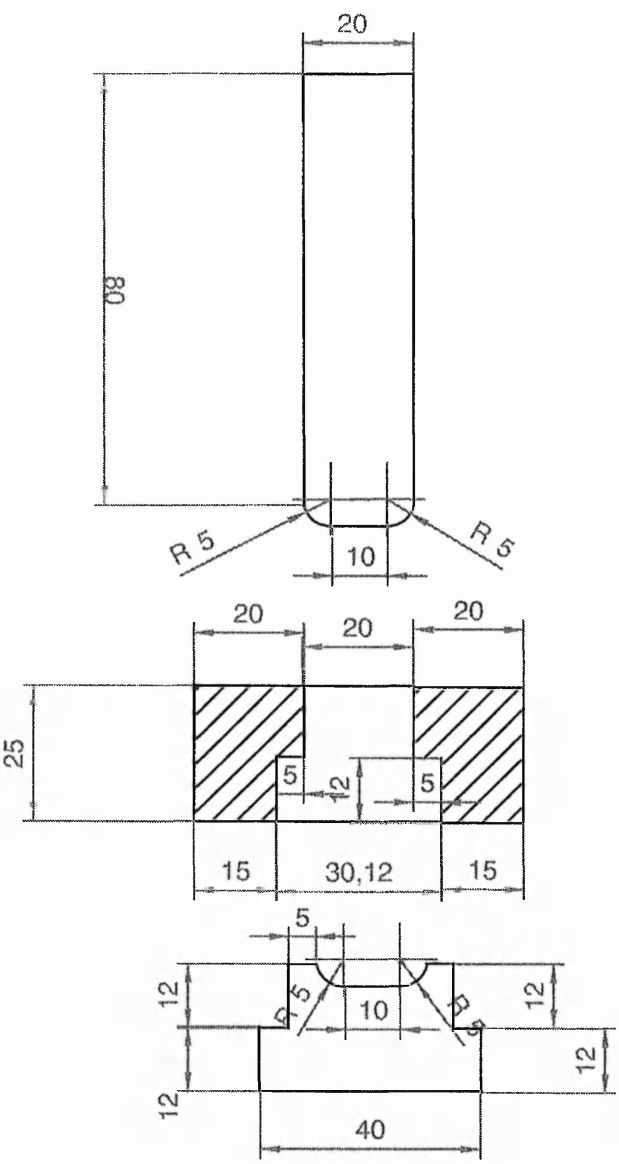

The Nottingham Trent University			
Faculty of Engineering and Computing Department of Mechanical and Manufacturing Engineering			
Tolerances : +/- 0.1 Unless Otherwise Stated	Material Mild Steel	Drawing No: F2	Scale: 1:1
Surface Finish Unless Otherwise Stated	Title: Die and punch 20mm interlayers		Units: mm
Author : Karim Khene			Date: 2000

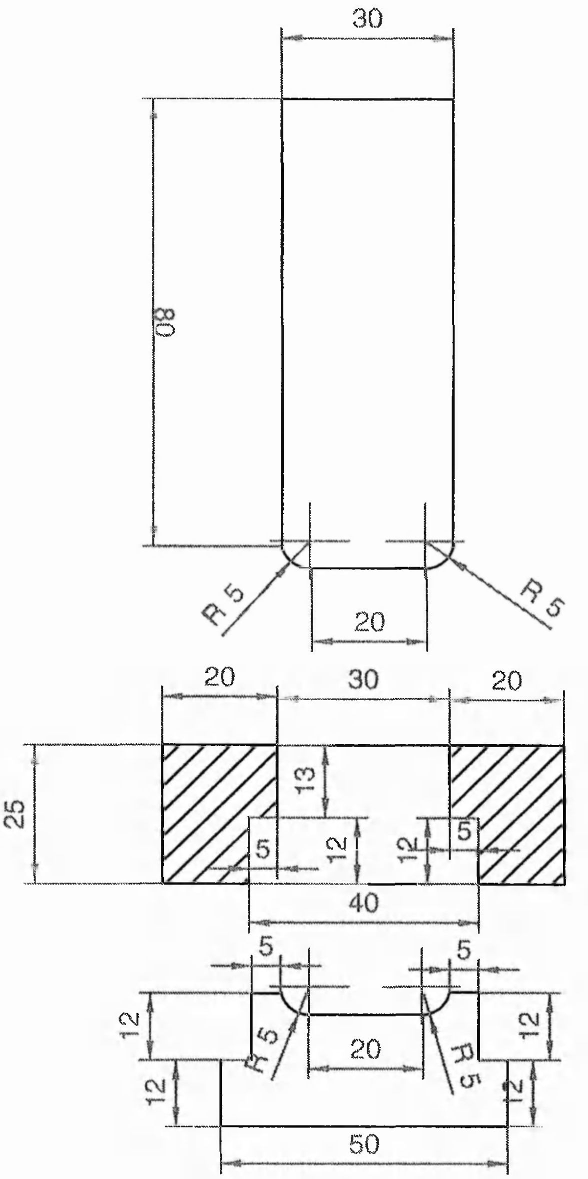

The Nottingham Trent University			
Faculty of Engineering and Computing Department of Mechanical and Manufacturing Engineering			
Tolerances : +/- 0.1 Unless Otherwise Stated	Material Mild Steel	Drawing No: F3	Scale: 1:1
Surface Finish Unless Otherwise Stated	Title: Die and punch 30mm interlayers		Units: mm
Author : Karim Khene			Date: 2000

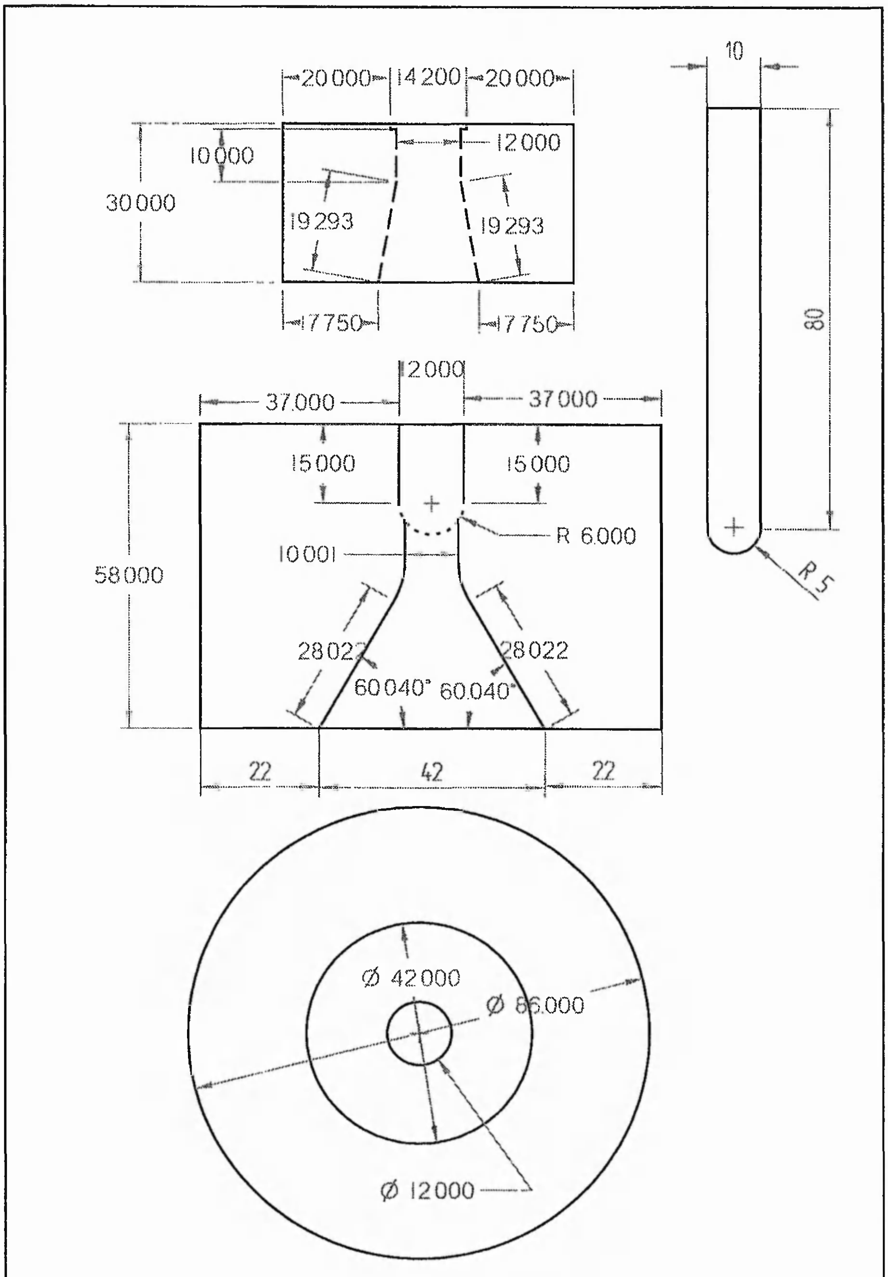

The Nottingham Trent University			
Faculty of Engineering and Computing Department of Mechanical and Manufacturing Engineering			
Tolerances : +/- 0.1 Unless Otherwise Stated	Material Mild Steel	Drawing No: F4	Scale: 1:1
Surface Finish Unless Otherwise Stated	Title: Special die and punch to shape copper layer		Units: mm
Author : Karim Khene			Date: 2000

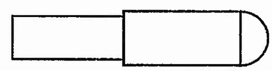

(a)

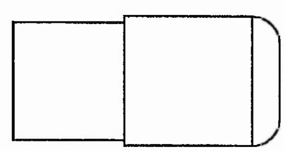

(b)

The Nottingham Trent University			
Faculty of Engineering and Computing Department of Mechanical and Manufacturing Engineering			
Tolerances : +/- 0.1 Unless Otherwise Stated	Material Mild Steel	Drawing No: F5	Scale: 1:1
Surface Finish Unless Otherwise Stated	Title:Madrill used during maching of copper cups		Date: 2000
Author : Karim Khene			

Appendix G

Copper casting

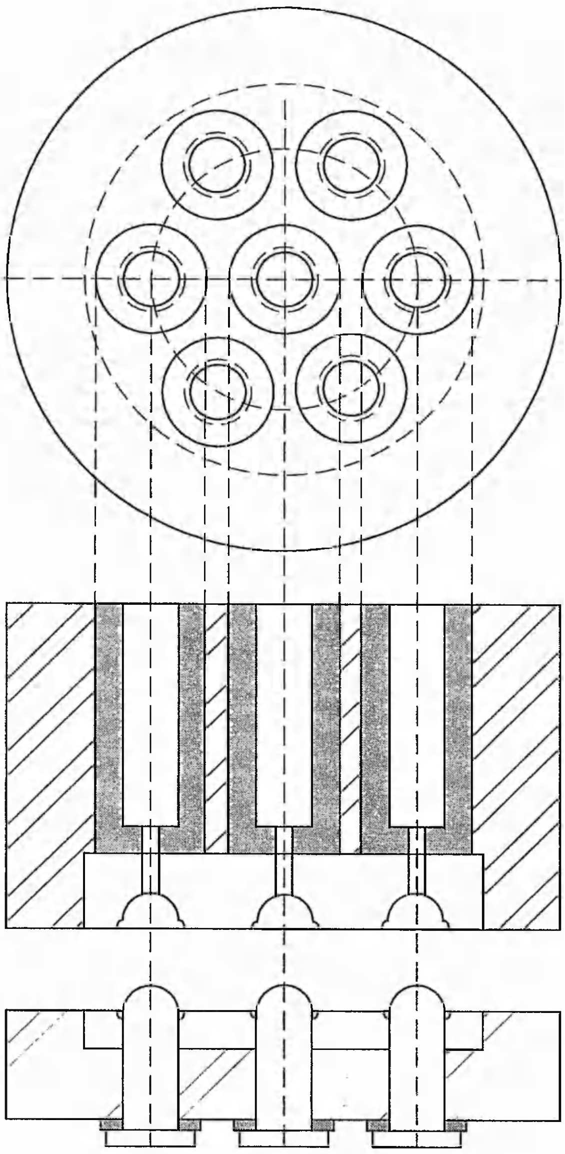

The Nottingham Trent University			
Faculty of Engineering and Computing Department of Mechanical and Manufacturing Engineering			
Tolerances : +/- 0.1 Unless Otherwise Stated	Material Graphite	Drawing No: G1	Scale: 1:1
Surface Finish Unless Otherwise Stated	Title:Proposed Casting mould to produce copper interlayers		
Author : Karim Khene	Date: 2000		

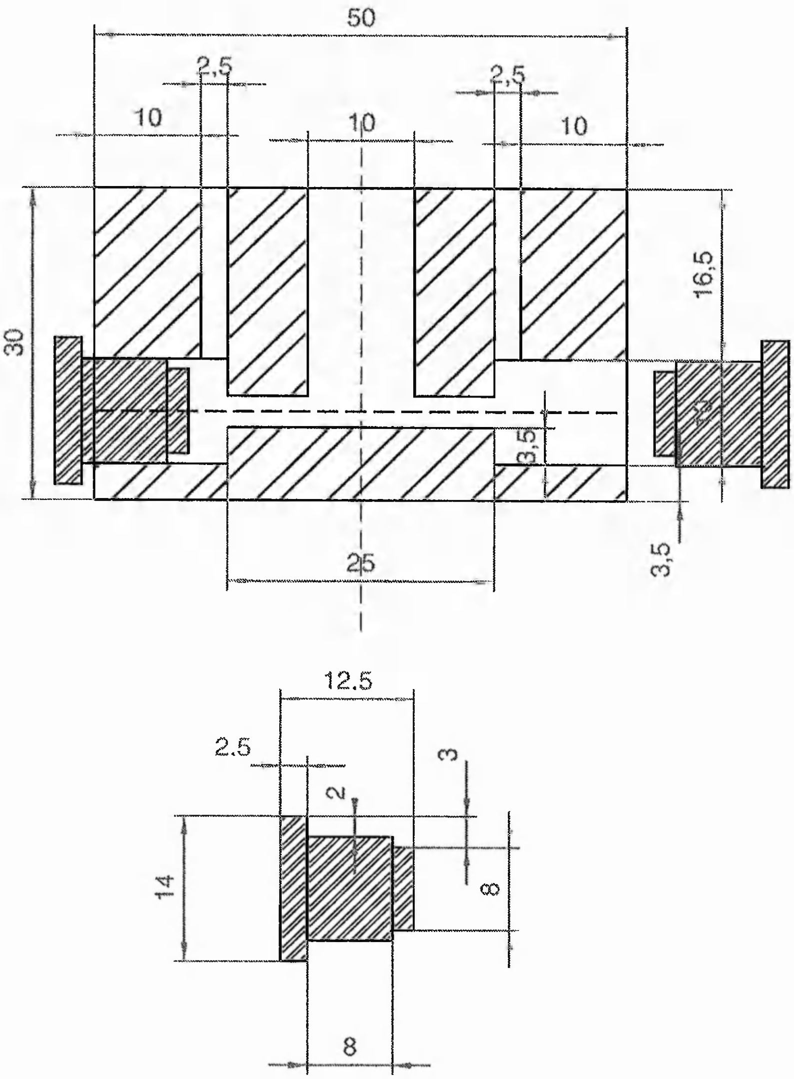

The Nottingham Trent University			
	Faculty of Engineering and Computing	Department of Mechanical and Manufacturing Engineering	
	Material Graphite	Drawing No: G2	Scale: 1:2
Tolerances : +/- 0.1 Unless Otherwise Stated	Title: Graphite die for casting copper prototype		
Surface Finish Unless Otherwise Stated			
Author : Karim Khene			Date: 2000

Appendix H

Drilling Jigs

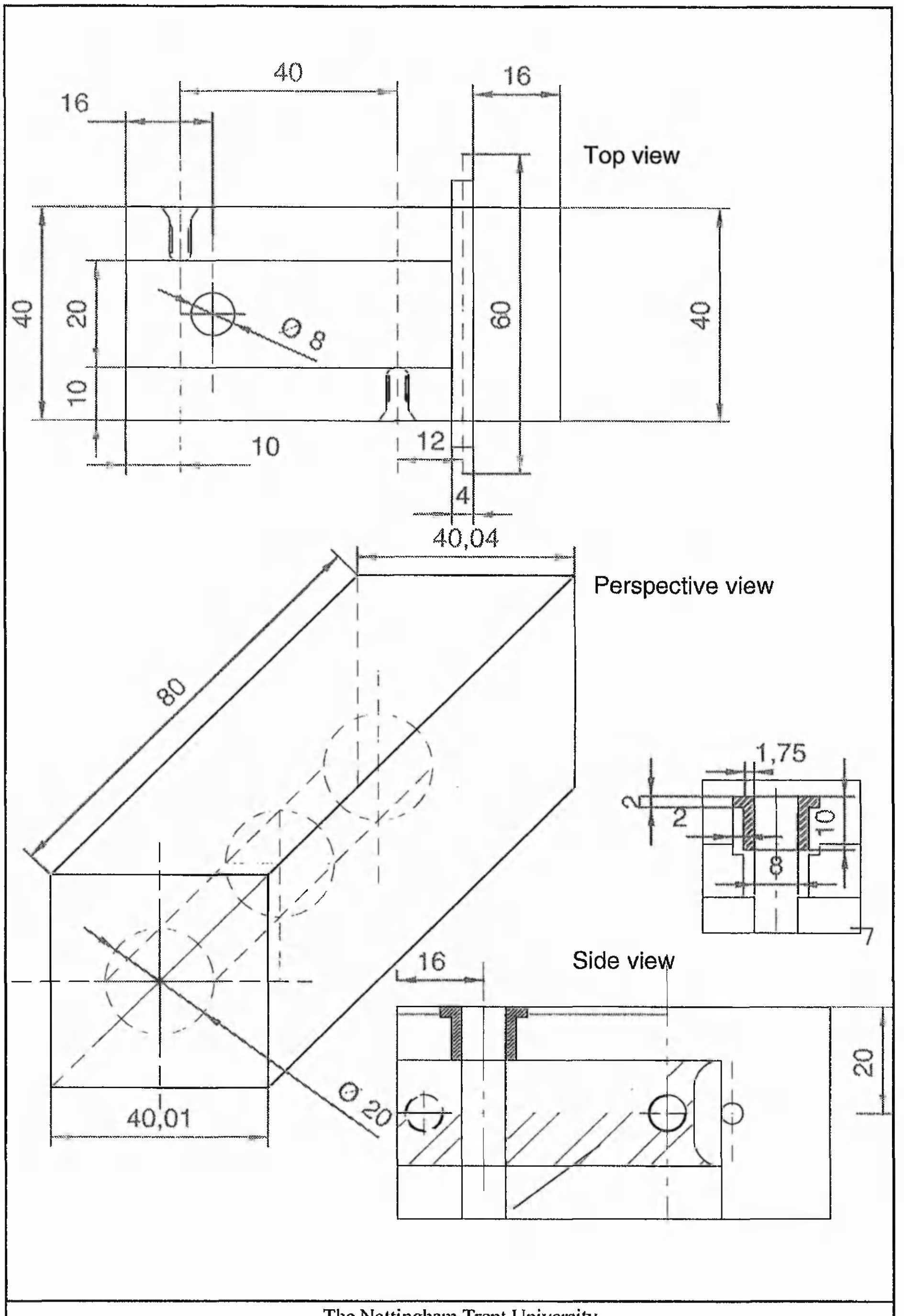

The Nottingham Trent University			
Faculty of Engineering and Computing Department of Mechanical and Manufacturing Engineering			
Tolerances : +/- 0.1 Unless Otherwise Stated	Material Aluminium /Silver steel	Drawing No: H1	Scale: 1:1
Surface Finish Unless Otherwise Stated	Title: Drilling Jig		
Author : Karim Khene	Date: 2000		

Appendix I

Chucks and grips

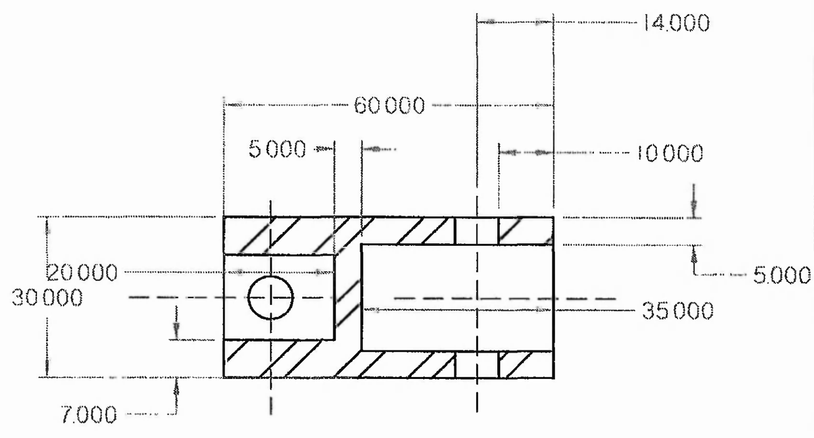

The Nottingham Trent University			
Faculty of Engineering and Computing Department of Mechanical and Manufacturing Engineering			
Tolerances : +/- 0.1 Unless Otherwise Stated	Material Mild Steel	Drawing No: 11	Scale
Surface Finish Unless Otherwise Stated	Title: Grips		Date: 2000
Author : Karim Khene			

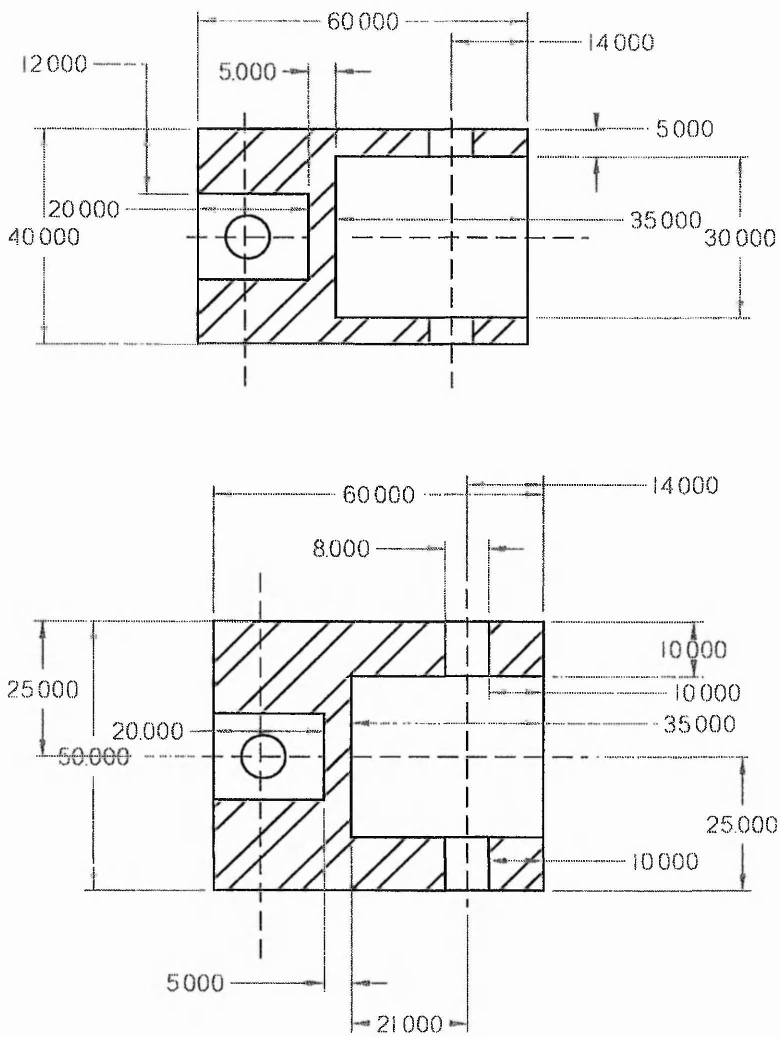

The Nottingham Trent University			
Faculty of Engineering and Computing Department of Mechanical and Manufacturing Engineering			
Tolerances : +/- 0.1 Unless Otherwise Stated	Material Mild Steel	Drawing No: I2	Scale: 1:1
Surface Finish Unless Otherwise Stated	Title: Grips		Date: 2000
Author : Karim Khene			

Appendix J

Annealing of AISI 321

Annealing of Stainless Steel - 10mm x 15mm x 20

Sample No	Hardness Hv20kg	Average	Sample No	Hardness Hv20kg	Average
1*	Before Annealing	294	6*	Before Annealing	302
	After Annealing	139		After Annealing	136
1**	Before Annealing	301	6**	Before Annealing	297
	After Annealing	136		After Annealing	139
2*	Before Annealing	298	7*	Before Annealing	306
	After Annealing	136		After Annealing	143
2**	Before Annealing	298	7**	Before Annealing	298
	After Annealing	139		After Annealing	144
3*	Before Annealing	297	8*	Before Annealing	245
	After Annealing	139		After Annealing	142
3**	Before Annealing	284	8**	Before Annealing	304
	After Annealing	139		After Annealing	141
4*	Before Annealing	292	9*	Before Annealing	295
	After Annealing	139		After Annealing	142
4**	Before Annealing	291	9**	Before Annealing	295
	After Annealing	139		After Annealing	141
5*	Before Annealing	299	10*	Before Annealing	303
	After Annealing	140		After Annealing	138
5**	Before Annealing	300	10**	Before Annealing	297
	After Annealing	134		After Annealing	144

Annealing of Stainless Steel 20mm x 15mm x 16

Sample No	Hardness HV20kg	Average	Sample No	Hardness HV20kg	Average
1*	Before Annealing	292	6*	Before Annealing	296
	After Annealing	136		After Annealing	140
1**	Before Annealing	283	6**	Before Annealing	296
	After Annealing	136		After Annealing	139
2*	Before Annealing	292	7*	Before Annealing	298
	After Annealing	135		After Annealing	144
2**	Before Annealing	296	7**	Before Annealing	302
	After Annealing	137		After Annealing	139
3*	Before Annealing	301	8*	Before Annealing	302
	After Annealing	144		After Annealing	145
3**	Before Annealing	301	8**	Before Annealing	296
	After Annealing	139		After Annealing	144
4*	Before Annealing	300	9*	Before Annealing	300
	After Annealing	137		After Annealing	134
4**	Before Annealing	306	9**	Before Annealing	249
	After Annealing	145		After Annealing	137
5*	Before Annealing	296	10*	Before Annealing	295
	After Annealing	138		After Annealing	139
5**	Before Annealing	296	10**	Before Annealing	299
	After Annealing	139		After Annealing	142

Sample No	Hardness HV20kg	Average	Sample No	Hardness HV20kg	Average
11*	Before Annealing	294	14*	Before Annealing	296
	After Annealing	139		After Annealing	145
11**	Before Annealing	303	14**	Before Annealing	302
	After Annealing	143		After Annealing	144
12*	Before Annealing	298	15*	Before Annealing	293
	After Annealing	142		After Annealing	145
12**	Before Annealing	299	15**	Before Annealing	298
	After Annealing	141		After Annealing	142
13*	Before Annealing	300	16*	Before Annealing	296
	After Annealing	144		After Annealing	145
13**	Before Annealing	298	16**	Before Annealing	295
	After Annealing	145		After Annealing	142

Annealing of Stainless Steel 30mm x 15mm x 8

Sample No	Hardness HV20kg	Average	Sample No	Hardness HV20kg	Average
1*	Before Annealing	299	5*	Before Annealing	294
	After Annealing	140		After Annealing	144
1**	Before Annealing	295	5**	Before Annealing	306
	After Annealing	143		After Annealing	147
2*	Before Annealing	304	6*	Before Annealing	301
	After Annealing	145		After Annealing	144
2**	Before Annealing	307	6**	Before Annealing	297
	After Annealing	144		After Annealing	140
3*	Before Annealing	304	7*	Before Annealing	289
	After Annealing	139		After Annealing	144
3**	Before Annealing	293	7**	Before Annealing	290
	After Annealing	142		After Annealing	142
4*	Before Annealing	296	8*	Before Annealing	296
	After Annealing	145		After Annealing	141
4**	Before Annealing	296	8**	Before Annealing	304
	After Annealing	139		After Annealing	141

Appendix K

AISI 321 physical properties

Stainless Steel AISI 321

Properties

Tensile strength	= 515 MPa
0.2% Yield Strength	= 205 MPa
Elongation	= 40%
Reduction in area	= 50%
Melting point range	= 1400 - 1427C

Composition

		%
Carbon	C	0.08
Manganese	Mn	2.00
Silicon	Si	1.00
Chromium	Cr	17.0 - 19.0
Nickel	Ni	9.0 - 12.0
Phosphorus	P	0.045
Sulphur	S	0.03

AISI 321 is a stabilised austentic chromium-nickel steel. Austentic stainless steels are a high temperature form of iron which can be used between 425 and 900°C. The structure is nonmagnetic. The annealing temperature is between 955 to 1065°C.

Titanium is added in 321 to a minimum of five times the carbon content. 321 has similar room temperature mechanical properties to basic austentic stainless steel. But with differences in corrosion performance and high temperature properties. Where stabilised, grades like 321 show resistance to creep and rupture, superior to that of basic grades at high temperatures

321 steel is formed into

Ingot
Slabs
Sheets
Strips

Typical uses include

Aircraft exhaust manifolds and flanges
Chemical equipment
Collectors rings
Heat exchangers
Jet engine parts
Fire walls
Pressure tanks

Appendix L

Syalon physical properties

Syalon 101 – Typical physical property data obtained under test conditions

PROPERTY	VALUE	UNITS
3 point Room Temperature Modulus of Rupture Specimen 3 x 3 x 350mm, span 19.05mm	945	MPa
Weibull Modulus	11	-
Room Temperature Unit Tensile Strength	450*	MPa
Room Temperature Compressive Strength	>3500	MPa
Room Temperature Young's Modulus of Elasticity	288	GPa
Room Temperature Hardness – (HRA)	91.0 - 91.2	-
Fracture Toughness (K1c)	7.7	M Pa $m^{1/2}$
Poisson's Ratio	0.23	-
Density	3,230 – 3,260	Kgm^{-3}
Thermal Expansion Coefficient (0 – 1200ºC)	3.04 x 10-6	K^{-1}
Specific Heat	620	$JKg^{-1}\ K^{-1}$
Room Temperature Thermal Conductivity	21.3	$Wm^{-1}\ K^{-1}$
Room Temperature Electrical Resistivity	1010	Ohm m
Room Temperature Permittivity – 10 GHz	8.165	-
Room Temperature Loss Tangent – 10 GHz	0.0019	-
Thermal Shock Resistance	up to 900	ΔTºC Quenched in cold water
Coefficient of Friction – Syalon on Syalon in 10W40 engine oil at 80ºC	0.04	-

* Minimum acceptable value 400 MPa

All properties have been measured by independent testing authorities. The values given only apply to test bodies on which they were determined, and therefore can only be recommended values

For further information contact:

Lucas Cookson Syalon Limited
Cranmore Boulevard - Shirley - Solihull - West Midlands B90 4ALL
Telephone: 021 744 2234 Telex: 33 85 26

SYALON

Syalon 201 – Typical physical property data obtained under routine test conditions

PROPERTY	VALUE	UNITS
3 point Room Temperature MOR (Specimen 3 x 3 x 350mm, span 20mm)	825	MPa
Weibull Modulus	8 - 13	-
Room Temperature Unit Tensile Strength	350*	MPa
3 Point MOR at 1400°C (Specimen 3 x 3 x 350mm, span 20mm)	600	MPa
Room Temperature Hardness (HRA)	92.5 – 93.0	-
Density	>3,240	Kgm^{-3}
Creep Strain (1277°C, 77MPa, 100hrs)	<0.02	%
Stress to Rupture (1200°C, 100hrs)	450	MPa

* Minimum acceptable value 300 MPa

All properties have been measured by independent testing authorities. The values given only apply to test bodies on which they were determined, and therefore can only be recommended values

For further information contact:

International Syalons Newcastle Ltd.

P.O. Box 26, Cookson House, Willington Quay, Wallsend, Tyne & Wear NE28 6DF

Telephone: +44 (0) 191 295 1010 **Fax:** +44(0) 191 263 3847

Syalon 501 – Typical physical property data obtained under test conditions

PROPERTY	VALUE	UNITS
3 point Room Temperature MOR	825	MPa
Weibull Modulus	8 - 14	-
Density	>3,950 x 10^3	Kgm^{-3}
Hardness – (HRA)	90.16 – 91.2	-
Specific Heat at 27°C	630	JKg^{-1} K^{-1}
Thermal Diffusivity	7.7	mm^2/sec
Thermal Conductivity	19.1	Wm^{-1} K^{-1}
Volume Electrical Resistivity	7.24 x 10^{-6}	Ohm m
Fracture Toughness	5.7 – 5.8	M Pa $m^{1/2}$
Thermal Shock Resistance	Up to 400	ΔT°C Quenched in cold water
Thermal Expansion Coefficient	5.6 x 10^{-6}	K^{-1} (from 20°C to 1100°C)

All properties have been measured by independent testing authorities. The values given only apply to test bodies on which they were determined, and therefore can only be recommended values

Appendix M

Electrical discharge machining

(EDM)

Summary of Electrical Discharge Machining Parameters

M = Machining Mode

1 = Standard
2 = Low wear
3 = Very low wear
4 = Microfine
6 = Super-Polishing
7 = Standard user

V Machining voltage

Value of V	2	3	4	5
Non-Load voltage/ V	80	120	160	200

If V = +ve then electrode is positive with respect to the workpiece
If V = -ve then electrode is negative with respect to the workpiece

P = Power available

Value of P	0	1	2	3	4	5	6	7	8	9	10	11
Maximum Current / A	0.5	1	1.5	2	3	4	6	8	12	16	24	32

Value of P	12	13	14	15
Maximum Current / A	48	64	96	128

A = Pulse Duration

Value of A	0	1	2	3	4	5	6	7	8
Duration / µs	0.2	0.8	1.6	3.2	6.4	12.8	25	50	100

Value of A	9	10	11	12	13
Duration / µs	200	400	800	1600	3200

RF = Reference Arc Voltage
This is fixed and depends on material Pair.

T = Selector of Secondary Parameters

T = 0: B, R, U, SV, PR are ignored-fixed parameters used.
T = 1: B, R, U, SV, PR are taken into account- fixed parameters are replaced-protection is not ensured.

B = Duration of Interval between two pulses

Value of B	0	1	2	3	4	5	6	7	8
Duration / µs	Opt	0.8	1.6	3.2	6.4	12.8	25	50	100

Value of B	9	10	11	12	13
Duration / µs	200	400	800	1600	3200

R = Withdrawal time
U = Machining time

Value of R or U	0	1	2	3	4	5	6	7	8
Duration / s	Opt	0.1	0.2	0.4	0.8	1.6	3.2	6.4	12.8

If U=9 the pulsations are stopped

SV = Reference mean waiting time (For = 1,2,3)
Between 10 and 50%
Mean voltage (for M= 4,5,6,7)
Adjustable between 50 and 70%

PR = Protection

Adjustable from 0 to 9 (0 = minimum, 5 = standard, 9 = Maximum)

Appendix N

Cooling Pattern

Predicted Cooling Pattern for a 5mm radius dome ceramic-metal joint

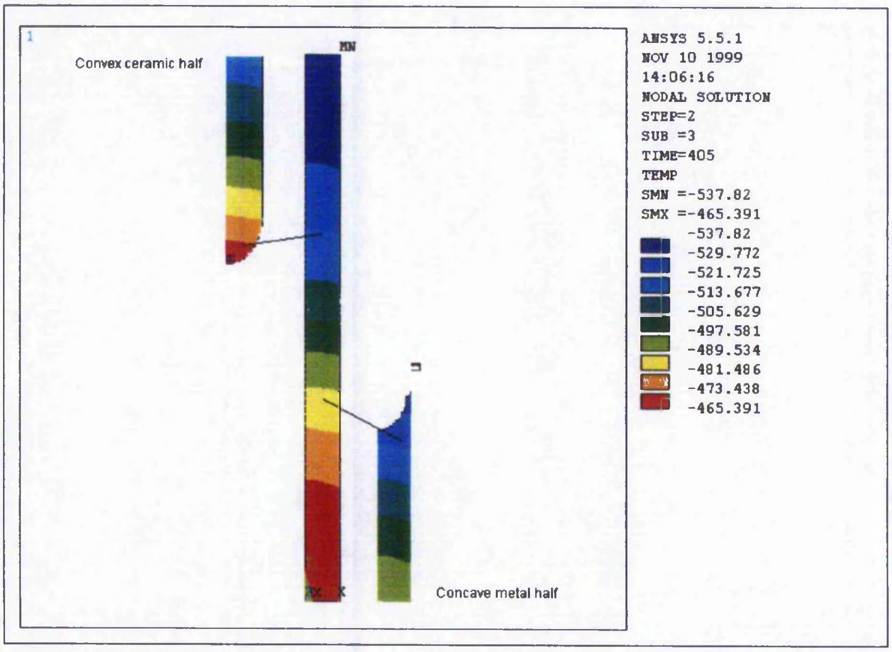

Instantaneous predicted temperature distribution in a 5mm dome ceramic-metal joint after 405s using ANSYS 5.5.1

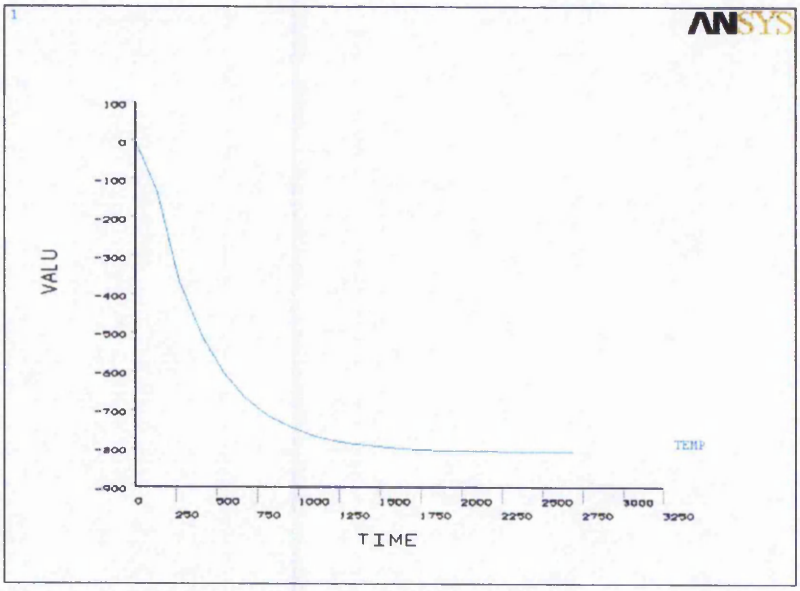

Cooling curve for a point near the free surface of the interface in a 5mm radius dome ceramic-metal joint

Appendix O

High Temperature Vacuum Induction Furnace

High Temperature Vacuum Induction Furnace
Safety Regulations

Safety Procedure

- Always have a member of staff present at all times
- Shut the laboratory door and place the no entry sign outside
- Locate the Radyne control cabinet
- Locate the Radyne remote controller
- Locate the Radyne emergency stop buttons

Authorised User Only

Assemble the furnace as instructed

Connect the furnace to the vacuum pumps using the copper tube and clamps etc.

Wear safety spectacles from this point

Authorised User Only

Evacuate the furnace using the rotary pump. When sufficient vacuum has been obtained (~ 9x 10-2 mbar) disconnect the rotary pump and evacuate the chamber using the diffusion pump (Again refer to the operating procedure on the wall).

Authorised User Only

Connect the induction coil to the Radyne taking care to tighten the nuts to eliminate any water leakage. Be careful when tightening the nuts not to twist the coil and put unnecessary force on the quartz tube which could damage the tube.

- Switch on the water pump [left side of the Radyne cabinet]

- Switch on the Radyne unit at the control cabinet and press the green button (heat off-reset) on the Radyne remote control unit. A green light should appear on the controller (ready). If it does not appear contact the member of staff immediately. Do not proceed beyond this point if the green light is on.

Use the microcomputer to program the necessary ramp rates and set points on the Eurotherm controller.

- Switch on the water cooling to the water jackets. Make sure there is sufficient water flow. Monitor the flow of water at all times.

- If you have followed the above procedures correctly, press the red button (heat on) on the Radyne remote controller. When pressed you should hear a slight humming from the Radyne transformer and the blue light (heat on) should appear on the Radyne remote control unit.

- Do not touch the induction coil or the furnace from this point onwards.
- If the coil start to vibrate on the quartz tube immediately stop the Radyne generator by pressing the red isolator on the Radyne remote controller or by switching the lever on the Radyne control cabinet. Contact a member of staff.

- When finished switch off the induction generator and leave to stand for at least one hour before attempting to handle the furnace. After on hour you may switch off the water cooling to the furnace. Test the temperature of the furnace using the temperature probe before handling (wear gloves).
- Switch off the vacuum pumps as defined by the operating procedure.
- Take extreme care when venting the furnace to the atmospheric pressure. Do it slowly.

Ask a member of staff if unsure

Appendix P

Proposed further FEA work

Ceramic-to-metal joint interface geometries investigated by FEA, but excluded from the main investigation

Before deciding to concentrate on the dome and dome-flat interface geometries a number of designs were considered that involved the introduction of various types of 'interpenetration' between interface to see whether these led to any useful stress reduction at the free edge.

In each design conducted the radiused 'domed' edge profile was retained

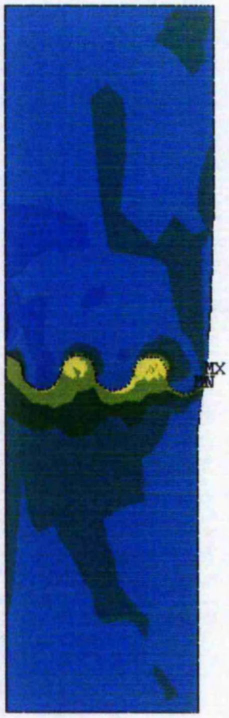

Figure P1: Ansys' stress plot for ceramic/metal assembly (ceramic top) after 540s of cooling from brazing temperature

Figure P2: Two-D Ansys plot of a ceramic/metal assembly after 9000s of cooling from the brazing temperature

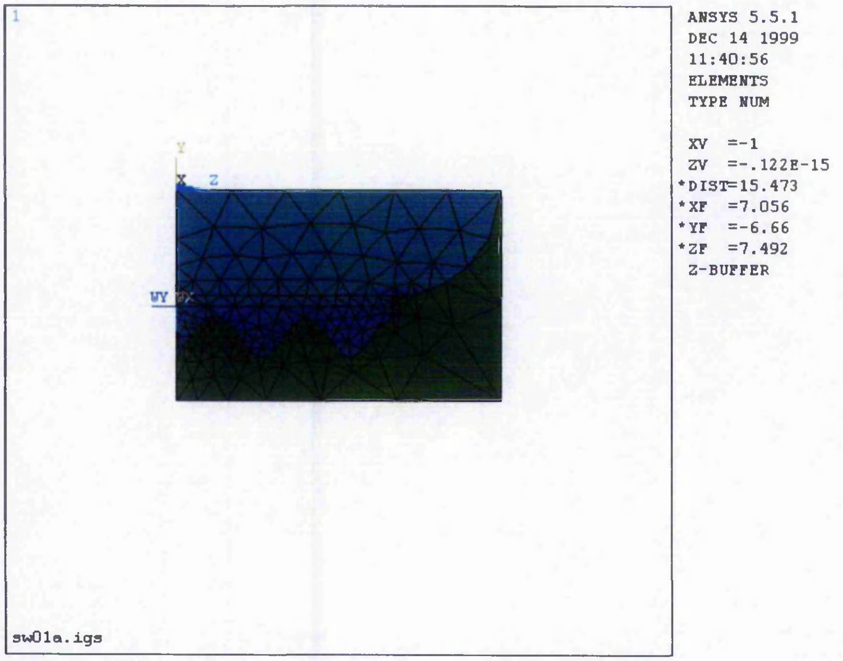

Figure P3: Side view of a 3-D ceramic-to-metal system

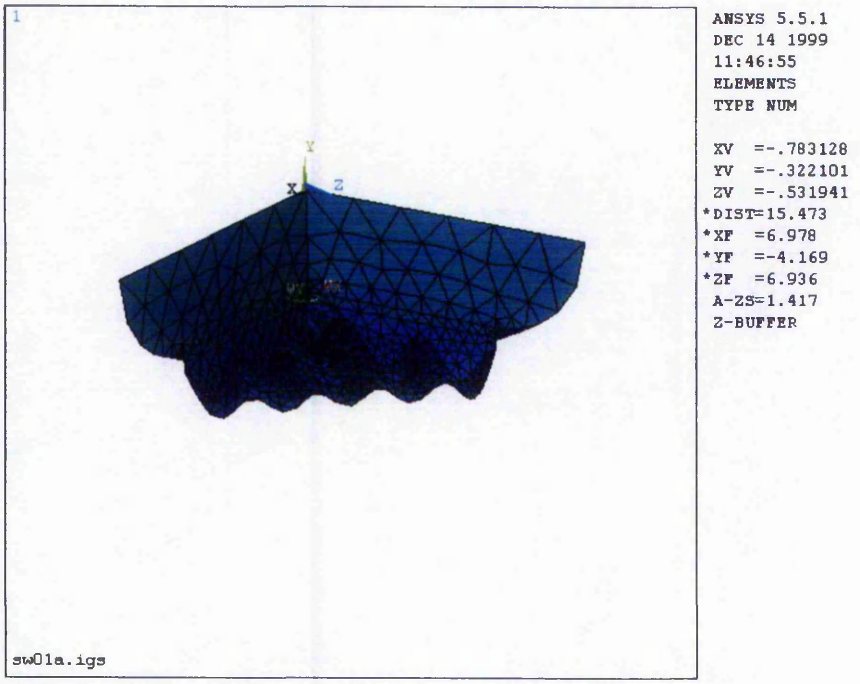

Figure P4: ¼ of 3-D ceramic member showing the repeating sine wave pattern

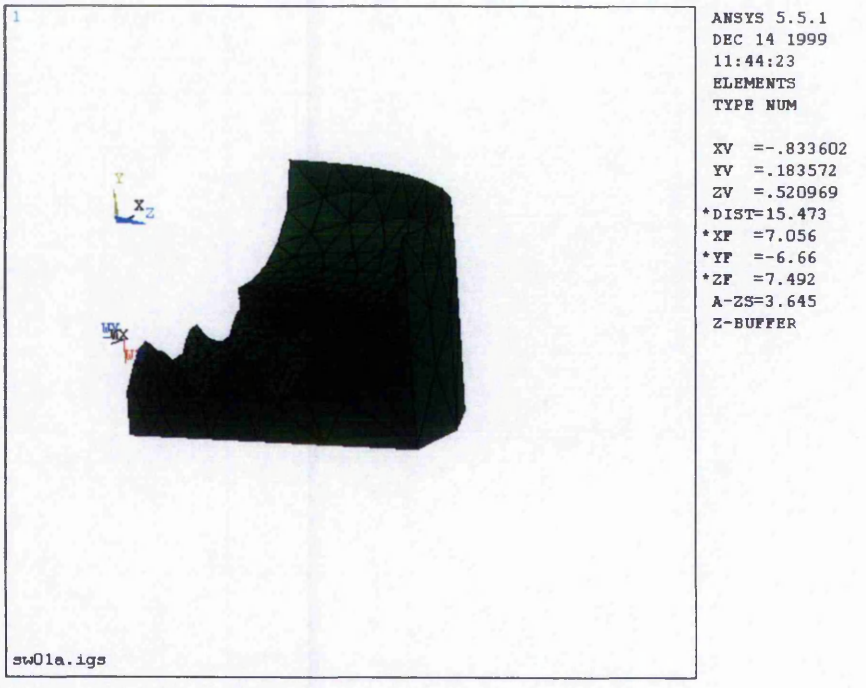

Figure P5: ¼ of 3-D metal member showing the repeating sine wave pattern

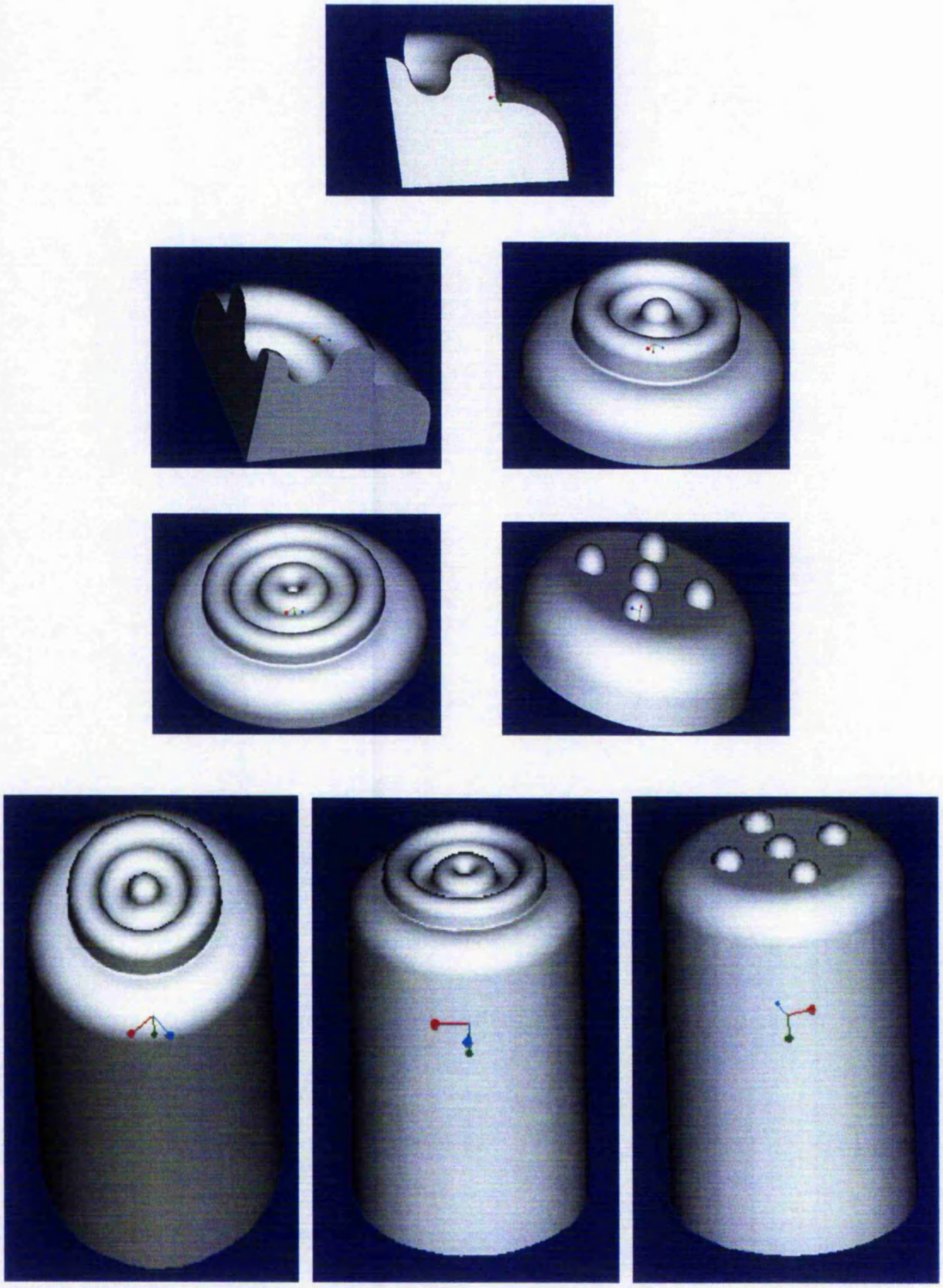

Figure P5: Different types of electrodes modelled

Appendix Q

The size reduction effect on ceramics' strengths

The size reduction effect on ceramics' strengths

Morrell[125] quotes the expression

$$\frac{\sigma_{V1}}{\sigma_{V2}} = \left(\frac{V_2}{V_1}\right)^{\frac{1}{m}}$$

Relating tensile strength (σ) to volume (V) under test.

In comparing cylindrical specimens for a particular ceramic, where each cylinder is of the same length, the ratio

$$\frac{V_2}{V_1} = \frac{A_2}{A_1} = \frac{d_2^2}{d_1^2}$$

Where A and d are the cross section area and diameter of each cylinder respectively.

To predict the fall in strength anticipated when the diameter of a 4mm diameter standard testpiece of strength 450MPa, taken from a population with Weibull modulus of 14 is extended successively to 10mm, 20mm and 30mm diameter, it can be shown that the strengths of these larger diameter cylinders will become σ_{10} , σ_{20} , σ_{30},

where

$$\frac{\sigma_{10}}{450} = \left(\frac{4^2}{10^2}\right)^{\frac{1}{14}}$$

$$\sigma_{10} = 450\ (0.16)^{0.0714} = 395\ \mathbf{MPa}$$

And, when Weibull modulus is 8,

$$\sigma_{10} = 450\ (0.16)^{0.125} = 358\ \mathbf{MPa}$$

Similarly, for a 4mm diameter reference specimen of strength 400MPa, from a population with Weibull modulus 14, the predicted strength for a 10mm diameter cylinder becomes

$$\sigma_{10} = 400\ (0.16)^{0.0714} = 351\ \mathbf{MPa}$$

and where Weibull modulus is 8

$$\sigma_{10} = 400\ (0.16)^{0.125} = 318\ \mathbf{MPa}$$

These calculations can be repeated for the $(\text{diameter})^2$ ratio

$$\frac{d_4^2}{d_{20}^2} = 0.04$$

giving values for σ_{20} of **267 MPa** and **318MPa** on the basis of a 400 MPa reference strength with 'm' equal to 8 and 14 respectively

and for the $(\text{diameter})^2$ ratio

$$\frac{d_4^2}{d_{30}^2} = 0.0178$$

giving values for σ_{30} of **242MPa** and **300MPa** on the basis of a 450MPa reference strength, with 'm' equal to 8 and 14 respectively

Appendix R

Standard Tensile Test Pieces

Standard test pieces used to investigate the tensile properties and work hardenability of copper and AISI 321 stainless steel

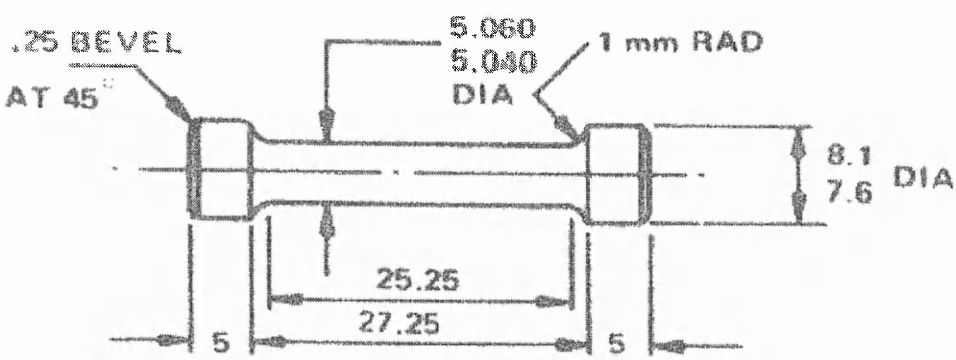

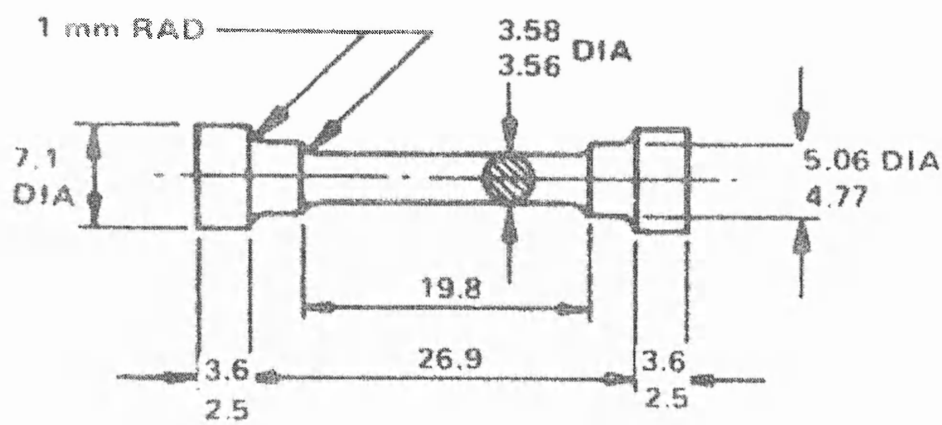
1 mm RAD
3.58
3.56 DIA
7.1
DIA
5.06 DIA
4.77
19.8
3.6
2.5
26.9
3.6
2.5

Appendix S

Investigation into level of work hardening achieved by annealed copper and stainless steel AISI 321

Investigation into level of work hardening achieved by annealed stainless steel AISI 321

Hardness after annealing at 1050°C for 30 minutes = **153 ± 5 HV100g**

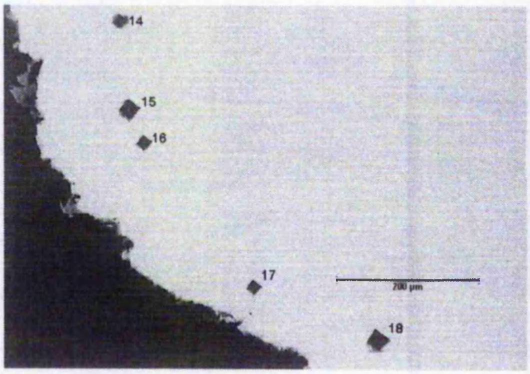

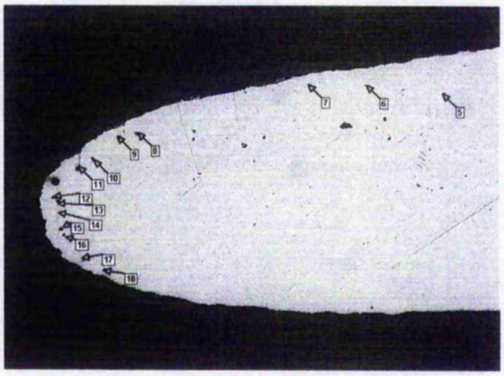

Position	Hardness (HV100g)	Hardness (HV200g)
1	-	197
2	-	317
3	-	368
4	-	379
5	445	-
6	446	-
7	453	-
8	426	-
9	-	427
10	-	454
11	-	450
12	432	-
13	-	522
14	462	-
15	-	514
16	476	-
17	432	-
18	-	416

Average of the 2 hardest values in center of necked region, 100μm from fracture face

= **518 ± 5 HV200g (520 ± 5 HV 100g)**

Investigation into level of work hardening achieved in annealed copper

Hardness after full simulated thermal history experienced by the copper interlayers
= 43 ± 1 HV100g

Position	Hardness (HV100g)	Comments
1	113	1.95mm from side, 4.06 mm from fracture surface
2	110	2.10mm from side, 3.68 mm from fracture surface
3	139	1.28 mm from side, 2.23 mm from fracture surface
4	169	0.44 mm from side, 1.05 mm from fracture surface
5	126	1.17 mm from side, 1.54 mm from fracture surface
6	143	0.46 mm from side, 0.51 mm from fracture surface
7	142	0.10 mm from side, 0.11 mm from fracture surface
8	159	0.08 mm from side, 0.69 mm from fracture face

Average of the 2 hardest values near fracture face = **164 ± 9 HV100g**

Appendix T

Publications

1) Khene, K., Trueman, C.S., Tinsley, N.D., Lacey, M.R. and Huddleston, J., "*A Novel Method of Joining Ceramic-Metal Systems to Reduce Thermally Induced Stresses*", Proceedings of 6th International Symposium on Functionally Graded Materials, Estes Park, Colorado, in Ceramic Transactions, Am. Ceram. Soc., **114**, pp 619-626, 2000

Abstract

A novel method for ceramic-metal joining, applicable for a wide range of emerging Ceramic Matrix Composites (CMC) and cermets is described. It combines singularity removal from the free surface with the introduction of a functional gradient zone, achieved by preshaping the mating parts to obtain typically a regularly repeating interpenetration of the two surfaces. This shaping is performed by CNC electrical discharge machining the CMC (generally containing conductive dispersoid nitrides, carbides or borides), by the preshaped metal part. This paper presents Finite Element Analysis predictions for a range of interface geometries, along with experimental results, illustrating the merits of the process as demonstrated through mechanical testing of finished joints

2) Khene, K., Trueman, C.S., Lacey, M.R. and Huddleston, J., "*Application of Innovative interface Design in Ceramic-Metal Joints to Reduce Thermally Induced Stresses*", Proceedings of the 16th Conference on Manufacturing Research, Advances in Manufacturing Technology-XIV, Edit. R. Perryman and C.D. Ellis, Publ. Professional Engineering Publishing Limited, pp 113-118, 2000

Abstract

Innovative interface configurations were introduced to investigate size and shape effects on the thermally induced residual stresses in ceramic-metal joints with and without soft metal interlayers. Predictive finite element analysis was used in this investigation. The authors found that introducing a new 'dome flat' interface configuration consisting of a flat surface contained between two 5mm-radius half domes identified a situation in which increasing induced residual stress accompanied increasing joint interface size . Moreover the results showed that although the predicted induced stresses increased with larger

components, they were lower than the tensile strength of the ceramic suggesting it is therefore possible to join components up to at least 30mm diameter. EDM shaping of these interfaces is proposed. The EDM-able ceramics demanded generate lower thermally induced stresses in these joints.